SYNTHESIS, STRUCTURE AND PROPERTIES OF SOME CHIRAL-AT-METAL TRANSITION METAL ORGANOMETALLICS

YONGFEI YU

Synthesis, Structure and Properties of Some Chiral-at-Metal Transition Metal Organometallics

by

© Yongfei Yu

B.Sc. (Hons.), Anhui Normal University, Anhui, China, 1984

M.Sc., Anhui Normal University, Anhui, China, 1987

A thesis submitted to the
School of Graduate Studies
in partial fulfilment of
the requirements for the degree of
Doctor of Philosophy

Department of Chemistry
Memorial University of Newfoundland

April 1998

St. John's Newfoundland

Abstract

Although chirality can arise in various guises in organometallic systems, metal centered chirality has become an ever growing concern due to its potential high efficiency in asymmetric synthesis. This thesis focuses on the synthesis, structure and properties of some chiral-at-metal transition metal organometallics.

Reactions of CpCo(X)(Y)(I) (X=(*S*)-$Ph_2PNHCH(Me)Ph$, Y=I, CF_3; XY=PhCH(Me)-N=CH-C_4H_3N) with $Et_2NP(OMe)_2$ toward diastereoselective synthesis of novel Co- and P-chiral amidophosphonate Co(III) complexes were studied by a combination of ^1H, ^{13}C, ^{19}F, ^{31}P NMR, proton NOED, CD spectroscopy and single crystal X-ray diffraction in order to rationalize the Co*→P chiral induction and to establish the solid-state structure, configuration and solid-state/solution conformations. The results show that chemical outcome varies from one system to another.

Study on reaction of a series of resolved chiral aminophosphine Co(III) complexes (CpCo(I)(P(O)(R)(OMe))($Ph_2NHCH(Me)Ph$)) with gaseous HCl shows that the reaction affords regioselective P-N bond cleavage products with retention of configuration at Co* and establishes a convenient method to obtain homochiral transition metal complexes. The regioselectivity was discussed based on EHMO

calculations. ^{1}H NMR evidence for the formation of isobutene, resulting from P-C bond activation via β-elimination in a diastereoselctive, Arbuzov dealkylation reaction involving dimethyl *t*-butylphosphite, was found.

A series of new chiral-at-metal and non-chiral titanocene derivatives with general formula $Cp(C_5R_5)Ti(X)(Ar)$ (R=Me, X=Cl, Ar=C_6F_5, *o*-FC_6H_4; R=H, X=Cl, Ar=C_6F_5, *o*-FC_6H_4; R=H, X=Ar=C_6F_5, *o*-FC_6H_4) was synthesized and characterized. The barrier of aryl rotation around Ti-C_{ipso} and the possibility of coordination of *ortho*-F to Ti were examined by variable temperature NMR, MMX and EHMO methods, as well as solid state single crystal X-ray diffraction.

Acknowledgements

I would like to express my appreciation to my supervisor, Professor Chet R. Jablonski, for his outstanding supervision, encouragement, and financial support throughout the course of thesis studies. His great assistance and patience in the preparation of this thesis are also gratefully acknowledged.

I am greatly indebted to Dr. John. N. Bridson and Mr. David Miller for the X-ray single crystal structural determination, to Ms. Nathalie Brunet and Mr. David Miller for numerous NMR spectroscopic measurements, to Dr. Dan Drummond (University of New Brunswick) for FAB mass spectrometry, to Dr. Kelvin E. Gilbert (Serena Software) for providing PCMODEL for Windows 6.0 and to Dr. Carlo Mealli (Italy) for providing the CACAO package for EHMO analysis.

I am very grateful to Drs. John. N. Bridson and Graham J. Bodwell for their patience in reviewing this thesis, and helpful comments and suggestions in shaping this thesis.

Many thanks are extended to the CRJ group and other members of the Chemistry Department for providing a pleasant working atmosphere and making the years at MUN enjoyable.

I wish to thank Memorial University of Newfoundland for the award of a

graduate fellowship.

Special thanks are extended to my wife, Fang Liu, for her steadfast encouragement and understanding and for her dedicated care of our son.

To My Wife, Fang Liu

and Our Parents

Table of Contents

List of Tables

List of Figures

List of Schemes

List of Abbrevations

BICHEP	2,2'-bis(dicyclohexylphosphino)-6,6'-dimethyl-1,1'-biphenyl
BDPP	2,4-bis(diphenylphosphino)pentane
BINAP	2,2'-bis(diphenylphosphino)-1,1'-binaphthyl
Bn	benzyl
BPPFA	*N,N'*-dimethyl-1-[1',2-bis(diphenylphosphino)ferrocenyl]-ethylamine
BPPM	*N-t*-butoxycarbonyl-4-diphenylphosphino-diphenylphosphino-methyl-pyrrolidine
CAMPHOS	1,2,2-trimethyl-1,3-bis(diphenylphosphino)cyclopentane
CD	circular dichroism
CHIRAPHOS	2,3-bis(diphenylphosphino)butane
CIP	Cahn-Ingold-Prelog
Cp	η^5-cyclopentadienyl
Cp*	η^5-pentamethylcyclopentadienyl
CSA	(+)-camphor-10-sulphonic acid
CT	centroid of cyclopentadienyl/pentamethyl cyclopentadienyl
CYCPHOS	1,2-bis(diphenylphosphino)-1-cyclohexylethane
de	diastereomeric excess

deg	degrees (°)
DIOP	4,5-bis(diphenylphosphinomethyl)-2,2-dimethyl-1,3-dioxolane
DIPAMP	1,2-bis[*o*-methoxyphenyl)phenylphosphino]ethane
DPCP	1,2-bis(diphenylphosphino)cyclopentane
$Eu(DPM)_3$	tris(dipivalomethanato)europium(III)
EAC	ethyl-2-acetamidocinnamate
ee	enantiomeric excess
EHMO	extended Hückel molecular orbital
HOMO	highest occupied molecular orbital
FAB	fast atom bombardment
FMO	fragment molecular orbital
Ind	indenyl
IR	infrared
isodiCp	isodicyclopentadienyl
L-Dopa	(*S*)-3,4-dihydroxyphenylalanine
LUMO	lowest unoccupied molecular orbital
MAC	methyl (*Z*)-α-(acetamido)cinnamate
Me/Et-DuPHOS	1,2-bis[(1,5-dimethyl/ethyl)-phospholano]benzene
MO	molecular orbital

mp	melting point
NMR	nuclear magnetic resonance
N-N*	(*S*)-PhC*H(Me)-N=CH-$C_4H_3N^-$ ($C_4H_3N^-$= pyrrolyl)
NOBA	3-nitrobenzyl alcohol
NOED	nuclear Overhauser effect difference
NORPHOS	2,3-bis(diphenylphosphino)bicyclo[2.2.1]hept-5-ene
PNH	(*S*)-diphenyl-((1-phenylethyl)amino)phosphine
ProNOP	*N*-diphenylphosphino-1-diphenylphosphinooxymethyl-pyrrolidine
PYRPHOS	3,4-bis(diphenylphosphino)-pyrrolidine
THF	tetrahydrofuran
TLC	thin layer chromatography
VT	variable temperature

Chapter 1

Transition Metal-Mediated Asymmetric Synthesis

1.1. Introduction

1.1.1. Why asymmetric synthesis? In general, a chiral compound which contains one stereogenic center exists as a pair of enantiomers, where an enantiomer is defined as "one of a pair of molecular species that are mirror images of each other and not superimposable."[1] However, although the difference in physical properties between two enantiomers is small,[2] their chemical properties including biological activity may vary dramatically.[3-5] The thalidomide tragedy[6] offers a noteworthy example. In the early 1960's the drug thalidomide was used therapeutically as a sedative and hypnotic. However, it was marketed in its racemic form and caused a high incidence of fetal deaths, neonatal deaths, and congenital malformations when taken by pregnant women.[6] Subsequently, it was found that the teratogenicity was attributed to the (*S*)-(-)-enantiomer.[7] This different biologic activity arises from the inherent chirality of the enzymes in biological systems which can differentiate two enantiomers of a specific molecule. Some examples including (*R*,*S*)-thalidomide which demonstrate stereospecificity through precise molecular recognition are given in Scheme 1-1.[9, 10] Potential benefits of therapeutic use of a single enantiomer, based on properties of

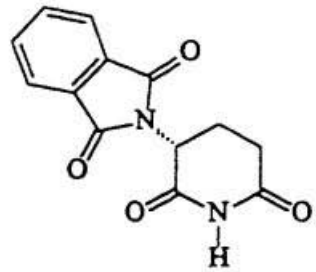

(*R*)-Thalidomide
Sedative

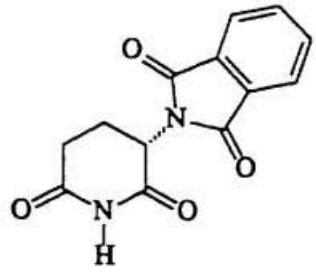

(*S*)-Thalidomide
Teratogen

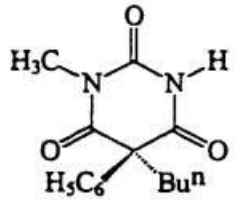

(*R*)
Narcotic

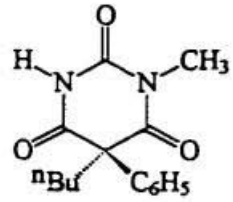

(*S*)
Anticonvulsant

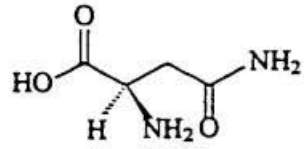

(*R*)-Asparagine
Sweet

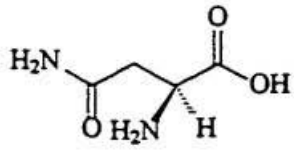

(*S*)-Asparagine
Bitter

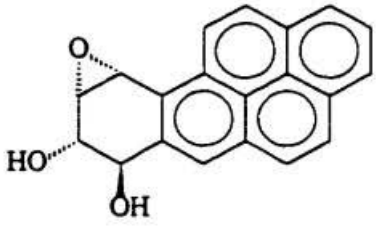

(+)-Metabolite of Benzo[A]pyrene
Carcinogen

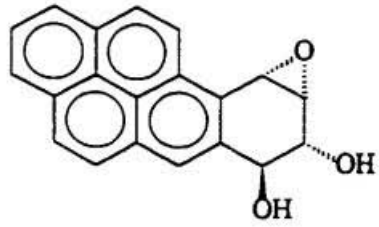

(-)-Metabolite of Benzo[A]pyrene
Innocuous

Scheme 1-1. Contrasting biological behavior exhibited by enantiomeric pairs[9, 10]

Table 1-1. Potential benefits of therapeutic use of a single enantiomer[8]

Properties of Racemate	*Potential Benefits of Enantiomer*
One enantiomer has exclusive activity	Reduce dose and load on metabolism
Other enantiomer is toxic	Increased latitude in dose and broader usage
Enantiomers have different pharmokinetics	Better control of kinetics and dose
Enantiomers metabolized at different rates (in one person)	Wider latitude in dose setting; less variability in patient response
Enantiomers metabolized at different rates (different people)	Reduction in variability of patient responses; large confidence in dose selection
One enantiomer prone to interaction with key detoxification pathways	Reduced interactions with other common drugs
One enantiomer is agonist, other antagonist	Enhanced activity and reduction of dose
Enantiomers vary in spectra of pharmacological action and tissue specificity	Increased specificity and reduced side effects for one enantiomer; use of other enantiomer for different indication

racemates, are summarized in Table 1-1.[8] The increasing awareness of the importance of enantiomeric purity in the study of biological activities and their applications in pharmaceutical, agrochemical, flavour and fragrance industries provides incentive for devising new methodology for the synthesis of pure enantiomers. Regulatory pressure from guidelines issued recently by the Food and Drug Administration (FDA)[11] in the United States are an added incentive.

Increasing environmental pressure serves as another impetus for enantioselective synthesis since unneeded by-products are reduced by up to 50%, thus minimizing

ecologic impact on the environment.[12, 13] Single enantiomers are also useful probes in the elucidation of chemical reactions and reaction mechanisms.[14] In addition, enantiomerically pure compounds have growing applications in areas of molecular electronics, optical data storage and speciality polymers such as high strength lightweight materials and liquid crystals.[15]

Lastly, asymmetric synthesis affects synthetic efficiency. It is well known that uncontrolled synthesis of n stereogenic centres produces 2^n stereoisomers. Clearly, without stereochemical control, the construction of a moderately sized molecule would be hopelessly inefficient. Without repeated separation of stereoisomers, chaos would occur. A non-stereoselective synthesis of a compound with 64 asymmetric carbons and 7 double bonds of a particular configuration would afford only one molecule with the correct stereochemistry out of each mole of substance — one in every 10^{23} molecules![10] A real example that has been achieved[16] is the total synthesis of a protected palytoxin carboxylic acid, which contains 65 asymmetric carbons and 6 double bonds!

1.1.2. Approaches to obtain enantiopure materials. The methods to achieve enantiomerically pure or enriched materials can generally be grouped into two

categories, although a variety of approaches[1, 8, 14, 17, 18] have been developed.

1.1.2.1. Resolution of racemates. Resolution, which includes separation of enantiomeric crystals (conglomerates),[14] conversion to and separation of diastereomers,[19, 20] employment of biochemical and chemical kinetic techniques,[19, 21-23] selective extraction[8] and chiral preparative chromatography,[1, 19] etc, served as the primary method to obtain enantiopure compounds until the early 1970's.[24] The technique of resolution via manual separation of enantiomeric crystals (conglomerates) was first employed by Louis Pasteur in 1848.[25] He obtained two types of crystals with different asymmetric faces by partial evaporation of aqueous solutions of ammonium-sodium double salts of racemic tartaric acid. In this regard, preferential crystallization coupled with spontaneous *in situ* racemization, known as second order asymmetric transformation, is a particularly attractive method for industrial synthesis since the theoretical yield is 100%. An elegant example[26] is shown in Scheme 1-2. A catalytic amount (3 mol%) of an aldehyde facilitates racemization in solution at ambient temperature via the imine and the desired (*S*)-amine continuously crystallizes as its (+)-camphor-10-sulphonic acid (CSA) salt in 91% yield and > 98% ee. It is important to add less than a full equivalent of (+)-CSA in order to maintain a concentration of free amine which ensures the racemization of

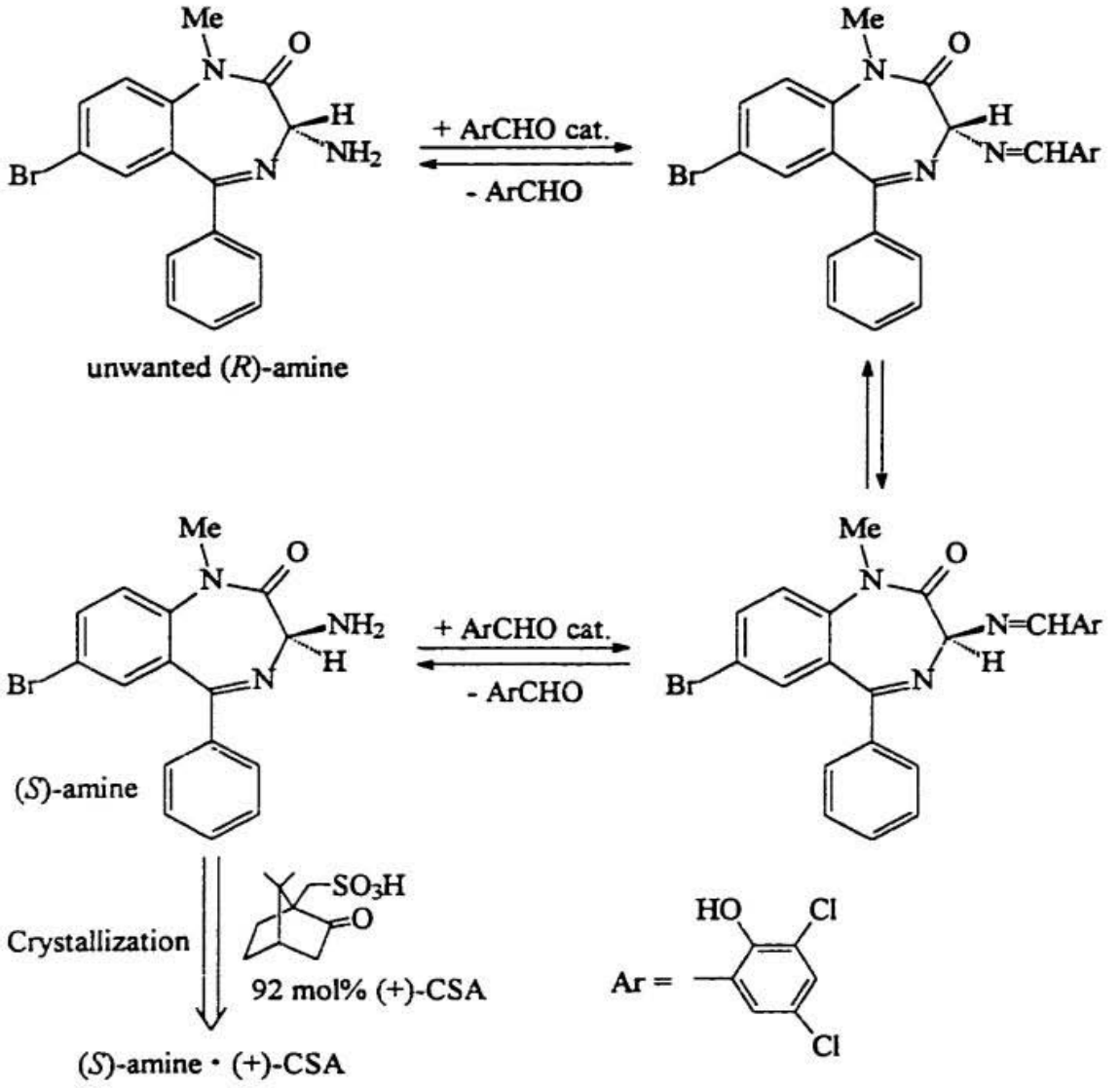

Scheme 1-2. Example of deracemization process[26]

the imine. This efficient, one-pot resolution-racemization process, designated as "deracemization", has been successfully used by Merck[26] on a 6 kg scale to produce an intermediate for a possible cholecystokinin antagonist.

The technique of resolution via the separation of diastereomers generally involves two steps. The racemate is converted into diastereomers by treatment with an optically active reagent (resolving agent) and the resulting diastereomers, which have distinct physical properties, are separated by distillation, chromatographic separation or fractional crystallization. The corresponding enantiomers are recovered by removing the resolving agent. Since the resolving agent for this method is crucial, it must be carefully chosen. A good resolving agent should be inexpensive, react easily and in good yield with the racemate to be resolved and be easily removed after separation.

Biochemical and chemical kinetic resolution depend on different reaction rates of each enantiomer with an enzyme and a chemical reagent, respectively. Recently, Jacobsen at Harvard University developed a direct and efficient route to enantiopure 1,2-amino alcohols from readily available epoxides by using catalytic kinetic resolution.[27] Enantiopure 1,2-amino alcohols are difficult to synthesize, but very useful for generating important synthetic intermediates. Jacobsen's approach is shown in Scheme 1-3. The catalyst delivers an azide group to a particular carbon atom of one of two enantiomers of the epoxide. Removal of the trimethylsilyl group and reduction of the azide group in the generated 1-azido-2-trimethylsiloxyalkane leads to 1,2-amino alcohol. The actual form (*R* or *S*) depends on the chirality of the

catalyst used.

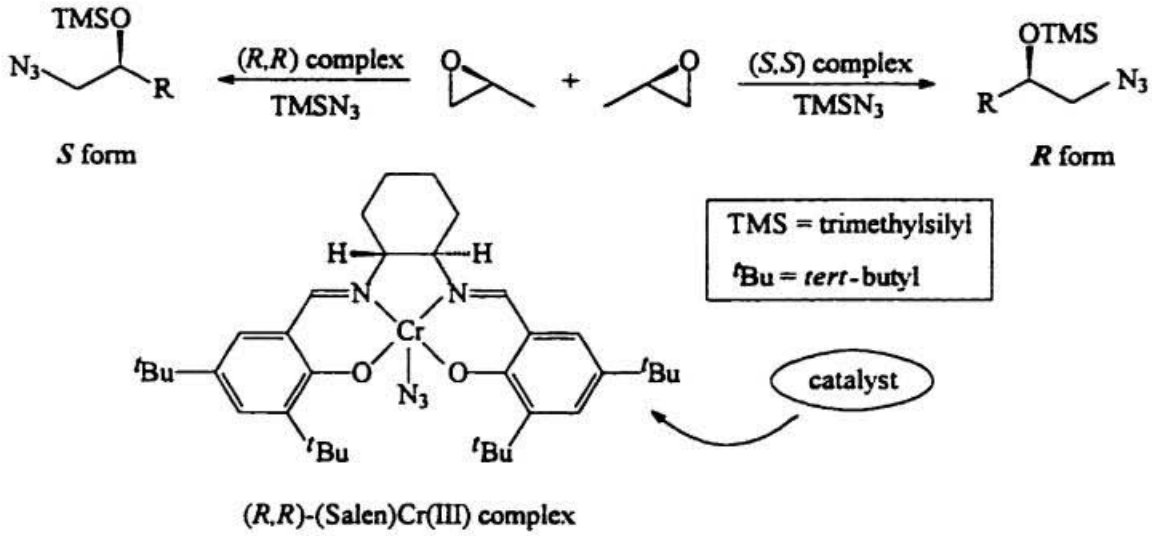

Scheme 1-3. Example of kinetic resolution[27]

All these resolution methods, except the second order asymmetric transformation, generally give, at the very best, a 50% yield of the desired enantiomers.[14] The situation worsens and makes resolution impractical, if not impossible, when a molecule contains more chiral centres since the number of stereoisomers is dramatically increased.

1.1.2.2. Asymmetric synthesis. This method is a solution to the aforementioned problem. Asymmetric synthesis is characterized by its generality, efficacy and

flexibility. These versatilities have been fully acknowledged by chemists in synthetic organic chemistry, medical chemistry, agricultural chemistry, natural products chemistry, pharmaceutical industries, and agricultural industries and clearly reflected by a huge number of publications dealing with asymmetric syntheses of enantiomerically pure or enriched compounds over the last two decades. Stereoselective synthesis, one of the most coveted and long-sought after goals of chemists, has now reached the level which allows organic compounds of virtually every type to be obtained in complete enantioselective or diastereoselective form.[28] The prominence of asymmetric synthesis is largely due to the explosive development of numerous new and efficient catalytic and stoichiometric methods during the last decade.

However, regardless of the method and its inherent efficiency, asymmetric synthesis requires the chemist to "pay the price." A chiral molecule, either in the substrate, the reagents, the catalyst, or the solvent must be incorporated. Without a chiral agent the isolated product(s) will be racemic and require resolution. Schematic representation[29] of this central idea on asymmetric synthesis is given in Scheme 1-4. Scheme 1-4 clearly demonstrates that chirality does not occur spontaneously and it must be imposed during the resolution (eq. 1) and the asymmetric synthesis (eq. 2-6 in

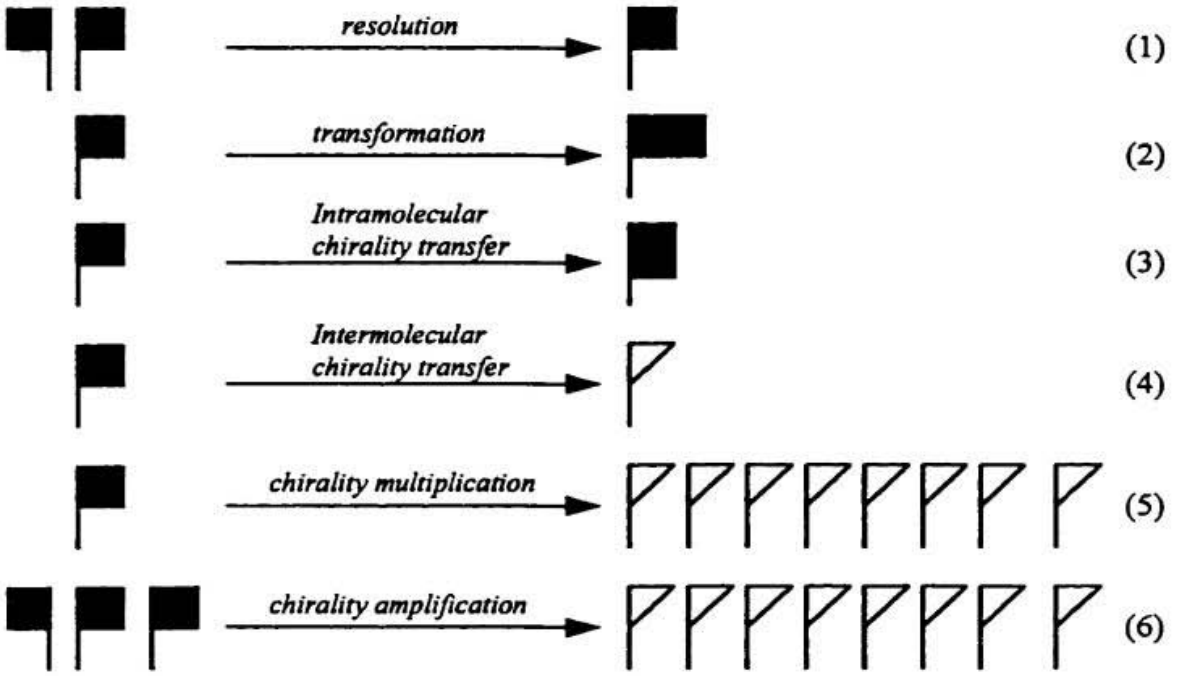

Scheme 1-4. Approaches to optically pure isomers[29]

Scheme 1-4). Transformation (eq. 2) as an approach is often referred to as the "chiral pool" method, which is only valid for the preparation of derivatives of inexpensive, readily available, natural optically pure compounds such as amino acids,[4, 19, 30] tartaric and lactic acids,[31] terpenes[32] and carbohydrates.[33] A limitation of this methodology results from the fact that not all materials isolated from natural sources are enantiopure. For example, many terpenes are obtained in "scalemic"[34] form in which one enantiomer predominates over the other. However the chiral pool is not a

stagnant pond. As enzymes and reagents are discovered and developed, they can be applied to produce large quantities of useful chiral starting material. A timely example is the use of Sharpless epoxidation of prochiral allylic alcohols to form homochiral glycidols (Scheme 1-5) by ARCO.[35]

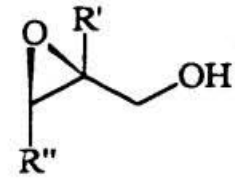

Scheme 1-5. Glycidol

Glycidols can then be converted into enantiomerically pure derivatives via conventional organic reactions involving retention or inversion of configuration or chirality transfer.

Other approaches such as intra- or inter- molecular chirality transfer (eq. 3, 4) as well as chirality multiplication or amplification (eq. 5, 6) involve the use of chiral auxiliaries to create new stereogenic centres, either stoichiometrically or catalytically. A great deal of effort devoted to these approaches has resulted in exponential growth of asymmetric synthesis in last decade. Among various possibilities, the use of chiral transition metal complexes, *i.e.*, transition metal-mediated (TMM) asymmetric synthesis[8, 17, 18, 24, 35–40] promises to be one of the most general and flexible methods and will continue to grow.

1.2. Transition-metal-mediated (TMM) asymmetric synthesis

Organic molecules can be bonded to transition metals in a great variety of ways due to the flexible bonding patterns, variable oxidation states and coordination numbers of transition metals. The reactivities of the organic compounds are often altered / regulated[37, 40-43] as a consequence of bonding to the central metal. In the context of organic synthesis, this change offers exciting and unconventional opportunities through the provision of new types of reactions to be harnessed for the construction of target molecules. Furthermore, geometric restrictions to the orientation of bonding ligands in many transition metal complexes determines the alignment of reacting species brought together by the metal and in turn provides control of stereoselectivity as well as chemical selectivity. The use of transition metals continues to provide a plethora of asymmetric reactions, and this trend will, no doubt, continue as organometallic chemistry sees further developments.[8]

Based on the position of the stereogenic centre in the transition metal chiral auxiliary, transition metal-mediated asymmetric synthesis can normally be divided into two groups (Scheme 1-6). The stereogenic centre is in the chiral ligand in the first group while the second group involves a chiral-at-metal organometallic species. In the first case the chiral source is "distal" to the prochiral target-T. In the second case the chiral source is "proximal" to the prochiral target. In principle, a proximal chiral

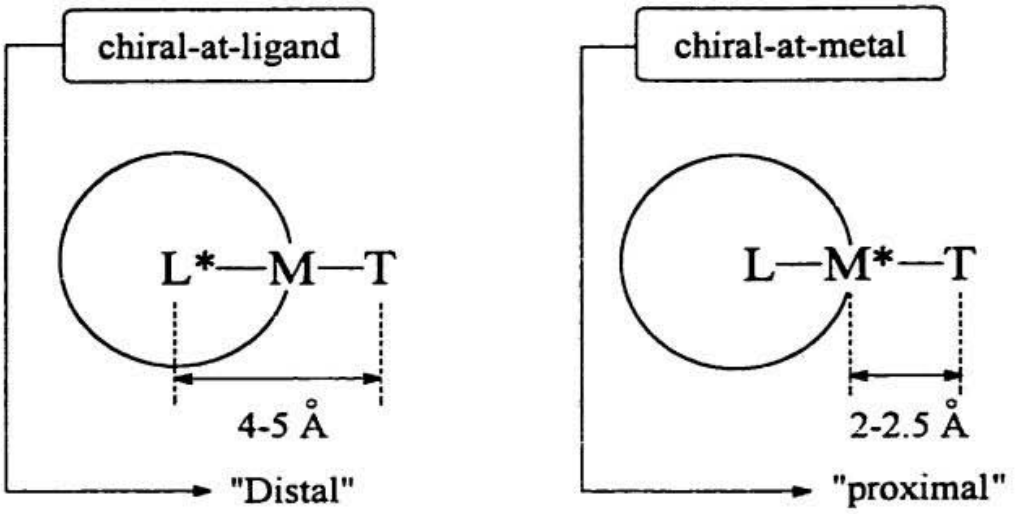

Scheme 1-6. Two types of chiral auxiliaries

centre would be expected to have larger influence (chiral induction) on the target molecule than the distal one. This is easy to be understood since the former chiral centre is relatively far from the target molecule. However a great deal of effort is being spent to extend the chirality of ligands into the active site of a target molecule via phenyl transmitter groups in expanded "dendrizyme" ligands. For instance, a two-layer dendrizyme as shown in Scheme 1-7 has recently been synthesized and examined by Brunner.[44]

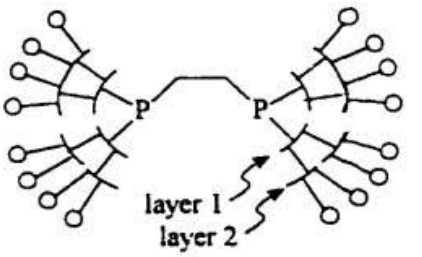

Scheme 1-7. Two-layer dendrizyme

1.2.1. TMM asymmetric synthesis with chiral ligand auxiliaries. This technique

is usually catalytic and represents one of the most promising methods for synthesis of optically active compounds, since a small amount of chiral material (catalyst) can produce naturally occurring and nonnaturally occurring chiral products in large quantities.[4, 18, 24, 35, 36, 45] Generally speaking, especially with respect to chiral induction, homogeneous catalysts are more selective than heterogeneous catalysts.[46] This argument is based on the proposal that only one catalytically active species is present in solution for an ideal homogeneous catalyst while a heterogenous catalyst is more likely to contain different catalytically active sites. In the latter case, overall low selectivity would be observed as each site has its own selectivity. In addition, it is more convenient to study catalytic mechanisms with a homogeneous system. However, it is easier to isolate desired products from a heterogeneous system. Recent advances in the area of catalytic TMM asymmetric synthesis have become industrial reality.[5, 24, 47, 48] Special attention in this regard has been given to reduction,[8, 17, 24, 29, 38, 46, 49-62] oxidation[8, 17, 49, 50, 63-69] and carbon-carbon bond formation.[8, 17, 38, 49, 50, 70-73]

"Heterogenized homogeneous catalysts" represent a bridge between homogeneous and heterogeneous catalysts and are known as the third generation catalysts. These third generation catalysts combine advantages of homogeneous and heterogeneous catalysts. However, a problem associated with third generation catalysts is the loss

of activity and selectivity due to metal leaching.[74]

These topics have been extensively covered by literature, hence only homogeneous catalytic hydrogenation promoted by transition metal complexes bearing chiral ligand auxiliaries will be highlighted since it provides exceptionally clear insight into the nature of TMM chiral synthesis.

The first homogeneous asymmetric hydrogenation, achieved via replacing triphenylphosphine in the Wilkinson catalyst[75] by a chiral tertiary phosphine, was reported independently by Horner[76] and Knowles[77] in 1968. However, the initial optical yield was very low (8-15% ee). Since then, significant improvements in optical yield have been achieved. Morrison[78] first recognized that phosphines achiral at phosphorus but bearing a chiral substituent may also serve as ligands for enantioselective hydrogenation. A further breakthrough in this area came when Kagan[79, 80] discovered that the optical yield could be greatly enhanced by the use of bidentate phosphines, which reduced the number of possible conformations and hence transition states. Some frequently used diphosphines are shown in Scheme 1-8.[57] Most have a C_2 symmetry axis which serves the important function of reducing the number of competing, diastereomeric transition states.[81] Soon after, it was found that

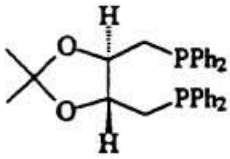

(*R*,*R*)-DIOP

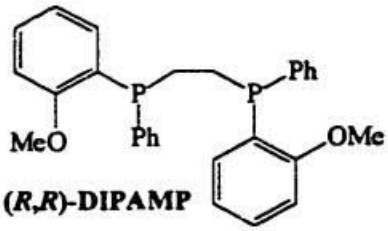

(*R*,*R*)-DIPAMP

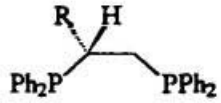

R=Me: (*S*)-PROPHOS
R=Ph: (*S*)-PHENPHOS
R=c-C_6H_{11}: (*S*)-CYCPHOS

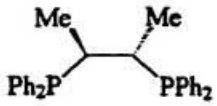

(*S*,*S*)-CHIRAPHOS

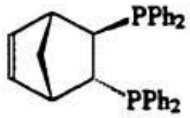

(*R*,*R*)-NORPHOS

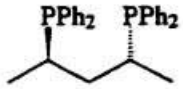

(*R*,*R*)-BDPP

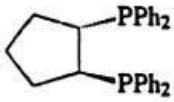

(*S*,*S*)-DPCP

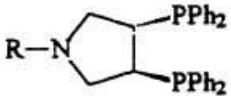

(*S*,*S*)-PYRPHOS

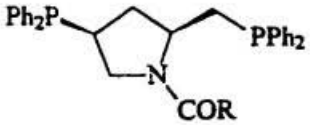

R=*t*-BuO: (*S*,*S*)-BPPM
R=R'NH: (*S*,*S*)-R'-CAPP
R'=C_6H_3-3,4-Cl_2;
C_6H_4-4-Br

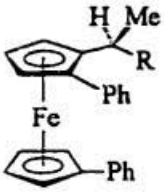

R=NMe_2: (*R*,*S*)-BPPFA
R=OH: (R,*S*)-BPPFOH
R'=N(Me)CH_2CH_2N

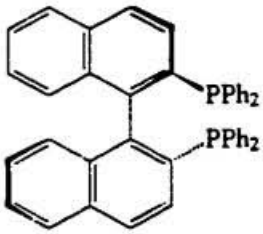

(*R*)-BINAP

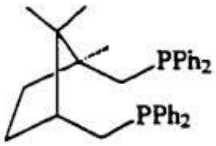

CAMPHOS

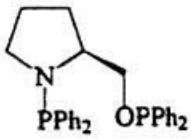

ProNOP

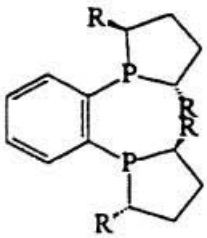

R=Me: Me-DuPHOS
R=Et: Et-DuPHOS

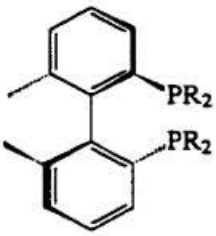

R=Ph: (*R*)-BIPHEMP
R=*c*-C_6H_{11}: (*R*)-BICHEP

Scheme 1-8. Frequently used chiral diphosphine ligands[57]

the best substrates for rhodium-catalyzed enantioselective hydrogenations were 2-acyl-aminocinnamic acids. Nowadays, a series of naturally and non-naturally occurring amino acids can be prepared routinely in greater than 90% ee using phosphine-Rh catalysts. Some examples[24] are shown in Scheme 1-9.

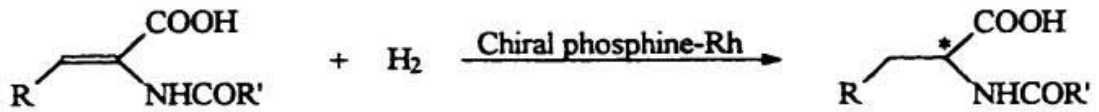

Phosphine Ligand	R	R'	%ee of product
(*S*)-BINAP	Ph	Ph	100(*R*)
(*S*)-BINAP	H	Ph	98(*R*)
(*S,S*)-BPPM	Ph	Me	91(*R*)
(*S,S*)-BPPM	H	Me	98.5(*R*)
(*S,S*)-CHIRAPHOS	Ph	Me	95(*R*)
(*S,S*)-CHIRAPHOS	H	Me	91(*R*)
(*R,R*)-DIPAMP	Ph	Me	96(*S*)
(*S,S*)-DIPAMP	H	Me	94(*S*)
(*S,S*)-Et-DuPHOS	Ph	Me	99(*R*)
(*S,S*)-NORPHOS	Ph	Me	95(*R*)

Scheme 1-9. Selected hydrogenation with Rh-P* system

Catalytic asymmetric hydrogenation with Rh-phosphine catalysts has been highly successful and has resulted in several commercial applications.[5, 82, 83] Examples of industrially relevant targets are given in Scheme 1-10.[5] Unfortunately, however, the

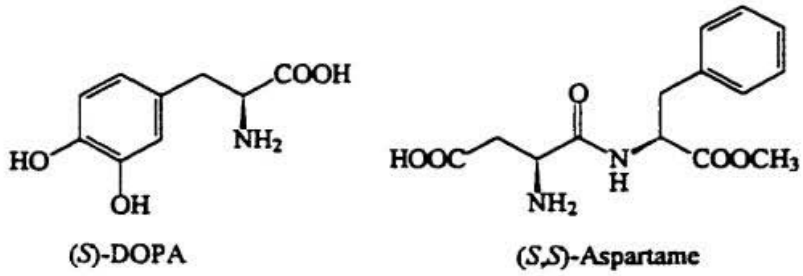

Scheme 1-10. Industrial process with Rh-P* system[5]

scope of the Rh-catalyzed system is very narrow. An extensive, systematic survey of these reactions indicates that an α-amido functional group must be present for efficient enantioface selection (Scheme 1-11). Some useful generalizations have emerged: (i) amide or related groups are necessary; if they are absent, high ee cannot be obtained with any catalyst system;[55] (ii) the phenyl group in position 2 may be replaced by any other aryl group, alkyl group, and even hydrogen; (iii) the hydrogen in position 3 is usually necessary; (iv) the carboxyl group in position 4 can be replaced by other electron-withdrawing groups. Generally, the most successful substrates in catalytic asymmetric hydrogenation are *N*-acylaminoacrylic acid derivatives, carboxylic acids, enamides, enol derivatives, allylic alcohols, and α,β-unsaturated esters, amides and

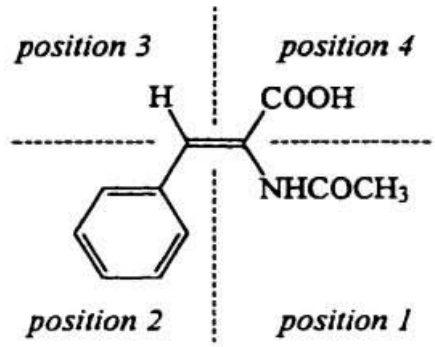

Scheme 1-11. Olefin requirement

ketones, as shown in Scheme 1-12.

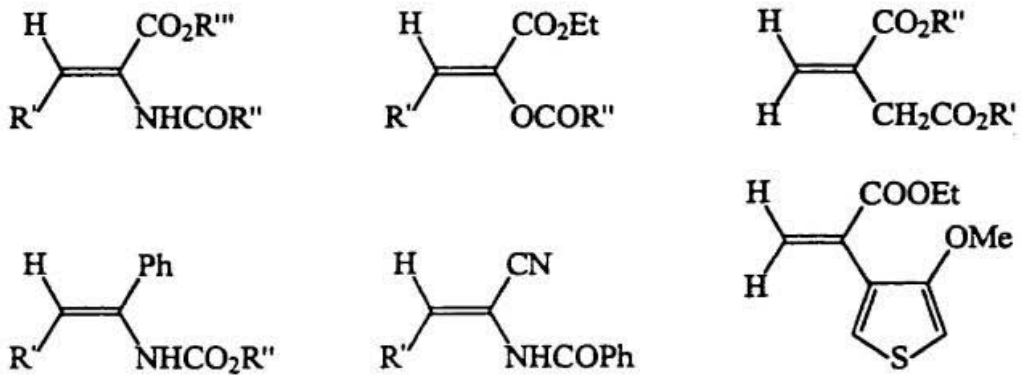

Scheme 1-12. Successful substrates with Rh-P* system

The limitations of the rhodium system stimulated development of a catalytic system which applies to a wider range of olefinic substrates. The BINAP-Ru(II) dicarboxylate complexes shown in Scheme 1-13 are excellent examples. This second generation system, developed by Noyori, can catalyze the hydrogenation of a variety

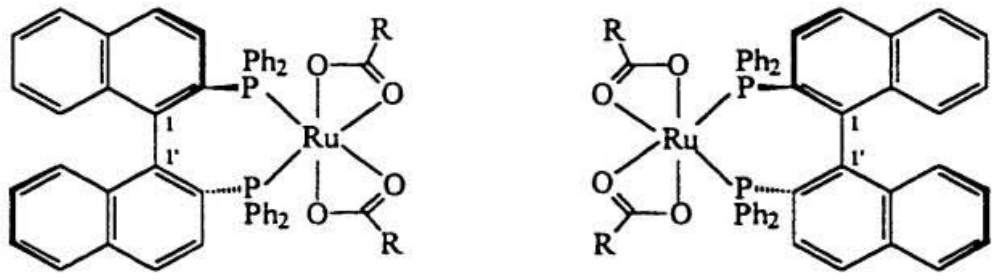

(*R*) (*S*)

Scheme 1-13. BINAP-Ru dicarboxylate catalyst

of functionalized prochiral olefins and ketones[24, 84] which is not possible with conventional Rh(I) systems. The high efficiency of the system is believed to be a result of the structure of the chiral diphosphine BINAP although the exact mechanism is unknown.[24, 29, 52, 59, 85] BINAP is an axially dissymmetric, C_2 chiral diphosphine (Scheme 1-13). The C_2 symmetry dramatically reduces the number of possible diastereomeric reactive intermediates and transition states.[81] The fully aromatic substitution exerts a strong steric influence and provides high polarizability. Due to its conformational flexibility, BINAP can accommodate a variety of transition metals by rotating around its C_1-$C_{1'}$ pivot and C_2-P or $C_{2'}$-P' bonds without serious increase of torsional strain. After coordination with transition metals the resulting seven-membered chelate ring is conformationally and skeletally unambiguous.[86] Some examples[24, 87-89] of BINAP-Ru(II) catalysts are shown in Scheme 1-14. The drawback of the ruthenium-based catalysts is that they require high pressure and sometimes elevated temperature. Therefore, their best field of application is where rhodium catalysts do not excel, for example, in carbonyl reductions (Scheme 1-14).

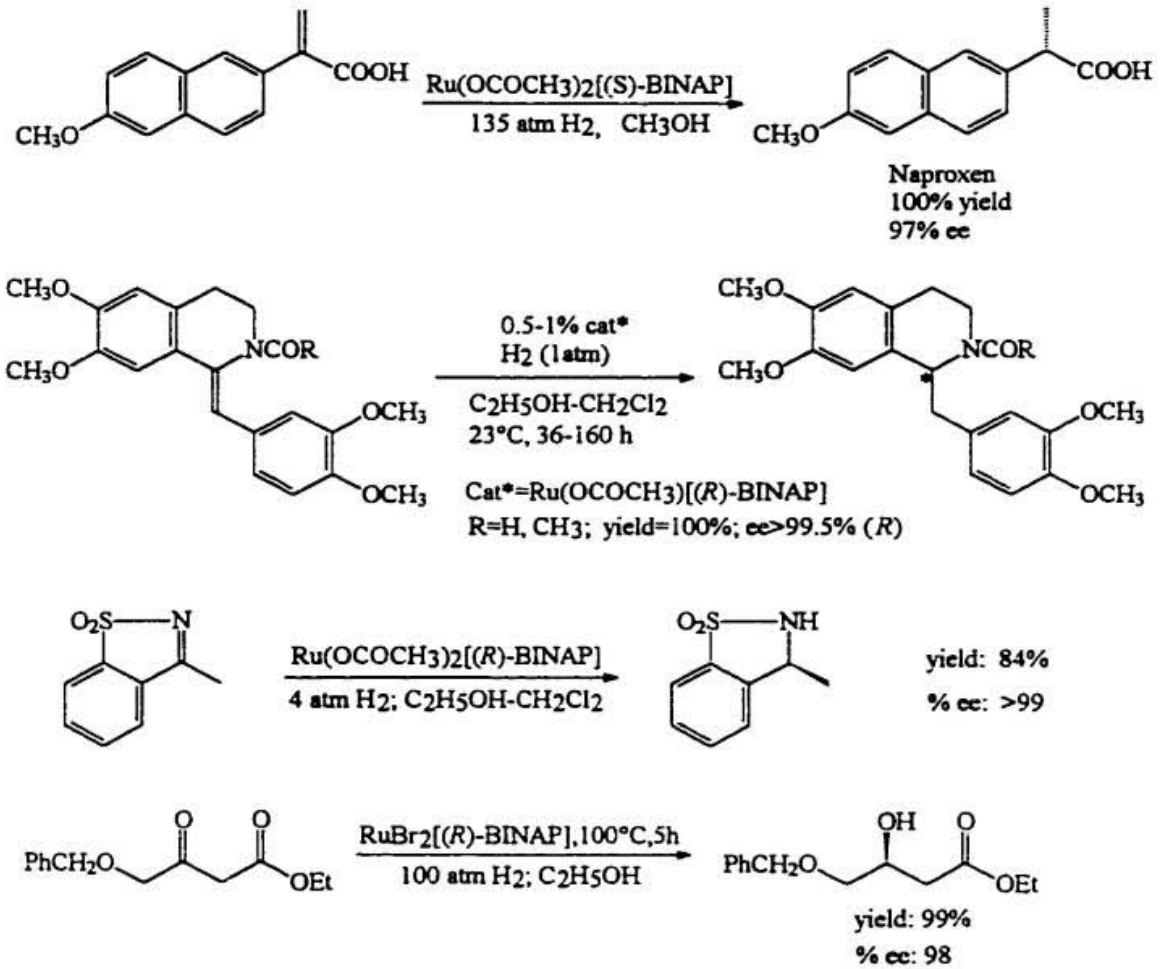

Scheme 1-14. Applications of Ru-BINAP catalytic hydrogenation[24, 87-89]

With both Rh(I) and Ru(II) systems, asymmetric hydrogenation of "simple" olefins that lack functional / secondary binding usually gives low ee. However, recently developed chiral complexes of group IVB metals and lanthanides have paved a road for asymmetric hydrogenation of simple olefins (Scheme 1-15).

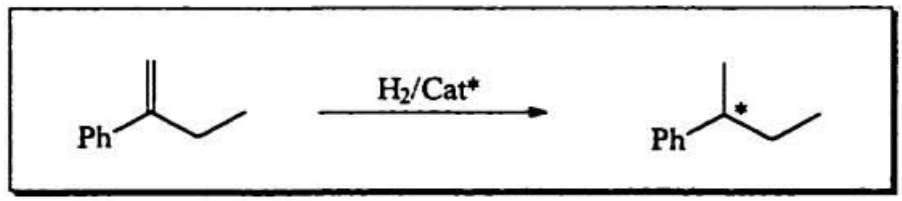

Cat*	Temp. (°C)	% ee
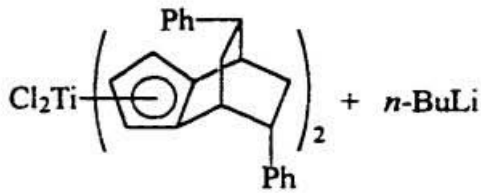	-75	95(*S*)
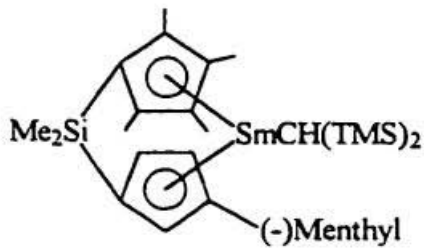 70/30 (*S*)/(*R*) #	-78	96(*S*)

(*S*) and (*R*) indicates the chirality of Cp group

Scheme 1-15. Hydrogenation of simple olefins

1.2.2. TMM asymmetric synthesis with chiral-at-metal auxiliaries.

1.2.2.1. Chiral-at-metal organometallics. Although the first chiral-at-carbon compound, tartaric acid, was resolved by Louis Pasteur in 1845, it was 66 years before the first optically active octahedral transition metal compound *cis*-$[Co(en)_2(NH_3)Cl]^{2+}$ (Scheme 1-16, A) was finally resolved via crystallization of the

3-bromocamphor-9-sulfonates by Werner after fifteen years of effort and failure.[14] Another 58 years passed before the first optically active pseudotetrahedral chiral-at-metal transition metal organometallic compound $[(C_5H_5)Mn(CO)(NO)(PPh_3)]^+$ PF_6^- (Scheme 1-16, B) was resolved by Brunner in 1969.[90] The resolution of chiral-at-metal complexes is generally achieved in two steps. Initial reaction of a racemic mixture with an optically active resolving agent affords a pair of diastereomers which are then separated by crystallization or chromatography. Individual enantiomers can then be recovered by chemical removal of the resolving agent from separated diastereomers. Scheme 1-17 shows the procedure for resolution of the first optically active organometallic complex with four different ligands surrounding the metal, $[(C_5H_5)Mn(CO)(NO)(PPh_3)]PF_6$. Treatment of the R,S_{Mn}-racemate with the sodium salt of the natural optically active alcohol (1*R*,3*R*,4*S*)-menthol gave two diastereomers with elimination of $NaPF_6$. The two diastereomers were separated on the basis of their solubility difference. The $(+)_{579}$-diastereomer is soluble in petroleum ether while the $(-)_{579}$-diastereomer is insoluble.[90] The menthoxide resolving handle was then

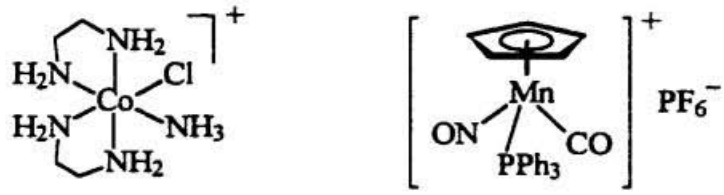

(A) (B)

Scheme 1-16. The 1st resolved octahedral (A) and tetrahedral (B) chiral-at-metal compounds

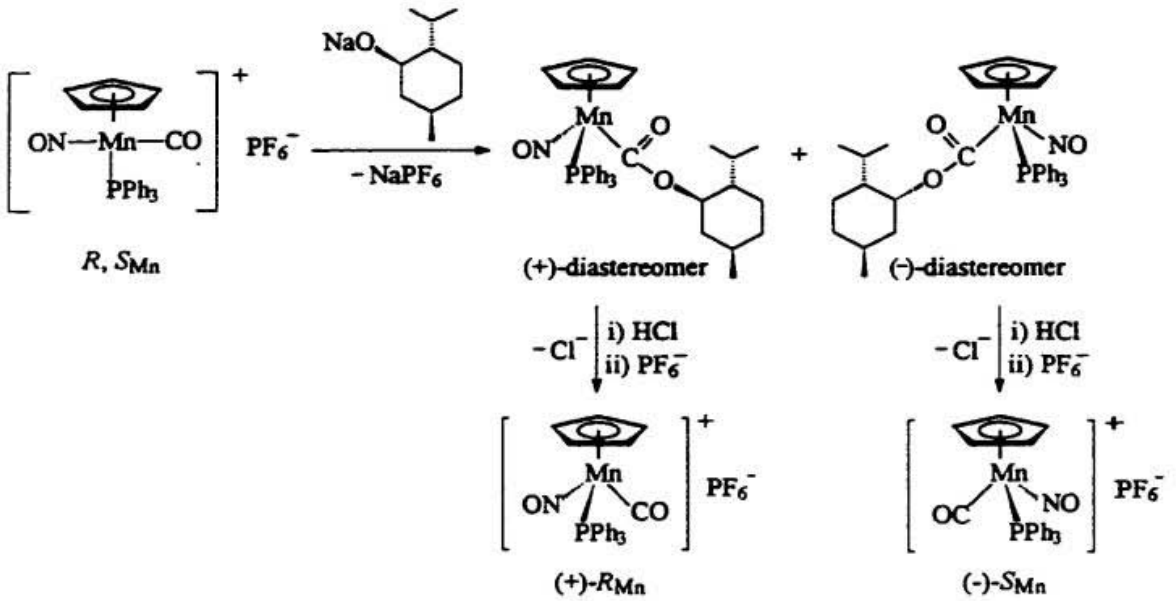

Scheme 1-17. Resolution of the 1st chiral-at-metal organometallics

removed from the separated diastereomers by passing a stream of gaseous HCl through a toluene solution of $(+)_{579}$- and $(-)_{579}$-$(C_5H_5)Mn(NO)(PPh_3)(COOC_{10}H_{19})$. The resulting salts $(+)_{579}$- and $(-)_{579}$-$[(C_5H_5)Mn(CO)(NO)(PPh_3)]^+Cl^-$, which are insoluble in toluene, were then dissolved in water and treated with NH_4PF_6 to afford the enantiomerically pure $(+)_{579}$- and $(-)_{579}$-$[(C_5H_5)Mn(CO)(NO)(PPh_3)]^+PF_6^-$.

1.2.2.1.1. Absolute configuration. Absolute configuration can be unequivocally determined by single crystal X-ray diffraction study using Rogers' η method[91] or by

comparing the difference of R factors after independent refinement of both enantiomers. In favourable cases absolute configurations can also be assigned based on chiroptical properties such as CD spectra.[92]

The descriptors (*R*, *S*) developed for chiral carbon atoms[93] can also be applied to describe the absolute configuration of a metal atom after extension[94, 95] to treat polyhapto ligands. Polyhapto ligands are treated as pseudo-atoms with atomic weight equal to the sum of the atomic weights of all atoms bonded to the metal atom. Using this extension, the frequently used polyhapto ligands such as η^6-C_6H_6, η^5-C_5H_5 and η^2-C_2H_4 can be considered as pseudo-atoms of atomic weight 72, 60 and 24 (or atomic number 36, 30 and 12), respectively.[94, 95] Based on Wojcicki's suggestion,[96] if a complex contains more chiral centers, the metal designation precedes that of carbon. According to these proposals[94-96] and conventional Cahn-Ingold-Prelog rules,[93] the ligand priority series in the complex (η^6-C_6H_6)Ru(Cl)(*o*-$OC_6H_4CH{=}NC^*H(Me)Ph$, as shown in Scheme 1-18, are C_6H_6 > Cl > O > N for Ru* and N > Ph > Me > H for C*, which specifies the absolute configuration of the complex as $R_{Ru}S_C$.

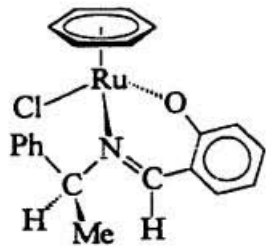

$R_{Ru}S_C$

Scheme 1-18. Application of modified CIP rule

1.2.2.1.2. Chiroptical properties. Unlike optically active organic compounds, optically active organotransition metal complexes exhibit extremely large specific rotations, often larger than those of organic compounds by a factor of one or two powers of ten.[97] These larger rotations are due to the fact that the optically active organotransition metal complexes are colored and thus show strong Cotton effects in the visible part of the spectrum.

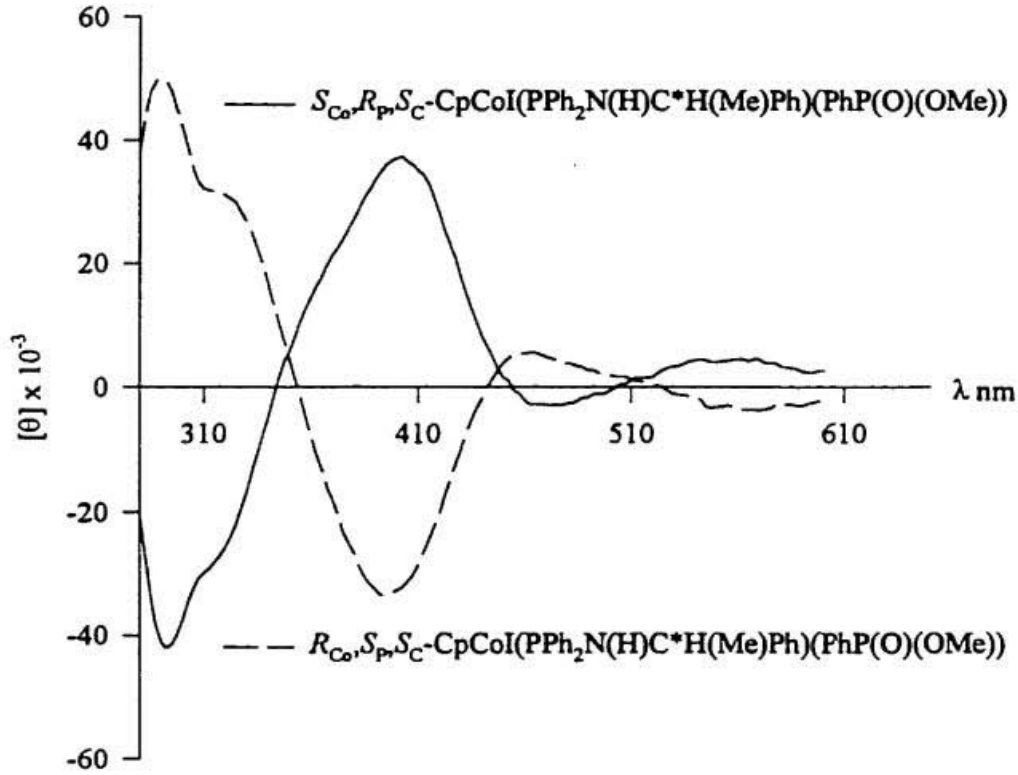

Scheme 1-19. CD spectra of two chiral-at-metal, M-epimeric diastereomers

Correlation of configuration of organotransition metal compounds with chiroptical properties has shown that chiroptical properties are generally dominated by the central metal atom.[92] In other words, the chirality of ligands makes only a minor contribution to chiroptical properties of chiral-at-metal compounds. Based on this empirical rule, the similarity between circular dichroism (CD) spectra of two species has been used to assign the same relative configuration to the central metal atoms while quasi-mirror morphology of two CD spectra indicates the opposite relative configuration at the central metal atoms. For example, the virtually mirror image morphology of the CD spectra of two diastereomers, (S_{Co},R_P,S_C-)-CpCoI(Ph_2PN(H)C*H(Me)Ph)(PhP(O)(OMe)) and (R_{Co},S_P,S_C-)-CpCoI(Ph_2PN(H)C*H(Me)Ph)(PhP(O)(OMe)), as shown in Scheme 1-19, suggests that the two diastereomers have opposite configurations at cobalt.[98]

1.2.2.1.3. Stereochemistry. Although optically active organometallics are configurationally stable at the metal center in the solid state, stereochemical studies of their solution behaviour show that retention, inversion and racemization may be observed[92, 99] in various chemical transformations.

A. Retention of configuration at metal. If reaction of an optically active chiral-at-

compound does not involve metal-ligand bonds, retention of configuration at metal will be achieved.[100, 101] Reaction of (+)-$[(C_5H_5)Mn(NO)(CO)P(C_6H_5)_3]^+PF_6^-$ with LiC_6H_5 serves as an example (Scheme 1-20). Due to attack of LiC_6H_5 on the Cp ring and the carbonyl group, two types of products are obtained.[102]

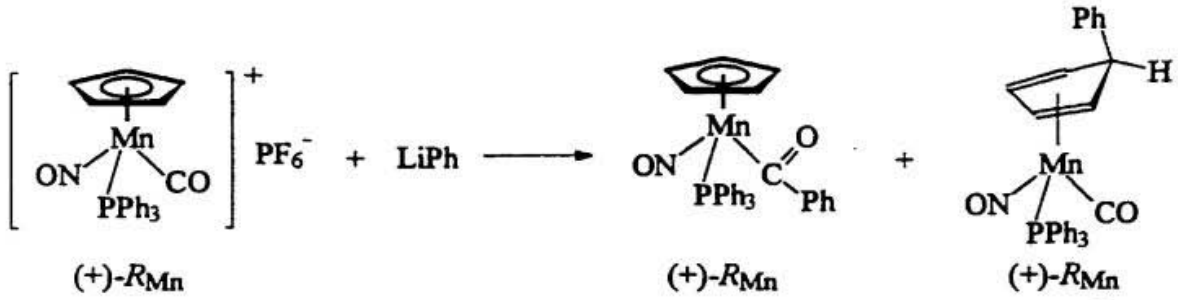

Scheme 1-20. Retention of configuration at metal

B. Inversion of configuration at metal. As shown in Scheme 1-21, reaction of the

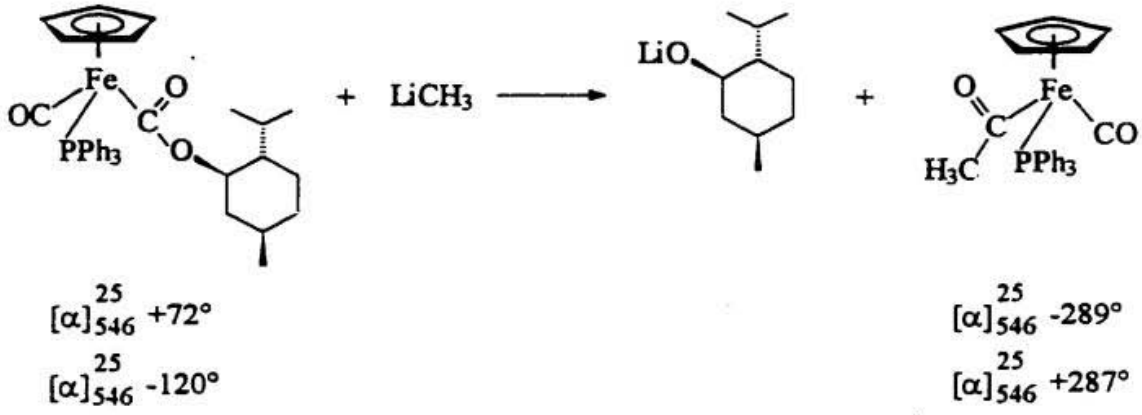

Scheme 1-21. Inversion of configuration at metal

optically active iron complex $CpFe(CO)(PPh_3)(COOC_{10}H_{19})$ with methyl lithium results in the elimination of lithium mentholate and formation of an acetyl complex $CpFe(CO)(COCH_3)(PPh_3)$. Interestingly, the optical rotations of starting material and the acetyl product have opposite signs and their CD spectra are almost mirror images, *i.e.*, starting with $(+)_{546}$ menthyl ester, the $(-)_{546}$ acetyl complex is obtained while $(-)_{546}$ menthyl ester gives the $(+)_{546}$ acetyl complex.[103-105] These chiroptical data suggested an inversion of configuration at Fe, which was unambiguously confirmed by a single crystal X-ray study of both starting material and product.[106-108] These results imply that attack of methyllithium does not occur at the ester group of the starting material as expected, but at the carbonyl group.[105, 109]

C. Racemization of configuration at metal. Racemization was demonstrated by the configurationally labile complexes, (+)- and (-)-$CpMn(NO)(COPh)(PPh_3)$,[110, 111] (Scheme 1-22). The half life (25°C, toluene) was determined to be 21 minutes by polarimetric kinetics. Mechanistic study shows that racemization depends on the concentration of triphenylphosphine. Half-life appreciably increases with the added

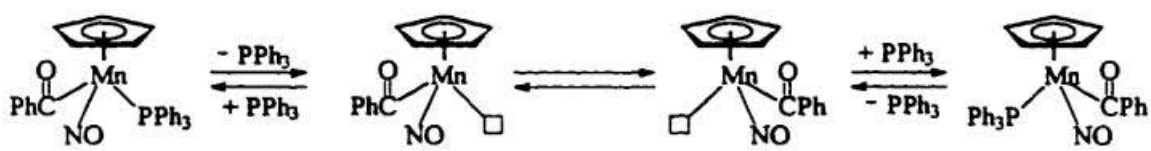

Scheme 1-22. Example of racemization reaction

amount of PPh_3.[110, 111] This observation suggested that configurational stability of the complexes increases on addition of PPh_3 and thus implied a dissociation mechanism (Scheme 1-22). It is believed that the first step, *i.e.*, the phosphine dissociation step, is the rate-determining step and involves a chiral intermediate [CpMn(NO)(COPh)] which has been trapped by CO giving an optically active CpMn(CO)(NO)(COPh)[112] with the same but stable, relative configuration. The tripod chiral intermediate may either invert chirality at Mn and then bind PPh_3 to form a Mn-epimer, or bind a PPh_3 with configuration change at Mn. The former process accounts for the observed racemization. Since the latter process is favored with increasing concentration of PPh_3, the slow racemization / longer half-lives will be achieved on addition of PPh_3.

1.2.2.2. TMM asymmetric synthesis of C*-materials. Many chiral-at-metal organometallic species[92] are potential auxiliaries for a wide range of asymmetric organic syntheses.[38] Here, only representative work with the chiral-at iron auxiliary [η^5-CpFe(CO)(PPh_3)] is highlighted to show how versatile the chiral-at-metal auxiliary is in stereochemical control in asymmetric synthetic transformations.

The chiral iron acetyl complex η^5-CpFe(CO)(PPh_3)($COCH_3$), which was first resolved by Brunner[103] and later extensively studied by Davies[113-116] and Liebeskind[117-121] for

synthesis of organic compounds through carbon-carbon bond forming reactions, exerts powerful stereochemical control over a variety of reactions of attached acyl ligands including alkylations, aldol reactions, tandem Michael additions, alkylations and Diels Alder reactions. The parent iron acetyl complex is commercially available in homochiral, (*R*) or (*S*), form.[99] This three-legged, piano-stool, pseudo-octahedral complex and most of its derivatives are air stable and thus easy to handle. They are also highly crystalline and coloured so that purification by crystallization or chromatography is relatively easy. The preferred conformation of the acetyl ligand places the acyl oxygen anti-periplanar to the carbon monoxide ligand.[122-124] In order to minimize steric interactions between the acetyl ligand and the phenyl rings, one of the three phenyl rings is face exposed under the acetyl ligand. Therefore, attacking substrates are blocked from one face of the acetyl group and high stereoselectivity results. This face selectivity has been well demonstrated in alkylation and tandem Michael addition-alkylation reactions.

Treating the acetyl complex with *n*-butyllithium cleanly generates the corresponding enolate, which may be trapped by alkyl halides. Further treatment with n-butyllithium leads to the corresponding *E*-enolate. Subsequent alkylation from the unhindered face generates a new chiral centre with complete stereocontrol. One

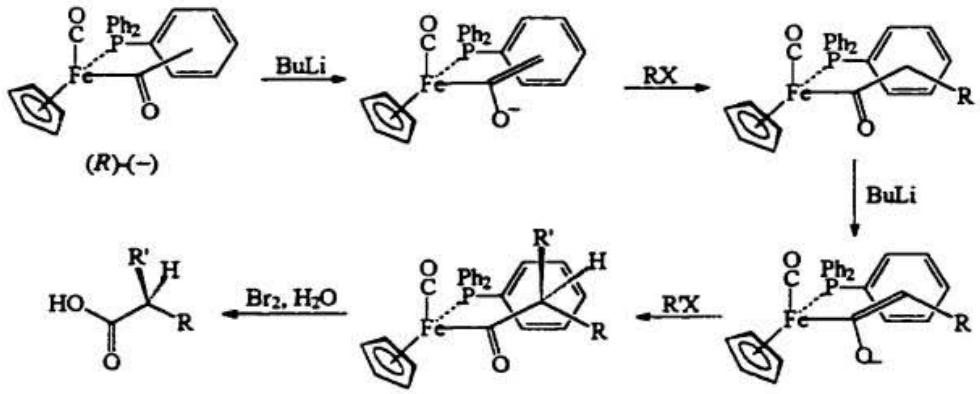

Scheme 1-23. Alkylation reaction mediated by a chiral iron auxiliary[126]

electron oxidation, most commonly with bromine in the presence of water, or alcohols or amines, liberates the corresponding carboxylic acids, esters and amines respectively, with retention at the new chiral centre (Scheme 1-23). The chirality of the newly generated stereogenic centre in the final product depends on the chirality of the starting chiral iron acetyl and on the order of the two alkylation reactions. This strategy has been used for drug syntheses of , for example, the antihypertensive drug (-)captopril[125] and the potent collagenase inhibitor (-)-actinonin[126] (Scheme 1-24).

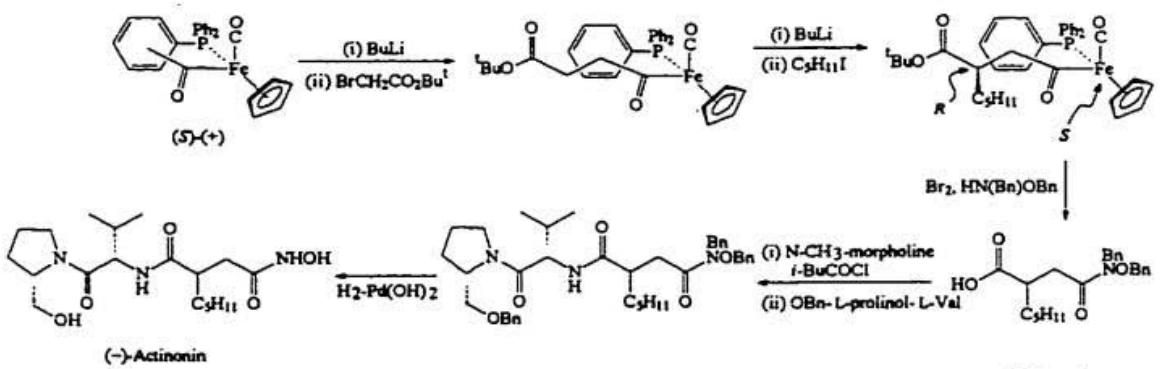

Scheme 1-24. Synthesis of (-)-actinonin via chiral iron auxiliary[126]

1.2.2.3. TMM asymmetric synthesis of P-chiral materials via Arbuzov-like dealkylation reactions. Numerous studies in asymmetric synthesis have established that P-chiral ligands play a crucial role in obtaining a high degree of stereoselectivity.[24, 127, 128] Enantiomers of P-chiral phosphorus compounds usually exhibit a variety of unique biological activities and hence could be used in chemotherapy, pest control, and bioorganic chemistry.[34, 58, 129, 130] In addition, P-homochiral materials are targets for basic studies of their stereochemistry and are widely used in asymmetric synthesis and asymmetric catalysis.[34, 58, 130] Since P-chiral materials cannot be found in the natural chiral pool, their preparation poses a challenge to chemists and must be achieved via synthesis. This thesis describes attempts to synthesize P-chiral materials via transition metal mediated Arbuzov reactions.

1.2.2.3.1. Classical Arbuzov reaction. The Arbuzov reaction, also known as the

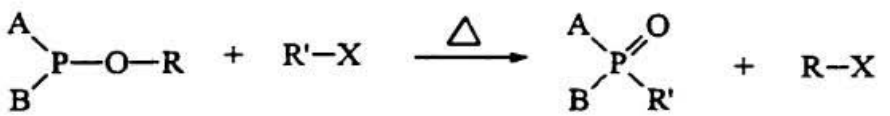

R, A, B = alkyl, aryl, ...
R' = alkyl, acyl, ...
X = Cl, Br, I

Scheme 1-25. Classical Arbuzov reaction

Arbuzov rearrangement, Arbuzov transformation, Michaelis-Arbuzov reaction, or Michaelis-Arbuzov rearrangement, is one of the most versatile methods for the formation of a phosphorus-carbon bond. The reaction, originally discovered by Michaelis and Kaehne in 1898 and explored extensively by Arbuzov[131-134] involves reaction of an ester of trivalent phosphorus with an alkyl halide as shown in Scheme 1-25. It has been widely used for the synthesis of phosphonates, phosphinates and phosphine oxides due to the availability of the required starting materials and the ease with which the reactions can be carried out. In most instances, little more than heating the reagents together in the absence of solvent followed by purification of the product by distillation is required.[135] Since the Arbuzov reaction transforms trivalent phosphorus compounds into potentially P-chiral pentavalent products, the reaction is stereochemically significant.

1.2.2.3.1.1. Mechanism. The widely accepted mechanism involves two steps.[133, 134, 136] In the first step, trivalent phosphorus displaces halide to form a phosphonium adduct / intermediate. Nucleophilic attack of halide on the alkyl group (R) of the phosphonium species results in the formation of the P=O bond (Scheme 1-26). Detailed study of these two steps has suggested that the mechanism for the Arbuzov reaction most commonly involves two sequential S_N2 processes and a quasi-

phosphonium intermediate, although autocatalytic and radical mechanisms have also been found.[133, 134, 136]

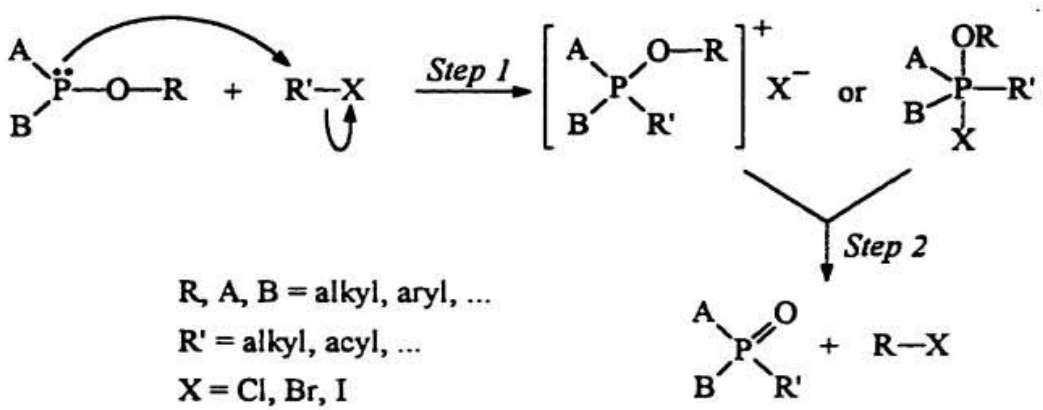

Scheme 1-26. Widely accepted Arbuzov reaction mechanism

From the mechanism shown above, it is clear that the driving force for the reaction is conversion of the >P-O-C linkage into >P(=O)-C which involves a net gain of an estimated 32 - 65 kcal/mol energy.[133] The second step is usually rate-determining.

1.2.2.3.1.2. Stereochemistry at phosphorus. Numerous investigations have been carried out on the stereochemistry of the phosphorus centre in Arbuzov chemistry. Experimental results have demonstrated that the stereochemistry at phosphorus depends on the reaction pathway. If a reaction proceeds through an intermediate phosphorane, the configuration at phosphorus will be lost due to rapid Berry

pseudorotation as outlined in Scheme 1-27. If reaction takes place through a quasi-

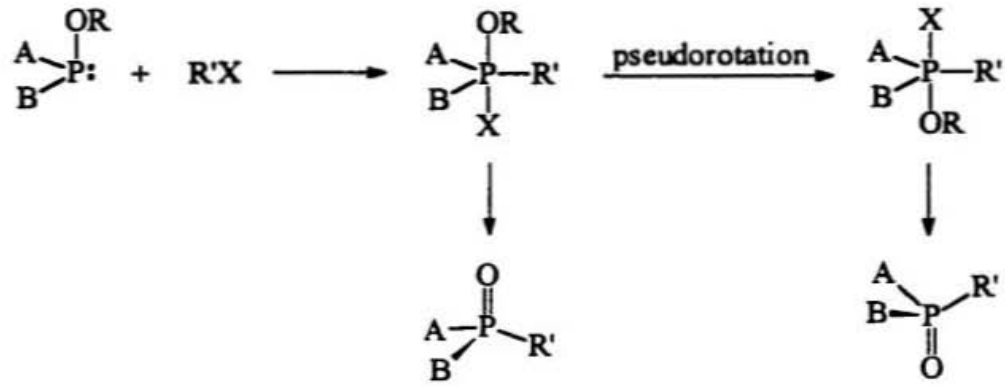

Scheme 1-27. Loss of configuration at P via rapid Berry pseudorotation

phosphonium intermediate, the configuration at phosphorus will be retained. Since the quasi-phosphonium is the dominant intermediate in most Arbuzov reactions, retention of configuration at a phosphorus centre can be anticipated[137] (Scheme 1-28).

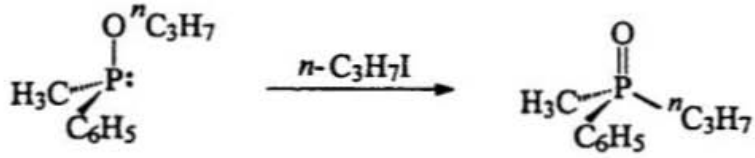

Scheme 1-28. Retention of chirality at P with Arbuzov reaction

1.2.2.3.1.3. Scope and limitations. As shown in Scheme 1-25, two reactants and five variables, *i.e.*, A, B, R, R', X are involved in Arbuzov reactions, hence the reaction provides a versatile synthetic method for the formation of P-C bonds.

(1). Phosphorus reagent ((A)(B)P-OR). Considerable structural variation of the phosphorus reagent is possible. The substituents A and B are commonly primary alkoxy, secondary alkoxy, aryloxy, alkyl, dialkylamino, halogen, or aryl groups and may be identical or different. Since the first step of the reaction involves S_N2 attack of the lone pair of electrons of phosphorus on the alkyl group in alkyl halide, it is evident that the reaction will be accelerated if A and B are electron-releasing groups and slowed if A and B are electron-withdrawing groups. The reactivity increases in the order A, B = halogen < aryloxy < alkoxy < aryl < alkyl < dialkylamino. For alkyl groups, the order of the reactivity of R is Me > Et > Pr. Although triaryl phosphites isomerize on heating with alcohols at higher temperature, they do not undergo the Arbuzov rearrangement.

(2). Alkyl halides (R'X). Except for those which contain potentially interfering groups (such as carbonyl or nitro, these groups may cause side reactions), any halide capable of undergoing S_N2 reactions may be used in the Arbuzov reaction. Primary alkyl halides are most common although other halides[133, 138] are possible. The usual reactivity sequence of organic halides is: acyl > primary alkyl > secondary alkyl >> tertiary alkyl and iodide > bromide > chloride.[139] The secondary and tertiary alkyl halides either fail to react or may give olefins by elimination. Aryl halides, tertiary

alkyl halides, vinyl halides and fluorides do not undergo the Arbuzov reaction under normal reaction conditions.[131]

The Perkow reaction competes when saturated α-chloro/bromo ketones and aldehydes react with trialkyl phosphites (Scheme 1-29). In these cases, Perkow products (P-O

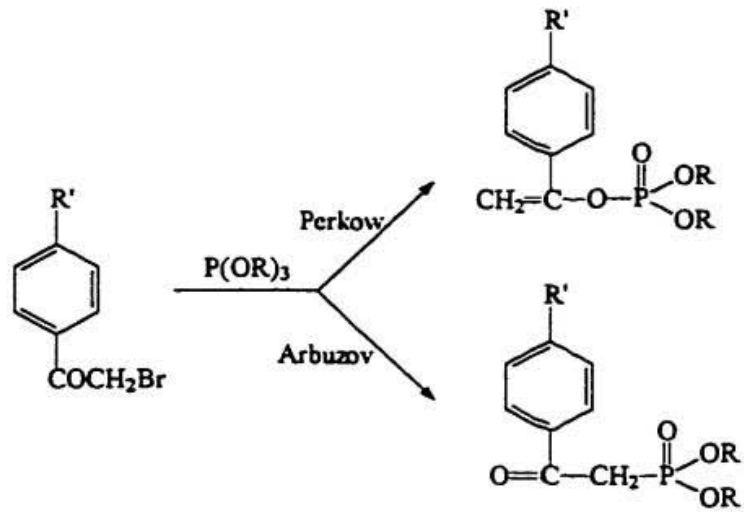

Scheme 1-29. Arbuzov reaction *vs* Perkow reaction

bond formation) are the main products while Arbuzov products (P-C bond formation) are minor products. The Perkow / Arbuzov product ratio decreases in the order R'=MeO, Me, H, F, Cl, Br, NO_2.[140] However, α-iodo ketones give normal Arbuzov product as the main product.[141] These observations were explained by the decreased electronegativity of iodine which exerts a smaller polarization effect on the carbonyl group and leads to greater reactivity in simple displacements (S_N2).

1.2.2.3.1.4. Synthetic applications. Applications of the Arbuzov reaction in organic synthesis are numerous. Scheme 1-30 shows applications for syntheses of phosphonates, phosphinates, novel phosphine oxides and unusual halides.[142]

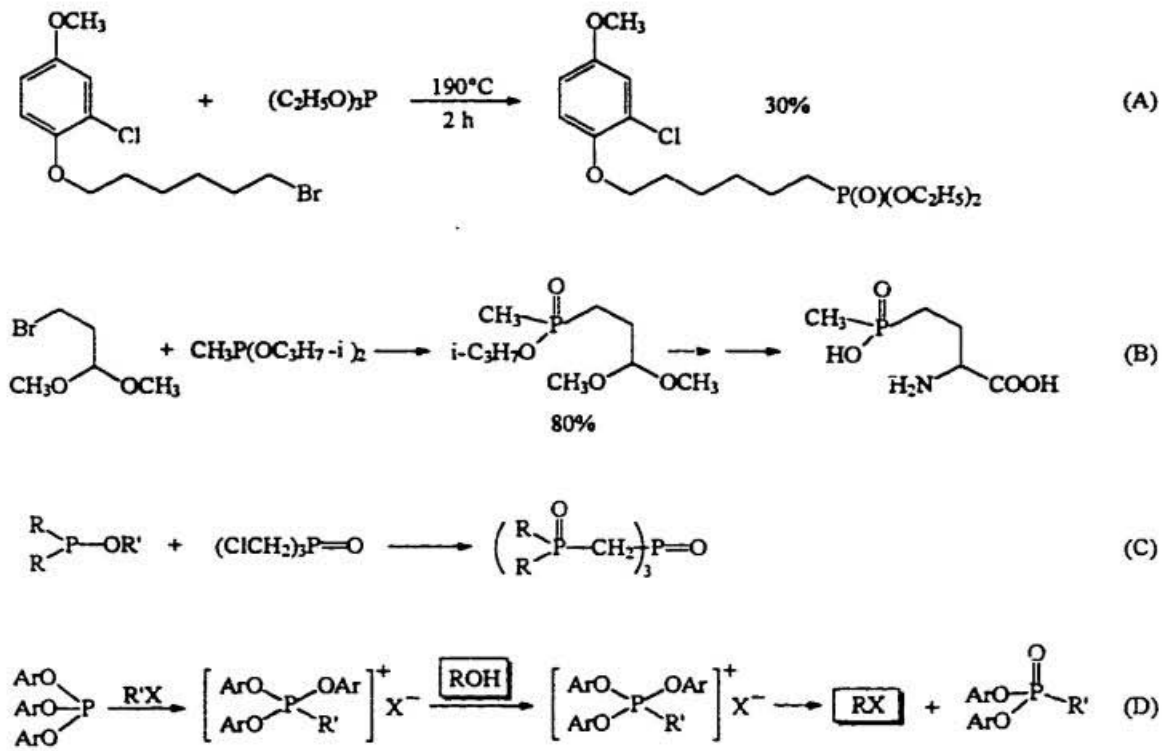

Scheme 1-30. Synthetic applications of traditional Arbuzov reactions

1.2.2.3.2. TMM Arbuzov reaction. When a transition metal halide ($L_n[M]X$) is used instead of ordinary halide in the traditional Arbuzov reaction (cf. Scheme 1-25), the reaction is referred to as a transition metal mediated Arbuzov reaction. The reaction,

R, A, B = alkyl, aryl, ...; X = Cl, Br, I, ...; [M] = transition metal; L = ligand

Scheme 1-31. Transition metal mediated Arbuzov reaction

as shown in Scheme 1-31, can be used to generate metallophosphonates (A, B = OR) / phosphinates(A = R, B = OR) / phosphine oxides (A, B = R). Most transition metal mediated Arubzov reactions studied to date involve a phosphite or phosphonite.[98, 138, 143-179] Comparison of transition metal mediated and traditional Arbuzov reactions shows some similarities and distinctions. The major distinction is that transition metal mediated Arbuzov reactions usually take place at room temperature or with gentle heating unlike traditional Arbuzov reactions which normally require prolonged heating. Double,[161, 164, 169, 180] triple[169] and quadruple[169] Arbuzov reactions have been achieved. The reaction has been used to prepare a synthetically useful, Cp-like, tripod Kläui ligand (Scheme 1-32).[154, 181-207]

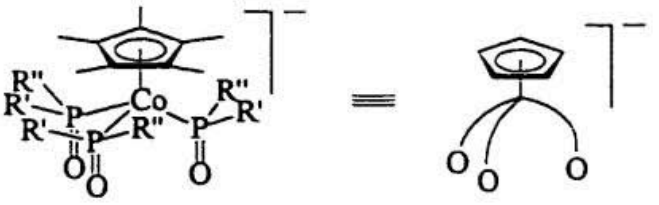

Scheme 1-32. Cp-like, tripod Kläui ligand

Like the classical Arbuzov reaction, the transition metal mediated Arbuzov reaction

usually proceeds through an ionic mechanism,[138] although radical[138, 208-211] and autocatalytic[138] mechanisms are possible. The ionic mechanism, as demonstrated in Scheme 1-33, almost always requires a coordinated phosphite in a cationic metal complex and availability of a nucleophile. Both the intermediate $\{CpCo(dppe)[P(OMe)_3]\}^{2+}$ and the final product $\{CpCo(dppe)[P(O)(OMe)_2]\}^{+}$ have been characterized by X-ray crystallography.[168]

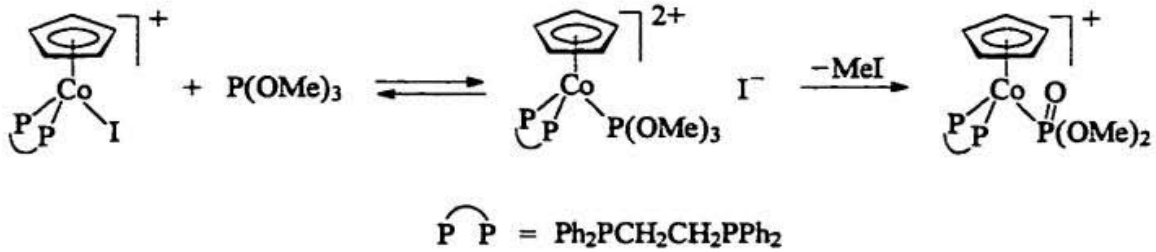

Scheme 1-33. Ionic mechanism for a TMM Arbuzov reaction[168]

Due to the mediation of a transition metal, transition metal Arbuzov reactions are much more versatile[138] than the classical case with respect to both chemistry and stereochemistry since the transition metal, through complexation, regulates reactions that occur in the coordination sphere.[37, 40, 41, 43] On the other hand, Arbuzov reactions involving a transition metal complex are less predictable, taking place not at all in some cases and occurring in seconds in other cases at room temperature.[138] For instance, CpFe(dppe)I, isoelectronic with $[CpCo(dppe)I]^{+}$, does not react with

$P(OMe)_3$ in refluxing CH_2Cl_2 after 3 hours whereas $[CpCo(dppe)I]^+$ reacts smoothly at room temperature.[167] This is probably due to a smaller residual positive charge (δ^+) on the carbon of the methyl group of coordinated $P(OMe)_3$ as a consequence of a relatively lower formal oxidation state on Fe. Therefore the rate-determining step, nucleophilic attack of I^- on the methyl group of the coordinated $P(OMe)_3$ does not take place or requires more forcing conditions.[212]

1.2.2.3.3. Synthesis of P-chiral materials via TMM Arbuzov reaction. Like the classical Arbuzov reaction, a new stereogenic centre will be formed during the formation of metallophosphonates / phosphinates / phosphine oxides (Scheme 1-31) in transition metal mediated (TMM) Arbuzov reactions which incorporate a prochiral phosphite, phosphonite or phosphinite, respectively. If a chiral metal auxiliary [M*] is used, some chiral induction from M*→P* could be expected. Due to the regulation of metal, more stereocontrol in transition metal mediated Arbuzov reactions is anticipated by modifying steric and electronic factors via changes in the supporting ligands L around a transition metal and the central metal M. In other words, a transition metal mediated Arbuzov reaction provides a route for diastereoselective synthesis of metallophosphonates, phosphinates or phosphine oxides via metal to phosphorus chiral induction. In this regard some P-chiral materials have been

diastereoselectively synthesized by employing an Arbuzov reaction of an asymmetric pseudooctahedral, piano-stool cobalt complex with a prochiral phosphonite.[98, 171-175] An example is given in Scheme 1-34.[172] However, attempts to react resolved P-chiral

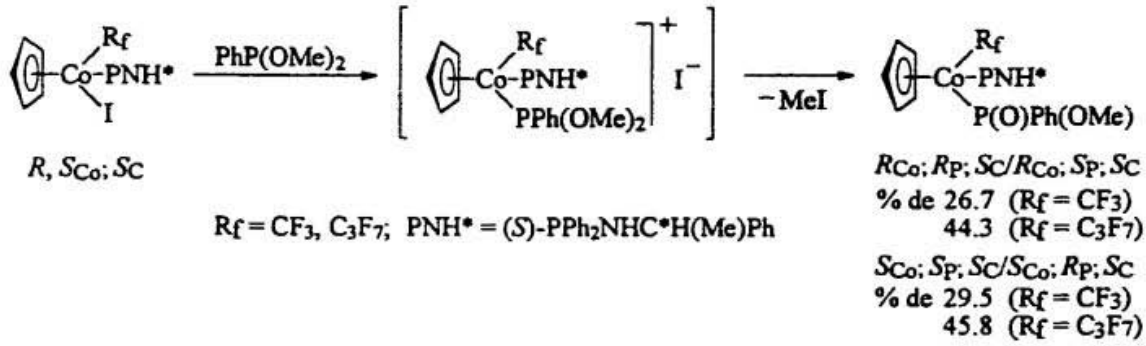

Scheme 1-34. Diastereoselective synthesis of P-chiral stereoisomers[172]

stereoisomers with common nucleophilic reagents such as Me^-, Et^-, MeO^- and Cl^- under various conditions were unsuccessful (Scheme 1-35). The negative results

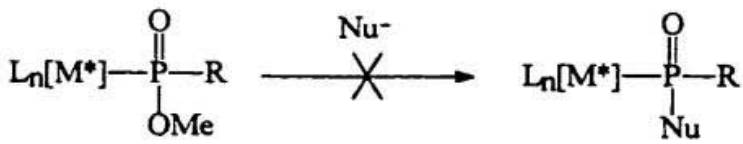

$L_n[M^*]$ = CpCo*(X)(PNH), X = I, CF_3, C_3F_7

PNH = (*S*)-(-)-$PPh_2NHC^*H(Me)Ph$

R = Ph, OMe

Nu^- = Me^-, Et^-, MeO^-

Scheme 1-35. Attempted substitution at P*

suggested that the inorganometallic phosphinate / phosphonate phosphorus (Scheme 1-35) is inert to nucleophilic substitution.

At this point the lack of nucleophilic reactivity at coordinated phosphorus compared to analogous free organophosphorus compounds is not well understood. One possible avenue toward phosphorus activation follows work done by Nakazawa.[213] Treatment of the amidophosphonate complex $CpFe(CO)_2[(Et_2NP(O)(OMe)]$ with two equivalents of boron trichloride followed by reaction with nucleophiles such as NaOMe, MeMgI and Et_2NH afforded the corresponding substituted products $CpFe(CO)_2[(Et_2NP(O)(Nu)]$ ($Nu^-/HNu = OMe^-$, Me and $HNEt_2$) via a intermediate $CpFe(CO)_2[(Et_2NP(O)(Cl)\cdot BCl_3]$. Although the phosphorus atom is chiral the stereochemistry at phosphorus was not investigated. Comparison of Nakazawa's starting complex with the model complexes of Scheme 1-35 suggests that the diethylamido group may activate phosphorus for substitution. To pursue this idea, a series of resolved, M- and P-chiral diethylamidophosphonate Co(III) complexes, which may show some chemical activity on the chiral P centre, was prepared. Examination of their absolute stereochemistry will be reported in Chapter 2.

Previous studies[98, 172] on the synthesis of chiral metallophosphinate

L_n[M*][PhP(O)(OMe)] employed a chiral aminophosphine resolving agent PNH* [(*S*)-PPh_2NHC*H(Me)Ph]. However, after resolution, the chiral moiety (*S*)-NHC*H(Me)Ph in the resolving handle was not removed. Chapter 3 describes a simple regiospecific method to cleave the chiral moiety (*S*)-NHC*H(Me)Ph in the resolving handle with gaseous HCl via P-N bond cleavage. In Chapter 3, ^{1}H NMR evidence for P-C bond cleavage resulting side products (R,S_{Co};S_C)-CpCoI(PNH*)[P(O)$(OMe)_2$] in the reaction of CpCoI_2(PNH*) with *t*-BuP$(OMe)_2$ will also be presented.

With regard to preparation of diastereoselective P-chiral isomers via Co*→P induction employing the TMM Arbuzov reaction, all previous studies[98, 170-179, 214, 215] used a late transition metal. The relatively large size and low ionization potentials of early transition metals combined with the possibility of high valence states containing few or no d electrons suggest substantial differences in chemical properties between the "early" and "late" organometallic complexes.[216, 217] Taken together with the fact that the previously examined cobalt systems showed limited reactivity regarding nucleophilic substitution at phosphorus, an attempt was made to study early transition metals and determine their effect on the chiral induction from metal to phosphorus in TMM Arbuzov reactions. A model early transition metal complex (η^5-

cyclopentadienyl)(η^5-pentamethylcyclopentadienyl) pentafluorophenyl chloro titanium CpCp*TiCl(C_6F_5) was chosen for this study. Synthesis, characterization and chemical properties, especially with respect to Arbuzov reaction of this new chiral-at-metal complex, will be discussed in Chapter 4.

Recently, internal fluorocarbon coordination M···F-C has been found to be a good mode of stabilizing hydrocarbyl group 4 metallocene cations, Cp_2MR^+, which are the reactive catalytic synthons in the homogeneous metallocene Ziegler catalysts.[218] During characterization of the new complex CpCp*TiCl(C_6F_5) (Chapter 4) it was found that the barrier to C_6F_5 rotation around the Ti-C_{ipso} bond is rather high (frozen even at 140°C) based on a variable temperature ^{19}F NMR study. In order to gain some insight into the origin of the rotation barrier around the Ti-aryl bond, and particularly the possibility of coordination from *ortho*-fluorine to metal titanium centre, *e.g.*, Ti···F-C, further isostructural titanocene derivatives with general formula (C_5H_5)(C_5R_5)TiX(Ar) (R = Me, X = Cl, *o*-FC_6H_4; R = H, X = Cl, Ar = C_6F_5, *o*-FC_6H_4, R = H, X = R = C_6F_5, *o*-FC_6H_4) were synthesized and investigated in Chapter 5 via variable temperature NMR, MMX and EHMO calculations as well as single crystal X-ray analysis.

Chapter 2

Synthesis, Structure and Conformational Analysis of Novel Co- and P-Chiral Amidophosphonate Co(III) Complexes

2.1. Introduction

One of most important reactions of organophosphorus compounds is nucleophilic substitution at P, which has been used for stereoselective synthesis of P-chiral materials.[34] An example[219] is presented in Scheme 2-1. Reaction of the phosphinates

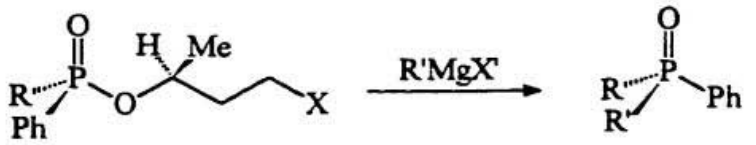

RX	R'X'	yield %	% ee	config. of prod.
MeI	$PhCH_2Cl$	32.7	77	*R*
$PhCH_2Cl$	MeI	10.3	94	*S*
EtI	MeI	56.6	100	*S*
n-PrBr	MeI	65.7	100	*S*
MeI	*n*-PrBr	22.3	76	*R*

Scheme 2-1. Nucleophilic substitution of organophosphinates

with excess of Grignard reagent afforded the corresponding phosphine oxides with inversion of configuration and high optical purity (76-100%) in yields of 10-57%.

However, inorganometallic[220] phosphinates ($L_n[M^*]$-P(O)(R)(OR)) and phosphonates ($L_n[M^*]$-P(O)$(OR)_2$) do not react with common nucleophilic reagents such as Me^-, Et^-, MeO^- and Cl^- (Scheme 1-35). It was concluded that, unlike organophosphorus analogs, the inorganometallic phosphinate / phosphonate phosphorus in the model complexes (Scheme 1-35) are surprisingly inert with respect to nucleophilic substitution. A clear understanding of the apparent lack of substitution chemistry at phosphorus for these complexes has not yet emerged. The reaction[221] of $CpFe(PMe_3)_2(P(O)(OMe)_2)$ with $C_4H_8N^-$ to give $CpFe(PMe)_2(P(O)(OMe)(NC_4H_8)$ under forcing conditions appears to be the only report of a nucleophilic displacement at an inorganometallic phosphonate.

The question to be asked is "can the model complex be modified to activate the phosphorus and develop the substitution chemistry on phosphorus?" One possible avenue toward phosphorus activation follows work reported by Nakazawa[213] (Scheme

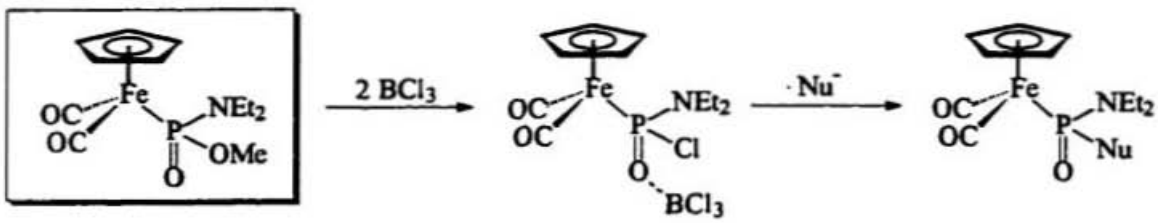

Nu^- / NuH = Me^-, Et^- / Et_2NH

Scheme 2-2. Successful nucleophilic displacement at P of metallophosphonate

2-2). Nakazawa activated the amidophosphonate complex by treatment with two equivalents of boron trichloride and obtained the corresponding chloro substituted complex which was then treated with several nucleophiles including NaOMe, MeMgI and Et_2NH. Although the phosphorus is chiral, no stereochemical information was investigated. Comparison of Nakazawa's starting complex with the model complexes of this study suggests that the diethylamido group may activate phosphorus. To pursue this idea, a series of resolved M- and P-chiral diethylamido phosphonate Co(III) complexes, which may show some chemical activity on the chiral P centre, were prepared, and their absolute stereochemistry examined.

2.2. Results and discussion

2.2.1. Reaction of 1a with $Et_2NP(OMe)_2$. Treatment of a deep purple solution of the three-legged piano stool complex **1a** (Scheme 2-3) with one equivalent of dimethyl diethylamidophosphite in benzene at ambient temperature gave a deep green reaction

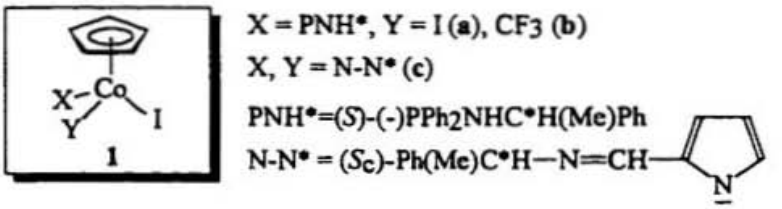

Scheme 2-3. Numbering scheme

mixture from which several products were isolated (Scheme 2-4). Preparative thick-layer radial chromatography separated starting material and six products which were identified, in order of decreasing TLC R_f values, as two of the four possible amidophosphonate diastereomers **3a-1** and **3a-2** (major products), two of the previously reported dimethyl phosphonates **4a-1** and **4a-2**[98] (minor products), and the remaining two amidophosphonate diastereomers **3a-3** and **3a-4** (minor products).

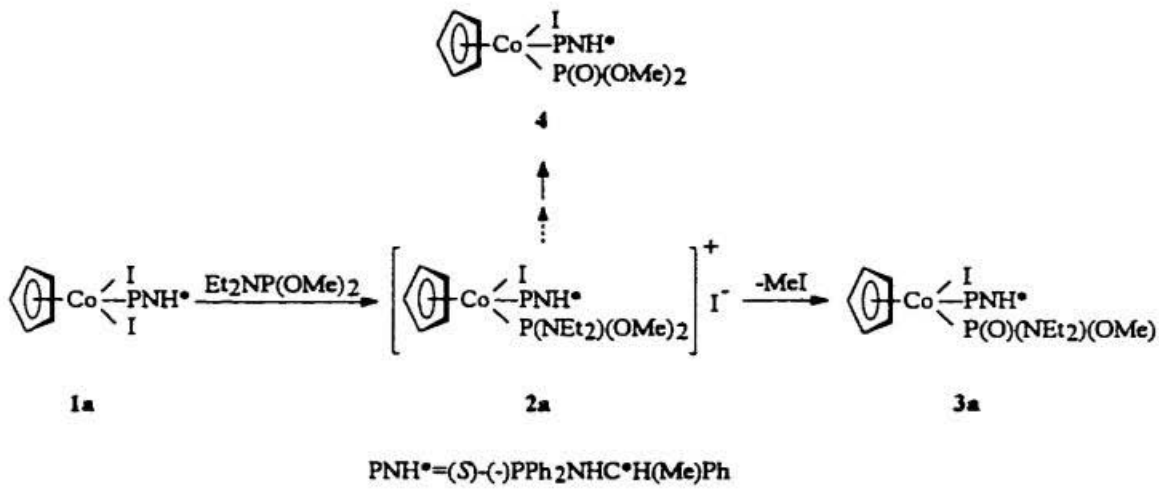

Scheme 2-4. Reaction of 1a with $Et_2NP(OMe)_2$

2.2.1.1. Characterization of the amidophosphonates 3a and phosphonates 4a. Complexes **3a -1, -2, -3 and -4** were characterized by elemental analysis, IR, ^1H, ^{13}C and ^{31}P NMR (Tables 2-1, 2-2 and 2-3). Complex **3a-2** was also characterized by an

X-ray crystallographic study. Infrared spectra showed strong $\nu_{P=O}$, δ_{P-OC}, and δ_{PO-C} modes in the ranges 1130-1132, 1020-1022, and 697-701 cm^{-1}, respectively, for all amidophosphonate complexes. The decreased phosphoryl stretching frequency compared to the related dialkyl phosphonate[151, 153] and alkylarylphosphinate complexes[151] can be attributed to a secondary bonding interaction at the basic phosphoryl oxygen. A broadened ν_{NH} compared to the starting material **1a** supports an intramolecular NH···O=P hydrogen bond which was confirmed in the solid state from crystallographic data of **3a-2**. All diastereomers displayed distinct ^{1}H, ^{13}C and ^{31}P NMR chemical shifts (Tables 2-2 and 2-3) consistent with their formulation as diastereomeric amidophosphonato complexes. All diastereomers except **3a-1** showed a doublet for the C**Me* and a multiplet for the C**H* of aminophosphine ligand[92] (Table 2-2). Consistent with the presence of a strong, intramolecular N−H···P=O hydrogen bond, the chemical shifts of the N-H proton of **3a** are relatively concentration independent and strongly deshielded (Table 2-2) compared to that of **1a**.[222] Intramolecular hydrogen bonding in **3a-2** was also confirmed from crystallographic data.

The presence of chiral Co, P, and C atoms results in diastereotopic PPh_2 and P−N(CH_2CH_3)$_2$ groups, which are reflected in the NMR spectra of the complexes **3a**.

Table 2-1. Physical and IR data

compd	color	mp(°C)	$[\alpha]_{436}$[a]	abs. config.	%de	ν_{P-O}, δ_{P-OC}, δ_{PO-C} (cm^{-1})
3a-1	dark green	125.2-125.8	-2.4×10^3	$S_{Co}R_PS_C$[b]	88[d]	1130, 1022, 697
3a-2	dark green	159.5-160.0	$+2.1 \times 10^3$	$R_{Co}S_PS_C$[c]		1132, 1020, 701
3a-3	green	128.4-130.1	$+1.1 \times 10^3$	$S_{Co}S_PS_C$[b]	88[e]	1131, 1021, 699
3a-4	green	155.7-158.2	-7.6×10^2	$R_{Co}R_PS_C$[b]		1132, 1020, 700
3b-2	yellow	199.3-200.4	$+1.9 \times 10^3$	$S_{Co}S_PS_C$[f]		1136, 1057, 705

[a]Unit is deg dL g^{-1} dm^{-1}; [b]determined from chiroptical data; [c]determined by X-ray crystallography study. [d]$S_{Co}R_PS_C/S_{Co}S_PS_C$. [e]$R_{Co}S_PS_C/R_{Co}R_PS_C$. [f]determined empirically.

Table 2-2. ^{1}H, ^{31}P and ^{19}F NMR data[a]

cpd	Ph	δ(NH)[b]	δ(Cp)	δ(OMe)	δ(N*CH₂*Me)	δ(C*H)[c]	δ(C*Me)	δ(NCH₂*Me*)	$^{31}P/^{19}F$
3a-1	7.93(m), 7.67(m), 7.42(m) 7.27(m), 6.92(m), 6.82(m)	6.65 (dd, 6.6, 6.0)	4.83 (s)	3.44 (d, 11.2)	3.39(m) 3.26(m)	3.65 (m)	1.32 (dd, 6.75,1.1)[d]	1.25 (t, 7.1)	89.86 (d,121.9) 81.93 (d, 121.9)
3a-2	7.92(m), 7.45(m), 7.23(m) 7.15(m), 7.01(m), 6.97(m)	6.37 (dd, 10.6, 7.5)	4.83 (s)	3.51 (d, 11.2)	3.40(m) 3.27(m)	3.89 (m)	1.26 (d, 7.1)	1.22 (t, 6.2)	87.19 (d, 122.1) 77.96 (d, 122.1)
3a-3	7.96(m), 7.84(m), 7.48(m) 7.26---6.9(m)	4.97 (dd, 15.5, 9.5)	4.84 (s)	3.41 (d, 11.3)	3.54(m) 3.42(m)	3.93 (m)	1.15 (d, 6.7)	1.22 (t, 7.0)	83.00 (d, 125.8) 71.44 (d, 125.8)
3a-4	8.20(m), 7.69(m), 7.52(m) 7.14(m), 7.07(m)	4.87[e]	4.86 (s)	3.51 (d, 11.2)	3.59(m) 3.43(m)	4.22 (m)	1.07 (d, 6.7)	1.25 (t, 7.0)	82.09 (d, 117.6) 72.02 (d, 117.6)
3b-1	[7.80(m), 7.57(m), 7.21(m) 7.00(m), 6.97(m), 6.88(m)][f]	6.40 (pt, 9.6)[g]	4.85 (s)	3.54 (d, 11.5)	3.23(m) 3.15(m)	3.83 (m)	1.33 (d, 6.6)	1.17[f] (t, 6.6)	94.17 (d, 128.9) 82.04 (d, 104.5) ^{19}F: 7.12(s)

Table 2-2. ^{1}H, ^{31}P and ^{19}F NMR data[a] *(cont'd)*

cpd	Ph	δ(NH)[b]	δ(Cp)	δ(OMe)	δ(N*CH*$_2$Me)	δ(C*H)[c]	δ(C*Me)	δ(NCH$_2$*Me*)	$^{31}P/^{19}F$
3b-2	7.99(m), 7.55(m), 7.30(m), 7.22-7.06(m)	6.42 (pt, 9.5)[g]	4.86 (s)	3.58 (d, 11.5)	3.30(m) 3.13(m	3.83 (m)	0.96 (d, 6.7)	1.19 (t, 7.1)	93.16 (d, 105.9) 81.55 (d, 108.3) ^{19}F: 7.09 (s)
4b-1	[7.95-7.79(m),7.51-7.43(m) 7.37 (m), 7.30 (m), 6.99(m)][h]	6.14(dd, 13.9, 9.6)[f]	4.89 (s)	3.90 (d, 9.9) 3.66 (d, 11.1)		4.39 (m)	1.58 (d, 6.7)		nm[i]
4b-2	[7.95-7.79(m),7.51-7.43(m) 7.37 (m), 7.30 (m), 6.99(m)][h]	5.90(dd, 15.5, 7.9)[f]	4.91 (s)	3.89 (d, 10.2) 3.67 (d, 11.1)		4.39 (m)	1.58 (d, 6.7)		nm[i]
5b			5.18 (s)	3.73 (d, 10.7) 3.57 (d, 10.7)	3.52(m)			1.20 (t, 7.0)	
3c-1	7.37(m), 7.36(m), 7.32(m) [H(1), 7.67 (d, 4.5) H(2), 6.23 (dd, 2.9, 1.8) H(3), 6.84 (d, 3.6) H(4), 7.10(s)][k]		4.74 (s)	3.27 (d, 11.3)	2.33(m) 2.13(m)	5.41[h] (m)	1.67 (d, 6.9)	0.86 (t, 7.1)	79.13 (s)

Table 2-2. ^{1}H, ^{31}P and ^{19}F NMR Data[a] *(cont'd)*

cpd	Ph	δ(NH)[b]	δ(Cp)	δ(OMe)	δ(N*CH*$_2$Me)	δ(C*H)[c]	δ(C*Me)	δ(NCH$_2$*Me*)	$^{31}P/^{19}F$
3c-2	7.37(m), 7.36(m), 7.32 (m) [H(1), 7.70 (d, 4.5) H(2), 6.29 (dd, 2.9, 1.8) H(3), 6.88 (d, 3.6) H(4), 7.15(s)][k]		4.75 (s)	3.74 (d, 11.3)	3.04(m)	5.39[h] (m)	1.66 (d, 7.0)	1.11 (t, 7.1)	73.12 (s)

[a] ^{1}H (300.1 MHz) NMR chemical shifts in ppm relative to internal TMS; ^{31}P (121.5 MHz) NMR chemical shifts in ppm relative to external 85% H_3PO_4; ^{19}F (282.4 MHz) NMR chemical shifts in ppm relative to external $CFCl_3$; *J* values in Hz given in parentheses; solvent=$CDCl_3$. Abbreviations: ; m, multiplet; s, singlet; d, doublet. [b]Doublet of doublets ($^{2}J_{PH}$, $^{3}J_{C*HH}$). [c]Multiplet($^{3}J_{PH}$, $^{3}J_{NHH}$, $^{3}J_{HH}$). [d]Doublet of doublets ($^{3}J_{C*HH}$, $^{4}J_{PH}$). [e] Overlapping with Cp. [f]Assignments ambiguous. [g]Pseudo-triplet. [h]Overlapped. [i]nm = not measured. [k]cf. Scheme 2-9.

Table 2-3. ^{13}C NMR data[a]

cpd	P-*Ph* *ipso* *ortho* *meta* *para*	C*-*Ph* *ipso* *ortho* *meta* *para*	δ(Cp)	δ(OMe)	δ(N*CH*$_2$Me)	δ(C*H)	δ(C*Me)	δ(NCH$_2$*Me*)
	132.70 (d, 55.93), nf[b]	147.51	87.82	54.62	41.70	49.90	26.62	14.57
3a-1	134.98 (d, 9.6), 131.52 (d, 10.0)	128.30	(p,2.5)[c]	(d, 7.9)	(d, 4.8)	(d, 10.7)	(d, 9.9)	(s)
	127.53 (d, 10.0), 127.11 (d, 10.4)	126.04						
	130.93 (d, 2.8), 129.27 (d, 2.7)	125.47						
	137.36 (d, 40.7), 133.62 (d, 61.3)	146.45(d, 3.5)	87.97	53.69	41.71[d]	50.16	27.09	14.41
3a-2	133.81 ((d, 9.4), 132.12 (d, 9.8)	128.31	(p,2.5)[c]	(d, 11.7)	(d, 4.9)	(d, 10.8)	(d, 4.5)	(s)
	127.84 (d, 9.3), 127.50 (d, 10.5)	125.84						
	130.52 (d, 2.7), 129.95 (d, 2.9)	125.51						
	136.17 (d, 53.7), 135.39 (d, 53.6)	145.63(d, 3.7)	89.44	54.04	40.73	49.18	26.40	14.61
3a-3	133.66 (d, 8.9), 133.30 (d, 10.6)	128.04	(p,2.5)[c]	(d, 10.9)	(d, 5.1)	(d, 12.3)	(d, 4.2)	(s)
	127.62 (d, 10.6), 127.45 (d, 11.4)	126.14						
	130.55 (d, 3.1), 130.15 (d, 2.9)	125.77						
	nf[b], nf[b]	nf[b]	89.34	53.68	40.86	49.10	27.18	14.69
3a-4	133.39 (d, 9.5), 133.19 (d, 10.3)	128.79	(p,2.5)[c]	(d, 10.9)	(d, 4.6)	(d, 12.3)	(d, 4.3)	(s)
	128.15 (d, 10.2), 127.10 (d, 9.9)	126.08						
	130.57 (d, 2.5), 130.24 (d, 2.7)	125.59						

Table 2-3. ^{13}C NMR data[a] *(cont'd)*

cpd	P-*Ph* *ipso* *ortho* *meta* *para*	C*-*Ph* *ipso* *ortho* *meta* *para*	δ(Cp)	δ(OMe)	δ(N*CH*$_2$Me)	δ(C*H)	δ(C*Me)	δ(NCH$_2$*Me*)
3b-2	137.83 (d, 39.9), 134.42 (d, 61.8) 132.96 (d, 10.2), 132.52 (d, 10.1) 127.89 (d, 11.1), 127.58 (d, 10.4)[f] nf[b], nf[b]	146.84(d, 4,3) 127.82[f] 125.78 125.58	89.55 (s)	53.62 (d, 12.0)	39.94 (d, 4.2)	49.64 (11.7)	26.39 (d, 3.6)	14.63 (s)

[a] ^{13}C (75.5 MHz) NMR chemical shifts in ppm relative to $CDCl_3$ @ 77.0; d=doublet; J values in Hz. [b]nf = not found. [c]p=pseudotriplet. [d]temperature independent to -90°C. [f]overlapped.

The ^{1}H NMR spectrum of the P–N(CH_2CH_3)$_2$ group in **3a** shows an ABM$_3$X pattern. Pairs of diastereotopic P*Ph*$_2$ *ipso, ortho, meta,* and *para* ^{13}C resonances were observed. However, only one set of CH_2CH_3 ^{1}H signals and one set of CH_2CH_3 ^{13}C signals are observed for the P–N(CH_2CH_3)$_2$ group which implies that the two ethyl groups are either in a plane or that the pyramidal nitrogen in P–N(CH_2CH_3)$_2$ inverts very rapidly at room temperature on the ^{1}H and ^{13}C NMR time scale.

In order to check the possibility of fast nitrogen inversion, variable temperature NMR spectra of both proton and carbon-13 were recorded for diastereomer **3a-2** in deuterated methylene chloride. However, even at -90°C no further splitting was observed. Taken together with the X-ray data for **3a-2**, which showed that the amidophosphonate nitrogen is non-planar, this observation suggests that either the low temperature limit for nitrogen inversion was not reached or that the two ethyl groups are accidentally isochronous. All phosphonate complexes **3a** showed well resolved ^{31}P AB or AX patterns with characteristic[138] chemical shifts for the phosphoryl (82–90 ppm) and phosphine (71-81 ppm) P-atoms.

^{1}H NMR analysis established that the low-yield products **4a-1** and **4a-2** were identical with authentic samples of the dimethyl phosphonate complexes $S_{C_\alpha}S_C$- and $R_{C_\alpha}S_C$-

$CpCoI(PPh_2NHC^*H(Me)Ph)(P(O)(OMe)_2)$ reported previously from the reaction of **1a** with trimethyl phosphite.[98] The possibility that **4a-1** and **4a-2** result from direct reaction with $P(OMe)_3$ present as an impurity in the $Et_2NP(OMe)_2$ sample, was discounted since a maximum yield of 2.8%, was calculated on the basis of ^1H NMR integration of the small δ 3.49 ppm doublet corresponding to $P(OMe)_3$ impurity in a fresh sample of $Et_2NP(OMe)_2$. Therefore, simple Arbuzov reaction of free $P(OMe)_3$ present as impurity cannot account for the total formation of **4a-1** and **4a-2** that were consistently isolated in "small" but reproducible total yields of *ca.* 8.6% (based on $Et_2NP(OMe)_2$). Consideration of the deamination mechanism proposed by Nakazawa for related Fe(II) amidophosphonates[221] and increased formal charge of Co(III) vs. Fe(II) suggests that the phosphonate products **4a-1** and **4a-2** originate from a cationic amidophosphite intermediate **2a** via direct attack of a trace amount of water, present in the reaction mixture, on the phosphoryl atom of the amido-substituted phosphite

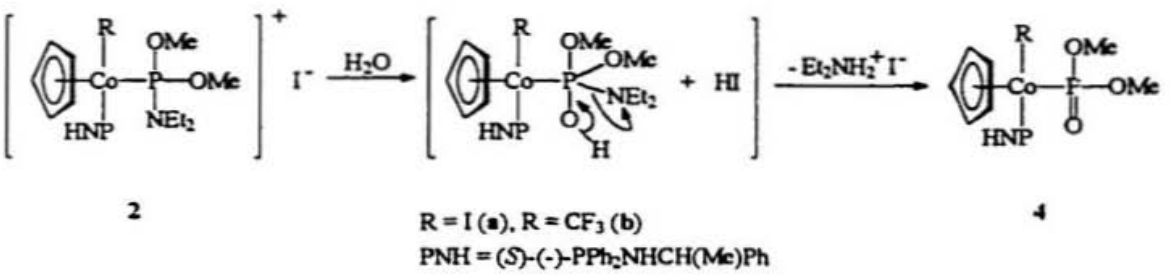

Scheme 2-5. Proposed mechanism for the formation of 4

in **2a**. The resulting metallophosphorane intermediate subsequently decomposes to afford **4a-1** and **4a-2** (Scheme 2-5). Although the phosphorus-nitrogen bond has π bond character[223] and most reactions leave the P-N bond intact, the P-N bond might be appreciably weakened by strong HO:→P π donation[221] (Scheme 2-5). The formation of a very stable phosphoryl group may be the driving force and the main reason for the observed selective deamination.[221]

In order to confirm the proposed hydrolysis mechanism for the formation of **4a**, the reaction of **1a** with $Et_2NP(OMe)_2$ was followed by ^1H NMR for samples dried with activated 4 Å molecular sieves and samples doped with deionized water. In both cases, an instantaneous color change from purple to brown was observed on the addition of the amidophosphite. Time dependent spectra (^1H NMR) for the reaction in the dry condition are depicted in Figure 2-1. The initial ^1H NMR spectrum showed that the Cp signal of iodide **1a** was replaced by a broad resonance at 5.03 ppm and two broad resonances at 5.41 and 5.34 ppm. The former was assigned to a fast equilibrium **1a** + $Et_2NP(OMe)_2$ ⇌ **2a** (Figure 2-1a and Scheme 2-4). The latter was assigned to Cp of diastereomeric cationic intermediate **2a**. Subsequent deamination and dealkylation reactions of **2a** resulted in the appearance of methyl iodide and Cp resonances corresponding to **4a-1** (δ = 4.90 ppm), **4a-2** (δ = 4.89 ppm), **3a-1** (δ =

4.83 ppm), **3a-2** (δ = 4.83 ppm), **3a-3** (δ = 4.84 ppm) and **3a-4** (δ = 4.86 ppm). A further Cp resonance at 5.23 ppm was assigned to an additional side product. For runs with less than one equivalent of dimethyl diethylamidophosphite, on complete reaction of $Et_2NP(OMe)_2$ the above equilibrium cannot be maintained and thus the Cp resonance (δ = 5.00 ppm) of the corresponding iodide **1a** gradually sharpened (Figure 2-1 c-f). Careful line fits of the time dependent spectra showed that the ratio of **1a**/(**3a**+**4a**) decreased toward a limiting value (1.45 for the data of Figure 2-1). Addition of a second aliquot of $Et_2NP(OMe)_2$ re-established the equilibrium as indicated by reappearance of characteristic broadened Cp signals observed on initial addition of amidophosphite. The product ratio of **3a**:**4a** after 12 hours reaction at 25°C, determined by line fit of the 300 MHz NMR Cp region, was 9.2:100 for "dry" vs. 120:100 for "wet" reactions. This product distribution showed the relative yield of side products dimethyl phosphonate **4a-1** and **4a-2** decreased on drying as required for the hydrolysis mechanism.

2.2.1.2. Solid-state structure, chiroptical properties, and absolute configuration. The solid-state structure of diastereomer **3a-2** was determined by single crystal X-ray diffraction in order to confirm the structure and to establish the absolute configuration. Crystallographic data are listed in Table 2-4. Atomic coordinates for

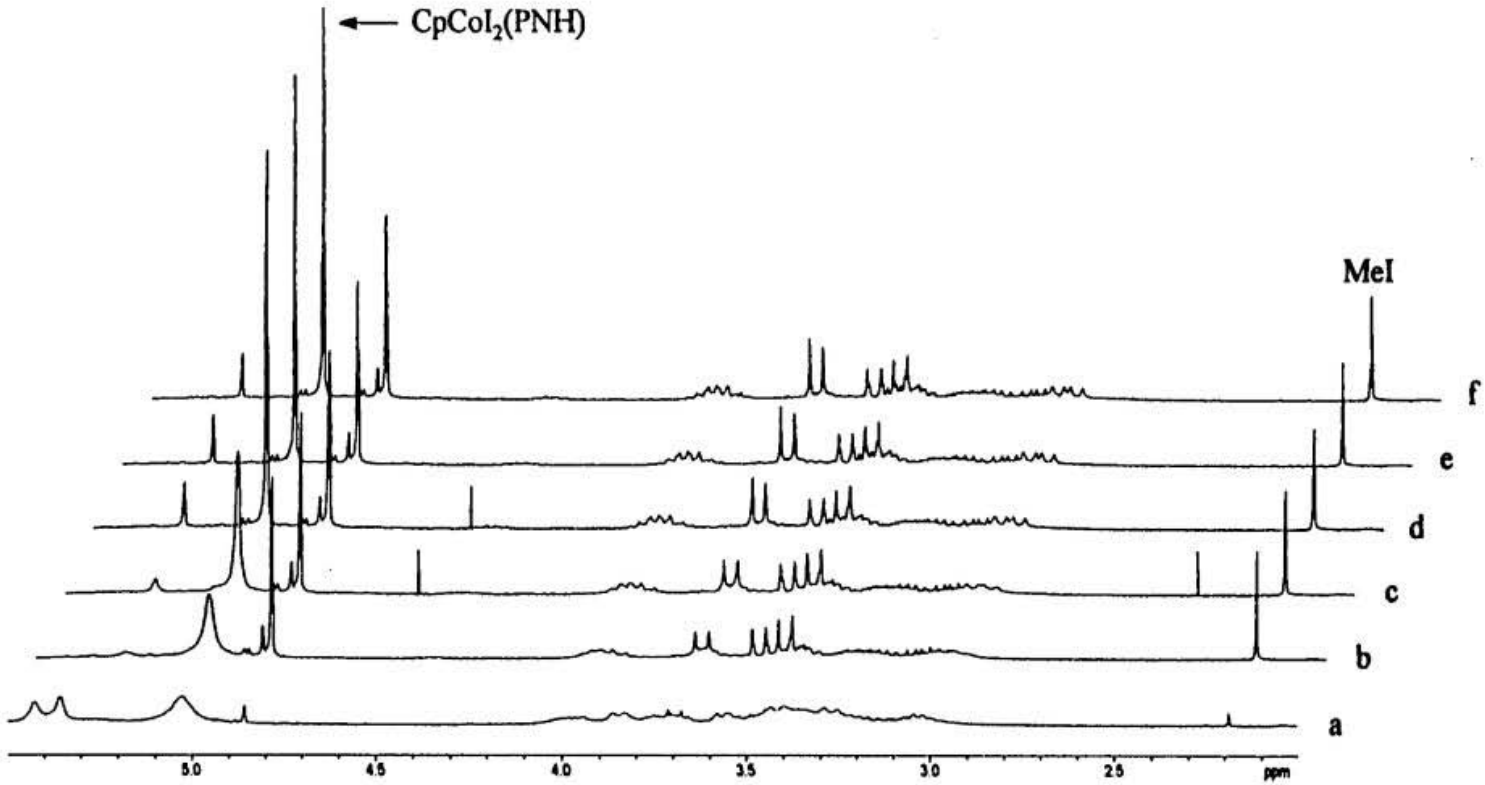

Figure 2-1. Time dependence for reaction of $CpCoI_2(PNH)$ (1a) with $Et_2NP(OMe)_2$ in $CDCl_3$ in dry condition at 25°C; a (2.5min), b (2h 35min), c (3h 26min), d (4h 17min), e (5h 08min), f (5h 59min)

non-hydrogen atoms, the N-H, selected bond distances and bond angles are presented in Tables 2-5 and 2-6. An ORTEP drawing of the molecular structure of **3a-2** is given in Figure 2-2. The coordination geometry is that of a pseudooctahedral, three-legged piano-stool. The η^5-Cp moiety occupies three facial coordination sites with iodide, aminophosphine, and monodentate, distorted pyramidal, P-bonded amido-phosphonate ligands completing the coordination sphere. Monodentate interligand bond angles (P(2)-Co-P(1)=92.33(7)°, P(2)-Co-I=89.84(5)°) approximate 90°. The phosphinato P atom shows a distorted tetrahedral geometry with an opened Co-P=O bond angle 116.2(2)° and a concomitant adjustment of the Co-P-OMe angle to 102.4(2)°. The phosphoryl bond is considered to have a bond order of two as with other related phosphonate and phosphinate complexes.[98, 164, 170, 172-176, 224, 225] Accordingly, the P=O bond distance (1.496(4)Å) is considerably shorter than the P-OMe bond distance (1.618(4)Å).

The presence of a strong N-H···O=P intramolecular hydrogen bond as found in spectroscopic data (^{1}H NMR and IR) is confirmed by the short N-H···O=P distance (O(1)-H(N(1))= 2.088 Å) which is considerably shorter than the sum of the van der Waals radii of O and H (2.60 Å) and well within the range considered diagnostic for hydrogen bonded N-H···O.[98, 170, 172, 173, 176, 227] This secondary hydrogen-bonding

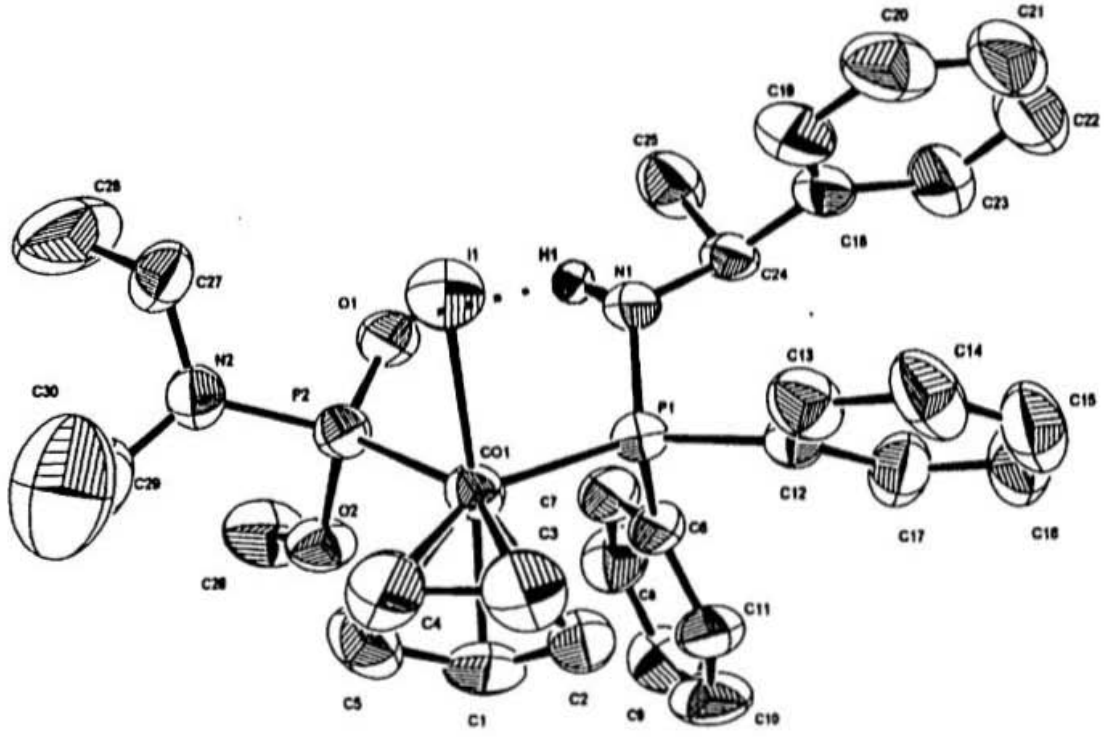

Figure 2-2. ORTEP representation for (η^5-Cp)CoI(PPh$_2$NHCH(Me)Ph)(P(O)(NEt$_2$)(OMe)), 3a-2. Hydrogens, except N-H, have been omitted for clarity.

Table 2-4. Summary of crystallographic data for 3a-2

Formula	$C_{30}H_{38}N_2O_2P_2CoI$
F.W. (G/mol)	706.43
Crystal color	dark green
Crystal Size (mm)	0.200x0.120x0.400
Crystal System	monoclinic
No. Reflections Used for Unit Cell Determination (2θ range)	21 (27.7 - 30.5°)
Omega Scan Peak Width at Half-height	0.33
Lattice Parameters	
a(Å)	12.883(4)
b(Å)	8.698(3)
c(Å)	14.532(6)
β(°)	107.19(3)
V(Å^3)	1555.6(9)
Space Group	$P2_1$ (#4)
Z	2
$D_{calc.}$ (g/cm^3)	1.508
F_{000}	716
μ (Mo Kα) (cm^{-1})	16.61
Scan Width (°)	1.57 + 0.35 tanθ
$2\theta_{max}$ (°)	50.1
No. Reflections Measured	
Total	6191
Unique	2965
Corrections[a]	Lorentz-polarization Absorption
Trans. factors:	0.91 - 1.00
Function Minimized	$\sum w(\|Fo\|-\|Fc\|)^2$
Least-squares Weights	$4Fo^2/\sigma^2(Fo)^2$
p-factor	0.01
Anomalous Dispersion	All non-hydrogen atoms
No. Observation (I>2.00σ(I))	2408
No. Variables	343
Reflection/Parameter Ratio	7.02
R[b]	0.027
R_w[c]	0.021
Goodness of Fit Indicator[d]	1.27
Max Shift/Error in Final Cycle	0.00
Maximum Peak in Final Diff. Map (e$^-$/Å^3)	0.31
Minimum Peak in Final Diff. Map (e$^-$/Å^3)	-0.35

[a] cf. Reference[226]. [b] $R=\sum||Fo|-|Fc||/\sum|Fc|$.
[c] $R_w=[\sum w(|Fo|-|Fc|)^2/\sum wFo^2]^{1/2}$. [d] $GOF=(\sum(|Fo|-|Fc|)/\sigma)/(n-m))$ where n= # reflections, m=#variables, and σ^2=variance of (|Fo|-|Fc|).

Table 2-5. Atomic coordinates ($\times 10^4$) and isotropic temperature factors ($pm^2 \times 10^{-1}$) for 3a-2

atom	x	y	z	B(eq)(Å^2)
I(1)	0.16022(3)	0.4668	0.10882(3)	4.88(2)
Co(1)	0.23543(6)	0.1920(1)	0.13396(5)	3.38(3)
P(1)	0.1791(1)	0.1406(2)	0.2609(1)	3.13(6)
P(2)	0.3945(1)	0.2827(2)	0.2261(1)	3.40(6)
O(1)	0.3948(3)	0.3494(5)	0.3210(2)	3.8(2)
O(2)	0.4723(3)	0.1333(5)	0.2393(3)	4.2(2)
N(1)	0.1903(3)	0.2852(5)	0.3372(3)	3.1(2)
N(2)	0.4606(4)	0.4086(6)	0.1772(4)	4.4(2)
C(1)	0.2697(5)	-0.025(1)	0.0972(4)	5.4(3)
C(2)	0.1551(5)	-0.009(1)	0.0657(5)	5.1(3)
C(3)	0.1278(5)	0.111(1)	0.0007(4)	5.8(4)
C(4)	0.2257(6)	0.169(1)	-0.0124(4)	5.9(4)
C(5)	0.3114(5)	0.081(1)	0.0448(5)	5.7(4)
C(6)	0.2536(4)	-0.023(1)	0.3289(4)	3.6(2)
C(7)	0.3428(5)	0.0037(7)	0.4098(4)	4.1(3)
C(8)	0.4047(5)	-0.1153(8)	0.4594(5)	5.1(3)
C(9)	0.3792(6)	-0.2640(8)	0.4275(6)	5.8(4)
C(10)	0.2931(7)	-0.2937(8)	0.3482(5)	6.0(4)
C(11)	0.2294(6)	-0.1731(8)	0.3005(5)	4.7(3)
C(12)	0.0348(4)	0.0870(7)	0.2328(4)	3.8(3)
C(13)	-0.0407(5)	0.1658(9)	0.1603(4)	5.2(3)
C(14)	-0.1513(5)	0.139(1)	0.1417(5)	6.7(4)
C(15)	-0.1841(6)	0.033(1)	0.1953(6)	7.7(5)
C(16)	-0.1131(6)	-0.044(1)	0.2661(5)	7.3(4)
C(17)	-0.0010(5)	-0.018(1)	0.2865(4)	5.6(3)
C(18)	0.0373(5)	0.3330(7)	0.4056(4)	3.8(3)
C(19)	-0.0077(5)	0.444(1)	0.3380(5)	5.5(3)
C(20)	-0.1141(6)	0.494(1)	0.3248(5)	6.7(4)
C(21)	-0.1731(5)	0.436(1)	0.3813(6)	7.3(5)
C(22)	-0.1284(6)	0.329(1)	0.4492(6)	7.1(5)
C(23)	-0.0249(5)	0.2757(9)	0.4611(5)	5.7(4)
C(24)	0.1527(4)	0.2769(7)	0.4237(4)	3.3(2)
C(25)	0.2316(5)	0.3694(9)	0.5039(4)	5.2(3)
C(26)	0.5774(5)	0.1373(9)	0.3118(5)	6.1(3)
C(27)	0.4514(6)	0.5744(9)	0.1935(6)	6.0(4)
C(28)	0.5547(7)	0.651(1)	0.2425(7)	10.5(6)
C(29)	0.5079(7)	0.370(1)	0.0988(6)	8.0(5)
C(30)	0.4471(7)	0.419(2)	-0.0041(7)	13.6(8)
H(1N)	0.242(4)	0.330(7)	0.343(4)	3.5(2)

Table 2-6. Selected bond distance (Å) and bond angles (deg) for 3a-2

atom	atom	distance	atom	atom	distance
I(1)	Co(1)	2.565(1)	P(1)	C(6)	1.832(7)
Co(1)	P(1)	2.218(2)	P(1)	C(12)	1.841(5)
Co(1)	P(2)	2.235(2)	P (2)	O(1)	1.496(4)
Co(1)	C(1)	2.042(8)	P(2)	O(2)	1.618(4)
Co(1)	C(2)	2.121(7)	P(2)	N(2)	1.669(5)
Co(1)	C(3)	2.141(6)	O(2)	C(26)	1.449(6)
Co(1)	C(4)	2.103(6)	N(1)	C(24)	1.476(6)
Co(1)	C(5)	2.077(6)	N(2)	C(27)	1.472(8)
P(1)	N(1)	1.655(4)	N(2)	C(29)	1.481(8)

bond	angle	bond	angle
I(1)-Co(1)-P(1)	95.94(5)	Co(1)-P(2)-O(2)	102.4(2)
I(1)-Co(1)-P(2)	89.84(5)	Co(1)-P(2)-N(2)	118.0(2)
P(1)-Co(1)-P(2)	92.33(7)	O(1)-P(2)-O(2)	111.7(2)
Co(1)-P(1)-N(1)	114.8(2)	O(1)-P(2)-N(2)	106.0(3)
Co(1)-P(1)-C(6)	110.9(2)	O(2)-P(2)-N(2)	101.7(2)
Co(1)-P(1)-C(12)	115.1(2)	P(2)-O(2)-C(26)	118.7(4)
N(1)-P(1)-C(6)	107.5(3)	P(1)-N(1)-C(24)	123.2(4)
N(1)-P(1)-C(12)	102.9(2)	P(2)-N(2)-C(27)	119.9(5)
C(6)-P(1)-C(12)	104.9(3)	P(2)-N(2)-C(29)	123.8(5)
Co(1)-P(2)-O(1)	116.2(2)	C(27)-N(2)-C(29)	114.7(6)

interaction controls the solid-state conformation and results in a distorted six-membered Co-P-O···H-N-P ring (Figure 2-3 A). The bond length of aminophosphine Co-P(1) (2.218(2) Å) is slightly shorter than that of phosphonato Co-P(2) (2.235(2) Å).

Bond angle summations around N(1) and N(2) of 350.1° and 357.5° as well as the mean deviations of 0.1003 Å and 0.0509 Å from least-squares planes of P(1), C(24), H(1N), N(1) and C(29), N(2), C(27), P(2) suggest a significant departure from trigonal pyramidal towards trigonal planar geometry, especially for the amidophosphonate nitrogen N(2). This indicates that the N(2) is essentially sp^2 hybridized. Therefore, significant π-donation from the nitrogen lone-pair to vacant phosphorus orbitals is postulated for N(2),[228] *i.e.*, the P-N(2) bond has significant π character. These observations are consistent with Nakazawa's prediction that at least one of the nitrogen atoms directly bonded to a phosphorus atom has a trigonal-planar geometry irrespective of the phosphorus valency and the coordination number.[229]

The absolute configuration of **3a-2** was unequivocally assigned from the X-ray structure. Significantly different Rw of 0.021 and 0.036 for both enantiomers of **3a-2** obtained from independent refinement with the Molecular Structure Corporation

TEXSAN software supports the absolute configuration of **3a-2** shown in Figure 2-2. The structure was also independently solved and refined using the NRCVAX X-ray software package.[230] The resulting Lapage η factor converged to 1 confirming the absolute stereochemistry assigned by the TEXSAN software. The stereogenic carbon center derived from the "chiral pool" was known to be *S* and provided an independent check for the correctness of the absolute configuration assignment. Consideration of the complex **3a-2** as pseudotetrahedral with an η^5-Cp occupying one coordination site and use of modified Cahn-Ingold-Prelog rules[95, 175, 214] with the ligand priority series I > η^5-Cp > P(O)(NEt$_2$)(OMe) > PPh$_2$NHC*H(Me)Ph for cobalt and Co > OMe > O > NEt$_2$ for phosphorus specifies the absolute configuration of **3a-2** as $R_{Co}S_PS_C$ (Figure 2-3 A).

The absolute configurations of the remaining three diastereomers **3a-1**, **3a-3** and **3a-4** were assigned on the basis of chiroptical evidence (circular dichroism (CD) spectroscopy, Figure 2-4). Ample literature precedent establishes that the morphology of the CD spectrum is dominated by metal-centered electronic transitions,[97] but it is clear that the chiral phosphorus center has a secondary effect.[98, 172] The similar CD morphology of **3a-2** and **3a-4** established that the absolute configurations of cobalt are identical and therefore R_{Co}. Since the configuration at the

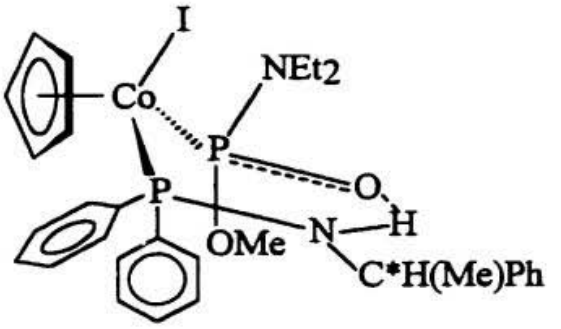

A

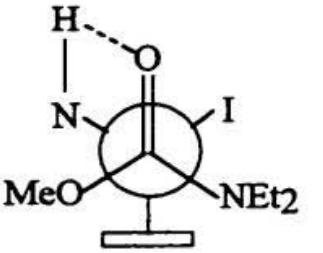

B

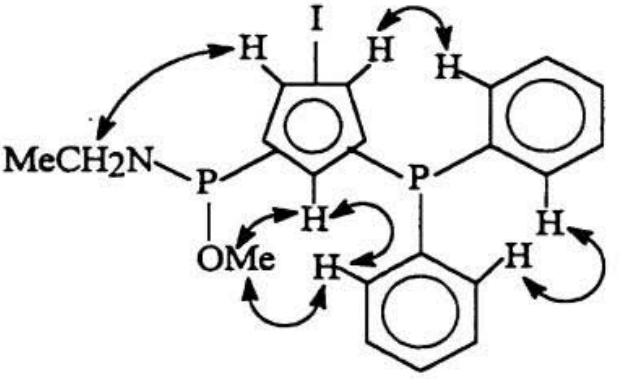

C

Figure 2-3. Conformational representations of 3a-2

aminophosphine carbon is known to be *S* (obtained from chiral pool) and **3a-2** is $R_{Co}S_PS_C$, the absolute configuration of P-epimeric **3a-4** must be $R_{Co}R_PS_C$. Since the CD spectra of **3a-1** and **3a-2** (Figure 2-4 A) as well as **3a-3** and **3a-4** (Figure 2-4 B) are quasi-mirror imagines, the absolute configurations of **3a-1** and **3a-3** can be assigned as $S_{Co}R_PS_C$ and $S_{Co}S_PS_C$, respectively. These assignments are confirmed by

the excellent correlation between the relative TLC R_f values and the absolute configurations for the isostructural chiral phosphinate complexes. It has been demonstrated that the absolute configurations of η^5-CpCo(X)($PPh_2NHC^*H(Me)Ph$)(P(O)R(OMe)) (X=I, R=Ph, Et, *t*-Bu,[98, 173]; X=C_nF_{2n+1}, R=Ph[159, 178]) consistently show decreasing TLC R_f values (from 1 to 4) assuming X is the largest group in these complexes along the series $S_{Co}R_PS_C$, $R_{Co}S_PS_C$, $S_{Co}S_PS_C$, and $R_{Co}R_PS_C$. The absolute configurations of **3a-1, -2, -3** and **-4** follow the same pattern.

2.2.1.3. Conformational analysis. The crystal structure of **3a-2** (Figure 2-2) shows that a "chaise longue"[173] conformation, formed as the result of intramolecular P=O···H−N hydrogen bonding, is established in the solid state (Figure 2-3 A). The N(1)−O(1) distance (2.770 Å) determined for **3a-2** reflects strong O···H−N hydrogen bonding[227, 231] typical for the basic phosphoryl P=O group. The solid-state conformation is remarkably similar to that found for other hydrogen-bonded aminophosphine phosphonate, phosphinate,[98, 170, 172, 173, 176] and acyl[227] analogs in which intramolecular, noncovalent interactions dominate stereo-electronic preferences. The η^5-Cp group occupies a pseudoequatorial and the iodide a pseudoaxial position in the Co−P−N−H···O=P six membered ring (Figure 2-3 A). An alternate conformation in

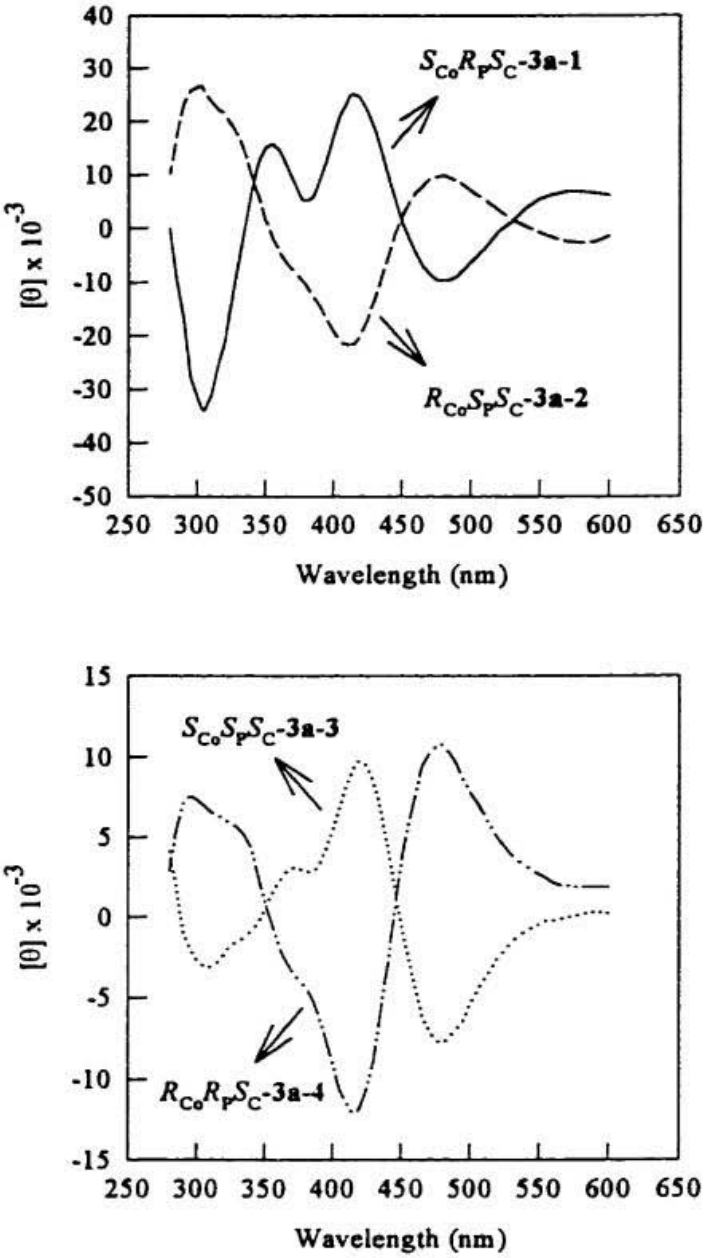

Figure 2-4. Circular dichroism spectra of (A) 3a-1 (___), 3a-2 (- - -); (B) 3a-3 (...), 3a-4 (- · · -)

which iodide is pseudoequatorial appears much less favourable since, as a consequence of the pseudooctahedral geometry at the metal and concomitant 90° interligand bond angles, iodide almost eclipses the pseudoaxial phosphorus substituents. In agreement with the proposed axial orientation of iodide the solid-state I–Co–P–O and I–Co–P–C torsion angles are in the range 169.7 and 161.0°, respectively (Figure 2-3). The P=O bond is *anti* to the η^5-Cp ring due to the N-H···O=P constraint (Figure 2-3 B).

The solution conformations of all four diastereomers **3a** were investigated by proton nuclear Overhauser effect difference spectroscopy (NOED).[98, 170, 172-176] The results are in accord with the retention of an intramolecular hydrogen-bonded quasi-chair conformation in solution. Partial saturation of the Cp resonance in **3a-2** gives positive Overhauser enhancements to the *ortho* hydrogens of the diastereotopic aminophosphine $P(C_6H_5)_2$, the $P(O)(N(CH_2CH_3)_2)$ and the $POCH_3$ substituents. These enhancements are confirmed by reverse irradiations at resonances for $P(C_6H_5)_2$, the $P(O)(N(CH_2CH_3)_2)$ and the $POCH_3$, respectively, (Figures 2-6 and 2-3 C). This conformational preference may result from the stabilizing interaction[232, 233] between the η^5-Cp ring and both face-exposed gauche aminophosphine phenyl groups which is possible only when the η^5-Cp ring is equatorial. Proton NOED spectra for **3a-1**

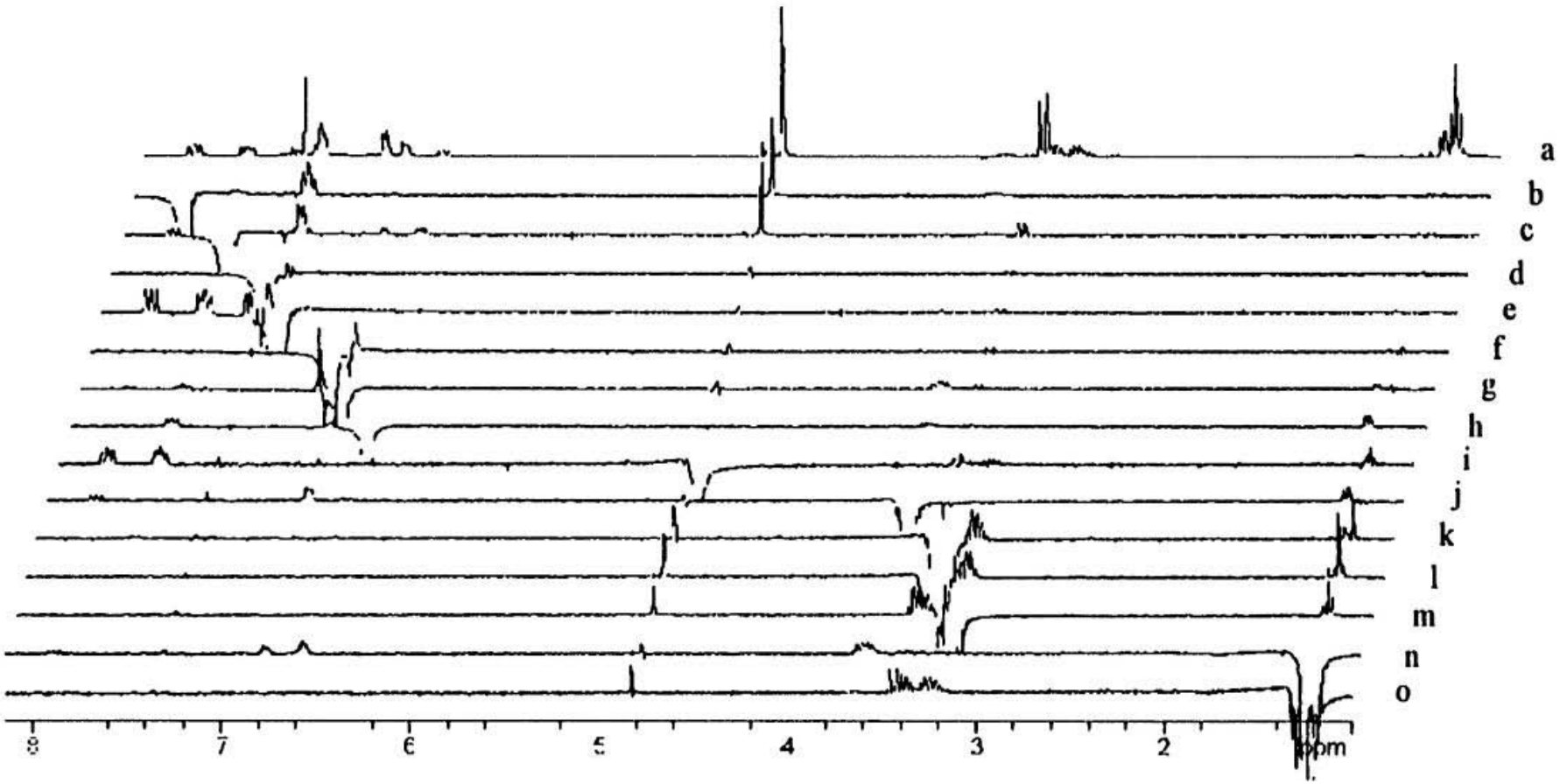

Figure 2-5. Proton NOED spectra of 3a-1: (a) reference spectrum; (b-o) difference spectra (16 X)

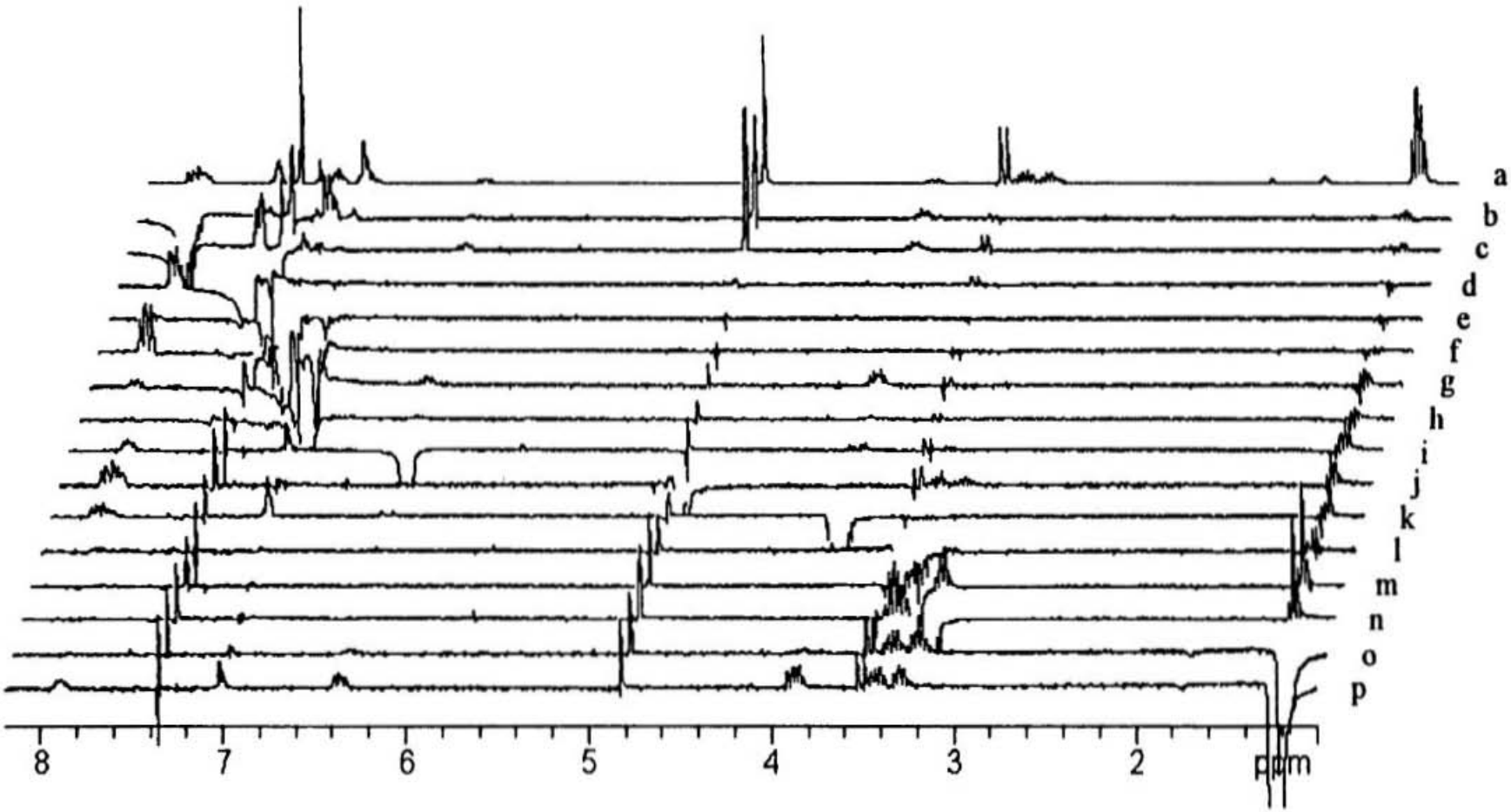

Figure 2-6. Proton NOED spectra of 3a-2: (a) reference spectrum; (b-p) difference spectra (64 X)

(Figure 2-5) parallels the results obtained for **3a-2** since the configuration at both chiral Co and P centers are opposite. The NEt_2 group is pseudo-equatorial in both diastereomers **3a-1** ($S_{Co}R_PS_C$) and **3a-2** ($R_{Co}S_PS_C$) (Figure 2-3). The minor diastereomers **3a-3** ($S_{Co}S_PS_C$) and **3a-4** ($R_{Co}R_PS_C$) are forced to accommodate the phosphonate amido group NEt_2 in the pseudoaxial position. A positive NOED enhancement to the Cp resonance on partial saturation of either the PO*Me* or $N(CH_2CH_3)$ signal for diastereomers **3a-3** and **3a-4** establishes a preference for equatorial Cp for diastereomers **3a-3** and **3a-4**.

2.2.1.4. Co*→P Chiral induction. The observed optical yield of 88% de for both $S_{Co}R_PS_C$ / $S_{Co}S_PS_C$ and $R_{Co}S_PS_C$ / $R_{Co}S_PS_C$ diastereomer pairs of **3a-1** shows a high chiral induction from Co* to P for the reaction of (*S*)-η^5-$CpCoI_2$(PNH) (PNH = (*S*)-(-)-$PPh_2NHC^*H(Me)Ph$)) **1a** with one equivalent of dimethyl diethylamidophosphite. The conformational bias for the major (**3a-1** and **3a-2**) and minor (**3a-3** and **3a-4**) diastereomers provides a rationale for the chiral induction from Co*→P on the formation of the chiral phosphorus centre. A model for the observed chiral induction is proposed in Scheme 2-6 based on solution conformation. Substitution of iodide in **1a** with $Et_2NP(OMe)_2$ gives us a cationic intermediate **2a**. Nucleophilic attack of iodide on the diastereotopic methoxy carbon of **2a** gives diastereomeric phosphinates

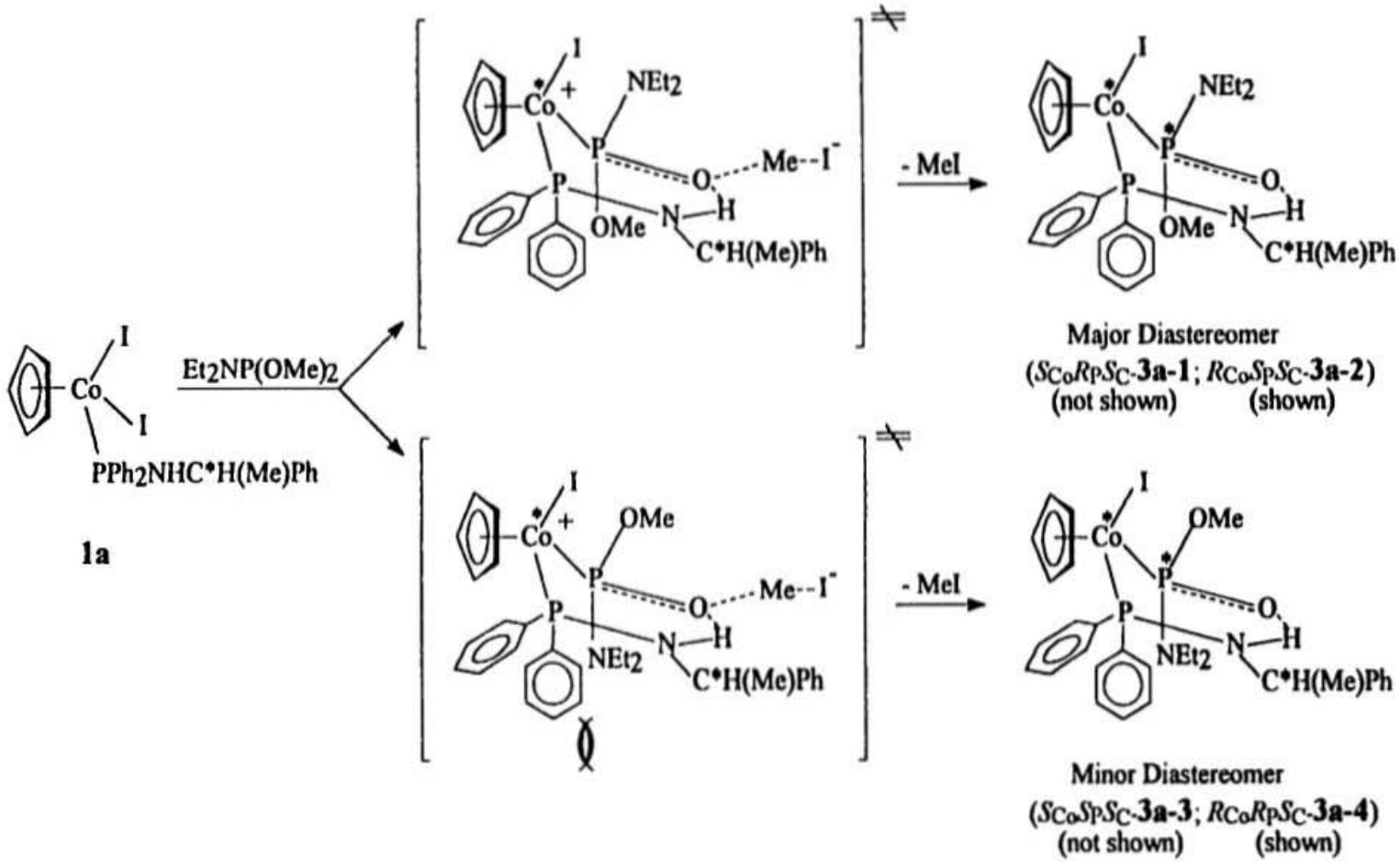

Scheme 2-6. Suggested mechanism for chiral induction Co*→P

3a with the release of MeI. The stereochemistry of this dealkylation is affected by the previously formed chiral Co center, *i.e.*, the chiral induction from Co*–P occurs on the transformation from **2a** to **3a**. The stability of the product-like transition state for the dealkylation of prochiral amidophosphite, where the P=O double bond and P=O···H-N hydrogen bond are sufficiently developed, will be controlled by 1,3-diaxial steric interactions between the phenyl group in the aminophosphine and the substituents on P(O) of the hydrogen-bonded "*chaise longue*". These interactions will in turn control the stereochemistry of products. According to this model, the $S_{Co}R_PS_C$ and $R_{Co}S_PS_C$ diastereomers will be the major products since intermediate **2a** with less severe 1,3-axial interactions between Ph and OMe is more stable. The $S_{Co}S_PS_C$ and $R_{Co}S_PS_C$ diastereomers are minor products due to the decreased stability of intermediate **2a** as a result of relatively stronger 1,3-axial interactions between Ph and NEt_2 (Scheme 2-6). This optical yield (88%) is higher than that obtained when the NEt_2 group is replaced by a Ph group[98] (78-80%) but a somewhat lower than that obtained when the NEt_2 group is replaced by a *t*-Bu group[173] (100%). This suggests that the NEt_2 group is sterically more bulky than a Ph group, but less bulky than *t*-Bu group.

2.2.2. Reaction of 1b with $Et_2NP(OMe)_2$ and characterization of the products.

Literature precedent shows that dissociation of labile cobalt-halide bonds[164-166, 180, 234] is a major source of loss of stereochemistry at the metal in piano stool complexes.[92, 235] The substitution-inert perfluoroalkyl group[172, 176, 232, 236] was introduced for the study of chiral induction from Co*→P. Reaction of R,S_{Co},S_C-CpCo(CF_3)(PNH*)(I) (**1b**) with dimethyl diethylamidophosphite in 1:1 molar ratio in benzene at room temperature is rather complicated compared to that of **1a**. The reaction proceeded with low chemical conversions (cf. experimental section). Two reaction channels were observed as shown in Scheme 2-7. The first channel results from iodide

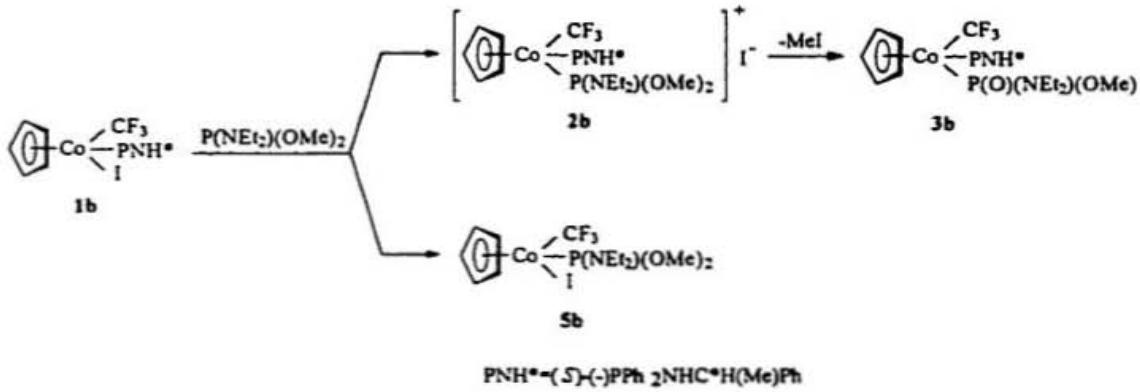

Scheme 2-7. Two reaction channels for 1b with $Et_2NP(OMe)_2$

displacement followed by Arbuzov dealkylation to give two of four possible diastereomers (**3b**). Pure, lower R_f diastereomer **3b-2** was isolated from the reaction mixture via preparative thick-layer radial chromatography while the higher R_f

diastereomer (**3b-1**) was obtained as a diastereomeric mixture with **1b**. **3b-2** was characterized by IR, ^{1}H, ^{13}C, ^{19}F and ^{31}P NMR (Tables 2-1, -2 and -3). ^{1}H, ^{19}F and ^{31}P NMR data assigned to **3b-1** are given in Tables 2-2 and 2-3.

Substitution of the aminophosphine ligand by dimethyl diethylamidophosphite to afford $CpCo(CF_3)(Et_2NP(OMe)_2)(I)$ (**5b**) was also observed (Scheme 2-7). The ^{1}H NMR of **5b** is given in Table 2-2. An additional reaction channel was indicated by isolation of a pair of diastereomers identified as **4b-1** and **4b-2** by comparison of ^{1}H NMR data reported for S_{Co},S_C- and $R_{Co}S_C$-$CpCo(CF_3)(PNH)P(O)(OMe)_2$.[176] Their formation can be explained by a mechanism akin to that suggested for the formation of **4a-1** and **4a-2** (Scheme 2-5).

2.2.2.1. Relative configuration of 3b. Previous work[98, 172, 173, 175, 176, 179] establishes an excellent correlation between relative TLC R_f values and absolute configurations for isostructural chiral phosphinate complexes CpCo(R')(PNH)(P(O)(R)(OMe)) (R' = I, CF_3, C_3F_7; R = Et, Ph, *t*-Bu; PNH = (S_C)-$PPh_2NHCH(Me)Ph$). For the isostructural perfluoroalkyl system,[172] the absolute configurations of four possible diastereomers are always $R_{Co}R_PS_C$, $S_{Co}S_PS_C$, $R_{Co}S_PS_C$ and $S_{Co}R_PS_C$ in order of decreasing TLC R_f values. The relative configuration of high- and low-R_f diastereomers **3b-1** and **3b-2**

was empirically assigned as $R_{Co}R_PS_C$ and $S_{Co}S_PS_C$, respectively, on the basis of comparison of chromatographic R_f values and on modified Cahn-Ingold-Prelog rules[94, 95, 237] with the ligand priority series for cobalt η^5-Cp > P(O)(NEt$_2$)(OMe) > PPh$_2$NHCH(Me)Ph > CF$_3$. Assumption that the morphology of the circular dichroism (CD) spectrum of an optically active chiral-at-metal complex is dominated by metal-centered electronic transitions[92] allows stereochemical assignment. A configuration of S_{Co} is consistent with the similar morphologies of the CD spectra of **3b-2** (Figure 2-7) and its analogs $S_{Co}S_C$-CpCo(R$_f$)(PNH*)(P(O)(OMe)$_2$)[176] and $S_{Co}S_PS_C$-CpCo(R$_f$)(PNH*)(P(O)(Ph)(OMe)).[172]

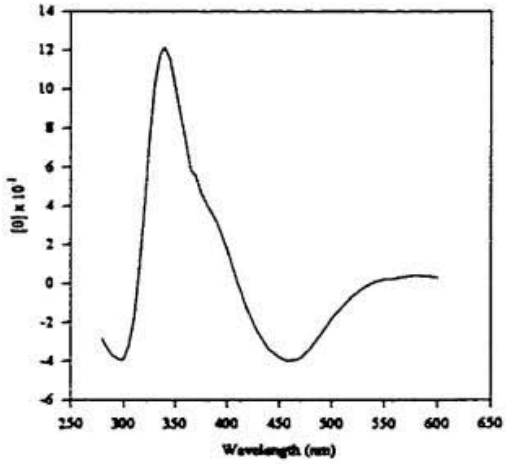

Figure 2-7. CD spectrum of 3b-2

2.2.3. Reaction of 1c with Et$_2$NP(OMe)$_2$ and characterization of the products. The stereochemical analysis for the reaction of **1a**, **b** with Et$_2$NP(OMe)$_2$ is consistent with previous studies[98, 170, 172, 173] of Arbuzov-like reactions[138] involving a diphenyl(1-phenylethyl)aminophosphine-substituted chiral cobalt auxiliary and a prochiral

phosphonite which concluded that the conformational mobility and thus the Co*→P chiral induction is controlled by intramolecular P=O···H-N hydrogen bonding at the nascent phosphoryl oxygen site (Scheme 2-6). The stereochemical outcome of these transition-metal-mediated Arbuzov reactions can be reliably predicted from the proposed transition state. Less hindered 1,3-diaxial interactions between the phosphonite substituent OMe and a pseudoaxial phenyl substituent of the aminophosphine will lead to major diastereomers while the larger 1,3-diaxial interactions give minor diastereomers (Scheme 2-6).

Attempts[176] have been made to assess the importance of intramolecular hydrogen bonding by use of *N*-alkylated aminophosphine ligands PNR* (PNR* = $Ph_2PNRC^*H(Me)Ph$, R = CF_3, Me, Et, CH_2Ph) which block intramolecular hydrogen bonding. However, these attempts were not successful.[176] In a search for an alternative, non-hydrogen bonding supporting ligand, chiral, bidentate, uninegative Schiff bases have been studied.[174] This work (Scheme 2-8) extends an early study[174] to a structurally analogous system where amidophosphite $Et_2NP(OMe)_2$ is involved.

Treatment of a dark blue solution of $R,S_{Co};S_C$-CpCo(N-N*)(I) (**1c**, N-N* = (S_C)-$Ph_2(Me)C^*H$-N=CH-$C_4H_3N^-$, $C_4H_3N^-$ = pyrrolyl) in benzene with dimethyl

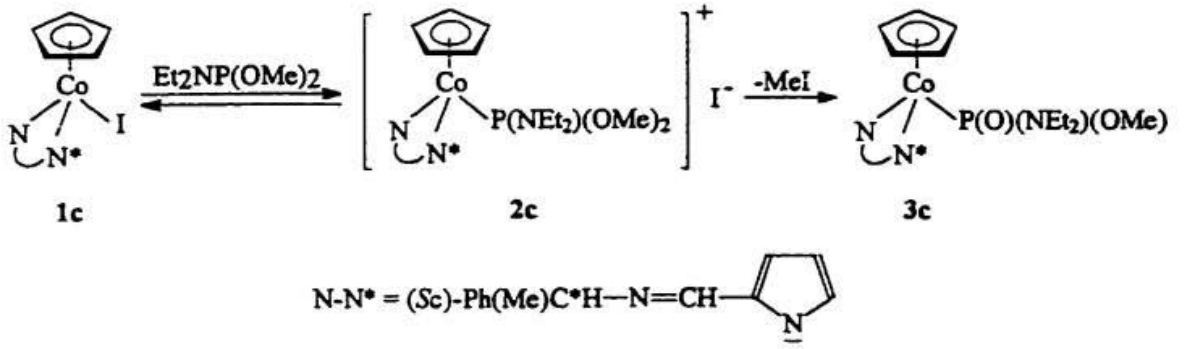

Scheme 2-8. Reaction 1c with $Et_2NP(OMe)_2$

diethylamidophosphite in a 1: 1 molar ratio at room temperature resulted in a deep red reaction mixture. Chromatography and ^{1}H NMR analysis showed both a higher-R_f and lower-R_f band to be a mixture of two distinct diastereomers. This suggests that the stereogenic cobalt center is labile at room temperature. The higher-R_f fraction was enriched with a diastereomer Cp = 4.74 ppm (assigned as **3c-1**) and the lower-R_f fraction was enriched with a diastereomer Cp = 4.75 ppm (assigned as **3c-2**) allowing assignment of their ^{1}H NMR spectra. The numbering scheme is given in Scheme 2-9 for the convenience of ^{1}H NMR assignment (Table 2-2). Analysis of a ^{31}P NMR

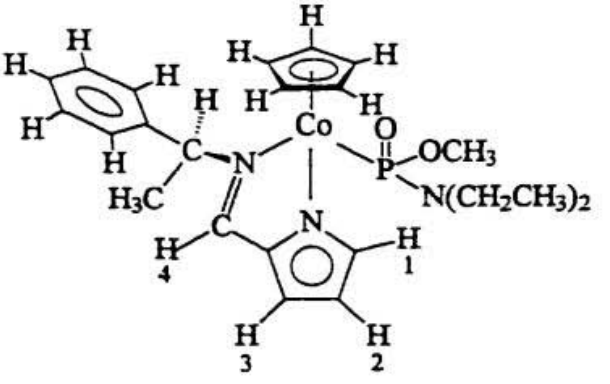

Scheme 2-9. Numbering scheme of 3c

spectrum of the higher-R_f fraction indicated that the chemical shifts of **3c-1** and **3c-2** are 79.13 ppm and 73.12 ppm, respectively. The CD spectrum of a mixture of **3c-1** and **3c-2** (*ca.* 60:40) is given in Figure 2-8.

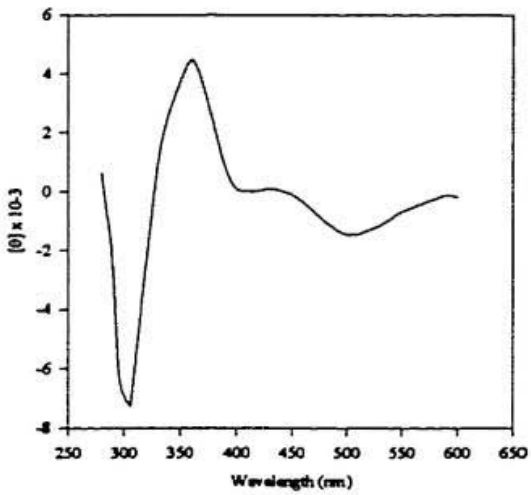

Figure 2-8. CD spectrum of 3c-1 & 3c-2 (*ca.* 60:40)

2.2.3.1. Mechanism of reaction of 1c with $Et_2NP(OMe)_2$. Analysis of ^{1}H NMR spectra of a reaction mixture (after removal of solvents) measured after 10 min and after 4 days (Figure 2-9) is consistent with substitution of iodide by amidophosphite and formation of a diastereomeric, cationic amidophosphite intermediate **2c**. Two broad Cp resonances at 4.81 ppm and 4.77 ppm and two methoxyl resonances and two sets of diastereotopic methylene resonances (Figure 2-9 bottom) were observed.

The broad Cp resonance at 4.88 ppm (Figure 2-9 bottom) can be assigned to a fast equilibrium **1c** + $Et_2NP(OMe)_2$ ⇌ **2c**. With decomposition of **2c** to form final Arbuzov-like dealkylation products **3c**, the equilibrium shifts to the right and eventually, on the completion of reaction, **2c** will be consumed and resonances corresponding to diastereomeric **2c** present in the equilibrium will disappear as shown in Figure 2-9 (top). This mechanism parallels that suggested for transition metal mediated Arbuzov reactions.[98, 138, 144, 147-149, 163, 167, 172-176, 180, 238]

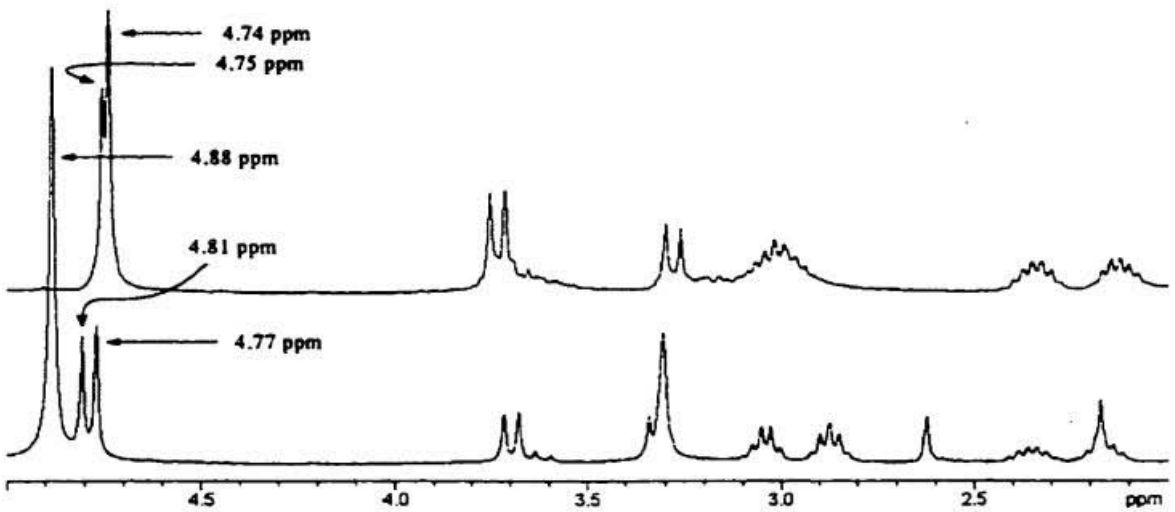

Figure 2-9. Time dependent ^1H NMR for reaction of 1c with $Et_2NP(OMe)_2$ after 10 min (bottom) and 4 days (top)

2.3. Summary

Reactions of CpCo(X)(Y)(I) (X=(*S*)-$Ph_2PNHCH(Me)Ph$, Y=I (**1a**); Y=CF_3 (**1b**) and XY= PhCH(Me)-N=CH-C_4H_3N (**1c**)) with $Et_2NP(OMe)_2$ have been studied. The chemical outcome varies from one system to another. For the system involving **1a**, all four possible $R,S_{Co};R,S_P;S_C$-CpCo(I)(PNH)(P(O)(NEt_2)(OMe)) (PNH = (*S*)-(-)-$PPh_2NHC^*H(Me)Ph$) diastereomers have been synthesized, resolved and fully characterized with high optical yield (88% de). The stereochemistry of all four possible diastereomers including solid-state structure and configurations as well as solid-state / solution conformations have been established by the combined use of single crystal X-ray diffraction, CD, and proton NOED spectra. The Co*–P chiral induction has been rationalized by steric interactions in the transition state for Arbuzov-like dealkylation reaction. A hydrolysis mechanism is proposed for the formation of the side products **4a**. For the system involving **1b**, more than two reaction channels are observed. Two of four desired diastereomers were isolated and characterized by spectroscopy (mainly by ^1H, ^{13}C, ^{19}F, ^{31}P NMR, CD and proton NOED). For the system involving **1c**, two of four possible diastereomers were isolated and characterized by ^1H and ^{31}P NMR. However, they epimerize at room temperature. In addition, two diastereomeric reaction intermediates and a fast equilibrium were observed by ^1H NMR in the reaction of **1c** with $Et_2NP(OMe)_2$.

2.4. Experimental

2.4.1. Reagents and methods. All manipulations were performed under a nitrogen or argon atmosphere using standard Schlenk techniques. Nitrogen or argon gas was purified by passing through a series of columns containing DEOX (Alpha) catalyst heated to 120 °C, granular P_4O_{10}, and finally activated 3 Å molecular sieves. Toluene, benzene, and ether were distilled under nitrogen from blue solutions of sodium benzophenone ketyl. Methylene chloride was distilled under nitrogen from P_4O_{10}. Acetone and ethyl acetate were distilled under N_2 from activated 4 Å molecular sieves. NMR solvents ($CDCl_3$ and CD_2Cl_2) were stored over activated 4 Å molecular sieves. Chromatographic separations were carried out using a Chromatotron (Harrison Associates) with 2-mm or 1-mm-thick silica $gel_{60}PF_{254}$ (Merck) absorbent. Thin-layer chromatographic separations were performed on analytical thin-layer precoated TLC plates (silica gel F-254, Merck). NMR spectra were recorded on a General Electric 300-NB Fourier transform spectrometer operating at a proton frequency of 300.1 MHz. Solution IR spectra were recorded in 0.1 mm path length KRS-5 cells on a Mattson Polaris FTIR spectrometer. Optical rotation measurements were determined in toluene (*ca.* 1 mg/mL) in a 1 cm path length cell on a Jasco DIP-370 digital polarimeter. Circular Dichroism (CD) spectra were determined in toluene

(*ca.* 1 mg/mL) on a Jasco J500A apparatus using a 0.1 or 0.05 cm path length cell. Melting points were determined in sealed capillaries by using a Büchi-SMP-20 apparatus and are uncorrected. Elemental analyses were performed by the Canadian Microanalytical Services (Delta, B.C.). The compounds η^5-$CpCoI_2$(PNH) (**1a**,[98] PNH = S_C-(-)-$Ph_2PNHCH(Me)Ph$) and η^5-CpCo(N-N*)(I) (**1c**)[232] were prepared using the established procedures. η^5-$CpCo(CF_3)$(PNH)(I) (**1b**)[176] was made by Professor H. Ma. Diethylamine was used as received. Methanol was refluxed over a small piece of sodium and freshly distilled before use. Triethylamine was refluxed and distilled from KOH.

Proton NOED spectra[239] were determined under steady-state conditions on a GE 300-NB instrument at 25.0 ± 0.1 °C. Data was collected on *ca.* 5 mg samples in 0.6 mL of $CDCl_3$ using a set of 16K interleaved experiments of 16 transients cycled 12-16 times through the list of decoupling frequencies. In each experiment, the decoupler was gated on in continuous wave (CW) mode for 3 s with sufficient attenuation to give an approximate 70-90% reduction in intensity of the irradiated peak. A 60 s delay preceded each frequency change. A set of four equilibrating scans was employed to equilibrate the spins prior to data acquisition. No relaxation delay was applied between successive scans of a given frequency. Difference spectra were

obtained on 16K or zero-filled 32K data tables which had been digitally filtered with a 0.1 Hz exponential line broadening function. Quantitative data were obtained by integration.

2.4.2. Crystal structure determination. Single crystals of **3a-2** suitable for X-ray crystallographic study were obtained from CH_2Cl_2/hexane by a diffusion method. Crystal data were collected at a temperature of 26±1 °C on a Rigaku AFC6S diffractometer with graphite monochromated Mo Kα radiation (λ=0.71069 Å), and a 2 kW sealed tube generator using the ω-2θ scan technique to a maximum 2θ value of 50.1°. Cell constants and an orientation matrix for data collection, obtained from a least-squares refinement using the setting angles of 21 carefully centred reflections in the range $27.72 < 2\theta < 30.53°$ are given in the Table 2-4. The space group $P2_1$ (#4) was determined on the basis of systematic absences of 0k0: $k \neq 2n$, a statistical analysis of intensity distribution and the successful solution and refinement of the structure. Omega scans of several intense reflections, made prior to data collection, had an average width at half-height of 0.33° with a take-off angle of 6.0°. Scans $(1.57 + 0.35 \tan \theta)°$ were made at a speed of 4.0 °/min (in Omega). Weak reflections ($I<10.0\sigma(I)$) were rescanned (maximum of 2 rescans) and the counts were accumulated to assure good counting statistics. Stationary background counts were

recorded on each side of the reflection. The ratio of peak counting time to background counting time was 2:1. The diameter of the incident beam collimator was 1.0 mm and the crystal to detector distance was 400.0 mm. The intensity of three representative reflections which were measured after every 150 reflections remained constant throughout data collection indicating crystal and electronic stability (no decay correction was applied). The linear absorption coefficient for Mo Kα is 16.6 cm^{-1}. An empirical absorption correction, based on azimuthal scans of several reflections, was applied which resulted in transmission factors ranging from 0.91 to 1.00. The data were corrected for Lorentz and polarization effects. A correction for secondary extinction was applied (coefficient = 0.11944E-6). The structure was solved by direct methods.[240] Non-hydrogen atoms were refined anisotropically. The hydrogen attached to nitrogen in the aminophosphine group was located in electron density difference maps. All other hydrogens were included in calculated positions then allowed to refine positionally (the methyl hydrogens with constrained H3 geometry), but fixed in the final rounds of least squares. Their isotropic thermal parameters were set 20% greater than those of their bonding partners at the time of inclusion. All calculations were performed using the TEXSAN crystallographic software package of Molecular Structure Corporation. The absolute configuration of **3a-2** (Figure 2-2) was determined by refining both enantiomers to convergence on

the complete data set with anomalous dispersion corrections included. The other enantiomer refined with significant higher R-values and GOF (0.040, 0.036, 2.13). This difference also showed up when the refinements on the two enantiomers were conducted leaving the I atom to refine isotropically. The data set was transferred to NRCVAX[230] and similar results were obtained. The eta refinement confirmed the absolute configuration and the statistical survey of Bijvoet[241] differences was consistent. Also the correct hand (*S*) was obtained for the chiral carbon derived from commercial (*S*)-(-)-(1-phenylethyl)amine.

2.4.3. Preparation of dimethyl diethylamidophosphite $Et_2NP(OMe)_2$. The amidophosphite $Et_2NP(OMe)_2$[148], b.p. 29.1-31.3 °C (2.5×10^{-4} mm Hg) was prepared by reacting Et_2NPCl_2[242], prepared from PCl_3 and Et_2NH in Et_2O, with MeOH in Et_3N according to the method for preparing $Me_2NP(OMe)_2$.[243] ^1H NMR ($CDCl_3$) 3.41 ppm (d, 12.6 Hz), 3.07 ppm (dq, 9.4, 7.1 Hz) and 1.06 ppm (t, 7.1 Hz).

2.4.4. Reaction of (*S*)-η^5-$CpCoI_2$(PNH) (PNH = (*S*)-(-)-$PPh_2NHCH(Me)Ph$)) (1a) with $Et_2NP(OMe)_2$. Preparation of ($R,S_{C*};R,S_P;S_C$)-(η^5-Cp)CoI($PPh_2NHCH(Me)Ph$)(P(O)(NEt_2)(OMe)) (3a) and ($R,S_{C*};S_C$)-(η^5-Cp)CoI($PPh_2NHCH(Me)Ph$)(P(O)$(OMe)_2$) (4a). A 55.20 mg (0.3340 mmol) of

$Et_2NP(OMe)_2$ was added slowly via syringe with stirring to a deep purple solution of 0.2282 g (0.3340 mmol) of **1a** in 50 mL of benzene at room temperature. The reaction mixture changed to black brown within 0.5 h. The resulting mixture was stirred for an additional 1.5 h. Removal of volatiles under vacuum left a black residue which was purified without protection from air by radial thick-layer chromatography on 2-mm silica gel plates. Elution with 5:1 benzene / ethyl acetate separated, in order of decreasing R_f values, purple starting material **1a** (23.1 mg, 10.1%) followed by two brown zones which contained **3a-1** and **3a-2** (74.5 mg, 35.1% and 72.0 mg, 34.0%, respectively, based on reacted **1**). After **3a-1** and **3a-2** were collected, the eluent was changed to 1:1 methylene chloride / ethyl acetate and in order of decreasing R_f values, four light brown zones containing **4a-1**, and **4a-2**, and **3a-3** and **3a-4** (10.1 mg, 5.1%, and 8.9 mg, 4.5%, and 4.6 mg, 2.2%, and 4.5 mg, 2.1% based on reacted **1a**), respectively, were eluted.

2.4.5. NMR Reaction of 1a with $Et_2NP(OMe)_2$. In a typical experiment 2.58 mg of $Et_2NP(OMe)_2$ (0.0156 mmol) was injected via microsyringe onto the neck of a screw-capped NMR tube held in a Schlenk adaptor which had been charged with 10.66 mg of **1a** (0.0156 mmol) and 0.6 mL of $CDCl_3$. After tightening the cap the reactants were mixed vigorously by inverting the NMR tube several times and immediately

placed into a thermostatted NMR probe. Spectra were acquired at 25.0°C every 5 minutes for a period of approximately 12 hours. Dried samples were obtained by cycling $CDCl_3$ solvent in the NMR tube through activated 4 Å molecular sieves prior to addition of solid **1a**. Wet samples were made by adding a drop of deionized water prior to mixing the two reactants.

2.4.6. Variable temperature NMR of 3a-2. A screw-capped NMR tube charged with approximately 10 mg of **3a-2** was connected to a vacuum/N_2 line. After several cycles of vacuum and N_2 filling, 0.6 mL of CD_2Cl_2 was added under nitrogen. After the sample was dissolved, the NMR tube was placed into a thermostatted NMR probe. ^1H and ^{13}C spectra were acquired at 25.0, -50.0, -90.0°C, separately.

2.4.7. Reaction of (R,S_{Co};Sc)-η^5-CpCo(CF$_3$)(PNH)(I) (PNH = (S)-(-)-PPh$_2$NH-CH(Me)Ph) (1b) with $Et_2NP(OMe)_2$. $Et_2NP(OMe)_2$ (54.26 mg, 0.3285 mmol) was added dropwise via syringe with stirring to a dark brown solution of **1b** (0.2054 g, 0.3285 mmol) in 40 mL of benzene at room temperature. After 24 hours all volatiles were removed under vacuum. Chromatographic separation on a 2-mm radial thick-layer silica gel plate (Chromatotron) eluting with ethyl acetate / hexane (1:5 v/v) resulted in, in order of decreasing TLC R_f values, a large brown zone (95.9 mg)

containing mainly starting material **1b**, two yellow zones which contained **3b-1** and **3b-2** (15.5 mg and 17.1 mg, respectively), and two slow moving brown zones from which **4b-1** and **4b-2** were obtained by manually extracting the separated silica gel powder with acetone.

2.4.8. Reaction of (R,S_{Co};Sc)-η^5-CpCo(N-N*)(I) (N-N* = (S_C)-Ph_2(Me)C*H-N=CH-$C_4H_3N^-$, $C_4H_3N^-$ = pyrrolyl) (1c) with $Et_2NP(OMe)_2$. After 0.2190 g (1.326 mmol) $Et_2NP(OMe)_2$ was added via syringe with stirring to a dark purple solution of 0.5942 g (1.326 mmol) **1c** in 40 mL benzene, an instantaneous color change from dark purple to deep red was observed. After four days' reaction, the mixture was filtered through a glass frit fitted with *ca.* 5 mm silica gel. Removal of solvent from the filtrate under aspirator and then oil pump pressure resulted in a deep red residue. Volatiles were removed from the deep red reaction mixture under water pump and then oil pump vacuum. Chromatographic separation on a 4-mm thick layer radial plate with 1:20 acetone / benzene gave two large red bands (0.2013 g and 0.2051 g, in order of decreasing TLC R_f values), which are enriched with **3c-1** and **3c-2**, respectively.

Chapter 3

Inorganometallic Phosphorus Chemistry: Regioselective Phosphorus-Nitrogen Bond Cleavage of Some Co(III) Complexes and Evidence for Phosphorus-Carbon Bond Activation

3.1. Introduction

As reviewed by Brunner[92] and discussed in Chapter 1, a common method for obtaining a homochiral-at-metal organometallic compound generally involves three steps: formation of diastereomers via reaction with a resolving agent, isolation of diastereomers and removal of the resolving handle. Both a proper resolving agent and suitable attachment chemistry have to be carefully chosen for the first step. The second step requires an efficient separation method. The third step requires a regiospecific reaction. Potential racemization / epimerization at the chiral metal center adds further difficulty to each step, making synthesis of homochiral organometallic compounds a formidable challenge. For these reasons relatively few M-chiral organotransition metal compounds are available in homochiral form, although they are valuable materials for catalysis, organic synthesis and stereochemical studies on reaction mechanisms.[92] Additionally, there is intrinsic

interest in the chemistry of chiral organotransition metal complexes.

Our research interest focuses on chiral induction from cobalt to directly attached phosphorus via the diastereoselective transition metal mediated (TMM) Arbuzov reaction. In order to understand the mechanism of Co*→P chiral induction, a large body of resolved, P-chiral metallophosphinates has been prepared.[98, 172, 174-176, 178, 179, 244] The resolution of these diastereomeric metallophosphinates requires a resolving agent. Optically active aminophosphines (*S*)-(-)-$Ph_2PN(R)C^*H(Me)Ph$ (R = H, Me, Et, CH_2Ph) are commonly used in this regard due to their optical stability, accessibility in large amounts and strong coordination ability to transition metals.[92, 245, 246] In this study, the resolving handle was not removed subsequent to chromatographic separation of diastereomers. This chapter describes a method for converting diastereoisomeric aminophosphine complexes into enantiomers, which provides a new route to optically active M-chiral organometallic compounds. Specifically, a method for preparation of homochiral metallophosphonates / phosphinates based on regiospecific HCl(g) induced P-N bond cleavage of the chiral moiety (*S*)-$NHC^*H(Me)Ph$ in the resolving handle will be discussed.

In addition, ^1H NMR evidence for P-C bond activation affording side products

(R,S_{Co},S_C)-(η^5-Cp)CoI($PPh_2NHC^*H(Me)Ph$)(P(O)$(OMe)_2$) in the reaction of (η^5-Cp)CoI_2($PPh_2NHC^*H(Me)Ph$) with *t*-BuP$(OMe)_2$) will also be presented.

3.2. Results and Discussion

3.2.1. Regiospecific P-N bond cleavage of chiral aminophosphine cobalt (III) complexes via reaction with HCl gas. Previous studies[247] on reactions of metallophosphonates/phosphinates [η^5-CpCo(X)($PPh_2NHCH(Me)Ph$)(RP(O)(OMe)), X=I, CF_3, C_3F_7; R=OMe, Ph] with common nucleophiles (NaOMe and RMgI, R=Me, Ph, MeC_6H_4) or BF_3 concluded that the metallophosphonates / phosphinates are

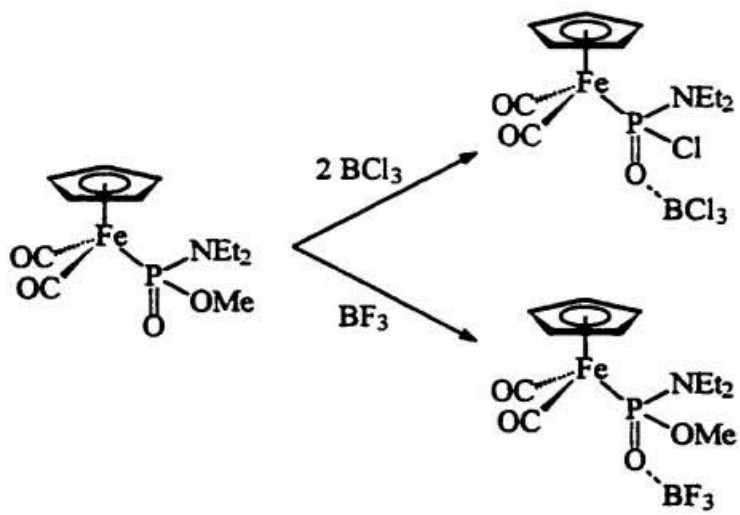

Scheme 3-1. Evidence showing phosphoryl oxygen is basic

chemically inert. Nevertheless, the phosphoryl group is anticipated to be relatively basic[213] (Scheme 3-1) hence reactivity with HCl(g) was tested. The initial results from a ^{1}H NMR study showed that a complicated reaction occurs. After examination of various reaction conditions, it was found that a mixed CCl_4/CH_2Cl_2 solvent system (v/v 5:1) works well at room temperature. Product analysis showed that the chiral moiety NHC*H(Me)Ph in the resolving handle PPh_2NHC*H(Me)Ph (PNH) was cleaved to give a homochiral organometallic product. Specifically, reaction of η^5-CpCo(I)(PPh_2NHC*H(Me)Ph)(P(O)(OMe)(R)) (R = OMe, Ph) under these conditions gave the P-N bond cleavage products as summarized in Scheme 3-2.

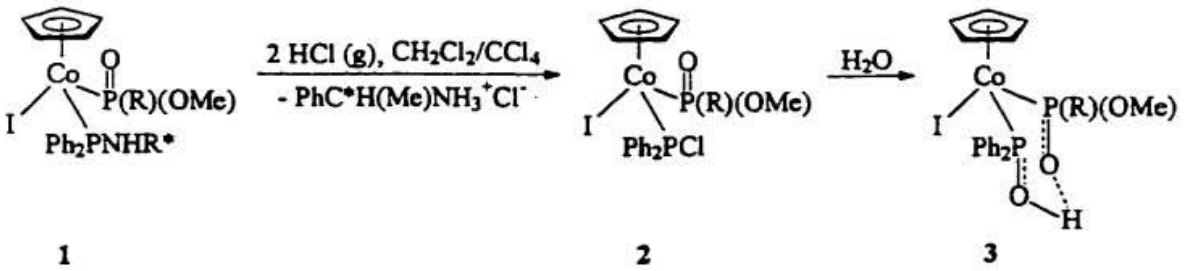

R* = C*H(Me)Ph

R	OMe	Ph
	$S_{Co}S_C$, **a-1**	$S_{Co}R_PS_C$, **b-1**
	$R_{Co}S_C$, **a-2**	$R_{Co}S_CS_C$, **b-2**
		$S_{Co}S_CS_C$, **b-3**
		$R_{Co}R_CS_C$, **b-4**

Scheme 3-2. Aminophosphine P-N bond cleavage

3.2.1.1. Reaction of CpCo(I)($PPh_2NHCH(Me)Ph$)(P(O)(OMe)(R)) (R = OMe, $S_{C*}S_{C'}$, 1a-1, $R_{C*}S_{C'}$, 1a-2; R = Ph, $S_{C*}R_PS_{C'}$, 1b-1, $R_{C*}S_PS_{C'}$, 1b-2; $S_{C*}S_PS_{C'}$, 1b-3, $R_{C*}R_PS_{C'}$, 1b-4) with HCl (g). Reactions were carried out at room temperature by adding HCl (g), slightly over one equivalent per time, via syringe to a stirred solution of diastereomerically pure **1** in the mixed solvent CCl_4/CH_2Cl_2 (v/v = 5:1). Reaction completion was monitored by following the decrease in intensity of the Me signal of CH*(Me)Ph in **1** by ^{1}H NMR. Careful workup gave a white precipitate, which was identified as 1-phenylethylammonium chloride by comparison of its ^{1}H NMR spectrum with that of an authentic sample, and homochiral CpCo(I)(PPh_2OH)(P(O)(OMe)(R) (R = OMe, Ph), **3**, the product of hydrolysis. The precursor of **3** was presumably CpCo(I)(PPh_2Cl)(P(O)(OMe)(R) (R = OMe, Ph), **2**, and formation of **3** results from facile hydrolysis of the P-Cl bond. Additional driving force for the hydrolysis of **2** may result from formation of a six-membered ring via hydrogen bonding (Scheme 3-2).

^{1}H NMR analysis of the crude reaction mixture was consistent with quantitative, regiospecific P-N cleavage. The products **3** were identified by ^{1}H, ^{13}C and ^{31}P NMR, IR and elemental analysis (Tables 3-1, 2, 3). All ^{1}H NMR spectra of three-legged piano stool complexes **3** show distinct resonances for η^5-Cp, P*Ph*, P(O)*Ph* and O*Me*

Table 3-1. Physical and IR data

compd	colour	mp(°C)	$[\alpha]_{436}$[a]	abs. config.	ν_{P-O}, δ_{P-OC}, δ_{PO-C} (cm^{-1})	anal. calcd (found) C, H
3a-1	brown-green	178-179	4.89×10^3	S_{Co}[b]	1100, 1061, 1011	40.60(40.32),3.94(3.88)
3a-2	brown-green	178-180	-4.91×10^3	R_{Co}[c]	1102, 1167, 1013	-
3b-1	green	186-188	1.24×10^3	$S_{Co}R_P$[c]	1106, 1081, 1029	47.39(46.89),3.98(4.06)
3b-2	green	184-186	-1.13×10^3	$R_{Co}S_P$[c]	1104, 1075, 1023	47.39(47.45),3.98(4.05)
3b-3	green	185-187	1.04×10^3	$S_{Co}S_P$[c]	1103, 1045, 1020	-
3b-4	green	186-188	-1.03×10^3	$R_{Co}R_P$[c]	1099, 1041, 1018	-

[a]Unit is deg dL g^{-1} dm^{-1}.
[b]determined by X-ray crystallography study.
[c]for Co, determined from chiroptical data; for P, assigned empirically

Table 3-2. ^{1}H and ^{31}P NMR data[a]

cpd	Ph	δ(Cp)	δ(OMe)	^{31}P
3a-1	7.99 (m), 7.53 (m), 7.44 (m), 7.40 (m), 7.37 (m)	5.02 (s)	3.87 (d, 10.1) 3.77 (d, 11.2)	119.01 (d, 127.8)[b] 112.47 (d, 138.1)[c]
3a-2	8.01 (m), 7.54 (m), 7.44 (m), 7.41 (m), 7.38 (m)	5.02 (s)	3.88 (d, 10.1) 3.78 (d, 11.2)	118.89 (d, 130.8)[b] 112.31 (d, 130.1)[c]
3b-1	8.02 (m), 7.87 (m), 7.51 (m), 7.46 (m) 7.40 (m)	4.95 (s)	3.74 (d, 10.9)	132.30 (d, 95.6)[b] 114.74 (d, 104.4)[c]
3b-2	8.02 (m), 7.87 (m), 7.50 (m), 7.45 (m) 7.40 (m)	4.95 (s)	3.69 (d, 10.8)	132.79 (d, 116.6)[b] 115.21 (d, 111.8)[c]
3b-3	8.03 (m), 7.87 (m), 7.52 (m), 7.46 (m), 7.40 (m)	4.95 (s)	3.69 (d, 10.8)	132.43 (d, 104.9)[b] 114.74 (d, 98.0)[c]
3b-4	8.03 (m), 7.88 (m), 7.53 (m), 7.47 (m), 7.41 (m)	4.96 (s)	3.70 (d, 10.9)	132.20 (d, 106.9)[b] 114.51 (d, 103.5)[c]

[a] ^{1}H (300.1 MHz) NMR chemical shifts in ppm relative to internal TMS; ^{31}P (121.5 MHz) NMR chemical shifts in ppm relative to external 85% H_3PO_4; *J* values in Hz given in parentheses; solvent = $CDCl_3$. Abbreviations: m, multiplet; s, singlet; d, doublet. [b] Phosphoryl P-atom. [c] Phosphinous acid P-atom.

Table 3-3. ^{13}C NMR data[a]

cpd	P-*Ph* *ipso* *ortho* *meta* *para*	P(O)-*Ph* *ipso* *ortho* *meta* *para*	δ(Cp)	δ(OMe)
3a-1	142.89 (d, 55.4), nf[b] 132.81 (d, 11.0), 129.69 (d, 10.4) 128.05 (d, 11.3)[c], 127.89 (d, 12.0)[c] 131.31[d], 130.20[d]	N/A	88.67 (s)	56.76 (d, 8.1) 51.25 (d, 10.1)
3a-2	143.02 (d, 54.4), nf[b] 132.87 (d, 10.5), 129.76 (d, 10.3) 128.11(d, 12.3)[c], 127.88 (d, 12.0)[c] 131.38[d], 130.24[d]	N/A	88.73 (s)	56.88 (d, 8.7) 51.31 (d, 9.7)
3b-1	141.13 (d, 66.7), 138.41 (d, 66.7) 132.91 (d, 10.6), 131.06 (d, 9.5) 130.66 (d, 2.0), 129.97 (d, 2.3) 127.98 (d, 3.0), 127.86 (d, 3.8)	143.96 (d, 54.4) 129.76 (d, 11.0) 131.93 (s) 127.74 (s)	88.51 (s)	52.69 (d,10.9)
3b-2	141.17 (d, 68.0), 138.45 (d, 65.7) 132.90 (d, 10.8), 131.48 (d, 9.1) 130.66 (d, 2.0), 129.97 (d, 2.3) 127.96 (d, 2.7), 127.84 (d, 3.7)	143.98 (d, 54.5) 129.72 (d, 10.6) 132.67 (s) 127.73 (s)	88.55 (s)	52.71 (d,11.1)

Table 3-3. ^{13}C NMR data [a] *(Cont'd)*

cpd	P-*Ph* *ipso* *ortho* *meta* *para*	P(O)-*Ph* *ipso* *ortho* *meta* *para*	δ(Cp)	δ(OMe)
3b-3	141.27 (d, 67.3), 138.58 (d, 63.8) 132.92 (d, 10.8), 131.24 (d, 9.7) 130.86 (d, 3.4), 130.07 (d, 2.5) 128.10 (d, 4.7), 127.98 (d, 2.8)	144.01 (d, 53.7) 129.87 (d, 10.3) 131.17 (s) 127.88 (d, 5.3)	88.57 (s)	52.78 (d, 10.9)
3b-4	141.22 (d, 67.8), 138.53 (d, 63.3) 132.99 (d, 10.8), 131.13 (d, 9.5) 130.76 (d, 3.3), 130.03 (d, 2.4) 128.03 (d, 4.4), 127.93 (d, 2.6)	144.09 (d, 53.7) 129.82 (d, 10.3) 131.15 (s) 127.83 (d, 4.9)	88.55 (s)	52.71 (d, 11.1)

[a] ^{13}C (75.5 MHz) NMR chemical shifts in ppm relative to $CDCl_3$ @ 77.0 ppm; s, singlet; d, doublet; J values in Hz. [b] nf = not found. [c] overlapped. [d] not resolved.

groups. For complexes **3a-1** and **3a-2**, diastereotopic OCH_3 groups gave distinct ^1H signals at 3.88 and 3.78 ppm and ^{13}C NMR resonances at 56.76 and 51.25 ppm (Table 3-2). The ^{13}C NMR (Table 3-3) of all complexes **3** showed diastereotopic *ipso*, *ortho*, *meta*, and *para* phenyl carbons for PPh_2. AB or AX patterns with characteristic[138] phosphoryl (119-132 ppm) and phosphinous acid (112-115 ppm) P-atoms were observed for all complexes **3** (Table 3-2). Complex **3a-1** was also characterized by a single crystal X-ray study.

3.2.1.2. Stereochemistry during the transformation of 1 to 3. Crystal structure of 3a-1. For the purpose of checking the stereochemistry during chemical transformation of **1** to **3**, the X-ray crystal structure of homochiral **1a-1** was determined. All hydrogen atoms were located in difference maps. The resulting molecular geometry and absolute configuration of **1a-1** is shown in Figure 3-1. A summary of crystallographic data, atomic coordinates, selected bond distances and bond angles are given in Tables 3-4, 5, 6 and 7, respectively. Complex **3a-1** is a pseudooctahedral, three-legged piano-stool. The η^5-Cp moiety occupies three facial coordination sites with iodide, P-bonded phosphinous acid and dimethyl phosphonato ligands completing the coordination sphere. Interligand bond angles (I-Co-P(1) = 92.02(5)°, I-Co-P(2) = 92.07(5)°, P(1)-Co-P(2) = 89.46(7)°) are approximately 90°.

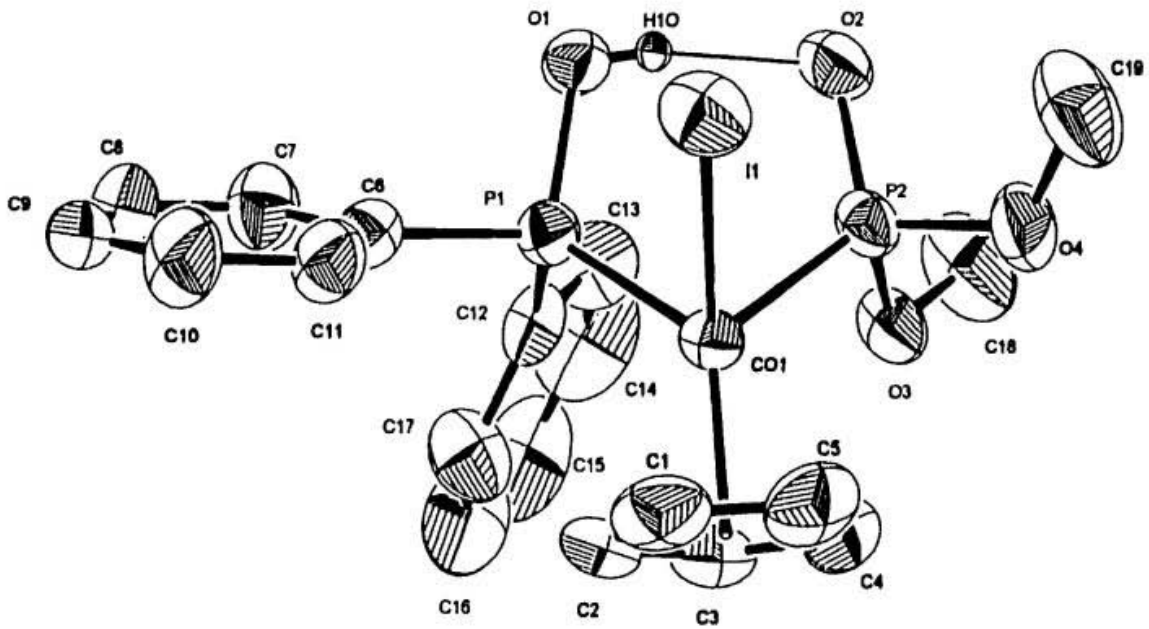

Figure 3-1. Molecular geometry and absolute configuration of S_{Co}-3a-1, hydrogens except O-H are removed for clarity.

Table 3-4. Summary of crystallographic data for 3a-1

Empirical Formula	$C_{19}H_{22}O_4P_2ICo$
Formula Weight	562.17
Crystal Colour	black
Crystal Dimensions (mm)	0.350 X 0.300 X 0.200
No. Reflections Used for Unit Cell Determination (2θ range)	24 (41.5 - 45.3°)
Omega Scan Peak Width at Half-height	0.34
Lattice Parameters:	
a (Å)	9.241 (4)
b (Å)	7.470 (2)
C (Å)	15.920 (2)
ß (°)	102.44 (1)
V = (Å^3)	1073.2 (5)
Space Group	$P2_1$ (#4)
Z value	2
$D_{calc.}$ (g/cm^3)	1.740
F_{000}	556
μ (MoKα) (cm^{-1})	23.89
Scan width (°)	1.57 + 0.30 tanθ
$2\theta_{max}$ (°)	50.1
No. of Reflections Measured	
Total	4357
Unique	2058
R_{int}	034
Structure Solution	Direct Methods
Refinement	Full-matrix least-squares
Corrections[a]	Lorentz-polarization Absorption
Trans. Factors	0.94 - 1.00
Function Minimized	$\Sigma w(\|Fo\| - \|Fc\|)^2$
Least-squares Weights	$4Fo^2/\sigma^2(Fo^2)$
p-factor	0.01
Anomalous Dispersion	All non-hydrogen atoms
No. Observations (I>2.00σ(I))	1890
No. Variables	243
Reflection/Parameter Ratio	7.78
R[b]	0.024
Rw[c]	0.022
Goodness of Fit Indicator[d]	1.67
Max Shift/Error in Final Cycle	0.00
Maximum Peak in Final Diff. Map	0.30 e$^-$/Å^3
Minimum Peak in Final Diff. Map	-0.25 e$^-$/Å^3

[a] cf. Reference[226]. [b] $R=\sum||Fo|-|Fc||/\sum|Fc|$. [c] $R_w=[\sum w(|Fo|-|Fc|)^2/\sum wFo^2]^{1/2}$.
[d] $GOF=(\sum(|Fo|-|Fc|)/\sigma)/(n-m))$ where n= # reflections, m=#variables, and σ^2=variance of $(|Fo|-|Fc|)$.

Table 3-5. Atomic coordinates ($\times 10^4$) and isotropic thermal parameters ($pm^2 \times 10^{-1}$) for 3a-1

atom	x	y	z	B(eq)
I(1)	0.43709(5)	0.0553	0.37224(2)	4.49(2)
Co(1)	0.49348(8)	0.3175(1)	0.28000(4)	2.76(3)
P(1)	0.7237(2)	0.2317(2)	0.2930(1)	2.99(6)
P(2)	0.4324(2)	0.1610(2)	0.1622(1)	3.24(6)
0(1)	0.7435(4)	0.0268(6)	0.2700(2)	3.9(2)
0(2)	0.5071(5)	-0.0179(5)	0.1599(2)	4.1(2)
0(3)	0.4588(4)	0.2854(6)	0.0860(2)	4.1(2)
0(4)	0.2557(4)	0.1328(6)	0.1317(3)	5.1(2)
C(1)	0.4346(8)	0.509(1)	0.3644(4)	5.3(4)
C(2)	0.5509(7)	0.575(1)	0.3289(4)	4.7(3)
C(3)	0.5005(6)	0.577(1)	0.2382(4)	4.2(3)
C(4)	0.3522(6)	0.520(1)	0.2196(4)	4.6(3)
C(5)	0.3147(7)	0.474(1)	0.2976(5)	5.2(3)
C(6)	0.8481(6)	0.2610(8)	0.3969(3)	3.4(2)
C(7)	1.0020(6)	0.255(1)	0.4020(4)	4.5(3)
C(8)	1.1004(7)	0.276(1)	0.4793(5)	4.8(3)
C(9)	1.0485(8)	0.308(1)	0.5530(4)	5.1(3)
C(10)	0.8982(9)	0.309(1)	0.5485(4)	5.3(3)
C(11)	0.7980(6)	0.290(1)	0.4719(4)	4.1(3)
C(12)	0.8172(6)	0.356(1)	0.2204(4)	3.8(3)
C(13)	0.8318(7)	0.280(1)	0.1446(4)	5.5(3)
C(14)	0.899(1)	0.380(2)	0.0876(5)	8.8(6)
C(15)	0.9433(9)	0.550(2)	0.1079(7)	8.5(6)
C(16)	0.9285(8)	0.625(1)	0.1836(6)	7.4(5)
C(17)	0.8651(7)	0.531(1)	0.2390(4)	5.3(3)
C(18)	0.449(1)	0.206(1)	0.0008(4)	7.3(4)
C(19)	0.1813(8)	-0.015(1)	0.1582(5)	6.9(4)
H(1O)	0.6798	-0.0002	0.2330	4.6
H(1)	0.4458	0.4817	0.4260	6.2
H(2)	0.6372	0.6135	0.3568	6.0
H(3)	0.5491	0.6059	0.1940	5.0
H(4)	0.2897	0.4880	0.1605	5.8
H(5)	0.2329	0.4379	0.3015	6.2
H(7)	1.0362	0.2445	0.3515	5.3
H(8)	1.2073	0.2760	0.4894	5.8
H(9)	1.1251	0.3424	0.6040	6.0
H(10)	0.8505	0.3149	0.5956	6.2
H(11)	0.6898	0.2939	0.4725	4.9
H(13)	0.8025	0.1750	0.1289	6.9
H(14)	0.8919	0.3089	0.0362	9.6
H(15)	0.9808	0.5969	0.0696	10.2
H(16)	0.9748	0.7351	0.1996	9.0
H(17)	0.8595	0.5734	0.2872	6.5
H(18A)	0.3584	0.1655	-0.0174	8.3
H(18B)	0.4379	0.2984	-0.0340	8.3
H(18C)	0.5609	0.1487	-0.0085	8.3
H(19A)	0.0750	-0.0292	0.1112	8.3
H(19B)	0.2244	-0.1171	0.1327	8.3
H(19C)	0.1599	0.0138	0.2034	8.3

Table 3-6. Selected bond distances (Å) for 3a-1

atom	atom	distance	atom	atom	distance
I(1)	Co(1)	2.5680(9)	C(2)	C(3)	1.418(8)
Co(1)	P(1)	2.189(2)	C(3)	C(4)	1.404(8)
Co(1)	P(2)	2.179(2)	C(4)	C(5)	1.402(8)
Co(1)	C(1)	2.111(6)	C(6)	C(7)	1.408(7)
Co(1)	C(2)	2.099(7)	C(6)	C(11)	1.387(7)
Co(1)	C(3)	2.053(7)	C(7)	C(8)	1.373(9)
Co(1)	C(4)	2.093(6)	C(8)	C(9)	1.380(9)
Co(1)	C(5)	2.094(6)	C(9)	C(10)	1.38(1)
P(1)	O(1)	1.593(4)	C(10)	C(11)	1.370(8)
P(1)	C(6)	1.813(5)	C(12)	C(13)	1.368(8)
P(1)	C(12)	1.836(6)	C(12)	C(17)	1.39(1)
P(2)	O(2)	1.508(4)	C(13)	C(14)	1.42(1)
P(2)	O(3)	1.587(4)	C(14)	C(15)	1.36(2)
P(2)	O(4)	1.614(4)	C(15)	C(16)	1.36(1)
O(3)	C(18)	1.468(8)	C(16)	C(17)	1.359(9)
O(4)	C(19)	1.410(8)	O(1)	H(10)	0.765
C(1)	C(2)	1.408(9)	O(2)	H(10)	1.767
C(1)	C(5)	1.385(9)			

Table 3-7. Selected bond angles[a] for 3a-1

atom	atom	atom	angle	atom	atom	atom	angle
I(1)	Co(1)	P(1)	92.02(5)	Co(1)	P(2)	O(4)	112.8(2)
I(1)	Co(1)	P(2)	92.07(5)	O(2)	P(2)	O(3)	110.7(2)
P(1)	Co(1)	P(2)	89.46(7)	O(2)	P(2)	O(4)	108.4(2)
Co(1)	P(1)	O(1)	114.6(2)	O(3)	P(2)	O(4)	99.1(2)
Co(1)	P(1)	C(6)	117.6(2)	P(2)	O(3)	C(18)	118.7(4)
Co(1)	P(1)	C(12)	111.8(2)	P(2)	O(4)	C(19)	122.6(5)
O(1)	P(1)	C(6)	104.2(2)	P(1)	C(6)	C(7)	118.8(4)
O(1)	P(1)	C(12)	104.4(3)	P(1)	C(6)	C(11)	122.7(4)
C(6)	P(1)	C(12)	102.8(3)	P(1)	C(12)	C(13)	119.6(6)
Co(1)	P(2)	O(2)	117.5(2)	P(1)	C(12)	C(17)	120.9(5)
Co(1)	P(2)	O(3)	106.8(2)	P(1)	O(1)	H(10)	108.85

[a]Angles are in degrees. Estimated standard deviations in the least significant figure are given in parentheses.

The phosphonato P atom has a distorted tetrahedral geometry[164, 168, 224] with an opened Co-P=O bond angle of 117.5(2)°. The Co-P-OMe bond angles differ (106.8(2)° and 112.8(2)°). The larger Co-P-OMe bond angle may be attributed to the stronger steric interaction with the bulky iodide atom (Figure 3-1). The O-H···O=P bond distance of 1.767Å, which is shorter than that (1.97Å) of the N-H···O=P hydrogen bond in its precursor **1a-1**[98], suggests very strong intramolecular O-H···O=P hydrogen bonding which completes a distorted six-membered Co-P-O···H-O=P ring (Figure 3-1).

The absolute configuration of **3a-1** shown in Figure 3-1 was determined by refinement of both enantiomers with Molecular structure Corporation TEXSAN software. Significantly different R/Rw/GOF (0.024/0.022/1.67 vs. 0.034/0.034/2.50) for both enantiomers established that the absolute configuration shown in Figure 3-1 was correct. A statistical survey of Bijvoet differences based on an independent solution of **3a-1** using the NRCVAX X-ray suite confirmed the above absolute stereochemistry assignment. The modified Cahn-Ingold-Prelog[95, 175, 214, 248] ligand priority series I > η^5-Cp > $P(O)(OMe)_2$ > PPh_2OH gives the absolute configuration of **3a-1** as S_{Co}.

Knowing that the absolute configuration of **1a-1** (the precursor of **3a-1**) is $S_{Co}S_C$, the

chemical transformation from **1a-1** to **3a-1** with P-N bond cleavage therefore proceeds with the expected retention of stereochemistry of the Co metal centre. The same conclusion can also be drawn by comparison of the CD (circular dichroism)[249] spectra of **1a-1** and **3a-1**, which show similar CD morphology (Figure 3-2). Since the CD morphology of a chiral-at-metal complex is normally dominated by chirality of the metal[92], it can be concluded that they have the same absolute configuration at Co.

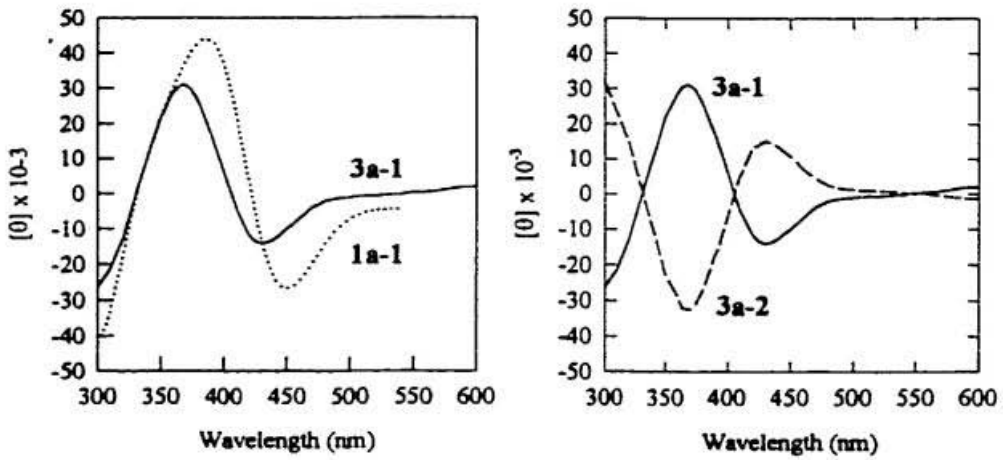

Figure 3-2. Circular dichroism (CD) spectra of 3a-1 (—) and 1a-1 (···)[98] (left); 3a-1 (—) and 3a-2 (---) (right)

The Newman projection (Figure 3-3) of **3a-1** along the O-P bonds based on the X-ray

structure demonstrates that a staggered conformation is adopted in the solid state. This conformation is retained in solution, which is reflected by the ^{1}H NOED spectrum (Figure 3-4).

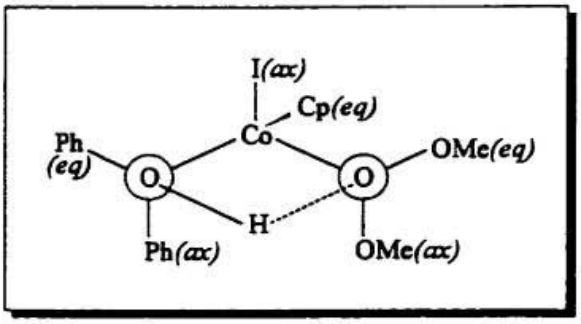

Figure 3-3. Newman projection of 3a-1

Circular dichroism (CD) spectra of **3b-(1-4)** are presented in Figure 3-5. Comparison of these spectra with those of their precursors **1b-(1-4)**[98] and assumption that the CD morphologies of chiral-at metal complexes is dominated by chirality of the metal,[92] suggests that transformation of **1b-(1-4)** to **3b-(1-4)** also proceeds with retention of absolute configuration at the cobalt centre. Efforts have been made to grow a single crystal from **3b** in order to determine the absolute configuration at the chiral P. Unfortunately, only twinned crystals were obtained and it was not possible to unambiguously assign the absolute configuration at chiral P. However, based on previous work[247] in this laboratory which concluded that neither epimerization nor ligand substitution occurred even with the strong nucleophile OMe^-, configurations at chiral P in **3b** were tentatively assumed to be the same as in its precusors **1b**.

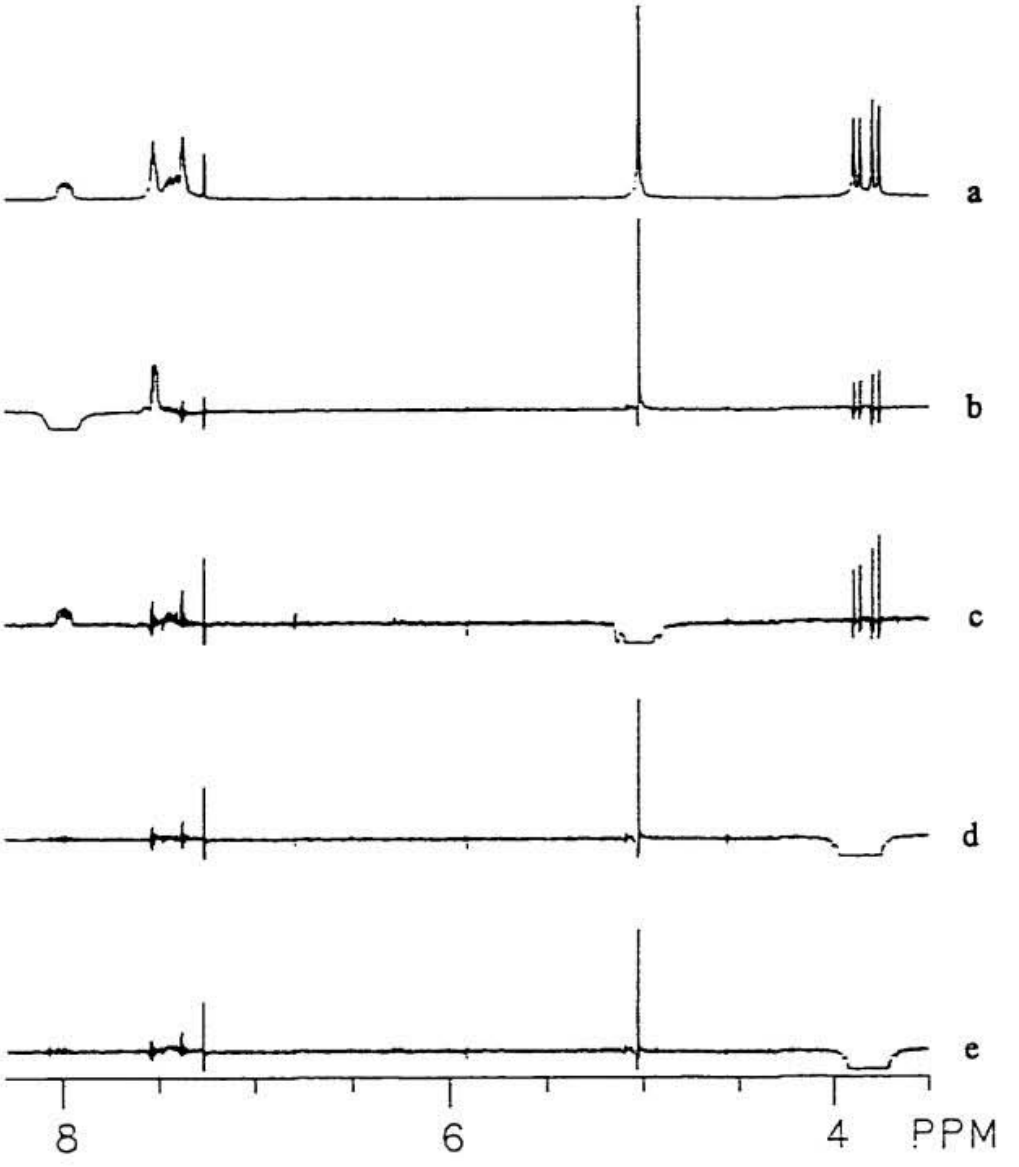

Figure 3-4. ^{1}H NOED spectra of 3a-1. (a) reference spectrum; (b)-(e) difference spectra

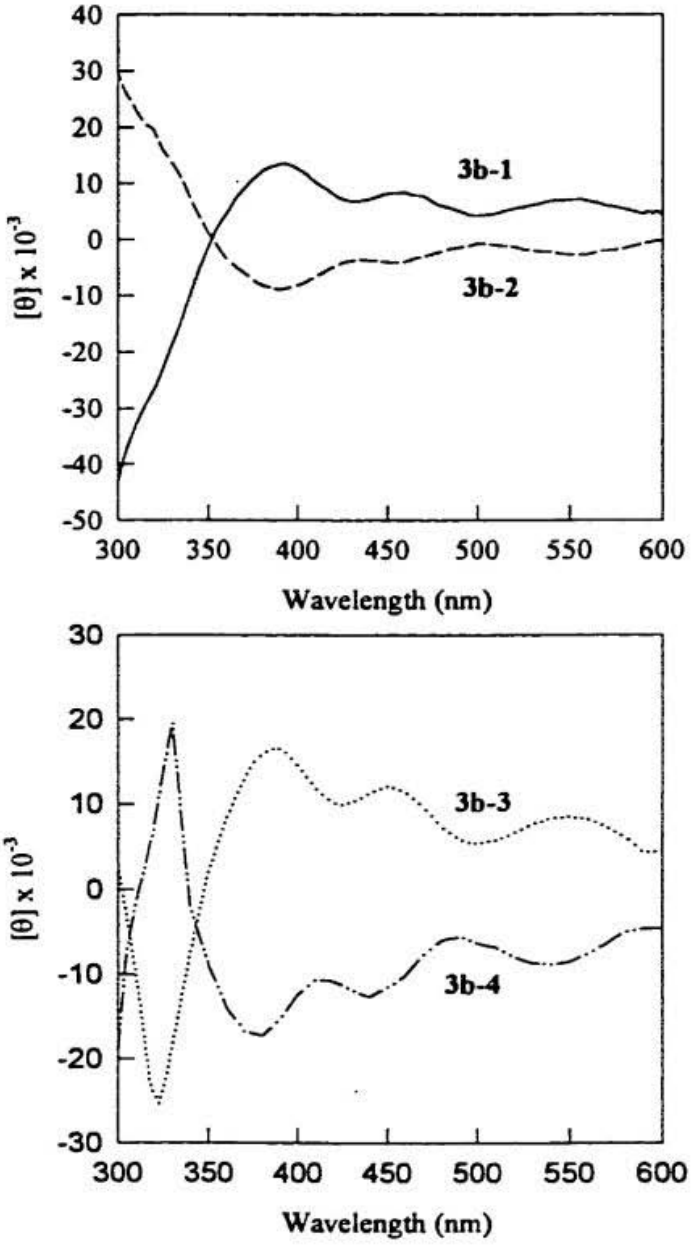

Figure 3-5. CD spectra of 3b-1 (—), 3b-2 (- - -), 3b-3 (·····) and 3b-4 (– ·· – ··)

3.2.1.3. Why regioselective P-N bond cleavage? Cleavage of M-C,[250, 251] P-N,[252-257] C-O,[258, 259] C-C[260] bonds and protonation[261] of phosphoryl oxygen by HCl (g) have all been reported. However, reactions of η^5-CpCo(I)($PPh_2NHC^*H(Me)Ph$)-(P(O)(OMe)(R)) (R = OMe, **1a**; Ph, **1b**) with HCl (g) are regiospecific although several alternative reactive sites (*Co*, *P*(O), *O*=P, *O*CH_3, *P*(Ph), *N*-Ph, etc.) are presented. To shed some light on this question, molecular orbital calculations at the extended Hückel level were performed for $S_{Co}S_C$-η^5-CpCo(I)($PPh_2NHC^*H(Me)Ph$)-(P(O)(OMe)$_2$) (**1a-1**) and $S_{Co}R_PS_C$-η^5-CpCo(I)($PPh_2NHC^*H(Me)Ph$)(PhP(O)(OMe)) (**1b-1**) as representatives using the CACAO package.[262] The starting geometry was taken from X-ray single crystal coordinates.[98] The calculated HOMO of **1a-1** is centered on the I atom (35%) with a major contribution from Co (23%) while the LUMO of **1a-1** is centered on Co (32%) with a major contribution from the I atom

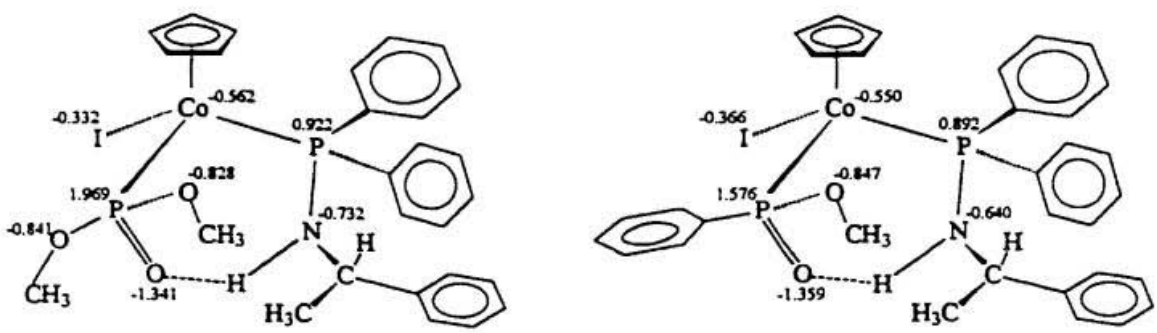

1a-1 **1b-1**

Scheme 3-3. Calculated net charges on heteroatoms in 1a-1 and 1b-1

(16%). For **1b-1,** the HOMO is dominated by Co (19%) and I (18%) while the LUMO is controlled by Co (32%) and I (17%) too. These results show that the reaction is not controlled by orbitals and suggest that the reaction is controlled by charges. The calculated net charges (at Hückel level) on relevant atoms are shown in Scheme 3-3.

Since the calculated net negative charges on heteroatoms in both **1a-1** and **1b-1** are in a decreasing order P(*O*) > P*O*Me > *N* > Co > I, assuming that the cleavage is protonation controlled, protonation will occur first on the phosphoryl oxygen and result in weakening of the existing P=O···H-N hydrogen bond. The second protonation may occur on the methoxy oxygen or nitrogen due to the relatively small charge difference. On protonation, the H-Cl bond will be polarized and the nucleophilicity of Cl will increase. However, even with this increased nucleophilicity and the high positive charge on *P*(O), products resulting from nucleophilic attack of Cl on *P*(O) have not been observed. On the contrary, nucleophilic attack on *P*-N with lower net positive charge was observed. This suggests that another driving force, presumed to be formation of the ammonium salt PhC*H(Me)$NH_3^+Cl^-$, controls regioselectivity. Nucleophilic substitution at *P*-N will give PhCH(Me)NH_2, which will react with a second equivalent of HCl to give a precipitate of

$PhC^*H(Me)NH_3^+Cl^-$. It is believed that the formation of the ammonium salt $PhC^*H(Me)NH_3^+Cl^-$ makes the P-N bond cleavage irreversible and controls the regiospecificity of the reaction (Scheme 3-4). However, if nucleophilic substitution at *P*(O) is reversible (slow or fast), the same result will be seen (Scheme 3-4).

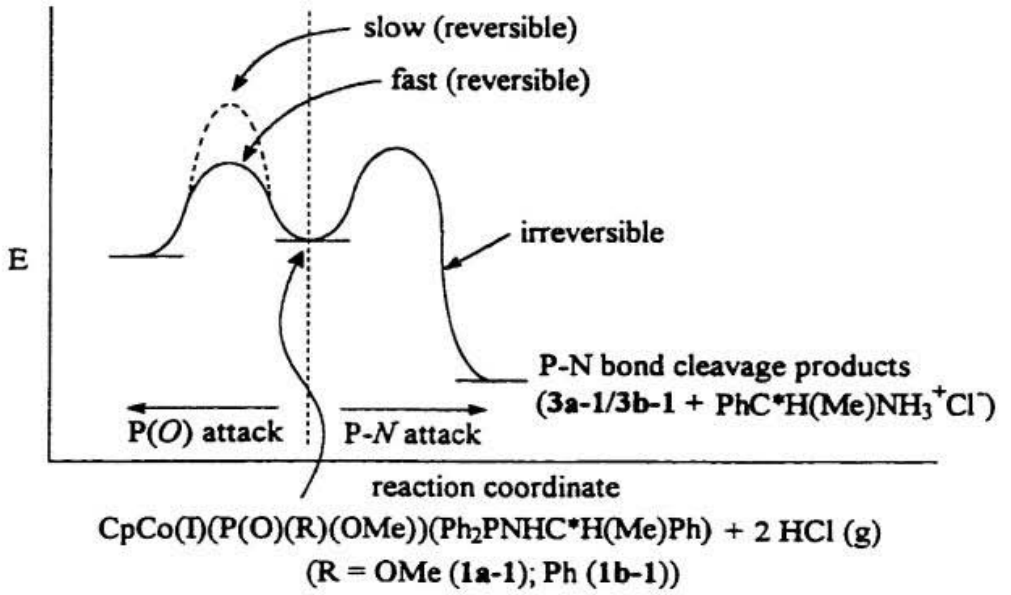

Scheme 3-4. Proposed energy profile for the reaction of $CpCo(I)(P(O)(R)(OMe))(Ph_2PNHC^*H(Me)Ph)$ with 2 equiv. of HCl(g)

3.2.2. Reaction of (*S*)-(η^5-Cp)$CoI_2(PPh_2NHC^*H(Me)Ph)$ (4) with *t*-$BuP(OMe)_2$. Previous research[98] on chiral induction from an asymmetric cobalt centre to a prochiral phosphorus atom via an Arbuzov-like dealkylation reaction concluded that the diastereoselectivity is controlled by P-N-H···O=P hydrogen bonding (Scheme 3-5) in a "product like" transition state. This strong hydrogen bonding interaction allows

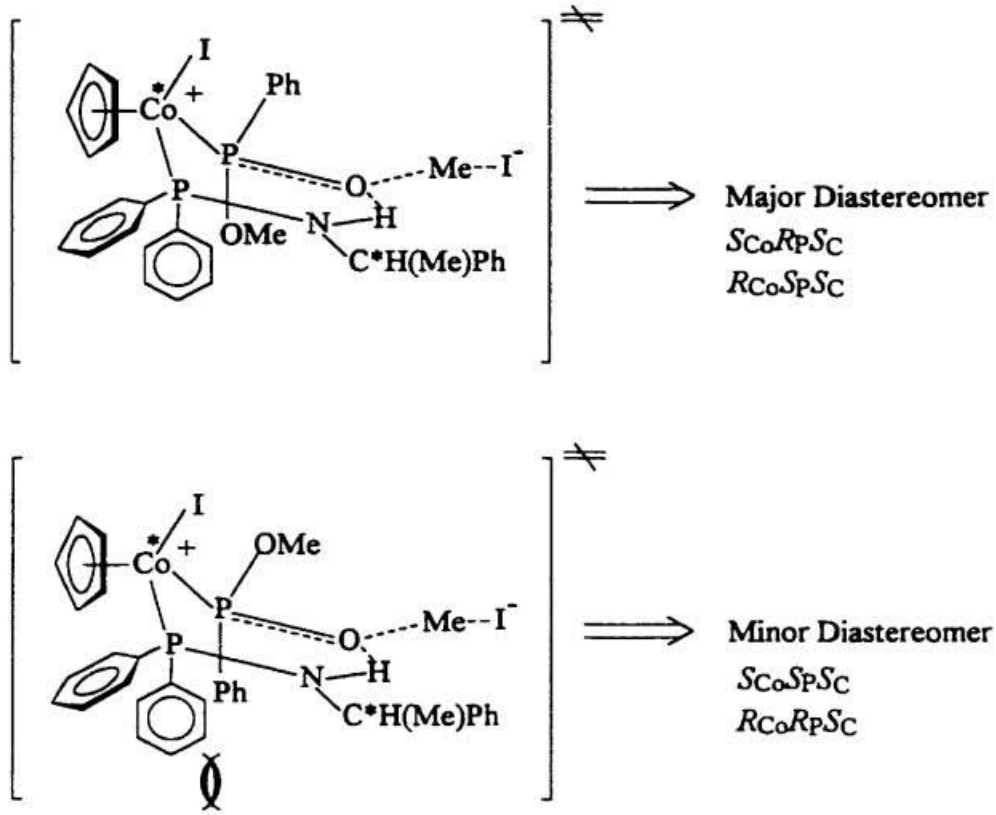

Scheme 3-5. Proposed Co* → P chiral induction model

the formation of a "*chaise longue*" conformation whose stability is determined by 1,3-diaxial steric interactions between phenyl groups on the aminophosphine and phosphite and in turn governs the stereochemical outcome. Based on this model the $R_{Co}S_PS_C$ (or $S_{Co}R_PS_C$) product is favoured compared to $R_{Co}R_PS_C$ (or $S_{Co}S_PS_C$) in agreement with experiment.[98]

To verify this model which suggests direct steric involvement of the phosphonite

substituents in Co*→P chiral induction, work[263] has been done with dimethyl *t*-butylphosphonite, which replaces a methoxyl or phenyl group with a bulky *t*-butyl group. Preliminary results[263] showed that reaction of (*S*)-(η^5-Cp)CoI_2(PPh_2NHC*H(Me)Ph) (**4**) with *t*-BuP$(OMe)_2$ in methylene chloride at room temperature proceeded with formation of ($S_{Co}S_C$)-(η^5-Cp)CoI(PPh_2NHC*H(Me)Ph)-(P(O)$(OMe)_2$) (**7-1**) and ($R_{Co}S_C$)-(η^5-Cp)CoI(PPh_2NHC*H(Me)Ph)(P(O)$(OMe)_2$) (**7-2**) in addition to two of four possible diastereomers ($S_{Co}R_PS_C$)-(η^5-Cp)-CoI(PPh_2NHC*H(Me)Ph)(*t*-BuP(O)(OMe)) (**6-1**) and ($R_{Co}S_PS_C$)-(η^5-Cp)-CoI(PPh_2NHC*H(Me)Ph)(*t*-BuP(O)(OMe)) (**6-2**) (Scheme 3-6). In order to confirm the formation of the P-C cleavage products **7-1** and **7-2**, the reaction was repeated.

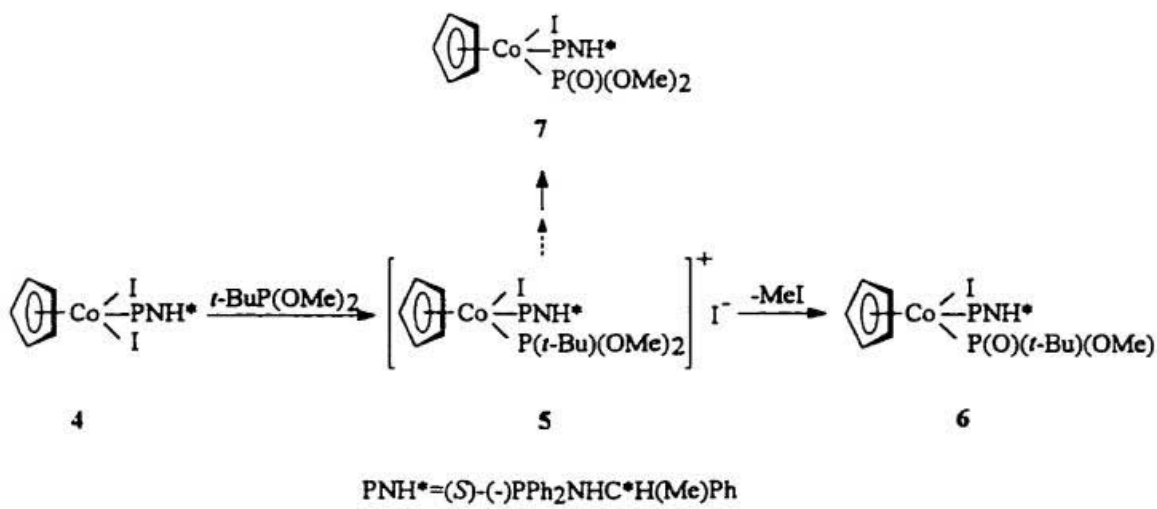

Scheme 3-6. Reaction of 4 with *t*-BuP$(OMe)_2$

The reaction was carefully carried out in a glove box which had been freshly purged using N_2 in order to minimize the possibility of adventitious water/oxygen.

Treatment of a deep purple solution of (*S*)-(η^5-Cp)CoI_2(PPh_2NHC*H(Me)Ph) (**4**) in CH_2Cl_2 with *t*-BuP$(OMe)_2$ taken from a freshly opened ampule in a glove box at room temperature gave a brown-green reaction mixture from which several products were isolated. Thick layer radial chromatography separated unreacted starting material **4** and four products which were characterized, in order of decreasing TLC R_f values, as two of four desired metallophosphinate diastereomers **6-1** and **6-2** and two minor dimethyl phosphonate "side" products, **7-1** and **7-2**.[98] All these complexes **6-1**, **6-2**, **7-1**, and **7-2** show substantial stability to air/water. These results confirmed initial experiments[263] except for small changes in product distribution.

3.2.2.1. Formation of 7-1 and 7-2 and evidence for P-C bond activation in 5. ^{1}H NMR showed that the lowest R_f, low yield products **7-1** and **7-2** were identical to authentic samples of ($S_{C\alpha}S_C$)- and ($R_{C\alpha}S_C$)-(η^5-Cp)CoI(PPh_2NHC*H(Me)Ph)-(P(O)$(OMe)_2$), respectively, which were rationally prepared from reaction of **4** with trimethylphosphite.[98] It is possible that **7-1** and **7-2** could form from the reaction of **4** with trimethylphosphite present as an impurity in the dimethyl *t*-butylphosphonite

since the dimethyl *t*-butylphosphonite was used as received from Alpha. However this possibility was eliminated by ^{1}H NMR impurity analysis of commercial dimethyl *t*-butylphosphonite through careful integration of the OMe group (δ = 3.49 ppm, J = 11 Hz) corresponding to $P(OMe)_3$ in a fresh sample of *t*-$BuP(OMe)_2$ under nitrogen against the ^{13}C satellite peaks of *t*-$BuP(OMe)_2$. This analysis showed that the level of trimethylphosphite was 0.21 mol %. Exposing CD_2Cl_2 solutions of *t*-$BuP(OMe)_2$ to air rapidly resulted in a complex mixture. However, even after exposure to air for 1 hour, ^{1}H NMR analysis showed that the impurity level of $P(OMe)_3$ only increased to 0.5 mol %. Comparison with the ~3% total isolated yield of **7-1** and **7-2** (based on *t*-$BuP(OMe)_2$) for the reaction of **4** with *t*-$BuP(OMe)_2$ under nitrogen atmosphere established that a low level of $P(OMe)_3$ impurity in *t*-$BuP(OMe)_2$ is unlikely to account for the formation of **7-1** and **7-2**. An argument can be made that the **7-1** and **7-2** originate from the P-C bond cleavage.[264-267]

P-C bonds tend to resist cleavage due to their high strength (259 kJ/mol) unless activated. Three possible classes of P-C bond cleavage of tertiary phosphine oxides have been identified by Edmundson.[267] Thermodynamic cleavage usually requires strong heating since P-C bonds have roughly the same bond energy as C-C bonds (259 kJ/mol vs. 268 kJ/mol). Cleavage by metals typically requires the presence of

alkali metals. Cleavage by nucleophiles is also possible. Potassium hydroxide is the most widely used nucleophile for the cleavage of P-C bonds, although others are possible. However, since ^{1}H NMR analysis of resolved products **6-1** and **6-2** indicates that they are stable under preparative conditions, the possibility that **7-1** and **7-2** derive from P-C bond cleavage of **6-1** and **6-2** can be eliminated. It is proposed that the metallophosphonates **7-1** and **7-2** form from the phosphonium intermediate **5** (Scheme 3-7). The proposed mechanism involves P-C bond cleavage via β-

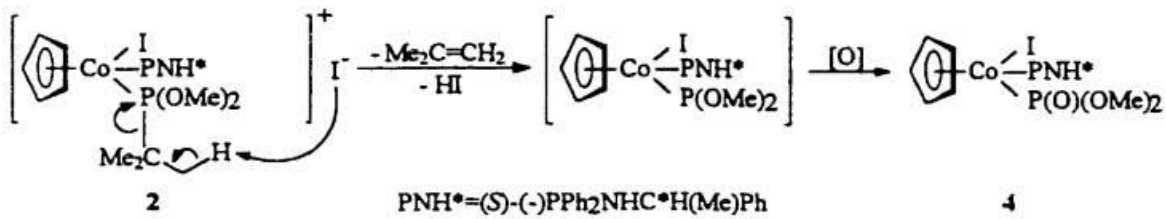

Scheme 3-7. Proposed P-C bond activation

elimination with formation of isobutene and a phosphito intermediate, **7'**. Oxidation of the phosphito intermediate[268] forms **7-1** and **7-2** as shown in Scheme 3-7. β-Elimination of phosphonium salts generally requires activation of the hydrogen β to the phosphorus.[26] In this case the organometallic species can function as an electron withdrawing group and thus activate the hydrogen β to the phosphorus. In addition, steric hindrance of the *t*-butyl group in the phosphonium salt should also favour the

elimination.[26] If this proposed mechanism is correct, isobutene should be formed in addition to **7-1** and **7-2**. This was confirmed by ^{1}H NMR studies in a screw capped NMR tube which showed multiplets at 4.66 and 1.73 ppm identical to those from authentic sample of isobutene from Aldrich (Figure 3-6).

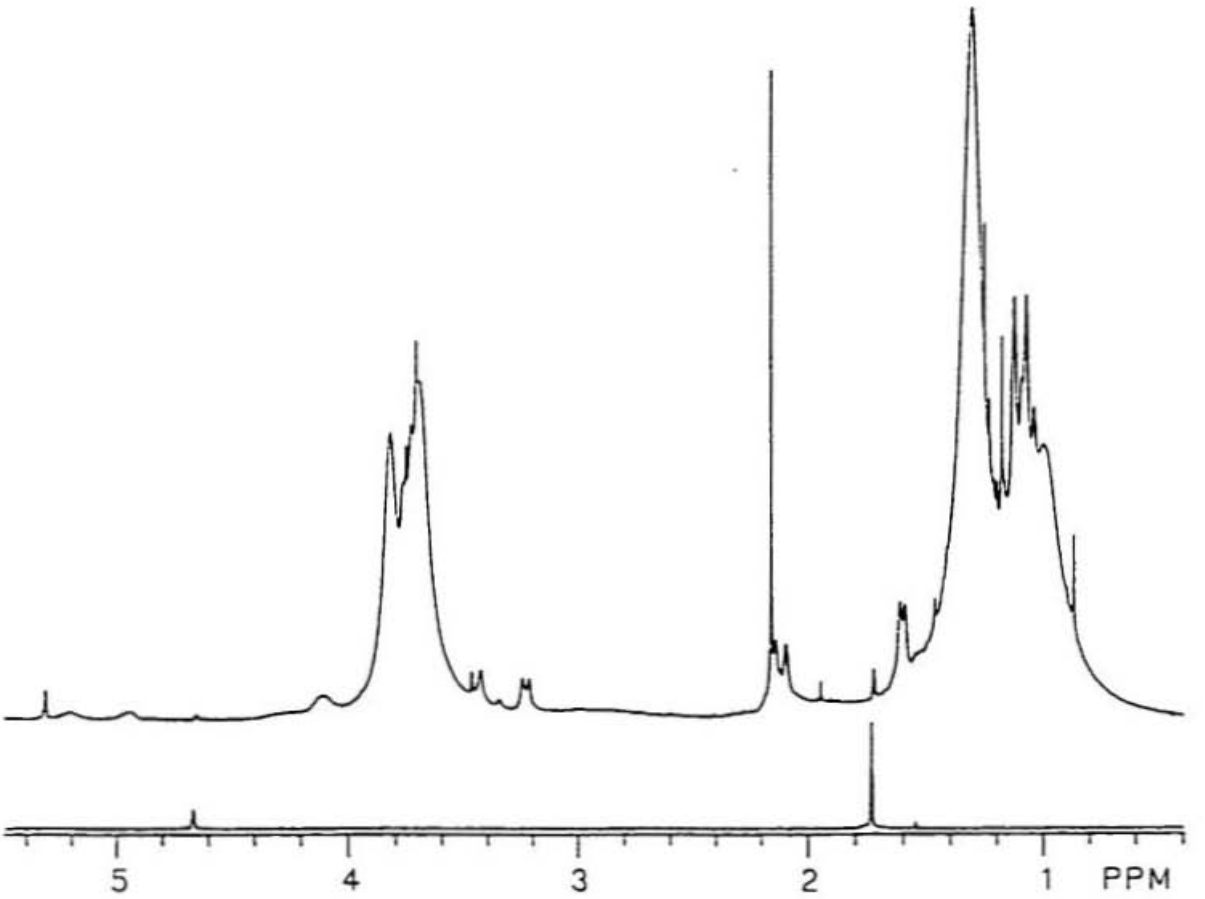

Figure 3-6. ^{1}H NMR of reaction mixture of 4 and *t*-BuP(OMe)$_2$ in CD_2Cl_2 (top) and authentic sample of isobutene (bottom, solvent: CD_2Cl_2)

3.3. Summary

A convenient and practical method to obtain homochiral transition metal complexes which are important to catalysis, organic synthesis and stereochemical studies was developed. Regioselective P-N bond cleavage reactions of chiral aminophosphine Co(III) complexes via gaseous HCl proceeds quantitatively with retention of configuration at Co*. The cleavage products have similar configuration in both solid state and solution. The regioselectivity has been discussed based on CACAO calculations.

Diastereoselective, Arbuzov-like dealkylation reactions involving dimethyl *t*-butylphosphonite and (η^5-Cp)CoI_2(PPh_2NHC*H(Me)Ph) were confirmed to give two P-C bond cleavage products in addition to two P-chiral metallophosphinates. The formation of isobutene, which provided a strong evidence for the proposed P-C bond cleavage mechanism involving β-elimination, was observed by ^{1}H NMR.

3.4. Experimental

3.4.1. General. All manipulations were performed under nitrogen by using an MBraun glove box (< 1 ppm O_2 / H_2O) or by using standard Schlenk techniques. Spectrograde CCl_4 was dried over 4 Å molecular sieves. (η^5-Cp)CoI(PNH)-(P(O)(OMe)$_2$) ($S_{Co}S_C$; **1a-1**; $R_{Co}S_C$, **1a-2**) and (η^5-Cp)CoI(PNH)(P(O)(Ph)(OMe)) ($S_{Co}R_PS_C$, **1b-1**; $R_{Co}S_PS_C$, **1b-2**; $S_{Co}S_PS_C$, **1b-3**; $R_{Co}R_PS_C$, **1b-4**) were prepared using the literature procedure.[98] HCl gas was purchased from Matheson and used as received. Other experiments were carried out by using the established procedures described in Chapter 2.

3.4.2. X-ray Crystallography. Black crystals of **3a-1** with well defined faces were obtained from methylene chloride / hexane. A fragment was cut and mounted on a glass fibre. All measurements were made on a Rigaku AFC6S diffractometer with graphite monochromated Mo Kα radiation (λ=0.71069 Å), and a 2 kW sealed tube generator. Unit cell parameters and an orientation matrix for data collection, obtained from a least-squares refinement using the setting angles of 24 carefully centred reflections in the range $41.52 < 2\theta < 45.32°$ are given in Table 3-4. The unit cell was identified as monoclinic, space group $P2_1$ (#4) on the basis of systematic absences of 0k0: $k \neq 2n$, on a statistical analysis of intensity distribution and on the successful solution and refinement of the structure. A data set was collected at a temperature of

26 ± 1 °C using the ω-2θ scan technique to a maximum 2θ value of 50.1°. Omega scans of several intense reflections, made prior to data collection, had an average width at half-height of 0.34° with a take-off angle of 6.0°. Scans $(1.57 + 0.30 \tan \theta)°$ were made at a speed of 8.0°/min (in Omega). Weak reflections ($I<10.0\sigma(I)$) were rescanned (maximum of 2 rescans) and the counts were accumulated to assure good counting statistics. Stationary background counts were recorded on each side of the reflection. The ratio of peak counting time to background counting time was 2:1. The diameter of the incident beam collimator was 1.0 mm and the crystal to detector distance was 400.0 mm. The intensity of three representative reflections which were measured after every 150 reflections remained constant throughout data collection indicating crystal and electronic stability (no decay correction was applied). The linear absorption correction coefficient for Mo Kα is 23.9 cm^{-1}. An empirical absorption, based on azimuthal scans of several reflections, was applied which resulted in transmission factors ranging from 0.94 to 1.00. The data were corrected for Lorentz and polarization effects. The data set collected included a complete set of Friedel mates which was included in the analysis of absolute configuration, but excluded from the final rounds of least squares refinement on which the solution is based. The structure was solved by direct methods.[240] All non-hydrogen atoms were refined anisotropically. The hydrogens were located from difference maps and

assigned isotropic thermal parameters 20% greater than those of their bonding partners. They were included but not refined in the last rounds of least squares. All calculations were performed using the TEXSAN crystallographic software package of Molecular Structure Corporation. The absolute configuration of **3a-1** (Figure 3-2) was determined by refining both enantiomers to convergence on the complete data set with anomalous dispersion corrections included. The other enantiomer refined with significantly higher R-values and GOF (0.034, 0.034, 2.50 vs 0.024, 0.022, 1.67) confirming that the absolute stereochemistry assigned is indeed correct. Further confirmation was obtained from a statistical survey of Bijvoet[241] differences using the program BIVOET from the NRCVAX[230] suite.

3.4.3. Preparation of S_{Co}-(η^5-Cp)CoI(PPh$_2$OH)(P(O)(OMe)$_2$) (3a-1). A Schlenk flask was charged with 65.5 mg (0.100 mmol) of $S_{Co}S_C$-(η^5-Cp)CoI-(PPh$_2$NHC*H(Me)Ph)(P(O)(OMe)$_2$) (**1a-1**), 2 mL CH_2Cl_2, 10 mL CCl_4 and a stir bar. Then, with stirring, 2.5 mL (~20 °C, ~1 atm) (*ca.* 0.102 mmol) of dry HCl gas was slowly added at room temperature via syringe. The colour of the reaction mixture gradually changed to brown-green. After 4 h stirring a second 2.5 mL aliquot of dry HCl gas was added. The reaction was then monitored by ^{1}H NMR to determine whether the doublet (1.23 ppm, solvent, $CDCl_3$) corresponding to the C*Me group of

1a-1 had disappeared. A further three portions of HCl gas were necessary for reaction completion. Removal of volatiles under reduced pressure gave a brown-green residue, which was transferred to a glass fritted funnel and washed with CCl_4. A small amount of white precipitate collected in the funnel was identified as $PhC^*H(Me)NH_3^+Cl^-$ by comparison of its ^1H NMR with that of an authentic sample. The washings were collected and dried under oil pump vacuum to give 55.0 mg of **3a-1**, yield 98%.

3.4.4. Preparation of R_{Co}-(η^5-Cp)CoI(PPh$_2$OH)(P(O)(OMe)$_2$) (3a-2). A similar procedure starting from 46.8 mg (0.0703 mmol) of $R_{Co}S_C$-(η^5-Cp)CoI-(PPh$_2$NHC*H(Me)Ph)(P(O)(OMe)$_2$) (**1a-2**) gave **3a-2** (38.1 mg, 96%).

3.4.5. Preparation of $S_{Co}R_P$-(η^5-Cp)CoI(PPh$_2$OH)(P(O)(Ph)(OMe)) (3b-1). A similar procedure starting from 0.2109 g (0.2965 mmol) of $S_{Co}R_PS_C$-(η^5-Cp)CoI-(PPh$_2$NHC*H(Me)Ph)(P(O)(Ph)(OMe)) (**1b-1**) gave 175.0 mg (97%) of **3b-1.**

3.4.6. Preparation of $R_{Co}S_P$-(η^5-Cp)CoI(PPh$_2$OH)(P(O)(Ph)(OMe)) (3b-2). A similar procedure starting from 66.1 mg (0.0929 mmol) $R_{Co}S_PS_C$-(η^5-Cp)CoI-(PPh$_2$NHC*H(Me)Ph)(P(O)(Ph)(OMe)) (**1b-2**) afforded 53.4 mg (95%) of **3b-2**.

3.4.7. Preparation of $S_{Co}S_P$-(η^5-Cp)CoI(PPh$_2$OH)(P(O)(Ph)(OMe)) (3b-3). A similar procedure starting from 20.4 mg (0.0287 mmol) $S_{Co}R_PS_C$-(η^5-Cp)CoI(PNH)-(P(O)(Ph)(OMe)) (**1b-3**), 16.3 mg (93%) (**3b-3**) were obtained.

3.4.8. Preparation of $R_{Co}R_P$-(η^5-Cp)CoI(PPh$_2$OH)(P(O)(Ph)(OMe)) (3b-4). A similar procedure starting from 21.3 mg (0.0299 mmol) $R_{Co}R_PS_C$-(η^5-Cp)CoI(PNH)-(P(O)(Ph)(OMe)) (**1b-4**) afforded 16.8 mg (92%) (**3b-4**).

3.4.9. Reaction of (η^5-Cp)CoI$_2$(PNH) (4) with *t*-BuP(OMe)$_2$. Preparation of (η^5-Cp)CoI(PNH)(P(O)(*t*-Bu)(OMe)) ($S_{Co}R_PS_C$, 6-1; $R_{Co}S_PS_C$, 6-2) and (η^5-Cp)CoI (PNH)(P(O)(OMe)$_2$) ($S_{Co}S_C$, 7-1; $R_{Co}S_C$, 7-2). In a glove box, a solution of 0.2147 g (1.430 mmol) of *t*-BuP(OMe)$_2$ in 10 mL of methylene chloride was added dropwise over 15 min to a stirred deep purple solution of 0.9793 g (1.461 mmol) of **4** in 40 mL of the same solvent. The solution became orange and then slowly turned brown-green. After 1.5 h additional stirring the crude reaction mixture was removed from the glovebox and filtered through a Schlenk filter fitted with a 2-cm Celite pad. A black residue was obtained by removing volatiles under vacuum. Then the residue was dissolved and loaded on a 2-mm silica gel radial thick-layer chromatographic plate. Elution with 3:1 (v/v) benzene / ethyl acetate afforded, in order of decreasing

R_f values, purple starting material **4** (0.4767 g, 48.8%) followed by two brown bands containing **6-1** and **6-2** (0.1213 g, 24.20% and 0.1265 g, 25.17%, respectively, based on the recovered **4**), and two yellow-brown bands containing **7-1** and **7-2** (12.6 mg, 2.58% and 13.3 mg, 2.72%, respectively, based on recovered **4**).

3.4.10. NMR reaction of (η^5-Cp)CoI_2(PNH) (4) with *t*-BuP(OMe)$_2$. In a glove box a 3.63 mg (0.0242 mmol) of *t*-BuP(OMe)$_2$ was added via syringe to a septum capped 5-mm NMR tube which was charged with 16.6 mg (0.0242 mmol) of **4** in 0.6 ml CD_2Cl_2. An instantaneous colour change from deep purple to dark brown was observed. A ^{1}H NMR spectrum of the reaction mixture taken 29 min after mixing the two reactants showed the existence of multiplets at δ 4.66 and 1.73 corresponding to isobutene.

Chapter 4
Synthesis, Structure and Reactivity of (η^5-Cyclopentadienyl) (η^5-Pentamethylcyclopentadienyl) Pentafluorophenyl Chloro Titanium Complexes

4.1. Introduction

Interest in the synthesis of optically active organophosphorus compounds via transition metal-mediated (TMM) chiral induction based on the Arbuzov reaction stems from the recognition of their value for a variety of industrial, biological, and chemical synthetic uses.[269] To this end, systems with different metal coordination environments and phosphorus substituents have been pursued. However, all previous work[98, 170-179, 214, 215] including the work described in chapter 2 and 3 focused on cobalt. This chapter describes work which extends effort to early transition metals. All the cobalt systems studied suffer from limited reactivity with respect to nucleophilic substitution at phosphorus which sharply restricts further synthetic elaboration.

Compared with late transition metals, the early transition metals (groups 3, 4, 5) have relatively few electrons outside a closed shell electron configuration. Nuclei are relatively well screened with low effective nuclear charge and hence the d-orbitals are

expanded with low ionization potentials with the consequence that high valence states containing few or no d electrons are common. Due to these characteristics it can be expected that there are substantial differences in chemical properties between early d - block organometallic complexes and those of the late d - block.[216, 217] Thus, it was anticipated that substituting a late transition metal by an early transition metal would have significant effects on the chiral induction to and reactivity at phosphorus. Nucleophilic substitution at a phosphorus bonded to an early transition metal would be easier than nucleophilic substitution at a phosphorus bonded to a late transition metal with the same oxidation state since an early transition metal usually contains few or no d electrons.

Titanium was chosen because of its position in the periodic table (one of the earliest transition metals), its high abundance (inexpensive), relatively low toxicity, and its relative inertness toward redox processes. It is also possible that its reactivity and selectivity can be adjusted by ligands.[39, 92, 270] The chirality of optically active titanium complexes can be ligand or metal based.[39, 92] Examples[39, 271] from each category are given in Scheme 4-1. Although the former type of titanium complexes are more common,[39] the latter type was chosen in the present study since the Arbuzov reaction of interest occurs at the metal, and metal-delivered chirality may exert considerably

more influence on the stereochemical outcome of the reaction under study than ligand-delivered chirality.[92, 272]

ligand-based chirality metal-based chirality

Scheme 4-1. Examples of two types of chiral titanium complexes

The chiral-at-metal target complex (η^5-cyclopentadienyl)(η^5-pentamethylcyclopentadienyl) pentafluorophenyl chloro titanium, CpCp*TiCl(C_6F_5) (Cp*=C_5Me_5, **5**), was designed based on several considerations. It is commonly believed that substitution of η^5-cyclopentadienyl ligand by the η^5-pentamethylcyclopentadienyl group can increase the solubility of Cp-based metal complexes and introduce larger steric effects.[41, 43] In order to obtain a stable stereogenic titanium centre and to enhance the electrophilicity of titanium which will favour the formation of a phosphonium intermediate in a proposed Arbuzov reaction (Scheme 4-5), a strong electron-withdrawing perfluoroaryl group,[41, 273-277] which can stabilize its corresponding metal complexes, was introduced in the model complex investigated. In addition, the

introduction of a perfluorophenyl group provides an additional investigation tool or ^{19}F NMR "handle" which is more sensitive to both its local and distal electronic environment[278] than ^{1}H NMR. Moreover, stripping of chlorine from the new chiral-at-titanium complex CpCp*TiCl(C_6F_5) (5), will afford a hydrocarbyl group 4 metallocene cation, CpCp*Ti(C_6F_5)$^+$, which is a potential Ziegler catalyst.[218] The presence of C-F bonds in the cation species provides a potentially useful internal Ti···F-C interaction which can result in an appreciable protection of the catalyst centre in the dormant stage but allow for low activation barrier decomplexation routes to be followed when necessary, *e.g.*, upon the addition of an olefin monomer. This chapter will focus on the synthesis, structure and reactivity of CpCp*TiCl(C_6F_5) (5) towards Arbuzov reactions, and its possible Ti···F-C interaction.

4.2. Results and discussion

4.2.1. Synthesis and characterization of (R,S_{Ti})-CpCp*TiCl(C_6F_5), 5. Since complexes of some transition metals (*e.g.*, Ti(IV)) in high oxidation states are prone to reduction with Cp*Li (Cp*=C_5Me_5), preparation of the new target complex (R,S_{Ti})-CpCp*TiCl(C_6F_5) (5) started from trivalent $TiCl_3$ (Scheme 4-2). Refluxing of $TiCl_3$,

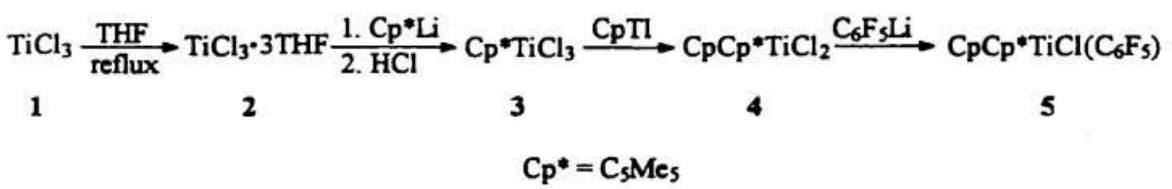

Scheme 4-2. Synthesis of CpCp*TiCl(C_6F_5) (5)

(1) for 24 hours in THF led to the formation $TiCl_3 \cdot 3THF$ (2).[279] Reaction of 2 with Cp*Li[280] followed by oxidation with HCl afforded Cp*$TiCl_3$ (3).[281] Sublimed 3 was reacted with an equimolar amount of CpTl in benzene at room temperature to give the desired mixed-ring complex CpCp*$TiCl_2$ (4) in quantitative yield.[282] The final complex, CpCp*TiCl(C_6F_5) (Cp*=C_5Me_5) (5), was prepared by reacting 4 with C_6F_5Li. Crystals suitable for X-ray analysis were obtained by slow diffusion of hexane into a CH_2Cl_2 solution of 5. The complex was also characterized by ^1H, ^{13}C, ^{19}F NMR, FT-IR, FAB MS as well as elemental analysis.

The infrared spectrum of compound 5 showed an absorption (ν_{C-H}) of a Cp ring at 3020 cm^{-1}. Of particular interest was the ^1H NMR spectrum of 5 which showed a doublet at 6.18 ppm with coupling constant of 1.1 Hz for the Cp group in addition to a sharp singlet corresponding to the Cp* group at 1.93 ppm. ^1H NMR was measured at different field strengths (7 T and 7/3 T) to verify that the observed "doublet" was

in fact due to *J*-coupling. This small coupling could be attributed to weak interaction between the Cp protons and one of two *ortho*-fluorine atoms of the perfluorophenyl group via a through-space interaction although a through-bond ^5J (H-C-Ti-C-C-F) coupling could not be ruled out entirely.

Another interesting feature of **5** was its ^{19}F NMR spectrum. At room temperature, it consisted of five distinct signals of equal intensity instead of the more usual three line pattern. This observation indicated a non-equivalent environment for each fluorine atom on the perfluorophenyl ring and implied that no rotation of the perfluorophenyl ring around the Ti-C_6F_5 bond occurred. A series of high temperature ^{19}F NMR spectra were measured in order to determine the coalescence temperature and activation parameters for this process. Unfortunately, high temperature ^{19}F NMR spectra measured at the highest temperature available (140 °C), did not show any visible change in comparison with the spectrum measured at room temperature, which suggests that the Ti-C_6F_5 rotation bond is still frozen at 140°C. The energy barrier is, accordingly, rather high. MMX and EHMO study on this barrier is presented in section 4.2.3. The energy barrier regarding Ti-C_{ipso} rotation in isostructural titanocene derivatives will be discussed in Chapter 5.

As observed for other pentafluorophenyl derivatives of metals,[283] the chemical shifts (-105.10, -112.37 ppm) of the *ortho* fluorine atoms in compound **5** are shifted to low field compared with those for the *para* fluorine atom (-158.87 ppm) and the *meta* fluorine atoms (-161.66, 164.46 ppm) in compound **5**. This could be explained by larger paramagnetic shifts on *ortho* fluorine atoms.[283]

4.2.2. X-ray structure of 5. Relatively few structurally characterized chiral-at-metal titanocene complexes containing a titanium-aryl bond have been reported [CpCp'Ti(OAr)(X) (Ar = 2,6-MeC_6H_3; Cp' = 1-Me-3-$^iPrC_5H_3$, X = Cl,[284] NCS;[285] Cp' = 1-Me-3-$C(Me)_2PhC_5H_3$, X= Cl;[94] Cp' = 1-Me-2-$^iPrC_5H_3$, X = Cl[286]) and CpTi(Ind)(Cl)(CH_2SiMe_3) (Ind = indenyl[287])]. For this reason and to investigate the structure of the ground state conformation, a single crystal X-ray analysis was performed on compound **5**. The data is as summarized in Table 4-1. Two distinct molecules (**5a** and **5b**), differing slightly in conformation were found in the asymmetric unit cell. The numbering schemes are depicted in Figure 4-1 and Figure 4-2, respectively. The relatively high *R* index is due to the fact that two molecules are in the asymmetric unit and one has a disordered Cp* group while the other has a disordered Cp group. Atomic coordinates, isotropic thermal parameters, bond distances as well as bond angles are presented in Tables 4-2, 4-3, and 4-4,

respectively. The molecular structures for both molecules in the asymmetric unit can be described formally as distorted pseudotetrahedral with a chlorine atom, a carbon atom of the perfluorophenyl group, and centroids of Cp and Cp* rings around the titanium atom. For the first molecule (**5a**) in the asymmetric unit, the angle CT(1)-Ti(1)-CT(2), where CT(1) is the centroid of Cp ring and CT(2) is the centroid of Cp* ring, is 135.1°. This is virtually the same as that in $Cp(C_5Ph_5)TiCl_2$ (134.9°),[288] larger than the value found in $CpCp^*TiCl_2$ (**4**, 132°),[282, 289] $Cp(C_5Bz_5)TiCl_2$ (133.6°),[288] and in $(CpR)_2TiCl_2$ (131.02 - 132.9°),[290] but smaller than that observed in $(C_5HMe_4)_2TiCl_2$ (139.0°).[291] The Cl(1)-Ti(1)-C(16) bond angle is 98.8(7)°, which lies in the range of 97.6 - 102.0° for $(isodiCp)_2TiCl(C_6F_5)$[292] but is larger than the Cl-Ti-Cl angle observed for $(C_5HMe_4)_2TiCl_2$ (94.2(1)°),[291] various $(\eta^5\text{-}RCp)_2MCl_2$ complexes (92.5 - 96.1°),[290, 293] $Cp_2TiCl(\mu\text{-}\eta^1{:}\eta^6\text{-}o\text{-}FC_6H_4)Cr(CO)_3$ (93.6°), and $Cp_2TiCl(\mu\text{-}\eta^1{:}\eta^6\text{-}p\text{-}CH_3C_6H_4)Cr(CO)_3$.[292, 294, 295] The angles for CT(1)-Ti(1)-Cl(1), CT(2)-Ti(1)-Cl(1), CT(1)-Ti(1)-C(16) and CT(2)-Ti-C(16) are 102.8, 106.3, 104.5, 103.9°, respectively. As observed in $CpCp^*TiCl_2$ (**4**),[282, 289] and $Cp_2Ti(O_2CC_6H_5)_2$[296] the Cp and Cp* rings are in a staggered conformation (Figure 4-3). As expected, the distance from the Cp centroid to the metal increases with the increasing steric demand of the Cp ligand.[297] The shorter value for CT(1)-Ti(1) (2.080 Å) compared to CT(2)-Ti(1) (2.12 Å) reflects that Cp* is a more steric demanding ligand than Cp. These distances are very

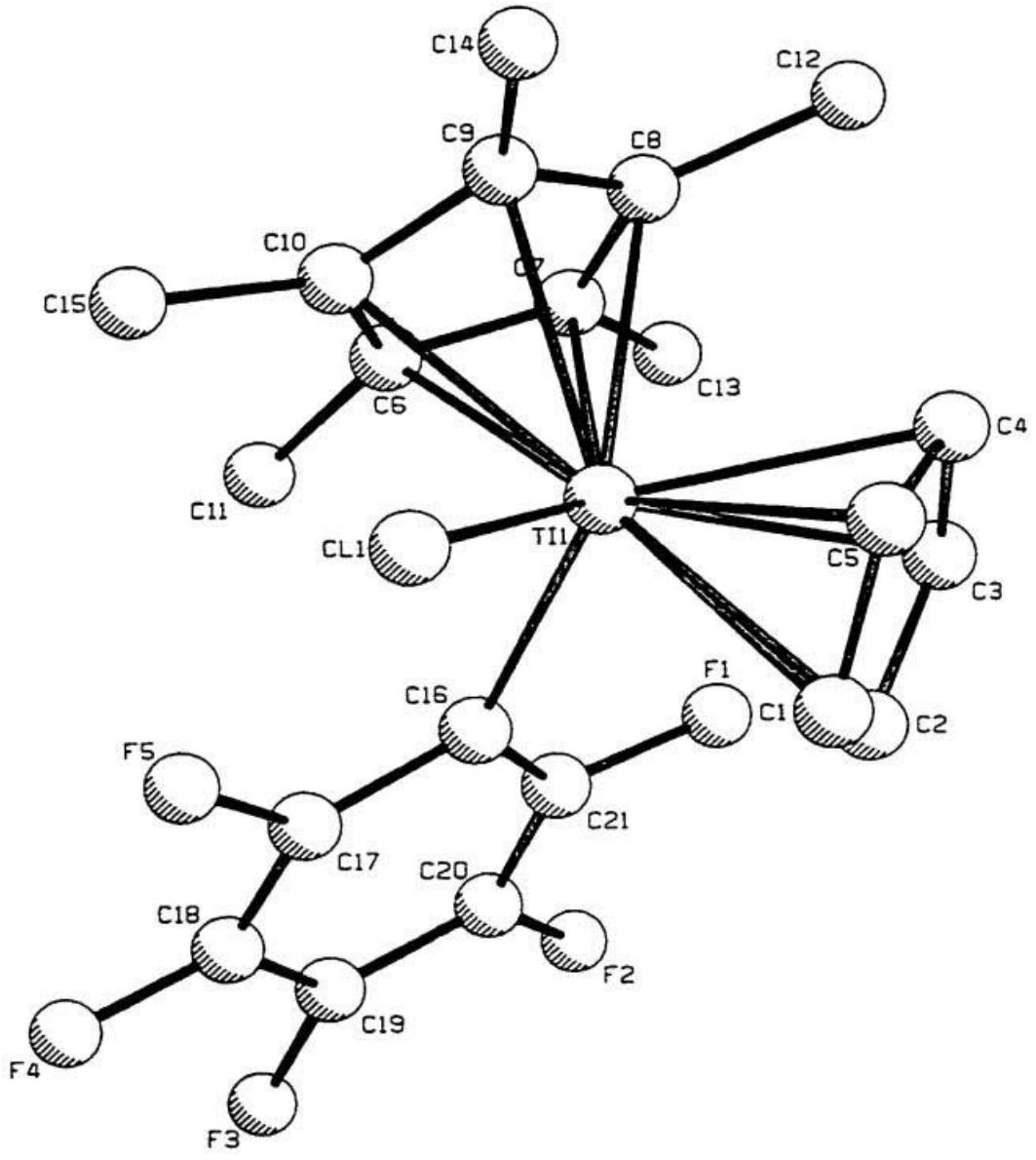

Figure 4-1. Solid state structure of CpCp*TiCl(C_6F_5), (5a)

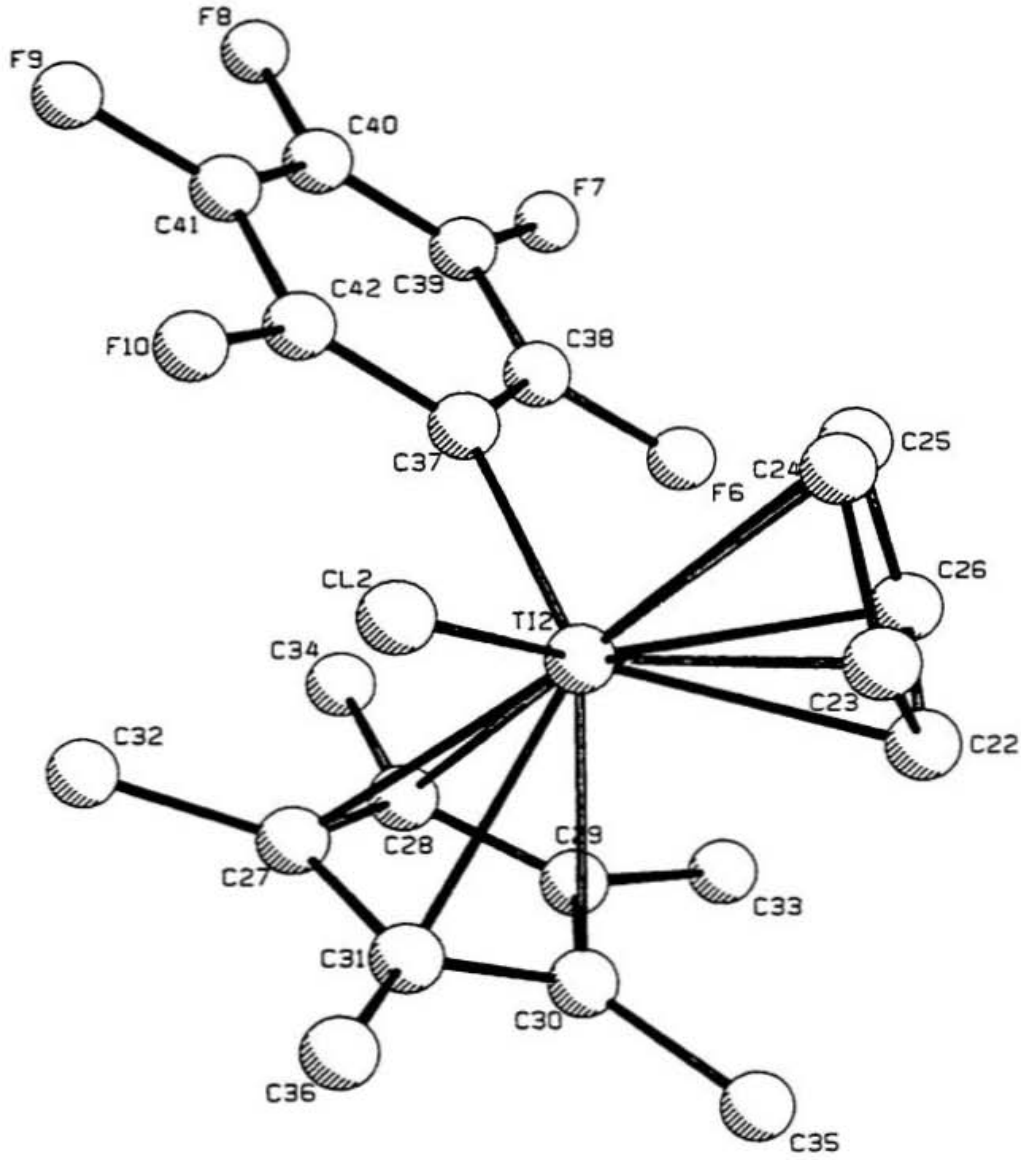

Figure 4-2. Solid state structure of CpCp*TiCl(C_6F_5), (5b)

Table 4-1. Summary of crystallographic data for 5

Empirical Formula	$C_{21}H_{20}F_5ClTi$
Formula Weight	450.73
Crystal Colour, habit	red, rect. plate
Crystal Dimensions (mm)	0.400 X 0.200 X 0.100
No. Reflections Used for Unit Cell Determination (2θ range)	21 (22.3 - 25.7°)
Omega Scan Peak Width at Half-height	0.45
Crystal System	triclinic
Lattice Parameters:	
a (Å)	15.935 (3)
b (Å)	16.422 (4)
c (Å)	8.568 (2)
α (°)	93.03(2)
β (°)	97.63 (2)
γ (°)	61.89(1)
V = (Å^3)	1960.1(8)
Space Group	P1 (#2)
Z value	4
$D_{calc.}$ (g/cm^3)	1.527
F_{000}	920
μ (MoKα) (cm^{-1})	6.16
Scan width (°)	1.68 + 0.30 tanθ
$2\theta_{max}$ (°)	45.1
No. of Reflections Measured	
Total	5375
Unique	5153
R_{int}	0.046
Structure Solution	Direct Methods
Refinement	Full-matrix least-squares
Corrections[a]	Lorentz-polarization Absorption Secondary Extinction (coefficient: 0.70766E-07)
Function Minimized	$\Sigma w(\|Fo\| - \|Fc\|)^2$
Least-squares Weights	$4Fo^2/\sigma^2(Fo^2)$
p-factor	0.01
Anomalous Dispersion	All non-hydrogen atoms
No. Observations (I>2.00σ(I))	2577
No. Variables	318
Reflection/Parameter Ratio	8.10
R[b]	0.116
Rw[c]	0.099
Goodness of Fit Indicator[d]	4.08
Max Shift/Error in Final Cycle	0.00
Maximum Peak in Final Diff. Map	0.79 e$^-$ /Å^3
Minimum Peak in Final Diff. Map	-0.71 e$^-$ /Å^3

[a] cf. Reference[226]. [b] $R=\sum||Fo|-|Fc||/\sum|Fc|$. [c] $R_w=[\sum w(|Fo|-|Fc|)^2/\sum wFo^2]^{1/2}$.
[d] $GOF=(\sum(|Fo|-|Fc|)/\sigma)/(n-m))$ where n= # reflections, m=#variables, and σ^2=variance of (|Fo|-|Fc|).

Table 4-2. Positional parameters for 5a and 5b

atom	x	y	z	B(eq)	occupancy
Ti(1)	0.9844(3)	0.3129(2)	0.3492(4)	3.0(3)	
Cl(1)	1.0951(4)	0.3666(4)	0.3439(7))	5.4(5)	
F(1)	0.882(1)	0.201(1)	0.112(1)	7(1)	
F(2)	0.933(1)	0.0851(9)	-0.117(1)	8(1)	
F(3)	1.103(1)	0.0276(8)	-0.230(1)	8(1)	
F(4)	1.220(1)	0.095(1)	-0.095(1)	7(1)	
F(5)	1.1778(8)	0.2096(9)	0.139(2)	6(1)	
C(16)	1.025(1)	0.213(1)	0.143(2)	3(2)	
C(17)	1.110(2)	0.183(2)	0.077(3)	4(2)	
C(18)	1.139(2)	0.123(2)	-0.039(3)	4(2)	
C(19)	1.077(2)	0.089(2)	-0.110(3)	5(2)	
C(20)	0.993(2)	0.117(1)	-0.052(3)	5(2)	
C(21)	0.970(2)	0.176(1)	0.068(3)	4(2)	
Ti(2)	0.4685(3)	0.3284(2)	0.2376(4)	3.0(3)	
Cl(2)	0.5749(4)	0.3900(4)	0.2984(7)	5.8(6)	
F(6)	0.385(1)	0.1981(8)	0.392(1)	6(1)	
F(7)	0.447(1)	0.079(1)	0.626(2)	10(2)	
F(8)	0.613(1)	0.032(1)	0.806(2)	11(2)	
F(9)	0.720(1)	0.117(1)	0.759(2)	12(2)	
F(10)	0.661(1)	0.240(1)	0.529(2)	9(2)	
C(37)	0.518(2)	0.227(1)	0.441(2)	4(2)	
C(38)	0.469(2)	0.183(1)	0.481(2)	4(2)	
C(39)	0.503(3)	0.117(2)	0.603(4)	7(3)	
C(40)	0.583(3)	0.097(3)	0.693(4)	9(3)	
C(41)	0.637(2)	0.138(2)	0.669(4)	7(3)	
C(42)	0.603(2)	0.200(2)	0.540(3)	5(2)	
C(1)	0.896(1)	0.446(1)	0.177(1)	3.8(5)	
C(2)	0.855(1)	0.3875(9)	0.139(1)	4.7(5)	
C(3)	0.815(1)	0.381(1)	0.271(2)	5.1(5)	
C(4)	0.832(1)	0.435(1)	0.390(1)	5.6(6)	
C(5)	0.882(1)	0.4753(9)	0.332(2)	5.9(6)	
C(6)	1.068(1)	0.155(1)	0.472(2)	2.5(8)	1/2
C(7)	0.974(1)	0.191(1)	0.505(2)	2.1(7)	1/2
C(8)	0.953(1)	0.267(1)	0.603(2)	3.0(8)	1/2
C(9)	1.035(1)	0.279(1)	0.630(2)	6(1)	1/2
C(10)	1.106(1)	0.210(1)	0.550(2)	4(1)	1/2
C(11)	1.121(2)	0.071(2)	0.369(3)	14(2)	1/2
C(12)	0.858(2)	0.327(2)	0.668(3)	8(1)	1/2

Table 4-2. Position parameters for 5a and 5b *(Cont'd.)*

atom	x	y	z	B(eq)	occupancy
C(13)	0.904(2)	0.152(2)	0.444(3)	6(1)	1/2
C(14)	1.046(2)	0.355(2)	0.732(3)	9(2)	1/2
C(15)	1.209(1)	0.197(2)	0.547(4)	11(2)	1/2
C(6A)	1.022(1)	0.168(1)	0.471(2)	3.3(9)	1/2
C(7A)	0.951(1)	0.240(1)	0.547(2)	5(1)	1/2
C(8A)	0.992(1)	0.292(1)	0.627(2)	2.2(7)	1/2
C(9A)	1.088(1)	0.251(1)	0.600(2)	2.4(8)	1/2
C(10A)	1.106(1)	0.175(1)	0.504(2)	2.5(8)	1/2
C(11A)	1.008(2)	0.094(2)	0.369(3)	9(2)	1/2
C(12A)	0.941(2)	0.378(1)	0.727(3)	5(1)	1/2
C(13A)	0.846(1)	0.259(2)	0.544(4)	13(2)	1/2
C(14A)	1.161(2)	0.285(2)	0.665(3)	5(1)	1/2
C(15A)	1.203(1)	0.110(2)	0.444(3)	5(1)	1/2
C(22)	0.307(3)	0.437(2)	0.144(2)	3(2)	1/2
C(23)	0.347(3)	0.489(2)	0.226(5)	4(2)	1/2
C(24)	0.366(3)	0.463(3)	0.386(4)	4(2)	1/2
C(25)	0.338(3)	0.396(3)	0.402(3)	3(2)	1/2
C(26)	0.302(2)	0.379(2)	0.253(4)	3(2)	1/2
C(27)	0.5975(6)	0.2065(7)	0.094(1)	3.9(5)	
C(28)	0.5350(7)	0.1705(6)	0.109(1)	4.4(5)	
C(29)	0.4467(7)	0.2271(7)	0.022(1)	4.9(5)	
C(30)	0.4547(7)	0.2980(6)	-0.047(1)	4.8(5)	
C(31)	0.5479(7)	0.2853(7)	-0.003(1)	5.2(5)	
C(32)	0.7025(7)	0.166(1)	0.169(2)	12(1)	
C(33)	0.3566(8)	0.214(1)	0.006(2)	11(1)	
C(34)	0.559(1)	0.0838(8)	0.205(2)	10.2(9)	
C(35)	0.375(1)	0.3763(9)	-0.153(2)	16(1)	
C(36)	0.589(1)	0.347(1)	-0.052(2)	14(1)	
C(22A)	0.303(3)	0.405(3)	0.205(5)	5(1)	1/2
C(23A)	0.327(3)	0.390(3)	0.368(5)	6(2)	1/2
C(24A)	0.372(3)	0.442(3)	0.428(2)	4(1)	1/2
C(25A)	0.376(2)	0.490(2)	0.302(4)	3.3(9)	1/2
C(26A)	0.334(3)	0.467(3)	0.164(3)	3.5(9)	1/2

Table 4-3. Selected bond distances[a] for 5a and 5b

atom	atom	distance	atom	atom	distance
Ti(1)	Cl(1)	2.32(1)	Ti(2)	C(24A)	2.48(3)
Ti(1)	C(16)	2.29(2)	Ti(2)	C(25A)	2.43(3)
Ti(1)	C(1)	2.42(1)	Ti(2)	C(26A)	2.32(3)
Ti(1)	C(2)	2.42(1)	F(6)	C(38)	1.37(3)
Ti(1)	C(3)	2.39(1)	F(7)	C(39)	1.35(5)
Ti(1)	C(4)	2.37(1)	F(8)	C(40)	1.35(4)
Ti(1)	C(5)	2.38(1)	F(9)	C(41)	1.34(4)
Ti(1)	C(6)	2.50(2)	F(10)	C(42)	1.38(4)
Ti(1)	C(9)	2.44(2)	C(37)	C(38)	1.36(4)
Ti(1)	C(10)	2.43(2)	C(37)	C(42)	1.39(3)
Ti(1)	C(6A)	2.42(2)	C(38)	C(39)	1.41(4)
Ti(1)	C(7A)	2.38(2)	C(39)	C(40)	1.31(5)
Ti(1)	C(8A)	2.40(2)	C(40)	C(41)	1.34(7)
Ti(1)	C(9A)	2.47(1)	C(41)	C(42)	1.41(4)
Ti(1)	C(10A)	2.48(1)	C(1)	C(2)	1.40(3)
F(1)	C(21)	1.36(3)	C(1)	C(5)	1.40(2)
F(2)	C(20)	1.36(4)	C(2)	C(3)	1.40(2)
F(3)	C(19)	1.36(3)	C(3)	C(4)	1.40(2)
F(4)	C(18)	1.29(3)	C(4)	C(5)	1.40(3)
F(5)	C(17)	1.38(3)	C(6)	C(7)	1.40(3)
C(16)	C(17)	1.39(3)	C(6)	C(10)	1.40(3)
C(16)	C(21)	1.37(4)	C(6)	C(11)	1.54(3)
C(17)	C(18)	1.33(3)	C(6)	C(6A)	0.67(3)
C(18)	C(19)	1.41(5)	C(6)	C(10A)	0.82(3)
C(19)	C(20)	1.35(4)	C(6)	C(11A)	1.82(4)
C(20)	C(21)	1.33(3)	C(7)	C(8)	1.40(3)
Ti(2)	Cl(2)	2.34(1)	C(7)	C(13)	1.54(4)
Ti(2)	C(37)	2.27(2)	C(7)	C(6A)	0.77(3)
Ti(2)	C(22)	2.39(3)	C(7)	C(7A)	0.80(3)
Ti(2)	C(23)	2.42(3)	C(7)	C(11A)	1.83(3)
Ti(2)	C(24)	2.46(3)	C(8)	C(9)	1.40(3)
Ti(2)	C(25)	2.45(4)	C(8)	C(12)	1.54(3)
Ti(2)	C(26)	2.41(4)	C(8)	C(7A)	0.64(3)
Ti(2)	C(27)	2.508(9)	C(8)	C(8A)	0.88(3)
Ti(2)	C(30)	2.464(9)	C(8)	C(13A)	1.78(3)
Ti(2)	C(31)	2.46(1)	C(9)	C(10)	1.40(2)
Ti(2)	C(22A)	2.30(4)	C(9)	C(14)	1.54(4)
Ti(2)	C(23A)	2.41(5)	C(9)	C(7A)	1.80(3)

Table 4-3. Selected bond distances[a] for 5a and 5b *(Cont'd.)*

atom	atom	distance	atom	atom	distance
C(9)	C(8A)	0.62(3)	C(22)	C(26A)	0.80(7)
C(9)	C(9A)	0.81(3)	C(23)	C(24)	1.40(6)
C(10)	C(15)	1.54(3)	C(23)	C(22A)	1.80(7)
C(10)	C(6A)	1.83(3)	C(23)	C(24A)	1.84(5)
C(10)	C(9A)	0.74(3)	C(23)	C(25A)	0.75(5)
C(10)	C(10A)	0.68(3)	C(23)	C(26A)	0.68(6)
C(11)	C(11A)	1.66(5)	C(24)	C(25)	1.40(7)
C(11)	C(15A)	1.74(4)	C(24)	C(23A)	1.60(7)
C(12)	C(13A)	1.56(4)	C(24)	C(24A)	0.49(6)
C(13)	C(11A)	1.68(4)	C(24)	C(25A)	0.93(6)
C(13)	C(13A)	1.79(4)	C(25)	C(26)	1.40(4)
C(14)	C(8A)	1.77(4)	C(25)	C(22A)	1.70(4)
C(14)	C(12A)	1.53(5)	C(25)	C(23A)	0.36(6)
C(14)	C(14A)	1.80(4)	C(25)	C(24A)	1.12(7)
C(15)	C(9A)	1.81(3)	C(26)	C(22A)	0.62(6)
C(15)	C(10A)	1.82(4)	C(26)	C(23A)	1.05(5)
C(15)	C(14A)	1.65(4)	C(27)	C(28)	1.40(2)
C(15)	C(15A)	1.67(5)	C(27)	C(31)	1.40(1)
C(6A)	C(7A)	1.40(2)	C(27)	C(32)	1.54(1)
C(6A)	C(10A)	1.40(3)	C(28)	C(29)	1.40(1)
C(6A)	C(11A)	1.54(4)	C(28)	C(34)	1.54(2)
C(7A)	C(8A)	1.40(3)	C(29)	C(30)	1.40(2)
C(7A)	C(13A)	1.54(3)	C(29)	C(33)	1.54(2)
C(8A)	C(9A)	1.40(2)	C(30)	C(31)	1.40(2)
C(8A)	C(12A)	1.54(3)	C(30)	C(35)	1.54(1)
C(9A)	C(10A)	1.40(2)	C(31)	C(36)	1.54(2)
C(9A)	C(14A)	1.54(4)	C(22A)	C(23A)	1.40(6)
C(10A)	C(15A)	1.54(3)	C(22A)	C(26A)	1.40(7)
C(22)	C(23)	1.40(6)	C(23A)	C(24A)	1.40(7)
C(22)	C(26)	1.40(5)	C(24A)	C(25A)	1.40(6)
C(22)	C(22A)	0.78(6)	C(25A)	C(26A)	1.40(5)

[a] Distances are in angstroms. Estimated standard deviations in the least significant figure are given in parentheses.

Table 4-4. Selected bond angles[a] for 5a and 5b

atom	atom	atom	angle	atom	atom	atom	angle
Cl(1)	Ti(1)	C(16)	98.8(7)	C(6)	C(7)	C(8)	108(2)
Cl(1)	Ti(1)	C(1)	78.2(5)	C(6)	C(7)	C(13)	126(2)
Ti(1)	C(16)	C(17)	124(2)	C(7)	C(8)	C(9)	108(2)
Ti(1)	C(16)	C(21)	125(2)	C(7)	C(8)	C(12)	126(2)
C(17)	C(16)	C(21)	112(2)	C(8)	C(9)	C(10)	108(2)
F(5)	C(17)	C(16)	121(2)	C(8)	C(9)	C(14)	126(2)
F(5)	C(17)	C(18)	112(2)	C(10)	C(9)	C(14)	126(2)
C(16)	C(17)	C(18)	127(3)	C(6)	C(10)	C(9)	108(2)
F(4)	C(18)	C(17)	125(3)	C(6)	C(10)	C(15)	126(2)
F(4)	C(18)	C(19)	117(2)	C(7A)	C(6A)	C(10A)	108(2)
C(17)	C(18)	C(19)	117(2)	C(7A)	C(6A)	C(11A)	126(2)
F(3)	C(19)	C(18)	120(3)	C(10A)	C(6A)	C(11A)	126(2)
F(3)	C(19)	C(20)	122(3)	C(6A)	C(7A)	C(8A)	108(2)
C(18)	C(19)	C(20)	118(2)	C(6A)	C(7A)	C(13A)	126(2)
F(2)	C(20)	C(19)	119(2)	C(8A)	C(7A)	C(13A)	126(2)
F(2)	C(20)	C(21)	120(3)	C(9A)	C(8A)	C(12A)	126(2)
C(19)	C(20)	C(21)	121(3)	C(8A)	C(9A)	C(10A)	108(2)
F(1)	C(21)	C(16)	120(2)	C(8A)	C(9A)	C(14A)	126(2)
F(1)	C(21)	C(20)	115(2)	C(10A)	C(9A)	C(14A)	126(2)
C(16)	C(21)	C(20)	125(2)	C(6A)	C(10A)	C(9A)	108(1)
Cl(2)	Ti(2)	C(37)	99.7(7)	C(6A)	C(10A)	C(15A)	126(2)
Ti(2)	C(37)	C(38)	125(1)	C(9A)	C(10A)	C(15A)	126(2)
Ti(2)	C(37)	C(42)	124(2)	C(23)	C(22)	C(26)	108(3)
C(38)	C(37)	C(42)	111(2)	C(22)	C(23)	C(24)	108(4)
F(6)	C(38)	C(37)	119(2)	C(23)	C(24)	C(25)	108(3)
F(6)	C(38)	C(39)	117(3)	C(24)	C(25)	C(26)	108(3)
C(37)	C(38)	C(39)	124(3)	C(22)	C(26)	C(25)	108(4)
F(7)	C(39)	C(38)	117(3)	C(28)	C(27)	C(31)	108.0(9)
F(7)	C(39)	C(40)	123(3)	C(28)	C(27)	C(32)	126(1)
C(38)	C(39)	C(40)	121(4)	C(31)	C(27)	C(32)	126(1)
F(8)	C(40)	C(39)	118(4)	C(27)	C(28)	C(29)	108.0(9)
F(8)	C(40)	C(41)	121(3)	C(27)	C(28)	C(34)	126.0(9)
C(39)	C(40)	C(41)	121(3)	C(29)	C(28)	C(34)	126(1)
F(9)	C(41)	C(40)	121(3)	C(28)	C(29)	C(30)	108(1)
F(9)	C(41)	C(42)	122(4)	C(28)	C(29)	C(33)	126(1)
C(40)	C(41)	C(42)	117(3)	C(30)	C(29)	C(33)	126.0(9)
F(10)	C(42)	C(37)	121(2)	C(29)	C(30)	C(31)	108.0(8)
F(10)	C(42)	C(41)	112(3)	C(29)	C(30)	C(35)	126(1)
C(37)	C(42)	C(41)	127(3)	C(31)	C(30)	C(35)	126(1)
C(2)	C(1)	C(5)	108(1)	C(27)	C(31)	C(30)	108(1)
C(1)	C(2)	C(3)	108(1)	C(27)	C(31)	C(36)	126(1)
C(2)	C(3)	C(4)	108(2)	C(30)	C(31)	C(36)	126.0(9)
C(3)	C(4)	C(5)	108(1)	C(23A)	C(22A)	C(26A)	108(4)
C(1)	C(5)	C(4)	108(1)	C(22A)	C(23A)	C(24A)	108(4)
C(7)	C(6)	C(10)	108(2)	C(23A)	C(24A)	C(25A)	108(3)
C(7)	C(6)	C(11)	126(2)	C(24A)	C(25A)	C(26A)	108(4)
C(10)	C(6)	C(11)	126(2)	C(22A)	C(26A)	C(25A)	108(3)

[a] Angles are in degrees. Estimated standard deviations in the least significant figure are given in parentheses.

close to the relevant distances in $CpCp^*TiCl_2$ (**4**, 2.06 and 2.10 Å)[282, 289] and in $(CpR)_2TiCl_2$ (2.058 - 2.093 Å).[290] The bond distance of Ti(1)-Cl(1) (2.32(1) Å) is slightly shorter than the Ti-Cl bond distance found in $(CpR)_2TiCl_2$ (2.361 - 2.372 Å).[290] The Ti(1)-C(16) bond distance (2.29(2) Å) is slightly longer than those (2.245 to 2.273 Å) for Ti-$C_{ipso}(C_6F_5)$ in $(isodiCp)_2TiCl(C_6F_5)$.[292]

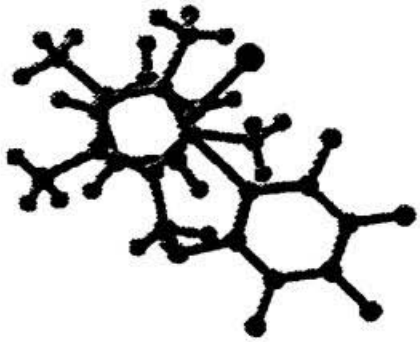

Figure 4-3. Projection (from the crystal structure, 5a) on Cl-Ti-C_{ipso} showing the satggered conformation of Cp and Cp* rings

The most interesting feature of this structure is that the pentafluorophenyl group lies almost in the plane defined by Cl(1), Ti(1) and C(16) (the torsion angle Cl(1)-Ti(1)-C(16)-C(17), 14.7°). This may result from the bent sandwich arrangement of Cp and Cp* groups which forces the pentafluorophenyl group to sit in the Cl-Ti-C_{ipso} plane in order to minimize steric interactions between the C_6F_5 group and Cp*, and between the C_6F_5 group and Cp ligand (Figure 4-5).

The second molecule (**5b**) in the asymmetric unit has nearly the same structural parameters as the first molecule (Table 4-3 and Table 4-4). However, the

conformation of Cp and Cp* rings in **5b** (Figure 4-4) is more nearly eclipsed than staggered as in **5a**. The observation (b) parallels Besancon's finding for CpCp'TiCl(OAr) (Cp' = 1-Me-2-^{i}PrC$_5$H$_3$, Ar = 2,6-Me$_2$C$_6$H$_3$)[286] where two conformations (staggered and eclipsed) in one single crystal were established by X-ray analysis for the racemic form of the compound.

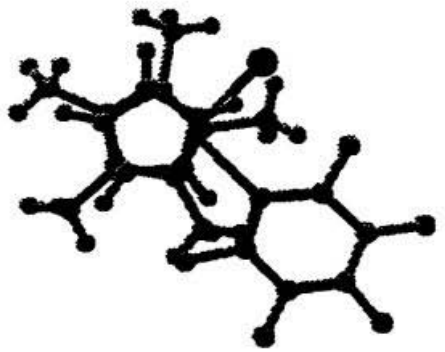

Figure 4-4. Projection (from the crystal structure, 5b) on Cl-Ti-C$_{ipso}$ showing nearly eclipsed conformation of Cp and Cp* rings

4.2.3. Molecular mechanics (MMX) and EHMO Analysis. As mentioned above, NMR data are consistent with a high rotation barrier of the Ti-perfluorophenyl bond in **5**. Molecular mechanics (MMX) modelling has become a valuable tool to assess the importance of steric effects on structure and reactions of inorganic and organometallic compounds.[298] Surprisingly, this method can be used to design catalysts[299] since it can provide insight into reaction mechanism. It has been found that MMX calculated ligand rotation conformational energy profiles are generally in excellent agreement with experimental rotation barriers as well as with experimental ligand conformational preference.[300-305] Molecular orbital calculations (EHMO) at the extended Hückel level have proven invaluable in exploring and understanding the

electronic nature of a variety of inorganic and organometallic compounds.[262, 296, 306-332] In order to more fully characterize the structure and bonding of the complex **5**, and in particular to probe the origin of the high rotation barrier suggested for the perfluorophenyl rotation in **5** by variable temperature ^{19}F NMR, both molecular mechanics modelling and molecular orbital calculations were carried out.

4.2.3.1. Molecular Mechanics (MMX) calculations. Optimization of the geometry of compound **5**, whose starting structure was obtained by use of the free drawing tool in PCMODEL[333, 334] for Windows 95 (version 6.0) resulted in a structure (Figure 4-5 (A)) which is similar to one obtained from the single crystal X-ray crystallographic analysis for the compound (Figure 4-1). Consistent with the X-ray structure, the perfluorophenyl group lies roughly in the plane defined by Cl-Ti-C_{ipso} (Figure 4-5 (B) (C)). The selected titanium-ligand bond distances and interligand bond angles from X-ray and MMX calculation are listed in Table 4-5.

The bond distances Ti-C_{ipso}, Ti-CT(1) and Ti-CT(2) are virtually the same (within 0.08 Å) as those found by X-ray analysis while the calculated Ti-Cl bond distance is *ca.* 0.2 Å longer than those (two asymmetric molecules in the unit cell of **5**) determined by X-ray. The larger relative discrepancy for the Ti-Cl bond might imply

Table 4-5. Comparison of selected crystallographic and MMX data for 5

parameter[a]	X-ray (5a)[b]	X-ray (5b)[c]	MMX[d]
Ti-Cl	2.32(1)	2.34(1)	2.541
Ti-C_{ipso}	2.29(2)	2.27(2)	2.249
Ti-CT(1)[e]	2.080	2.111	2.155
Ti-CT(2)[f]	2.120	2.197	2.199
Cl-Ti-C_{ipso}	98.8(7)	99.7	99.5
CT(1)-Ti-C_{ipso}	104.5	104.8	103.8
CT(2)-Ti-C_{ipso}	103.9	102.7	106.5
CT(1)-Ti-Cl	102.8	104.8	96.4
CT(2)-Ti-Cl	106.3	106.6	107.5
CT(1)-Ti-CT(2)	135.1	131.8	137.2
Cl-Ti-C_{ipso}-C_{ortho}	14.7	13.6	6.3

[a] units for bond distance and bond / torsion angle are Å and °; [b] the first molecule in the asymmetric unit cell; [c] the second molecule in the asymmetric unit cell; [d] a pre-optimized structure was obtained by using free drawing tools in the PCMODEL for Windows 95 (Version 6.0); [e] CT(1) is the centroid of Cp; [f] CT(2) is the centroid of Cp*.

some π donation by chloride. The π-donor ability of chloride has also been demonstrated[335] in other titanium complexes of $(\eta^5\text{-}C_5H_5)_2Ti(OC_2H_5)Cl$ and $[(\eta^5\text{-}C_5H_5)Cl_2Ti]_2O_2C_2(CH_3)_4$ *via* direct comparison of structural parameters from X-ray with each other and with those of Cp_2TiCl_2. The interligand bond angles as well as a dihedral angle are generally well within the range 0.2 - 8.4°, respectively (Table 4-5). The strong correlation between the crystallographic data and the calculated data suggests that the solid state structure and conformation of **5** is essentially dominated

by steric effects.

The dihedral driver built in PCMODEL[334, 336] was employed to compute the conformation energy profile with respect to perfluorophenyl rotation around the Ti-C_{ipso} bond in **5**. The calculated conformation energy profile is illustrated in Figure 4-6. As expected, two maxima corresponding to two perpendicular orientations of the perfluorophenyl ring were found during Cl-Ti-C_{ipso}-C_{ortho} torsion angle change over the range 0 - 360°. The calculated steric rotation barrier is about 22.6 kcal/mol, which is higher than the upper limit of 18 kcal/mol found for hindered rotation about the rhodium-aryl bond in a series of four-legged piano stool complexes $(C_5Me_5)Rh(PR'_3)(R)(X)$.[337]

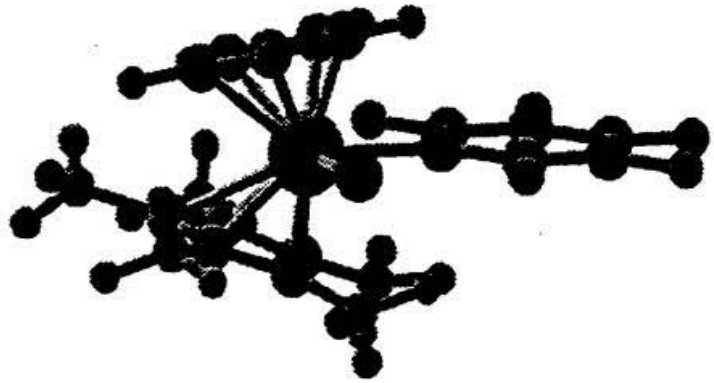

(A)

(B)

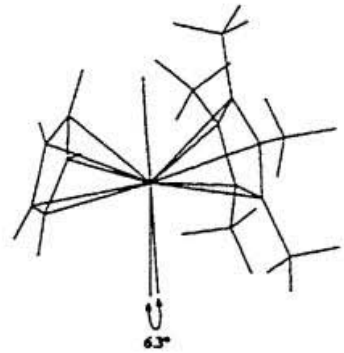

(C)

Figure 4-5. (A) Lowest energy conformer of 5 from PCMODEL (MMX); (B) view of the conformer down the Ti-C_{ipso} bond; (C) stick drawing of (B)

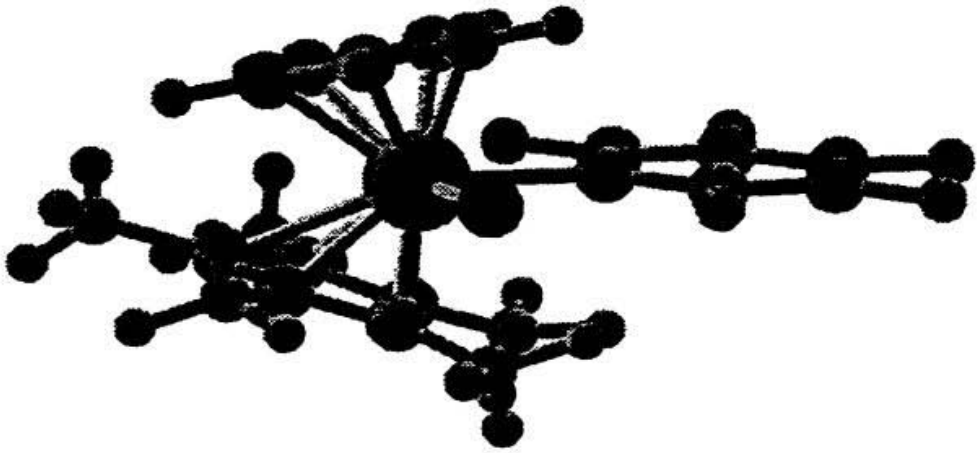

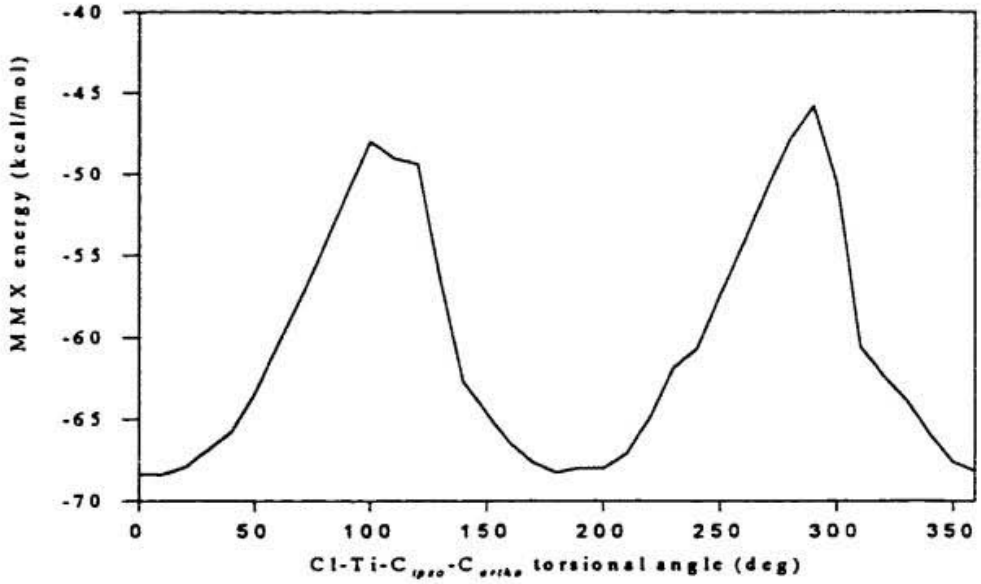

Figure 4-6. Lowest energy (MMX) conformer of 5 with dihedral driven atoms labelled (top); conformational energy profile for perfluorophenyl rotation in 5 (bottom)

4.2.3.2. Molecular Orbital Calculations. In light of the MMX studies of the steric barriers towards rotation of the perfluorophenyl group around the Ti-C_{ipso} bond, molecular orbital calculations at the extended Hückel level were performed to probe the electronic impact on the rotation barrier of the perfluorophenyl group around the Ti-C_{ipso} bond in **5** by use of CACAO.[262] To perform the fragment molecular orbital (FMO) analysis in the EHMO study the molecule **5** was ideally separated as two fragments: the CpCp*TiCl unit and the perfluorophenyl group. The partial orbital interaction diagram and calculated rotational energy profile obtained are shown in Figures 4-7 and 4-8, respectively. The torsional angles of Cl-Ti-C_{ipso}-C_{ortho} (Figure 4-6, top) corresponding to steps 1-15 are at -14.7 (=τ), 0, τ+30, τ+60, τ+90, τ+120, τ+150, τ+180, 180, τ+210, τ+240, τ+270, τ+300, τ+330, τ+360°. The three-dimensional CACAO drawings of HOMOs (MO 61, 62) and LUMOs (MO 63, 64) in compound **5** are depicted in Figure 4-9 with atomic orbital contributions from Cl, Ti, and C_6F_5 showing. Mulliken analysis on molecular orbitals in **5** indicates that the LUMO (MO 61, -7.979 eV) is primarily a mix of FMO 107 (70%) and FMO 46 (24%) (Figure 4-10) while the LUMO (MO 62, -9.070 eV) is fragment 1 like and mainly a mix of FMO 47 (67%) and 48 (28%) (Figure 4-11). The HOMO (MO 63, -11.804 eV) is dominated by FMO 49 (92%) with minor contribution from FMO 110 (4%) (Figure 4-12) while the HOMO (MO 64, -11.905 eV) is principally a sum of

FMO 50 (71%) and FMO 110 (11%) (Figure 4-13). Examination of the low-lying fragment molecular orbitals (FMO 46, 47, 48, Figure 4-14) in the fragment CpCp*TiCl clearly shows that all of them are largely metal-based and comprised primarily of metal d_{xz} with minor d_{yz}; d_{xy} with minor $d_{x^2-y^2}$; and $d_{x^2-y^2}$ with minor out-of-phase contributions from d_{z^2} and d_{xy}, respectively. Further visual inspection of these three orbitals demonstrates that metal based FMO 47 has a major lobe pointing in the +x+y direction while the FMO 48 has a major lobe pointing in the -x+y direction in addition to a slightly twisted, metal d_{xz} like FMO 46 (Figure 4-14). Inspection of the total rotational energy profile in Figure 4-8 shows that it is controlled by the HOMOs (MO 63 and 64). As the C_6F_5 group has a 2-fold axis, the profile exhibits the expected 2-fold rotational barrier, *i.e.*, has a repeat period of 360°/2 (=180°), with three lowest minima (Cl-Ti-C_{ipso}-C_{ortho} torsional angle: ϕ = -14.7°(step 1), -14.7+180° (step 8) and -14.7+360° (step 15)) and two local minima (ϕ = -14.7+90° (step 5), -14.7+270° (step 12)). The Mulliken overlap populations corresponding to perfluorophenyl rotation are documented in Table 4-6.

Mulliken overlap population for the Ti-C_{ipso} bond given in Table 4-6 correlates with E_{rot} and must represent π components for the Ti-C_{ipso} bond in compound **5**. This π interaction is clearly seen in HOMO (MO 63, Figure 4-12) which controls the E_{rot}

(Figure 4-8). Data for the Ti-Cl bond presented in Table 4-6 surprisingly shows that has some contribution to the rotation barrier. In other words, some π bonding character of the Ti-Cl bond is involved in the C_6F_5 rotation around the Ti-C_{ispo} bond, which is not in the direction initially expected. The π contribution of the Ti-Cl bond to the rotation barrier might be introduced through the π conjugation of p_z of Cl, d_{z^2} of Ti, p_z of C_{ipso} and p_z of C_{ortho} (E_{rot} controlling HOMO/MO 63 in Figure 4-9). The π character of the Ti-Cl bond will increase the bond energy and affect the reactivity of Ti-Cl in **5** by making the substitution of Cl more difficult (cf. sections 4.2.4 and 4.2.5). Table 4-6 also shows that at lowest energy conformation (step 1 and step 8) the coordination to titanium from the *ortho* fluorine (Ti···F-C) is negligible.

Table 4-6. Mulliken overlap populations for selected bonds as a function of Ti-C_{ipso} rotation

Step	E_{total}[a]	torsion angle[b]	Ti-C_{ipso}	Ti -Cl	Ti-F_{ortho1}[c]	Ti-F_{ortho2}[d]
1	-2903.6	-14.7°(=τ_0)	0.380	0.770	0.010	0.003
2	-2901.3	0	0.383	0.768	0.009	0.002
3	-2893.7	τ_0 + 30	0.352	0.509	-0.020	0.004
4	-2878.9	τ_0 + 60	0.424	0.518	-0.048	0.008
5	-2890.7	τ_0 + 90	0.444	0.545	-0.026	0.002
6	-2881.8	τ_0 + 120	0.442	0.543	-0.021	-0.029
7	-2897.5	τ_0 + 150	0.388	0.777	0.004	-0.002
8	-2903.6	τ_0 + 180	0.381	0.770	0.003	0.011
9	-2901.1	180	0.384	0.769	0.002	0.010
10	-2893.6	τ_0 + 210	0.352	0.509	0.004	-0.019
11	-2878.0	τ_0 + 240	0.435	0.519	0.008	-0.049
12	-2890.3	τ_0 + 270	0.443	0.545	0.002	-0.026
13	-2882.5	τ_0 + 300	0.442	0.544	-0.026	-0.023
14	-2897.1	τ_0 + 330	0.389	0.776	-0.002	0.004
15	-2903.6	τ_0 + 360	0.380	0.770	0.010	0.003

[a] unit, eV; [b] torsion angle: Cl-Ti-C_{ipso}-C_{ortho1} (Figure 4-6); [c] the *ortho* fluorine connected to C_{ortho1} which has been labelled as C_o in Figure 4-6; [d] the other *ortho* fluorine in Figure 4-6.

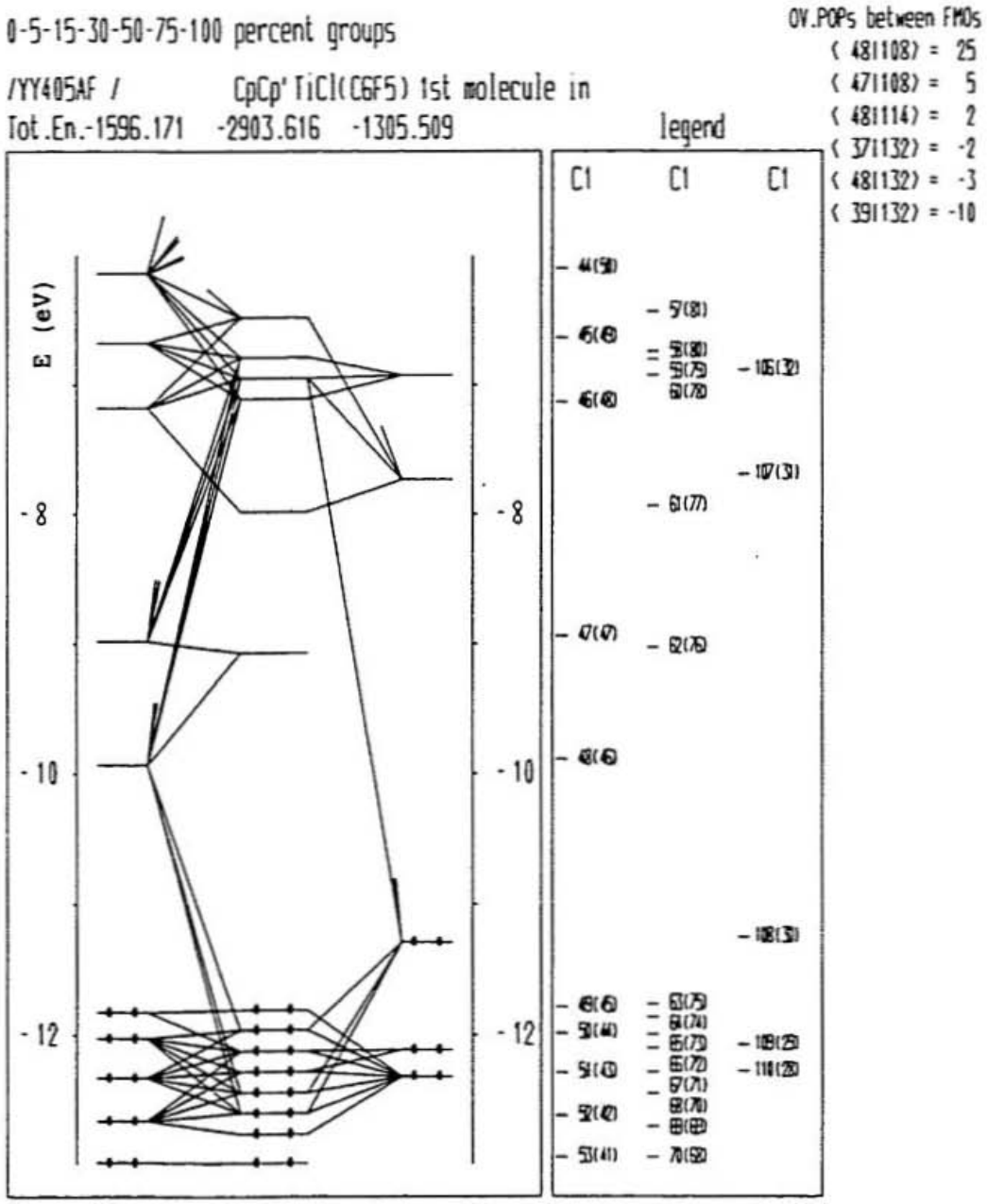

Figure 4-7. EHMO scheme showing the interaction between CpCp*TiCl and C_6F_5 to form 5

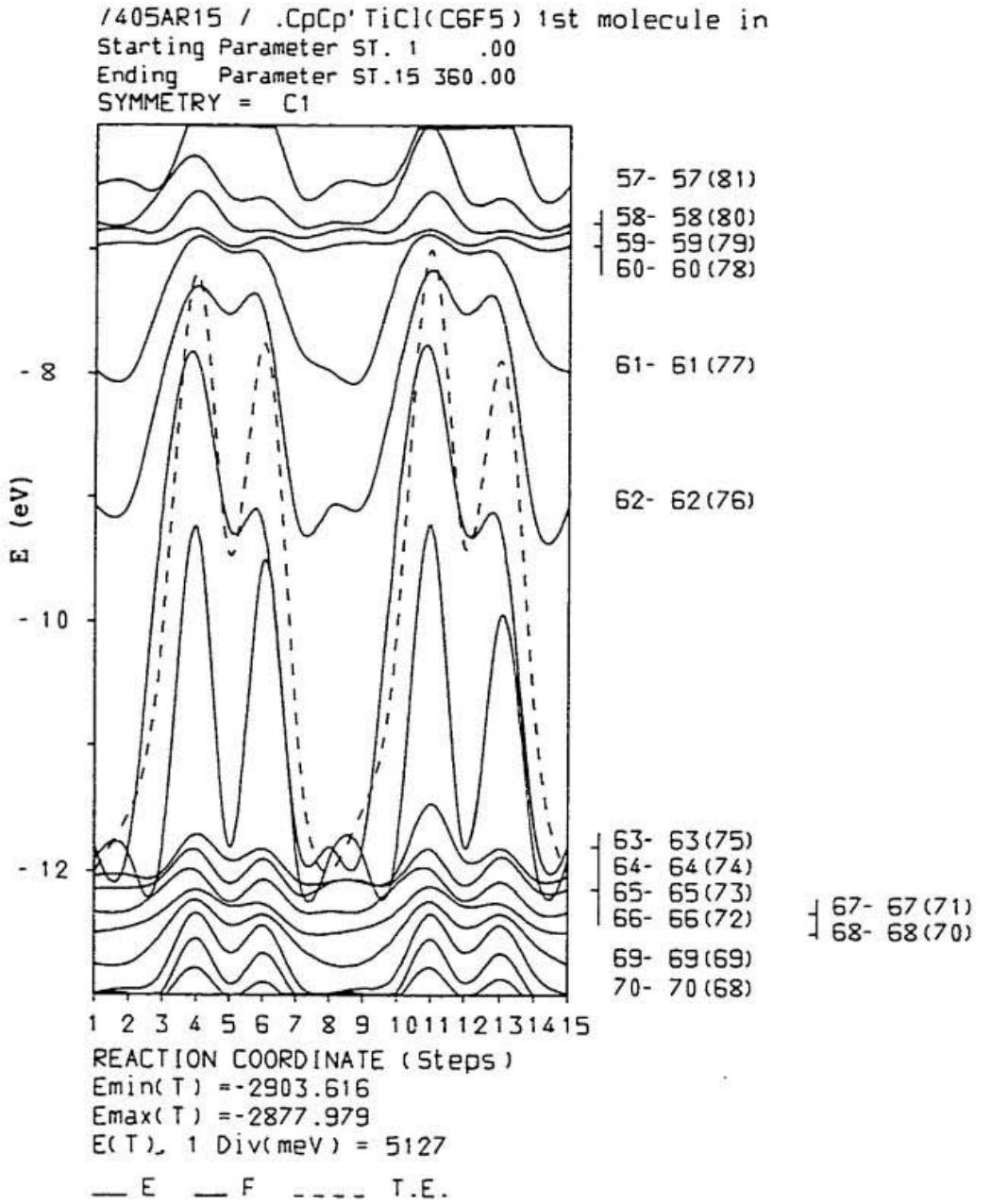

Figure 4-8. Energy profile with respect to the C_6F_5 group rotation around Ti-C_{ipso} for 5

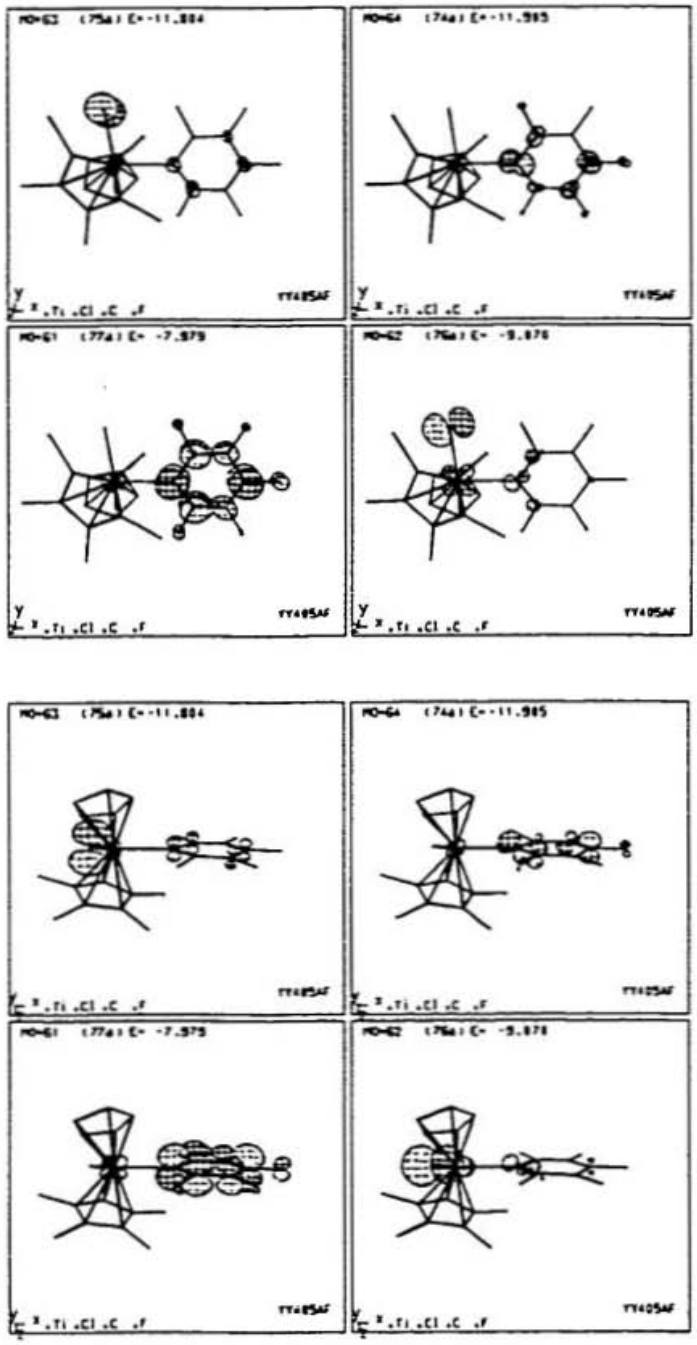

Figure 4-9. LUMO (MO 61, 62) and HOMO (MO 63, 64) for 5, top(top); side(bottom) view

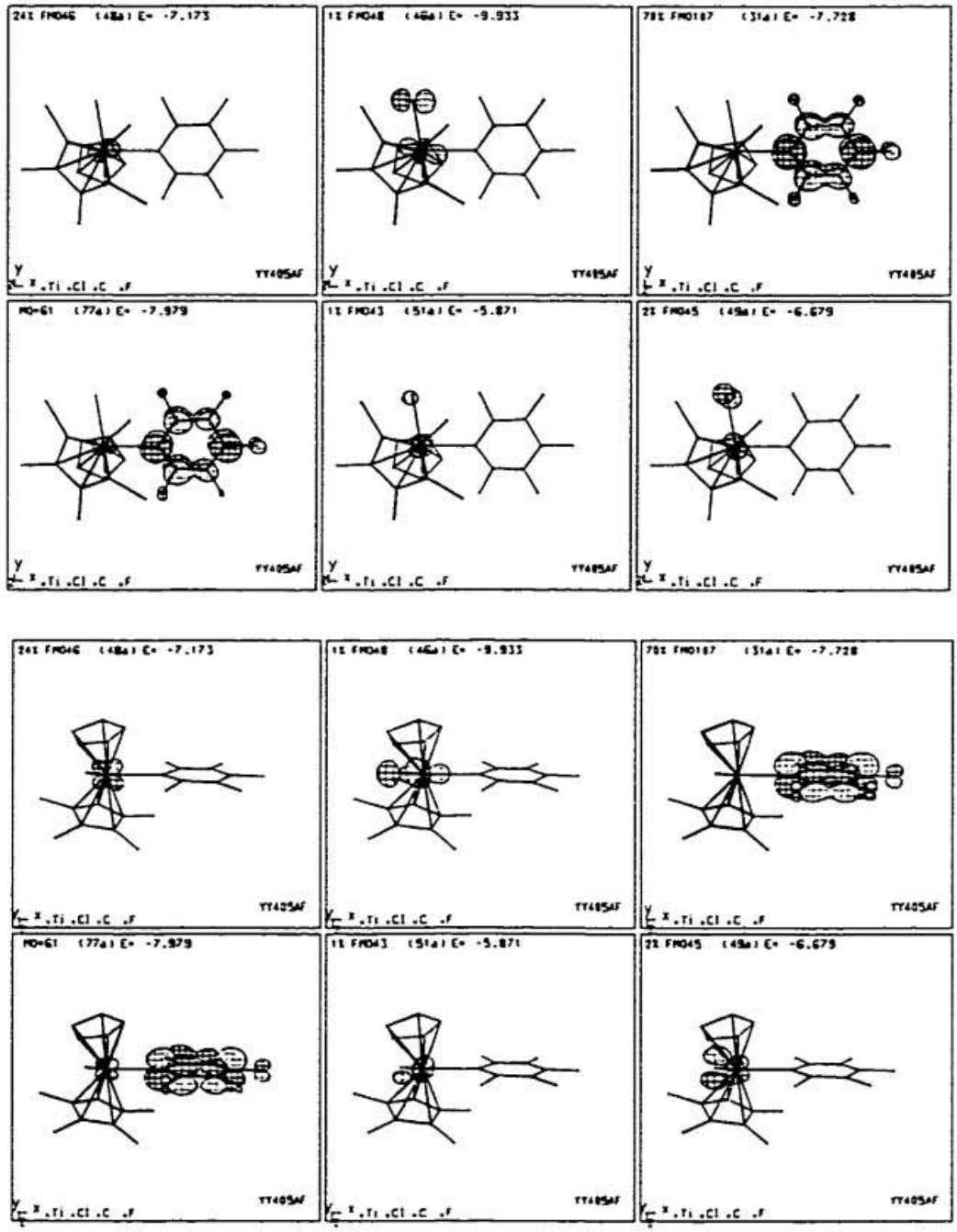

Figure 4-10. Composition of LUMO (MO 61) in terms of FMO, top (top); side (bottom) view

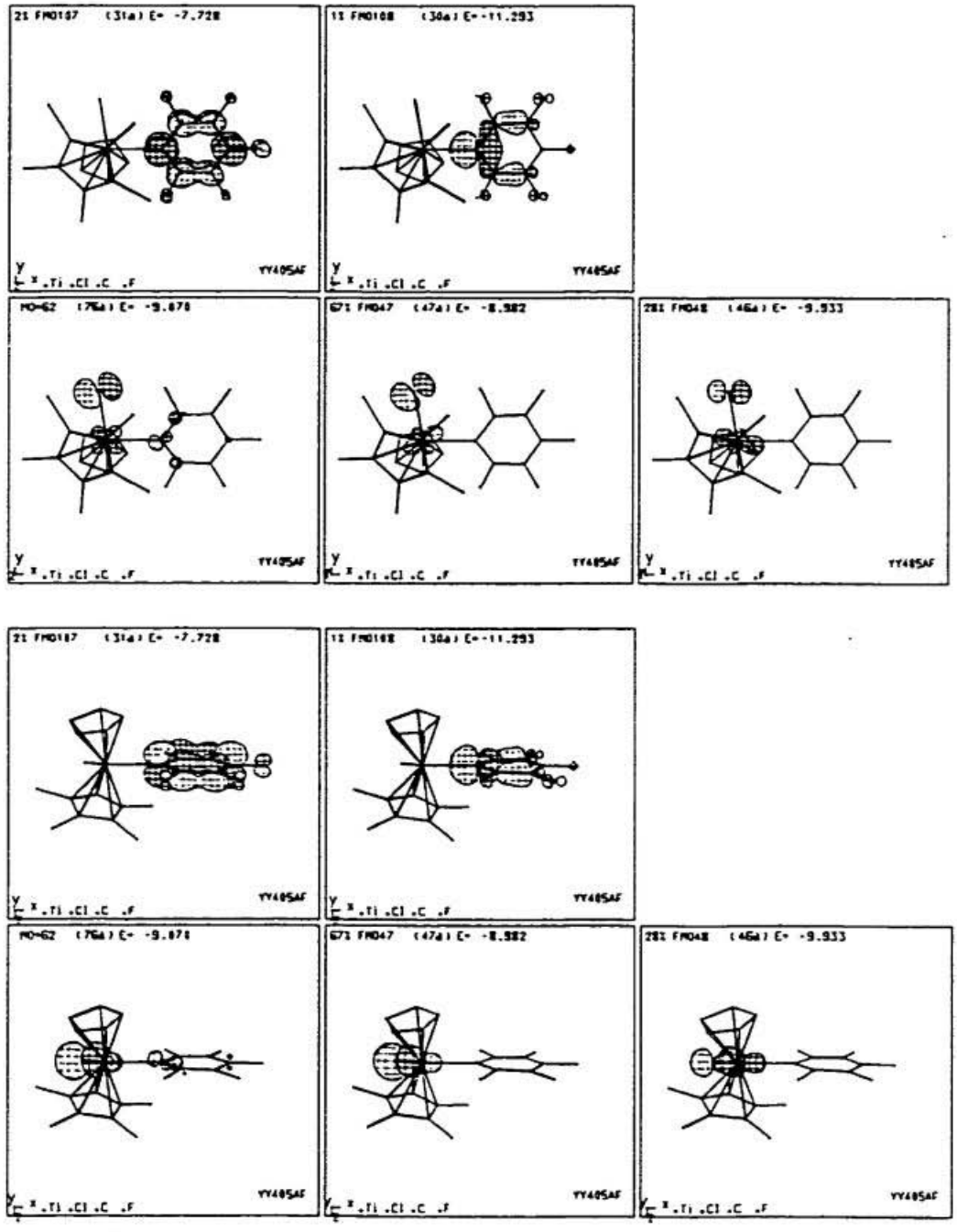

Figure 4-11. Composition of LUMO (MO 62) in terms of FMO, top (top); side (bottom) view

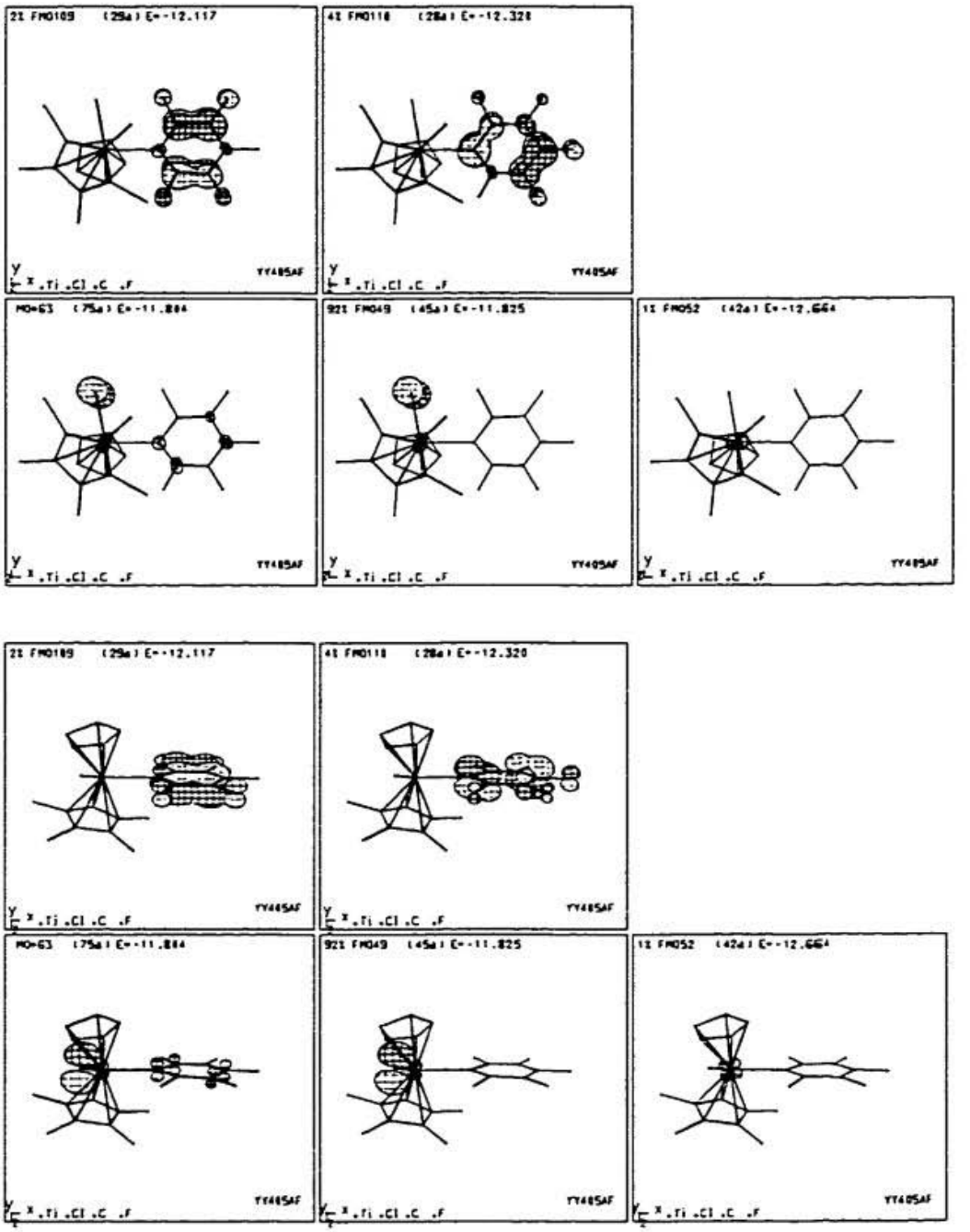

Figure 4-12. Composition of HOMO (MO 63) in terms of FMO, top (top); side (bottom) view

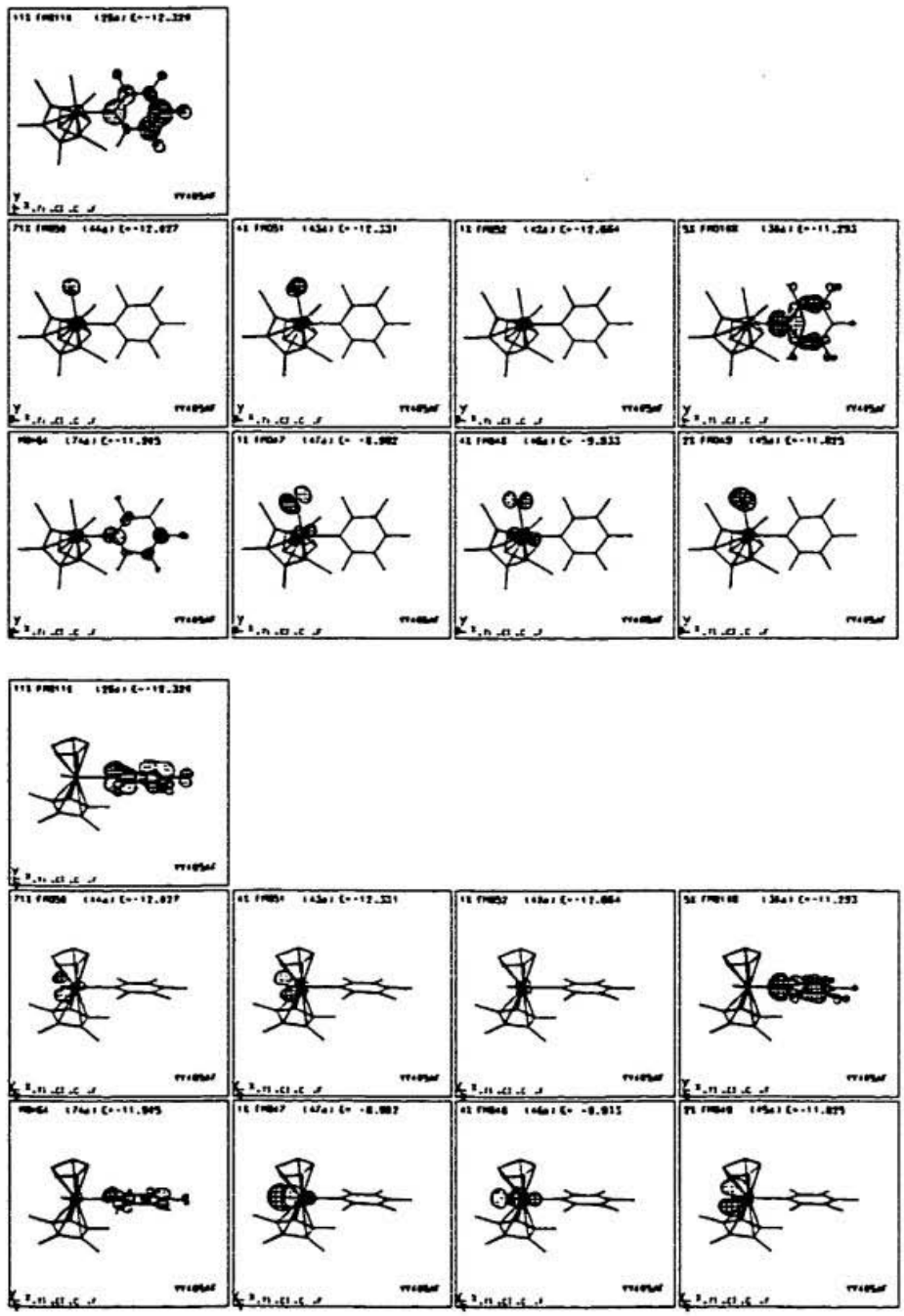

Figure 4-13. Composition of HOMO (MO 64) in terms of FMO, top (top); side (bottom) view

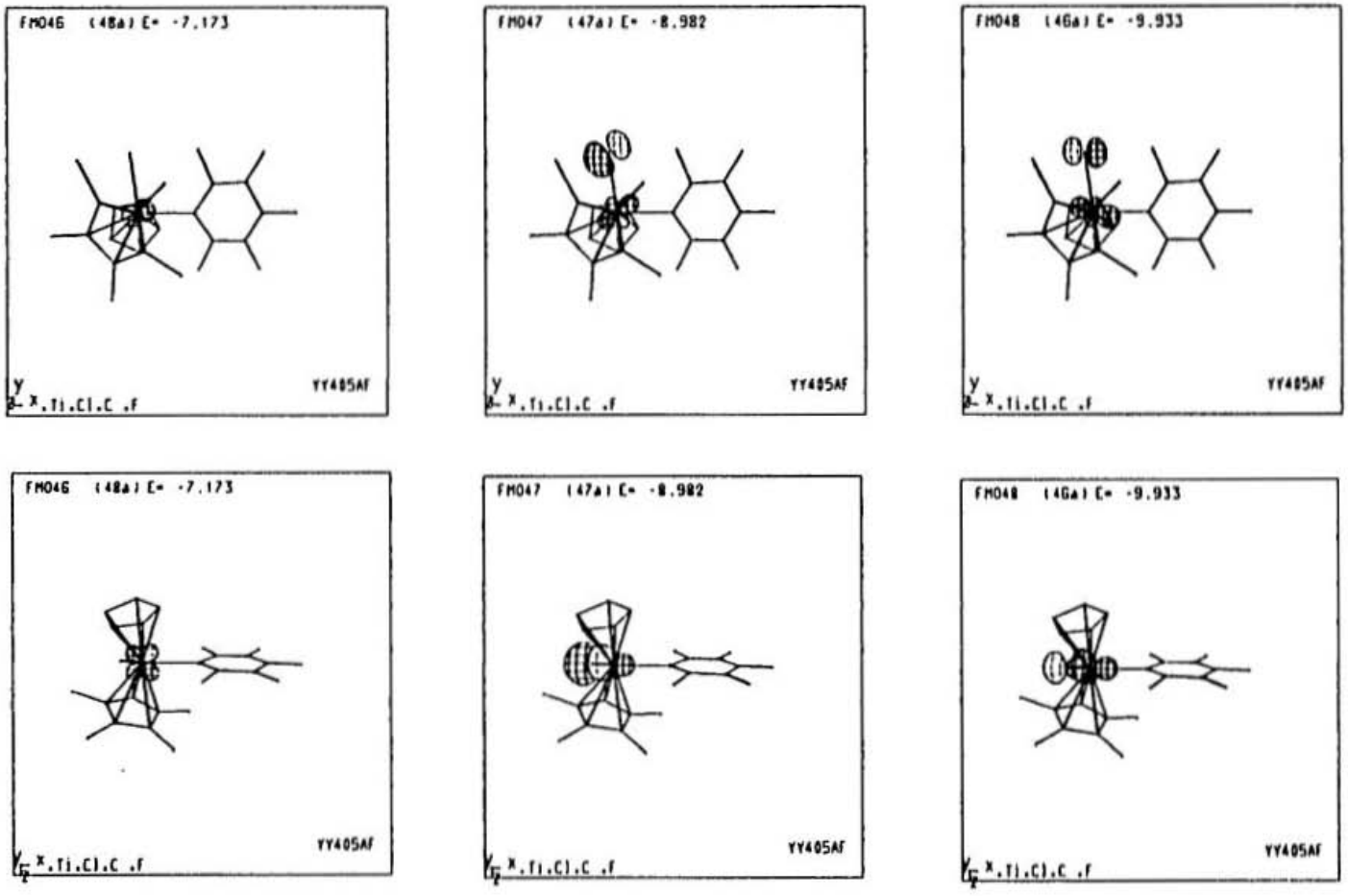

Figure 4-14. Low-lying LUMOs in the fragment CpCp*TiCl, view down z axis (top); view down y axis (bottom)

4.2.4. Attempted resolution of 5. The chiral-at-titanium compound **5** obtained by the procedure describe above is racemic. Resolution of the two Ti-enantiomers was attempted.

4.2.4.1 Chemical resolution. Attempted resolution followed a route described in Scheme 4-3.

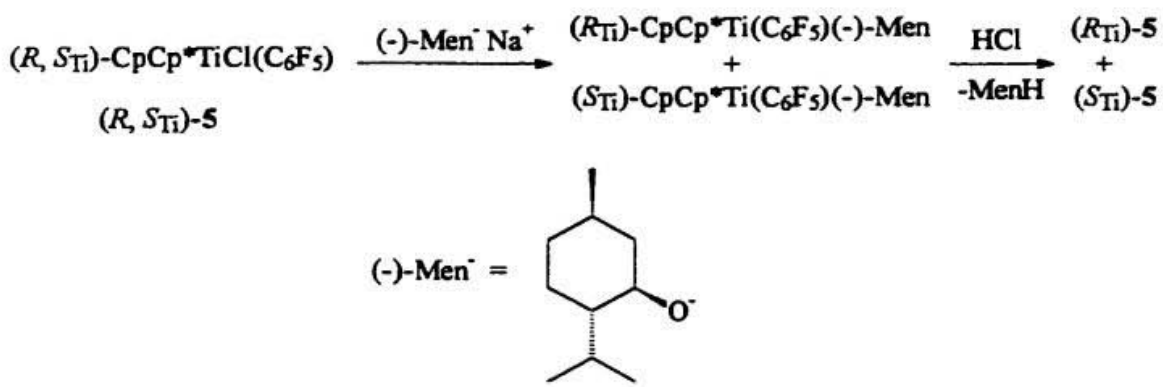

Scheme 4-3. Proposed procedure for resolution of (R, S_{Ti})-5

The resolution reagent used was the sodium salt of easily available (-)-menthol. Reaction was attempted in THF at room temperature and at -78°C, however only starting materials were recovered after workup. The inertness of Cl toward substitution may be attributed to the strong π interaction between Ti-Cl (Table 4-6). This observation also parallels Bochmann's previous observation[338] that no reaction took place between $Cp_2TiMeCl$ and $NaBPh_4$, $AgBPh_4$ or $TlBPh_4$ in THF.

4.2.4.2. NMR resolution. (a) Reaction of **5** with homochiral aminophosphine (*S*)-$PPh_2NHC^*H(Me)Ph$[98] in $CDCl_3$ was probed. However, the doublet at 6.18 ppm and a singlet at 1.93 ppm corresponding to Cp and Cp*, respectively, as well as signals of (*S*)-$PPh_2NHC^*H(Me)Ph$, did not shift after 32 h reaction. This observation suggested that the racemic **5** cannot be resolved by use of the chiral aminophosphine (*S*)-$PPh_2NHC^*H(Me)Ph$ and implies no / very weak interaction between Ti and P (cf. further discussion in section 4.2.5.4).

(b) Another attempted NMR resolution of **5** was attempted by adding homochiral lanthanide NMR shift reagent (+)-$Eu(DPM)_3$ to a solution of **5** in $CDCl_3$. After addition of several portions (totally 40 μL of shift reagent solution), the proton NMR spectrum showed no change, presumably due to the lack of an appropriate functional group (electron donor) in **5** for coordination to Eu in the NMR shift reagent (+)-$Eu(DPM)_3$.

4.2.5. Arbuzov reactivity. Arbuzov reaction of an alkylated nucleophile, such as an alkyl halide, with a phosphorus(III) ester, such as a trialkyl phosphite, generally

$$RX + P(OR')_3 \xrightarrow{\Delta} RP(O)(OR')_2 + R'X$$

Scheme 4-4. Classical Arbuzov reaction

affords an organophosphorus(V) compound with alkyl transfer. The reaction normally requires prolonged heating (Scheme 4-4). When a transition metal halide $L_n[M]X$ is used instead of a classical organic halide RX, a transition metal phosphorus complex will be obtained (Scheme 4-5). Mechanistic investigations for

$$L_n[Ti]X + R_iP(OR')_{3-i} \xrightarrow{\text{step 1}} \{L_n[Ti]\text{-}P(OR')_{3-i}R_i\}^+X^- \xrightarrow{\text{step 2}} L_n[Ti]\text{-}P(O)(OR')_{2-i}R_i + R'X \qquad i = 0,1,2$$

Scheme 4-5. Attempted titanium mediated Arbuzov reaction

reactions involving a transition metal centre demonstrate that the predominant mechanism is an ionic,[98, 138, 144, 147-149, 163, 167, 172-175, 178, 180, 238] two step sequence as shown in Scheme 4-5. Substitution of halide at the transition metal centre affords a cationic complex which is then attacked by the halide ion at the α-carbon of the coordinated phosphorus group leading to a metallo-phosphonate (i = 0), phosphinate (i = 1), phosphine oxide (i = 2) (Scheme 4-5). As discussed in Chapter 1, the transition metal mediated Arbuzov reaction differs from the classical case in that it is "less predictable,"[138] *i.e.*, the reaction does not occur at all for some compounds and rapidly at room temperature for others. Although $PhP(OMe)_2$ is a potentially more interesting substrate than $P(OMe)_3$ in terms of M*→P chiral induction,[98, 172-174] the latter is more reactive.[98, 138, 178] Therefore, the reactivity of **5** and related compounds toward the Arbuzov reaction was tested with $P(OMe)_3$.

4.2.5.1. Reaction of 5 with $P(OMe)_3$. A reaction was carried out by adding an equimolar amount of $P(OMe)_3$ to **5** in $CDCl_3$ in a NMR tube and monitored by ^1H NMR. However, no Arbuzov reaction products $CpCp^*Ti(C_6F_5)P(O)(OMe)_2$ were observed. This may be due to a steric hindrance of Cp^*[297] to the coordination of $P(OMe)_3$ to the titanium centre or difficult substitution of Cl in **5** by $P(OMe)_3$.

4.2.5.2. Reaction of $Cp_2TiCl(C_6F_5)$ with $P(OMe)_3$. To test the idea whether the Cp* group in **5** caused the suppressed reactivity of **5** in an Arbuzov reaction with $P(OMe)_3$, $Cp_2TiCl(C_6F_5)$, where the Cp* group was replaced by another Cp group, was prepared by the established literature method.[339] One equivalent of $P(OMe)_3$ was added via syringe to an orange solution of $Cp_2TiCl(C_6F_5)$ in CH_2Cl_2 at room temperature and reacted for 24 hrs. An orange crystalline solid was obtained after removal of volatiles from the reaction mixture under vacuum. The ^1H NMR spectrum of the crude product shows that the starting material $Cp_2TiCl(C_6F_5)$ (^1H NMR/$CDCl_3$, δ = 6.42 ppm) was recovered. This result suggested that the modified target compound $Cp_2TiCl(C_6F_5)$ might still be too sterically saturated for $P(OMe)_3$ coordination (Scheme 4-5).

4.2.5.3. Reactions of Cp_2TiCl_2 with $P(OMe)_3$. To further reduce the degree of steric

saturation at the central titanium atom in $Cp_2TiCl(C_6F_5)$, commercially available Cp_2TiCl_2 was utilized to perform the desired Arbuzov reaction with $P(OMe)_3$. Reaction of equal molar amounts of $P(OMe)_3$ and Cp_2TiCl_2 was carried out in CH_2Cl_2, THF, and in benzene (20°C, 55°C) with stirring at room temperature. The ^1H NMR in $CDCl_3$ (δ = 6.60 ppm) shows that no reaction occurred in each case. All these observations indicate that chlorides $CpCp^*TiCl(C_6F_5)$, $Cp_2TiCl(C_6F_5)$ and Cp_2TiCl_2 are inert towards reaction with $P(OMe)_3$ under the above conditions.

4.2.5.4. Reactions of Cp_2TiBr_2 with $P(OMe)_3$. The possibility that the low reactivity of the chlorides $CpCp^*TiCl(C_6F_5)$, $Cp_2TiCl(C_6F_5)$ and Cp_2TiCl_2 toward Arbuzov reaction with $P(OMe)_3$ might be improved by using bromide instead of chloride was investigated since bromides generally show a higher reactivity to Arbuzov reaction.[138] Deep red Cp_2TiBr_2[340] was prepared from the reaction of Cp_2TiCl_2 with BBr_3 in CH_2Cl_2. The dibromide was reacted with $P(OMe)_3$ in benzene at room temperature for 3 days. ^1H NMR spectra showed that no reaction had occurred.

All results above show that compound **5** and related titanocene derivatives possess limited substitution chemistry. One explanation is that the π character of the Ti-Cl bond (Table 4-6) makes the substitution difficult. Alternatively, an argument can be

made using Pearson's hard/soft acids/bases principle.[341] Based on Pearson's classification, Ti^{+4} is a hard acid while $P(OMe)_3$ is a soft base. By using Pearson's principle governing the stability of complexes formed between acids and bases, *Hard acids prefer to bind to hard bases and soft acids prefer to bind soft bases*, the presumed intermediate $[CpCp^*Ti(C_6F_5)(P(OMe)_3)]^+Cl^-$ and products (*R*,*S*)-$CpCp^*Ti(C_6F_5)[P(O)(OMe)_2]$ (Scheme 4-5) have low stability. This low stability may make the investigated Arbuzov reactions of L_nTiX with $P(OMe)_3$ an unfavourable process.

4.3. Summary

A new chiral-at-titanium compound $(C_5H_5)(C_5Me_5)TiCl(C_6F_5)$ (**5**) was synthesized and fully characterized by spectroscopic and X-ray single crystal diffraction. Complex **5** is the first structurally characterized chiral-at-titanium compound containing a Ti-aryl bond. Variable temperature ^{19}F NMR shows that the rotation of the perfluorophenyl group around Ti-C_{ipso} bond is frozen, even at 140°C. The high barrier of this rotation and other properties were probed in terms of steric and electronic contributions using molecular modelling (MMX field) and extended Hückel

molecular orbital (EHMO) calculations. The theoretical results were compared with experimental data. The attempted resolution of racemic **5** was unsuccessful. The lack of reactivity of **5** and related compounds towards Arbuzov reactions was explored and interpreted in terms of the π character of the Ti-Cl bond and Pearson's HSAB principle.

4.4. Experimental

4.4.1. General procedure. All manipulations were carried out under dry, purified nitrogen by using standard Schlenk or glove box techniques. Tetrahydrofuran (THF) was predried over KOH, dried over sodium wire, and finally distilled from blue sodium-benzophenone ketyl under nitrogen. Ethyl ether was predried over sodium wire, and distilled from blue sodium-benzophenone ketyl under nitrogen. Pentane was dried over calcium hydride and distilled under nitrogen. Trichlorotris(tetrahydrofuran) titanium (III)[279] (**2**), Cp^*TiCl_3[342] (**3**), $Cp^*CpTiCl_2$[282] (**4**), $Cp_2TiCl(C_6F_5)$,[339] and C_6F_5Li[343] were prepared according to literature procedures. Cp_2TiBr_2 was made by reaction of Cp_2TiCl_2 with BBr_3.[340] Cyclopentadienyl thallium and the NMR shift reagent (+)-Eu(DPM) were purchased from Aldrich and used as

received. VT ^{19}F NMR spectra were recorded on a General Electric GN 300-NB spectrometer operating at 282.37 MHz. Mass spectra (FAB) were recorded by Mass Spectroscopic Laboratory in the Department of Chemistry at University of New Brunswick using a NOBA matrix. Other experiments were conducted by using the procedures described in Chapter 2.

4.4.2. X-ray crystallography. Red crystals of **5** with well defined faces were obtained from methylene chloride / hexane. A rectangular plate crystal having dimensions of 0.400 x 0.200 x 0.100 mm was cut and mounted on a glass fibre. All measurements were made on a Rigaku AFC6S diffractometer with graphite monochromated Mo Kα radiation (λ=0.71069 Å), and a 2 kW sealed tube generator. Cell constants and an orientation matrix for data collection, obtained from a least-squares refinement using the setting angles of 21 carefully centred reflections in the range $22.25 < 2\theta < 25.71°$ are given in Table 4-1. Based on packing considerations, a statistical analysis of intensity distribution and the successful solution and refinement of the structure, the unit cell was identified as triclinic with space group $P\bar{1}$ (#2). The data was collected at 26 ± 1 °C using the ω-2θ scan technique to a maximum 2θ value of 45.1°. Omega scans of several intense reflections, made prior to data collection, had an average width at half-height of 0.45° with a take-off angle

of 6.0°. Scans (1.68 + 0.30 tan θ)° were made at a speed of 4.0°/min (in Omega). Weak reflections ($I < 10.0\sigma(I)$) were rescanned (maximum of 2 rescans) and the counts were accumulated to assure good counting statistics. Stationary background counts were recorded on each side of the reflection. The ratio of peak counting time to background counting time was 2:1. The diameter of the incident beam collimator was 1.0 mm and the crystal to detector distance was 400.0 mm. The intensity of three representative reflections which were measured after every 150 reflections remained constant throughout data collection indicating crystal and electronic stability (no decay correction was applied). The linear absorption coefficient for Mo Kα is 6.2 cm^{-1}. Azimuthal scans of several reflections indicated no need for an absorption correction. The data were corrected for Lorentz and polarization effects. A correction for secondary extinction was applied (coefficient = 0.70766E-07). The structure was solved by direct methods.[240] The non-hydrogen atoms were refined anisotropically or isotropically. All calculations were performed using the TEXSAN crystallographic software package of Molecular Structure Corporation.

4.4.3. Molecular Mechanics Modelling. The MMX calculation was performed on an IBM compatible PC with a Pentium-133 CPU using PCMODEL[334, 336] for Windows version 6.0. The starting structure for minimization was obtained by assembling

related structural components via the PCMODEL drawing tool. The Cp, Cp*, and C_6F_5 groups were constructed as substructures by the free drawing tool and have been separately minimized several times before assembly. The rotational conformational energy profile was calculated utilizing the dihedral driver within PCMODEL. The dihedral angle for perfluorophenyl rotation was defined as Cl-Ti-C_{ipso}-C_{ortho} (Figure 4-6).

4.4.4. Molecular orbital calculations. Extended Hückel calculations were carried out with the EH program contained in the CACAO package (version 4.0).[262] The standard atomic parameters associated were used in all calculations. Although the CACAO package can read directly fractional coordinates generated from X-ray analysis, the fractional coordinates cannot be used to examine variable coordinates which are necessary for routines such as group translation and / or rotation. For the purpose of using free variables, internal coordinates must be used. To this end, a coordinates conversion program CHANGE[344] was written. Although the CHANGE program was mainly designed to translate X-ray coordinates (internal coordinates) it can also set any real / dummy atom to the origin and / or place it in a plane or align a bond to a specific coordinate axis of the Cartesian coordination system. The program allows coordinate transformations in three ways: a) from X-ray to Cartesian; b) from

Cartesian to internal; c) from X-ray to internal. The calculated internal coordinates from X-ray data of **5** via CHANGE were used as input to CACAO for the fragment molecular orbital and rotational energy barrier study. Orbital exponents supplied with CACAO were used for all calculations.

4.4.5. Preparation of CpCp*TiCl(C_6F_5) (Cp*=C_5Me_5) (5). A 250 mL, three-neck, round-bottom flask equipped with a magnetic stirring bar, pressure-equalizing addition funnel, nitrogen inlet and outlet was charged with 3.5211 g (11.03 mmol) CpCp*$TiCl_2$ (**4**) in 100 mL Et_2O and cooled to -78°C. By way of the addition funnel, 11.03 mmol of ether-pentane solution of C_6F_5Li, freshly made from C_6F_5Br and 2.5 M *n*-BuLi in pentane,[343] was added dropwise with stirring. After stirring at -78°C for 2 hours, the reaction mixture was allowed to warm to room temperature and stirred for 30 hours. The precipitated LiCl was removed by filtration. Removal of solvents from the red filtrate under oil pump vacuum afforded 4.8230 g (97%) of compound **5**. Compound **5** obtained in this manner was used without further purification for further reactions. A highly pure sample was obtained by recrystallization using slow diffusion of hexane into a CH_2Cl_2 or acetone of **5**. *Anal.* Found(calcd.): C, 55.81 (55.96), H, 4.28 (4.47). ^{1}H NMR ($CDCl_3$, ppm): δ = 6.18 (d, 5H, Cp, J = 1.1 Hz), 1.93 (s, 15H, C_5Me_5); ^{13}C NMR ($CDCl_3$, ppm): 117.05(Cp), 13.28(Me); ^{19}F ($CDCl_3$;

δ, ppm; J, Hz): -105.10 (pseudo dt, 30.5, 9.4), -112.37 (pseudo dt, 32.0, 9.0), -158.87 (t, 19.9), -161.66 (dddd, 30.5, 19.9, 8.7, 3.1), 164.46 (dddd, 32.0, 19.9, 9.6, 3.1). MS (Fast Atom Bombardment), (*m/e*): 450 (M^+), 415 (M^+ - Cl), 385 (M^+ - Cp). M.P.:193.5-195.3°C.

4.4.6. Reaction of 5 with the sodium salt of (-)-Menthol. *(a) Reaction at room temperature.* A slurry of 14 mg (0.583 mmol) NaH in 5 mL THF was added to a solution of 48 mg (0.307mmol) (-)-menthol in 10 mL THF and stirred for 2.5 hours. The mixture was then directly filtered through a fritted funnel into a solution of 135.6 mg (0.301 mmol) **5** in 20 mL THF. Solvent was removed under vacuum after overnight reaction. The ^{1}H NMR of the residue showed unreacted **5** and sodium salt of (-)-menthol. *(b) Reaction at -78 °C.* The above reaction was also carried out under -78 °C. The same result was obtained.

4.4.7. Reaction of 5 with (*S*)-PPh$_2$NHC*H(Me)Ph. 8.37 mg (2.74 x 10^{-2} mmol) (*S*)-PPh$_2$NHC*H(Me)Ph and 12.36 mg (2.74 x 10^{-2} mmol) **5** was mixed in *ca.* 0.7 mL $CDCl_3$ in a NMR tube. No change in the NMR spectrum was found after 32 hr reaction at room temperature.

4.4.8. Attempted NMR resolution of 5. Homochiral NMR shift reagent (7.43 mg (10.6 μmol) of (+)-$Eu(DPM)_3$ was dissolved in 0.6 ml $CDCl_3$) was added to a solution of 3.40 mg (7.54 μmol) of **5** in 0.6 mL $CDCl_3$. After each addition (5, 10, 20, 40 μL), a proton NMR spectrum was taken and no change was observed.

4.4.9. Reaction of 5 with $P(OMe)_3$. A reaction in an NMR tube was carried out by adding 1.05 mg (8.46×10^{-3} mmol) $P(OMe)_3$ to 3.81 mg (8.45×10^{-3} mmol) **5** in *ca.* 0.7 mL $CDCl_3$. After a total of eight days, no Arbuzov reaction products $CpCp^*Ti(C_6F_5)(P(O)(OMe)_2)$ were observed via ^1H NMR.

4.4.10. Reaction of $Cp_2TiCl(C_6F_5)$ with $P(OMe)_3$. 24.4 μL $P(OMe)_3$ (*ca.* 0.207 mmol) was added via syringe to an orange solution of 78.8 mg (0.207 mmol) $Cp_2TiCl(C_6F_5)$ in 20 mL CH_2Cl_2 at room temperature. The reaction was stopped after stirring for 24 hrs at room temperature. An orange crystalline solid was obtained after removal of volatiles under vacuum. The ^1H NMR of the residue showed that the starting material $Cp_2TiCl(C_6F_5)$ (^1H NMR/$CDCl_3$, δ = 6.42 ppm) was virtually quantitatively recovered.

4.4.11. Reaction of Cp_2TiCl_2 with $P(OMe)_3$. *(a)* 0.201 mL (*ca.* 1.71 mmol) $P(OMe)_3$

was added via syringe to a red solution of 0.4247 g (1.71 mmol) Cp_2TiCl_2 in 30 mL CH_2Cl_2 with stirring at room temperature. The volatiles were removed after 24 hours under aspirator pressure and the residue was dried under oil pump vacuum. Its ^1H NMR in $CDCl_3$ ($\delta = 6.59$ ppm) showed that the residue was unreacted Cp_2TiCl_2. *(b)* The same result was obtained by running the reaction at room temperature in THF. *(c)* The same result was obtained by running the reaction in benzene at room temperature; or at 55°C for 14 hrs.

4.4.12. Reaction of Cp_2TiBr_2 with $P(OMe)_3$. 80 μL $P(OMe)_3$ (*ca.* 79.6 mmol) was added to a suspension of 0.2281g Cp_2TiBr_2 in 10 mL benzene at room temperature. ^1H NMR spectra of the crude reaction products, taken after 3 hours or 3 days, showed only unreacted starting materials.

Chapter 5

Rotational Barrier and Conformational Preference of a Fluorine Substituted Aryl Group in Titanocene Derivatives: Experimental and Theoretical Approaches

5.1. Introduction

The conformations of a molecule are generally defined as those arrangements of its atoms in space that can be interconverted purely by rotation about single bonds.[345] The study of rotational barriers and conformations has been a long-standing subject of concern to chemists as the magnitude of a rotational barrier is directly related to chemical bonding and stereospecific reactivity.[337, 346] The preferred conformations, identified through conformational analysis, often critically determine the physical, chemical and biological properties of a molecule.[347] In the course of study on chiral organometallic complexes, the chiral-at-metal titanium complex cyclopentadienyl pentamethylcyclopentadienyl pentafluorophenyl titanium chloride CpCp*TiCl(C_6F_5) (1) was prepared and showed some interesting spectroscopic properties (cf. Chapter 4). A variable temperature ^{19}F NMR study on CpCp*TiCl(C_6F_5) (1) concluded that C_6F_5 rotation around Ti-C_{ipso} bond was frozen even at 140°C which implied a rather

high rotational barrier similar to that found for the rotation of the phenyl ligand in the sterically very saturated Ti(IV) metal centre of $Cp^*_2TiCl(Ph)$.[348] The rotational barrier in **1** was also investigated using molecular mechanics (MMX) and molecular orbital methods (EHMO) which suggests that coordination from the *ortho*-fluorine to the titanium centre was negligible although this type of coordination has been observed for other group 4 metal zirconium complexes.[349, 350]

Although it was concluded that steric effects dominate the conformation of **1**, no generalities have been established. To this end, efforts to gain insight into the origin of the rotation barrier around the Ti-aryl bond, and particularly the possibility of coordination from the *ortho*-fluorine to the titanium have been made. As mentioned in Chapter 4, internal fluorocarbon coordination (M···F-C) can be used as a tool for the protection of active catalytic sites and has led to a much increased general interest in the structural features and chemical properties of the M···F-C interaction.[218] In this chapter, o-FC_6H_4 is studied since it lacks a C_2-axis and offers a good choice to study "in" / "out" fluorine orientation (cf. section 5.2.3) in complexes such as $(C_5H_5)(C_5Me_5)TiCl(o\text{-}FC_6H_4)$ (**2**). Also, further isostructural titanocene derivatives with the general formula $(C_5H_5)(C_5R_5)TiX(Ar)$ (R = Me, X = Cl, o-FC_6H_4, (**2**); R = H, X = Cl, Ar = C_6F_5, (**3**), o-FC_6H_4, (**4**); R = H, X = R = C_6F_5, (**5**), o-FC_6H_4, (**6**)) have

been synthesized and examined via a combination of variable temperature NMR, MMX and EHMO approaches, as well as solid state X-ray single crystal analysis.

5.2. Results and discussion

5.2.1. Synthesis of complexes. The numbering scheme of fluorine substituted phenyl titanocene derivatives used in the study of the barrier to rotation of the aryl group about the Ti - aryl bond is presented in Scheme 5-1. Literature methods were

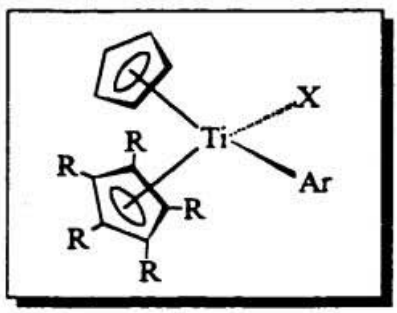

R=Me, X=Cl, Ar=C_6F_5	**(1)**
R=Me, X=Cl, Ar=*o*-FC_6H_4	**(2)**
R=H, X=Cl, Ar=C_6F_5	**(3)**
R=H, X=Cl, Ar=*o*-FC_6H_4	**(4)**
R=H, X=Ar=C_6F_5	**(5)**
R=H, X=Ar=*o*-FC_6H_4	**(6)**

Scheme 5-1. Selected fluorine substituted phenyl titanocene derivatives

followed to make known compounds **3**,[339] **4**,[351] **5**[339] and **6**.[351] A similar strategy, shown in Scheme 5-2, was applied to synthesize the new complex **2**. Treatment $CpCp^*TiCl_2$ with freshly-synthesized *o*-FC_6H_4Li at -78°C in ether, after

$$(C_5H_5)(C_5Me_5)TiCl_2 \xrightarrow{o\text{-}FC_6H_4Li} (C_5H_5)(C_5Me_5)TiCl(o\text{-}FC_6H_4) \quad (2)$$

Scheme 5-2. Synthetic route for complex 2

chromatographic separation (eluent: 1: 4 ether / hexane), gave **2** as dark red crystalline solid in a yield of 66%.

5.2.2. NMR observations on $(C_5H_5)(C_5Me_5)TiCl(o\text{-}FC_6H_4)$ (2). The ^1H NMR spectrum of **2** in $CDCl_3$ showed a sharp singlet for Cp at 6.20 ppm, a sharp singlet for C_5Me_5 at 1.88 ppm and four groups of multiplets for the $o\text{-}FC_6H_4$ group at 7.11, 6.92, 6.76 and 6.66 ppm. The ^{13}C NMR showed signals at 141.03(d, 17.8), 127.68(s), 126.03(d, 8.0), 123.56(s), 119.84(s), 117.21(s, Cp) and 113.76(d, 32.8). The ^{19}F NMR of **2** in $CDCl_3$ at room temperature showed a singlet at -87.66 ppm. This means at room temperature rotations of $o\text{-}FC_6H_4$ around Ti-C_{ipso} are either very fast or very slow (frozen). However the lack of observable splitting of the singlet (-87.66 ppm, $o\text{-}FC_6H_4$) at -60 and 140°C suggested the rotation at room temperature is frozen.

5.2.3. Solid state conformation of $(C_5H_5)(C_5Me_5)TiCl(o\text{-}FC_6H_4)$ (2). Group 4 metallocene complexes Cp_2TiX_2 are formally d^0, 16-electron species. Theoretical calculations show that the LUMO in these complexes is primarily a metal-centered orbital which lies in the MX_2 plane, as shown in Figure 5-1.[315, 352, 353]

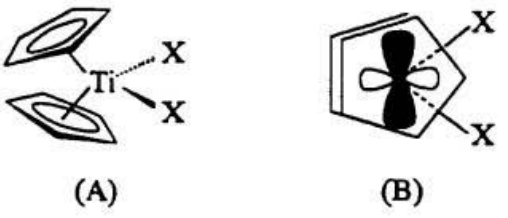

Figure 5-1. Structure (A) and proposed LUMO (B) of Cp_2TiX_2

Strong π donation and ligand to metal charge transfer involving this vacant metal orbital are observed for carboxylate ligands,[296, 354] alkoxide ligands and halides.[335, 355] More interestingly, the η^2-acyl group 4 complexes $Cp_2Ti(COCH_3)Cl$[356] and $Cp_2Zr(COCH_3)Cl$[357] show "O-in" geometry while the acyl in thorium analogue $Cp^*_2Th(COCH_2\text{-}t\text{-}Bu)Cl$[358] trends to be "O-out" (Figure 5-2) implying coordination to the metal based LUMO and coordinative saturation (18 e⁻). In order to determine if the *ortho* fluorine of the $o\text{-}FC_6H_4$ group can coordinate in a similar fashion, an X-ray crystallographic analysis of complex **2** was carried out. An ORTEP diagram showing the molecular structure of **2** is shown in Figure 5-3. Experimental parameters are collected in Table 5-1. The atomic coordinates, intramolecular bond distances and angles are located in Tables 5-2, 3 and 4, respectively. The geometry of the molecule is as expected, pseudotetrahedral, with the Cp and Cp* centroids, Cl and $o\text{-}FC_6H_4$ group each occupying a coordination position around the central metal. The Cp and Cp* rings are slightly staggered in projection on the Cl-Ti-C_{ipso} plane (Figure 5-4). The Ti-CT1 and Ti- CT2, where CT1 and CT2 represent centroids of Cp and Cp*, are 2.071 and 2.089 Å, respectively. They are slightly shorter than corresponding

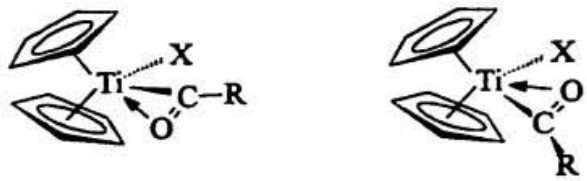

"O-out" η2-acyl "O-in" η2-acyl

Figure 5-2. Two types of η^2-acyl orientations

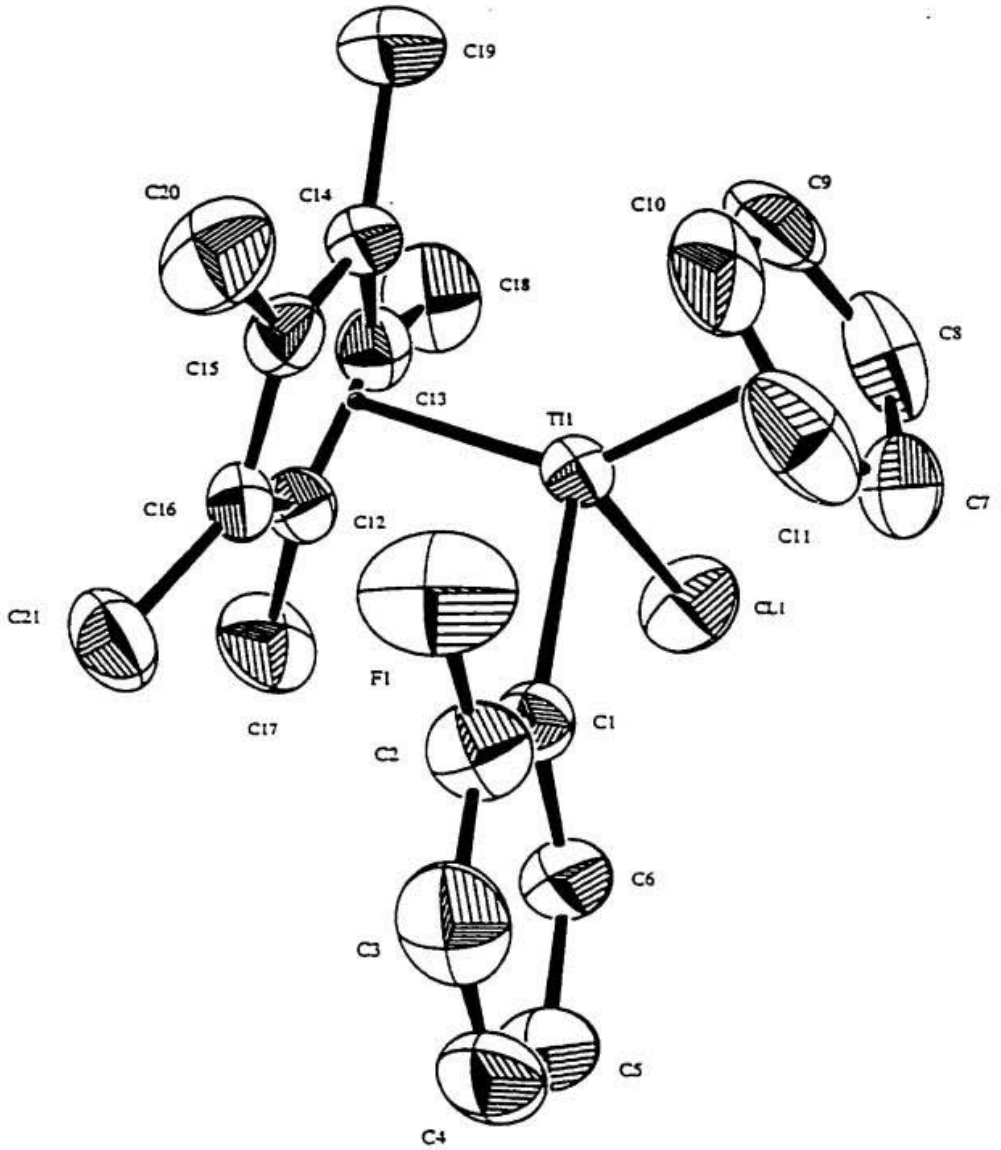

Figure 5-3. ORTEP representation of the molecular structure of CpCp*TiCl(*o*-FC_6H_4) (2)

Table 5-1. Summary of crystallographic data for 2

Empirical Formula	$C_{21}H_{24}ClFTi$
Formula Weight	378.77
Crystal Colour, Habit	red, irregular
Crystal Dimensions (mm)	0.300 X 0.250 X 0.400
No. Reflections Used for Unit Cell Determination (2θ range)	23 (36.4 - 40.9°)
Omega Scan Peak Width at Half-height	0.31
Crystal System	monoclinic
Lattice Parameters:	
a (Å)	8.584(4)
b (Å)	16.309(2)
c (Å)	13.241(3)
β (°)	97.48(2)
V = (Å^3)	1838.0(9)
Space Group	$P2_1/n$ (#14)
Z value	4
$D_{calc.}$ (g/cm^3)	1.369
F_{000}	792
μ (MoKα) (cm^{-1})	6.14
Scan width (°)	1.57 + 0.35 tanθ
$2\theta_{max}$ (°)	50.1
No. of Reflections Measured	
Total	3621
Unique	3388
R_{int}	0.019
Structure Solution	Direct Methods
Refinement	Full-matrix least-squares
Corrections[a]	Lorentz-polarization Absorption Secondary Extinction (coefficient: 0.56385E-06)
Function Minimized	$\Sigma w(\|Fo\| - \|Fc\|)^2$
Least-squares Weights	$4Fo^2/\sigma^2(Fo^2)$
p-factor	0.01
Anomalous Dispersion	All non-hydrogen atoms
No. Observations (I>2.00σ(I))	2565
No. Variables	218
Reflection/Parameter Ratio	11.77
R[b]	0.038
Rw[c]	0.037
Goodness of Fit Indicator[d]	2.38
Max Shift/Error in Final Cycle	0.00
Maximum Peak in Final Diff. Map	0.25 e$^-$/Å^3
Minimum Peak in Final Diff. Map	-0.23 e$^-$/Å^3

[a] cf. Reference[226]. [b] $R=\sum||Fo|-|Fc||/\sum|Fc|$. [c] $R_w=[\sum w(|Fo|-|Fc|)^2/\sum wFo^2]^{1/2}$.
[d] $GOF=(\sum(|Fo|-|Fc|)/\sigma)/(n-m))$ where n= # reflections, m=#variables, and σ^2=variance of $(|Fo|-|Fc|)$.

Table 5-2. Atomic coordinates ($\times 10^4$) and isotropic thermal parameters ($pm^2 \times 10^{-1}$) for 2

atom	x	y	z	B(eq)
Ti(1)	0.60460(6)	0.33539(3)	0.28723(4)	2.39(2)
Cl(1)	0.5251(1)	0.22751(5)	0.17261(7)	4.41(4)
F(1)	0.4541(3)	0.5155(1)	0.3623(2)	6.4(1)
C(1)	0.3970(3)	0.4125(2)	0.2382(2)	2.9(1)
C(2)	0.3548(4)	0.4845(2)	0.2809(2)	4.0(2)
C(3)	0.2227(4)	0.5314(2)	0.2504(3)	5.2(2)
C(4)	0.1208(4)	0.5038(3)	0.1690(3)	5.5(2)
C(5)	0.1539(4)	0.4327(2)	0.1213(3)	4.8(2)
C(6)	0.2880(3)	0.3882(2)	0.1553(2)	3.6(1)
C(7)	0.4421(5)	0.2666(3)	0.3940(3)	5.7(2)
C(8)	0.5754(6)	0.2228(2)	0.3993(3)	6.1(2)
C(9)	0.6973(5)	0.2695(3)	0.4416(3)	6.1(2)
C(10)	0.6353(6)	0.3464(3)	0.4658(2)	6.2(2)
C(11)	0.4771(6)	0.3416(3)	0.4366(3)	6.1(2)
C(12)	0.7376(3)	0.3778(2)	0.1472(2)	2.9(1)
C(13)	0.8429(3)	0.3283(2)	0.2116(2)	3.1(1)
C(14)	0.8795(3)	0.3706(2)	0.3047(2)	3.1(1)
C(15)	0.7945(3)	0.4443(2)	0.2987(2)	3.2(1)
C(16)	0.7099(3)	0.4498(2)	0.1999(2)	2.9(1)
C(17)	0.6797(4)	0.3623(2)	0.0367(2)	5.0(2)
C(18)	0.9165(4)	0.2499(2)	0.1835(3)	5.2(2)
C(19)	1.0120(4)	0.3491(2)	0.3860(3)	5.7(2)
C(20)	0.8176(4)	0.5129(2)	0.3753(3)	5.5(2)
C(21)	0.6311(4)	0.5249(2)	0.1518(3)	4.7(2)

Table 5-3. Bond distances (Å) for 2

atom	atom	distance	atom	atom	distance
Ti(1)	Cl(1)	2.365(1)	C(4)	C(5)	1.367(5)
Ti(1)	C(1)	2.209(3)	C(5)	C(6)	1.386(4)
Ti(1)	C(7)	2.391(3)	C(7)	C(8)	1.342(5)
Ti(1)	C(8)	2.394(3)	C(7)	C(11)	1.364(6)
Ti(1)	C(9)	2.354(3)	C(8)	C(9)	1.355(5)
Ti(1)	C(10)	2.351(3)	C(9)	C(10)	1.416(6)
Ti(1)	C(11)	2.385(3)	C(10)	C(11)	1.365(5)
Ti(1)	C(12)	2.402(3)	C(12)	C(13)	1.411(4)
Ti(1)	C(13)	2.395(3)	C(12)	C(16)	1.401(4)
Ti(1)	C(14)	2.411(3)	C(12)	C(17)	1.504(4)
Ti(1)	C(15)	2.403(3)	C(13)	C(14)	1.412(4)
Ti(1)	C(16)	2.431(3)	C(13)	C(18)	1.496(4)
F(1)	C(2)	1.380(4)	C(14)	C(15)	1.404(4)
C(1)	C(2)	1.372(4)	C(14)	C(19)	1.502(4)
C(1)	C(6)	1.403(4)	C(15)	C(16)	1.415(4)
C(2)	C(3)	1.384(4)	C(15)	C(20)	1.505(4)
C(3)	C(4)	1.373(5)	C(16)	C(21)	1.501(4)

Table 5-4. Intramolecular bond angles[a] for 2

atom	atom	atom	angle	atom	atom	atom	angle
Cl(1)	Ti(1)	C(1)	94.61(8)	C(8)	Ti(1)	C(16)	163.5(1)
Cl(1)	Ti(1)	C(7)	83.6(1)	C(9)	Ti(1)	C(10)	35.0(1)
Cl(1)	Ti(1)	C(8)	77.4(1)	C(9)	Ti(1)	C(11)	55.9(1)
Cl(1)	Ti(1)	C(9)	104.7(1)	C(9)	Ti(1)	C(12)	131.3(1)
Cl(1)	Ti(1)	C(10)	133.4(1)	C(9)	Ti(1)	C(13)	97.5(1)
Cl(1)	Ti(1)	C(11)	116.0(1)	C(9)	Ti(1)	C(14)	79.0(1)
Cl(1)	Ti(1)	C(12)	81.11(7)	C(9)	Ti(1)	C(15)	97.6(1)
Cl(1)	Ti(1)	C(13)	83.49(8)	C(9)	Ti(1)	C(16)	131.2(1)
Cl(1)	Ti(1)	C(14)	115.83(8)	C(10)	Ti(1)	C(11)	33.5(1)
Cl(1)	Ti(1)	C(15)	136.66(8)	C(10)	Ti(1)	C(12)	138.7(1)
Cl(1)	Ti(1)	C(16)	111.08(8)	C(10)	Ti(1)	C(13)	115.8(2)
C(1)	Ti(1)	C(7)	86.0(1)	C(10)	Ti(1)	C(14)	84.6(1)
C(1)	Ti(1)	C(8)	118.2(1)	C(10)	Ti(1)	C(15)	83.9(1)
C(1)	Ti(1)	C(9)	133.1(1)	C(10)	Ti(1)	C(16)	114.8(1)
C(1)	Ti(1)	C(10)	103.5(2)	C(11)	Ti(1)	C(12)	160.7(1)
C(1)	Ti(1)	C(11)	77.3(1)	C(11)	Ti(1)	C(13)	149.1(1)
C(1)	Ti(1)	C(12)	93.2(1)	C(11)	Ti(1)	C(14)	117.4(2)
C(1)	Ti(1)	C(13)	127.2(1)	C(11)	Ti(1)	C(15)	107.3(2)
C(1)	Ti(1)	C(14)	129.4(1)	C(11)	Ti(1)	C(16)	127.0(1)
C(1)	Ti(1)	C(15)	96.5(1)	C(12)	Ti(1)	C(13)	34.22(9)
C(1)	Ti(1)	C(16)	76.1(1)	C(12)	Ti(1)	C(14)	56.5(1)
C(7)	Ti(1)	C(8)	32.6(1)	C(12)	Ti(1)	C(15)	56.6(1)
C(7)	Ti(1)	C(9)	55.2(1)	C(12)	Ti(1)	C(16)	33.71(9)
C(7)	Ti(1)	C(10)	55.9(1)	C(13)	Ti(1)	C(14)	34.18(9)
C(7)	Ti(1)	C(11)	33.2(1)	C(13)	Ti(1)	C(15)	56.8(1)
C(7)	Ti(1)	C(12)	164.6(1)	C(13)	Ti(1)	C(16)	56.4(1)
C(7)	Ti(1)	C(13)	145.2(1)	C(14)	Ti(1)	C(15)	33.91(9)
C(7)	Ti(1)	C(14)	134.0(1)	C(14)	Ti(1)	C(16)	56.14(9)
C(7)	Ti(1)	C(15)	138.8(1)	C(15)	Ti(1)	C(16)	34.03(9)
C(7)	Ti(1)	C(16)	157.4(1)	Ti(1)	C(1)	C(2)	127.7(2)
C(8)	Ti(1)	C(9)	33.1(1)	Ti(1)	C(1)	C(6)	120.0(2)
C(8)	Ti(1)	C(10)	56.1(1)	C(2)	C(1)	C(6)	112.3(3)
C(8)	Ti(1)	C(11)	54.7(1)	F(1)	C(2)	C(1)	117.8(3)
C(8)	Ti(1)	C(12)	142.9(1)	F(1)	C(2)	C(3)	115.1(3)
C(8)	Ti(1)	C(13)	112.7(1)	C(1)	C(2)	C(3)	127.1(3)
C(8)	Ti(1)	C(14)	107.6(1)	C(2)	C(3)	C(4)	117.5(3)
C(8)	Ti(1)	C(15)	130.7(1)	C(3)	C(4)	C(5)	119.5(3)

Table 5-4. Intramolecular Bond Angles[a] for 2 *(Cont'd)*

atom	atom	atom	angle	atom	atom	atom	angle
C(4)	C(5)	C(6)	120.5(3)	Ti(1)	C(13)	C(14)	73.5(2)
C(1)	C(6)	C(5)	123.2(3)	Ti(1)	C(13)	C(18)	123.8(2)
Ti(1)	C(7)	C(8)	73.8(2)	C(12)	C(13)	C(14)	107.5(3)
Ti(1)	C(7)	C(11)	73.2(2)	C(12)	C(13)	C(18)	126.7(3)
C(8)	C(7)	C(11)	108.4(4)	C(14)	C(13)	C(18)	125.5(3)
Ti(1)	C(8)	C(7)	73.6(2)	Ti(1)	C(14)	C(13)	72.3(2)
Ti(1)	C(8)	C(9)	71.8(2)	Ti(1)	C(14)	C(15)	72.7(2)
C(7)	C(8)	C(9)	109.3(4)	Ti(1)	C(14)	C(19)	130.8(2)
Ti(1)	C(9)	C(8)	75.0(2)	C(13)	C(14)	C(15)	108.3(2)
Ti(1)	C(9)	C(10)	72.4(2)	C(13)	C(14)	C(19)	125.1(3)
C(8)	C(9)	C(10)	107.3(4)	C(15)	C(14)	C(19)	125.4(3)
Ti(1)	C(10)	C(9)	72.6(2)	Ti(1)	C(15)	C(14)	73.3(2)
Ti(1)	C(10)	C(11)	74.6(2)	Ti(1)	C(15)	C(16)	74.1(2)
C(9)	C(10)	C(11)	106.0(4)	Ti(1)	C(15)	C(20)	128.3(2)
Ti(1)	C(11)	C(7)	73.6(2)	C(14)	C(15)	C(16)	107.9(3)
Ti(1)	C(11)	C(10)	71.9(2)	C(14)	C(15)	C(20)	125.2(3)
C(7)	C(11)	C(10)	109.0(4)	C(16)	C(15)	C(20)	125.7(3)
Ti(1)	C(12)	C(13)	72.6(2)	Ti(1)	C(16)	C(12)	72.0(2)
Ti(1)	C(12)	C(16)	74.3(2)	Ti(1)	C(16)	C(15)	71.9(2)
Ti(1)	C(12)	C(17)	124.9(2)	Ti(1)	C(16)	C(21)	130.8(2)
C(13)	C(12)	C(16)	108.4(2)	C(12)	C(16)	C(15)	107.9(3)
C(13)	C(12)	C(17)	126.6(3)	C(12)	C(16)	C(21)	124.7(3)
C(16)	C(12)	C(17)	124.7(3)	C(15)	C(16)	C(21)	126.3(3)
Ti(1)	C(13)	C(12)	73.2(2)				

[a]Angles are in degrees. Estimated standard deviations in the least significant figure are given in parentheses.

distances (2.080 and 2.12 Å) in **1**. The Ti-Cl distance 2.365(1) Å is longer than 2.32(1) Å in **1**, which reflects a weaker coordination of Cl to Ti in **2** and may be a result of a stronger electron-withdrawing character of C_6F_5 compared to *o*-FC_6H_4. This electronic effect will cause a larger formal positive charge on Ti in **1** which in turn makes coordination stronger from Cl to Ti. The Ti-C_{ipso} distance 2.209(3) Å is shorter than 2.29(2) Å in **1**, consistent with a smaller steric effect between Ti and the *o*-FC_6H_4 group. The CT1-Ti-CT2 angle (134.5°) is within 135.1° and 131.8° (two molecules in an asymmetric unit) found for $(C_5H_5)(C_5Me_5)TiCl(C_6F_5)$ (**1**). The Cl-Ti-C_{ipso} angle 94.6° is significantly smaller than 98.8(7) and 99.7(7) found for the two asymmetric molecules in the unit cell of **1**. This observation is consistent with a smaller steric interaction between Cl and the *o*-FC_6H_4 group in (**2**) and implies that interaction between the Cl atom and the C_6F_5 group in **1** is stronger. As observed in **1**, the *o*-FC_6H_4 group lies almost in the plane defined by Cl, Ti and C_{ipso} with a Cl-Ti-C(1)-C(2) torsion angle of 172.8(3)°.

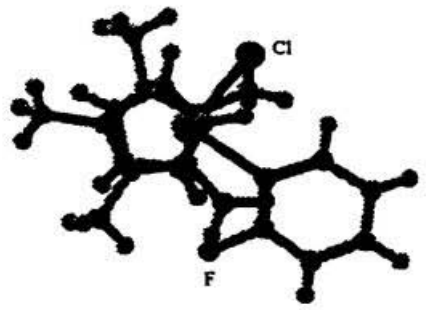

Figure 5-4. Ball-Stick drawing (from X-ray crystal data) of Cp and Cp* projection on Cl-Ti-C_{ipso} plane

The most surprising feature of this key structure is that the *ortho* fluorine atom of the

o-FC_6H_4 group is not in the expected "in" coordination position (in the Cl-Ti-C_{ipso} plane and close to the Cl atom) but in the "out" position (in the Cl-Ti-C_{ipso} plane and away from the Cl atom). A question immediately rises: what causes this particular orientation of the *ortho* fluorine of the *o*-FC_6H_4 group? A combined MMX and EHMO study, described in sections 5.2.9 and 5.2.10, concluded that the solid state configuration is a result of steric and electronic effects.

5.2.4. ^{19}F NMR observations on $(C_5H_5)_2TiCl(C_6F_5)$ (3). Compound **3** has been prepared previously,[359] however no ^{19}F NMR data was reported. It has been documented[360] that the pentafluorophenyl groups are particularly good for detecting rotation because 1) the *ortho* fluorine signals are well separated and are easy to detect; 2) the chemical shift difference in Hz between the two nonequivalent *ortho* fluorine signals in the same aryl ring is larger than the corresponding two nonequivalent *ortho* proton signals; 3) the ^{19}F NMR spectra are usually simple, compared to ^{1}H NMR. Therefore, for the purpose of studying the Ti-aryl rotation, $(C_5H_5)_2TiCl(C_6F_5)$ (**3**) was synthesized and its ^{19}F NMR was measured.

The ^{19}F NMR spectrum of $(C_5H_5)_2TiCl(C_6F_5)$ (**3**) at room temperature shows five sets of distinct peaks at -105.14, -116.19, -159.66, -161.75 and -165.03 ppm relative to

$CFCl_3$ rather than three resonances expected for a freely rotating C_6F_5 group. Non-equivalence of the two *ortho*-fluorine atoms as well as the two *meta*-fluorine atoms was attributed to a tilting of a static C_6F_5 group with respect to the plane which is approximately perpendicular to the Cl-Ti-C_{ipso} plane and bisects two Cp rings.

Variable temperature ^{19}F NMR (VT ^{19}F NMR) spectra (Figure 5-5) were measured to determine activation parameters. With increasing temperature the two downfield *ortho*-fluorine resonances as well as the two resonances corresponding to the two *meta*-fluorines at higher field gradually merge and finally collapse to a singlet. These observations suggested rapid exchange of two *ortho*-fluorine atoms and two *meta*-fluorine atoms at high temperature. Coalescence of the less separated *meta*-fluorine resonances occurs at 35°C while coalescence of the well separated *ortho*-fluorine resonances is evident at 55°C (Figure 5-5). This dynamic process can be explained by hindered rotation about the Ti-C_6F_5 bond.

In order to obtain the kinetic parameters of this process a total line shape analysis was performed using DNMR5.[361, 362] The procedure for obtaining activation parameters is outlined in Scheme 5-3. NUTS[363] data (ppm vs intensity) of an extracted ^{19}F NMR spectrum was generated from FID (free induction decay) by YYU[364] was used to

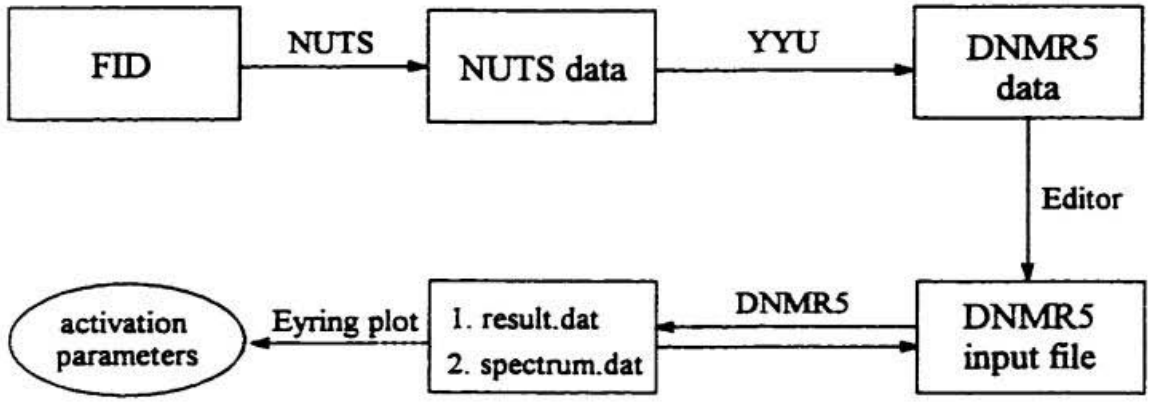

Scheme 5-3. Flow chart for obtaining activation parameters

convert NUTS data to DNMR5 acceptable data (normalized intensity). The final DNMR5 input file was obtained by adding information, such as chemical shifts, effective relaxation time T_2*, rate constants, sweep width, etc., to the DNMR5 data file by using a DOS Editor. The best fit, *i.e.*, rate, was obtained running DNMR5 in iterative mode with varied parameters of chemical shifts, effective relaxation time T_2*, rate constants, baseline increment and baseline tilt, through visual examination of the DNMR5 generated difference spectrum between the calculated spectrum and the experimental spectrum. The calculated spectra of $(C_5H_5)_2TiCl(C_6F_5)$ (**3**) at various temperatures are shown in Figure 5-6, which is in good agreement with the experimental data (Figure 5-5).

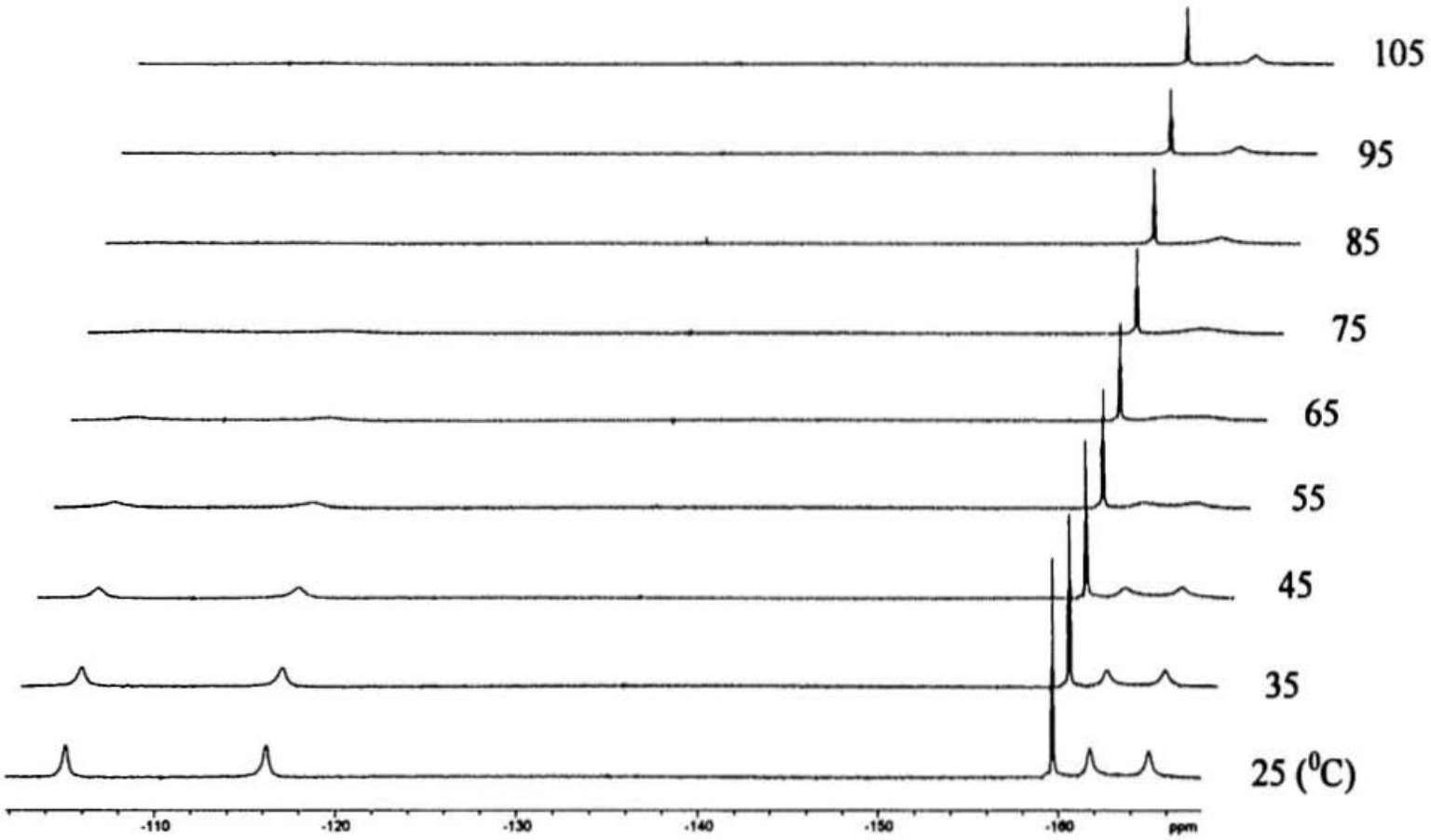

Figure 5-5. Variable temperature ^{19}F NMR of $Cp_2TiCl(C_6F_5)$ (3) in d^8-toluene

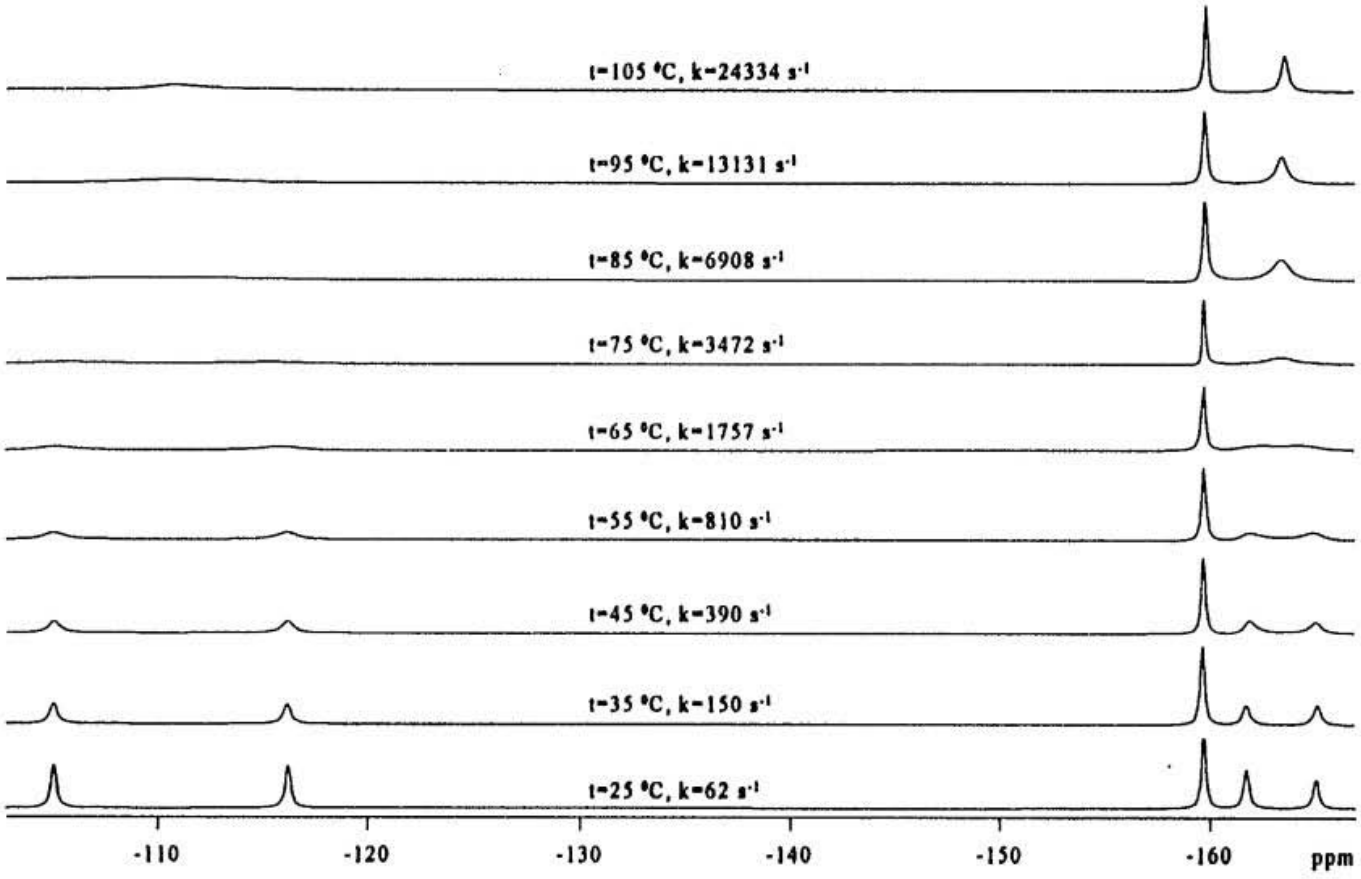

Figure 5-6. Calculated VT ^{19}F NMR of $Cp_2TiCl(C_6F_5)_2$ (3)

The activation parameters ($\Delta H^{\ddagger}$ = 16.0 kcal/mol and $\Delta S^{\ddagger}$ = 1.72 eu) for the rotation of the C_6F_5 group were determined from the slope and intercept of an Eyring plot (Figure 5-7) based on the standard equation:

$$\ln\left(\frac{k}{T}\right) = \ln\left(\frac{h}{k_B}\right) - \frac{\Delta H^{\ddagger}}{R \cdot T} + \frac{\Delta S^{\ddagger}}{R}$$

where k is rotation rate, T is temperature in Kelvins and k_B, h, and R are Boltzmann's, Planck's, and the gas constants, respectively. The calculated $\Delta H^{\ddagger}$ for the C_6F_5 rotation around the Ti-C_{ipso} bond in **3** is slightly higher than the reported range (11.5 - 15.5 kcal/mol) while the $\Delta S^{\ddagger}$ is within the range -9.5 - 2.3 eu found for C_6F_5 rotation around Pd-C_{ipso} / Pt-C_{ipso} bonds in a series of square planar Pd / Pt complexes with general formula $[M(C_6F_5)X(OPPy_nPh_{3-n})]$ (M = Pd, Pt; X= C_6F_5; halide; n = 1-3).[360] However, both $\Delta H^{\ddagger}$ and $\Delta S^{\ddagger}$ are larger than those for the p-$CH_3C_6H_5$ rotation in $(C_5Me_5)Rh(PMe_3)(p\text{-tol})Cl$ (9.8 kcal/mol, -13.7 eu) and $(C_5Me_5)Rh[P(C_6D_5)_3](p\text{-tol})Br$ (11.0 kcal/mol, -9.8 eu).[337]

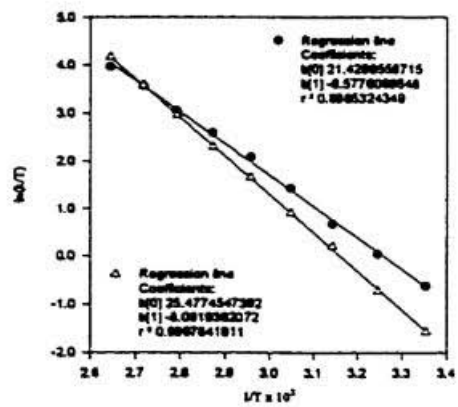

Figure 5-7. Eyring plots for 3 (Δ) and 5 (•)

5.2.5. NMR observations on $(C_5H_5)_2TiCl(o\text{-}FC_6H_4)$ (4). Although ^1H NMR data of **4** in $CDCl_3$ have been reported[351] at 100 MHz (6.8-7.6 (4H, m) and 6.51 (10H, s)), no ^{13}C and ^{19}F NMR data were recorded. In order to better characterize this compound, multinuclear NMR (^1H, ^{13}C and ^{19}F) were measured at 300 MHz. The ^1H NMR data for **4** [6.90 (m, 1H), 6.85 (m, 2H), 6.71 (m, 1H), 6.41 ppm(s, 10H)] were generally in agreement with literature data.[351] The ^{13}C NMR spectrum of **4** showed resonances at 165.66 (s, C-F), 139.69 (d, 15.7), 126.47 (d, 7.6), 124.69 (s), 119.57(d, 52.7), 117.07 (s, Cp) and 113.26 ppm (d, 31.9 Hz). The C_{ipso} was not observed. The ^{19}F NMR spectrum of **4** showed a singlet at -91.00 ppm at 22.4°C. On lowering the temperature to -60°C, no splitting corresponding to "out" and "in" rotamers was observed.

5.2.6. ^{19}F NMR observations on $(C_5H_5)_2Ti(C_6F_5)_2$ (5). The ^{19}F NMR spectrum of **5** was first studied in 1963. Only three non-equivalent sites (115.6, 158.7 and 163.7 ppm, relative to $CFCl_3$) corresponding to *ortho*, *meta*, *para* fluorine were reported[283] suggesting free C_6F_5 rotation around the Ti-C_{ipso} bonds on the time scale of the NMR spectrometer used.[283] In the course of this study on the C_6F_5 rotation around Ti-C_{ipso} bonds, VT ^{19}F NMR spectra of **5** were measured at 300MHz (proton frequency) and analysed using DNMR5.[361, 362] It is interesting to find that the ^{19}F NMR of **5** in $CDCl_3$

at room temperature displayed five signals at δ 114.46, 116.84, 158.35, 163.30 and 163.80 ppm relative to $CFCl_3$ (Figure 5-8). This observation implies that the two C_6F_5 groups in this molecule are equivalent. The X-ray single crystal structure (Figure 5-10) revealed that the molecule has C_2 symmetry in the solid state. As temperature was raised, the two down field *ortho*-fluorine resonances as well as two higher field *meta*-fluorines resonances broadened and finally coalesced.

This dynamic process can be attributed to hindered rotation of the C_6F_5 groups about their Ti-C_{ipso} bonds. Another interesting feature associated with this dynamic process is that the C_2 symmetry is maintained during the rotation since no second set of ^{19}F NMR resonances was observed on raising the temperature (Figure 5-8). In other words the C_6F_5 rotations are geared[365, 366] in such a way as to maintain C_2 symmetry (Figure 5-11). A total line shape analysis was performed for this process by use of DNMR5 with the same strategy employed for compound **3**. The calculated spectra depicted in Figure 5-9 are in good agreement with the experimental VT NMR data (Figure 5-8). The corresponding Eyring plot is shown in Figure 5-7.

Based on the Eyring plot (Figure 5-7) the $\Delta H^{\ddagger}$ and $\Delta S^{\ddagger}$ for this process are 13.1 kcal/mol and -2.33 eu, respectively. Interestingly this $\Delta H^{\ddagger}$ is smaller than the 16.0

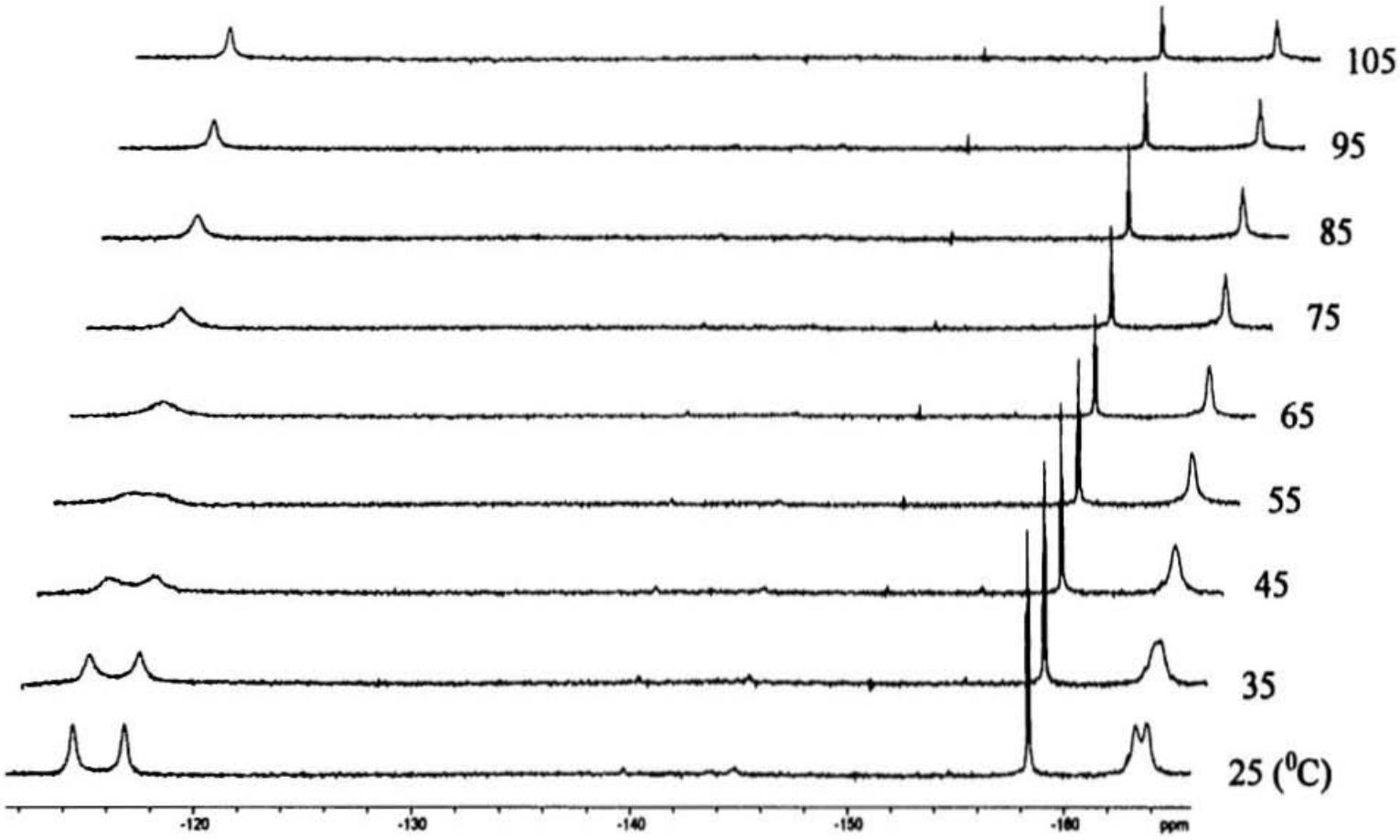

Figure 5-8. Variable temperature ^{19}F NMR of $Cp_2Ti(C_6F_5)_2$ (5) in d^8-toluene

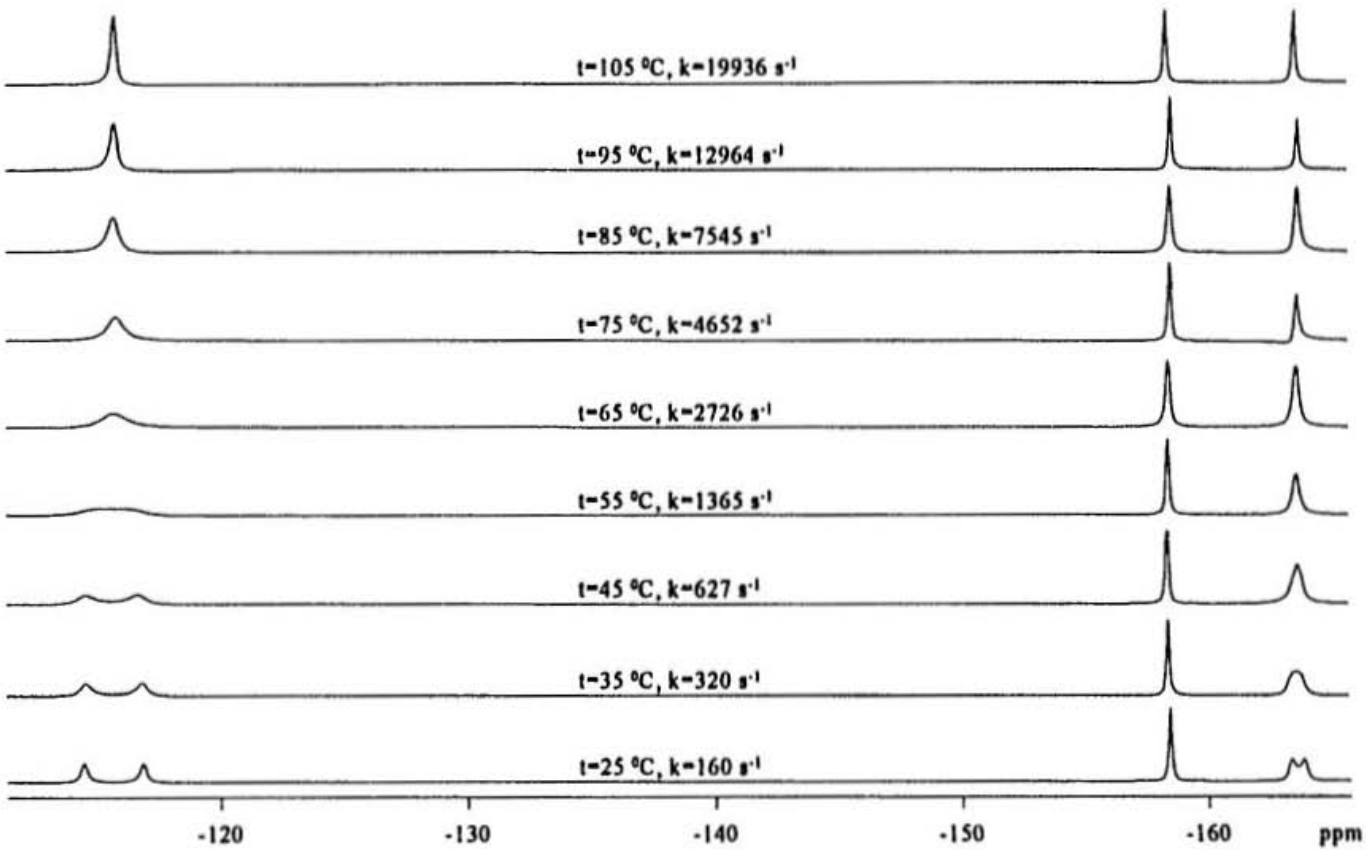

Figure 5-9. Calculated VT ^{19}F NMR spectra of $Cp_2Ti(C_6F_5)_2$ (5)

kcal/mol exhibited by compound **3**, but larger than those for the *p*-$CH_3C_6H_5$ rotations around the Rh-C_{ipso} bonds in $(C_5Me_5)Rh(PMe_3)$(*p*-tol)Cl and $(C_5Me_5)Rh[P(C_6D_5)_3]$(*p*-tol)Br[337] and within the range 11.5 - 15.5 kcal/mol for the C_6F_5 rotation about Pd-C_{ipso} / Pt-C_{ipso} bonds observed in complexes $[M(C_6F_5)X(OPPy_nPh_{3-n})]$ (M = Pd, Pt; X= C_6F_5; halide; n = 1-3).[360] The $\Delta S^{\ddagger}$ is larger than those for the *p*-$CH_3C_6H_5$ rotations around Rh-C_{ipso} bonds observed in $(C_5Me_5)Rh(PMe_3)$(*p*-tol)Cl (-13.7 eu) and $(C_5Me_5)Rh[P(C_6D_5)_3]$(*p*-tol)Br (-9.8 eu)[337] but within the range -9.5 - 2.3 eu for the C_6F_5 rotation around Pd-C_{ipso} / Pt-C_{ipso} bonds observed in a series of square planar Pd / Pt complexes with general formula $[M(C_6F_5)X(OPPy_nPh_{3-n})]$ (M = Pd, Pt; X= C_6F_5; halide; n = 1-3).[360]

5.2.7. Solid state conformation of $(C_5H_5)_2Ti(C_6F_5)_2$ (5). Although compound **5** has been known for more than three decades, no single crystal X-ray study has been performed.[339,367] Crystallographic data obtained in this study for **5** is summarized in Table 5-5. The ORTEP drawing of the molecular structure of **5** is illustrated in Figure 5-10. The atomic parameters are listed in Table 5-6 and details of bond distances and angles are given in Tables 5-7 and 5-8, respectively. Compound **5** is isostructural with $Cp_2Ti(C_6H_5)_2$,[368] $(C_5H_5)(C_5Me_5)TiCl(C_6F_5)$ (1) and $(C_5H_5)(C_5Me_5)TiCl(o\text{-}FC_6H_4)$ (2) with the expected pseudotetrahedral coordination of the central metal atom. The

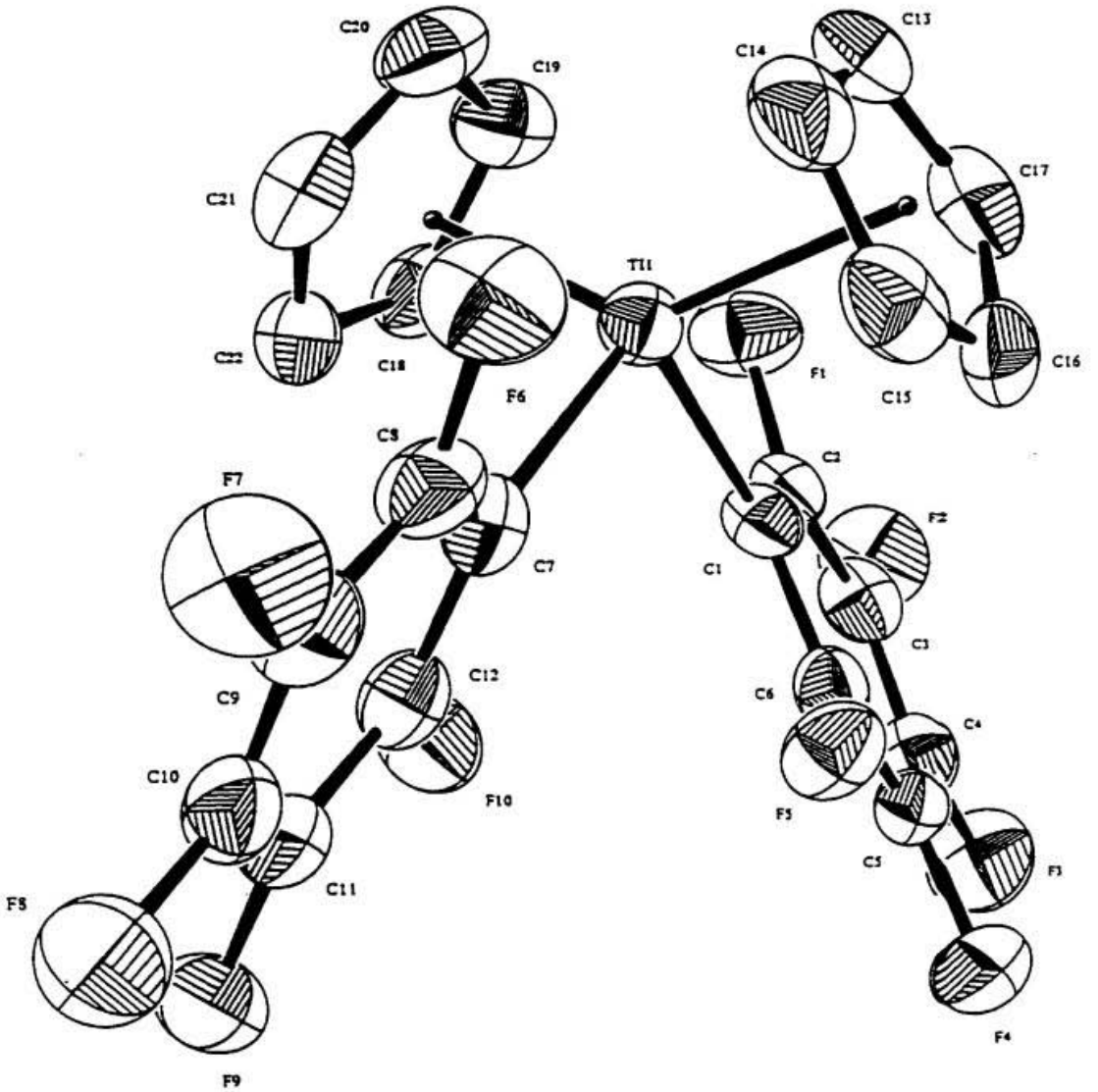

Figure 5-10. ORTEP drawing of X-ray crystal structure of $Cp_2Ti(C_6F_5)_2$ (5)

Table 5-5. Summary of Crystallographic Data for 5

Empirical Formula	$C_{22}H_{10}F_{10}Ti$
Formula Weight	512.21
Crystal Colour, habit	orange, irregular
Crystal Dimensions (mm)	0.300 X 0.050 X 0.400
No. Reflections Used for Unit Cell Determination (2θ range)	21 (20.2 - 28.9°)
Omega Scan Peak Width at Half-height	0.31
Crystal System	monoclinic
Lattice Parameters:	
a (Å)	14.241(4)
b (Å)	7.565(7)
c (Å)	17.381(5)
β (°)	91.16(2)
V = (Å^3)	1872(2)
Space Group	$P2_1/c$ (#14)
Z value	4
$D_{calc.}$ (g/cm^3)	1.817
F_{000}	1016
μ (MoKα) (cm^{-1})	5.53
Scan width (°)	1.10 + 0.35 tanθ
$2\theta_{max}$ (°)	50.1
No. of Reflections Measured	
Total	3734
Unique	3584
R_{int}	0.035
Structure Solution	Direct Methods
Refinement	Full-matrix least-squares
Corrections[a]	Lorentz-polarization Absorption Secondary Extinction (coefficient: 0.51403E-06)
Function Minimized	$\Sigma w(\|Fo\| - \|Fc\|)^2$
Least-squares Weights	$4Fo^2/\sigma^2(Fo^2)$
p-factor	0.01
Anomalous Dispersion	All non-hydrogen atoms
No. Observations (I>2.00σ(I))	1892
No. Variables	299
Reflection/Parameter Ratio	6.33
R[b]	0.044
Rw[c]	0.034
Goodness of Fit Indicator[d]	1.47
Max Shift/Error in Final Cycle	0.00
Maximum Peak in Final Diff. Map	0.25 e$^-$/Å^3
Minimum Peak in Final Diff. Map	-0.39 e$^-$/Å^3

[a] cf. Reference[226]. [b] $R=\sum||Fo|-|Fc||/\sum|Fc|$. [c] $R_w=[\sum w(|Fo|-|Fc|)^2/\sum wFo^2]^{1/2}$.
[d] $GOF=(\sum(|Fo|-|Fc|)/\sigma)/(n-m))$ where n= # reflections, m=#variables, and σ^2=variance of $(|Fo|-|Fc|)$.

Table 5-6. Atomic Coordinates (× 10^4) and Isotropic Thermal Parameters (pm^2 × 10^{-1}) for 5

atom	x	y	z	B(eq)
Ti(1)	0.74750(6)	0.8156(1)	0.06102(5)	2.74(4)
F(1)	0.5596(2)	1.1165(4)	0.0471(1)	4.5(1)
F(2)	0.4803(2)	1.3289(4)	0.1475(2)	5.0(2)
F(3)	0.5413(2)	1.3385(4)	0.2961(2)	5.1(2)
F(4)	0.6790(2)	1.1144(4)	0.3446(1)	4.3(1)
F(5)	0.7637(2)	0.9034(4)	0.2452(1)	3.8(1)
F(6)	0.9355(2)	0.5203(4)	0.0685(2)	5.1(2)
F(7)	1.1075(2)	0.5391(4)	0.1258(2)	6.1(2)
F(8)	1.1688(2)	0.8361(5)	0.2015(2)	5.8(2)
F(9)	1.0524(2)	1.1162(4)	0.2134(2)	5.2(2)
F(10)	0.8784(2)	1.1033(4)	0.1567(2)	4.3(1)
C(1)	0.6728(3)	1.0055(6)	0.1383(2)	2.6(2)
C(2)	0.5980(3)	1.1158(6)	0.1202(2)	3.0(2)
C(3)	0.5528(3)	1.2254(6)	0.1709(3)	3.2(2)
C(4)	0.5822(3)	1.2306(6)	0.2458(3)	3.3(2)
C(5)	0.6534(3)	1.1184(6)	0.2698(2)	3.0(2)
C(6)	0.6959(3)	1.0136(6)	0.2159(3)	2.9(2)
C(7)	0.8936(3)	0.8067(7)	0.1134(2)	3.2(2)
C(8)	0.9588(4)	0.6713(7)	0.1070(3)	3.6(2)
C(9)	1.0496(3)	0.6775(8)	0.1354(3)	4.0(3)
C(10)	1.0808(3)	0.8248(8)	0.1726(3)	4.0(3)
C(11)	1.0214(3)	0.9673(7)	0.1799(3)	3.5(3)
C(12)	0.9307(3)	0.9539(7)	0.1502(3)	3.4(2)
C(13)	0.6465(4)	0.5803(7)	0.0214(3)	4.2(3)
C(14)	0.7341(4)	0.5104(7)	0.0445(3)	4.5(3)
C(15)	0.7433(4)	0.5371(7)	0.1243(3)	4.3(3)
C(16)	0.6646(4)	0.6265(7)	0.1490(3)	4.4(3)
C(17)	0.6053(3)	0.6533(6)	0.0854(3)	4.1(3)
C(18)	0.7397(4)	1.0701(6)	-0.0195(3)	3.7(3)
C(19)	0.6937(3)	0.9310(7)	-0.0565(3)	3.8(3)
C(20)	0.7609(4)	0.8028(7)	-0.0756(2)	4.2(3)
C(21)	0.8469(4)	0.8607(8)	-0.0467(3)	4.5(3)
C(22)	0.8340(4)	1.0263(7)	-0.0129(3)	4.1(3)

Table 5-7. Bond Distances (Å) for 5

atom	atom	distance	atom	atom	distance
Ti(1)	C(1)	2.249(4)	C(1)	C(2)	1.385(6)
Ti(1)	C(7)	2.255(5)	C(1)	C(6)	1.382(6)
Ti(1)	C(13)	2.381(5)	C(2)	C(3)	1.378(6)
Ti(1)	C(14)	2.334(5)	C(3)	C(4)	1.361(6)
Ti(1)	C(15)	2.378(5)	C(4)	C(5)	1.380(6)
Ti(1)	C(16)	2.420(5)	C(5)	C(6)	1.377(6)
Ti(1)	C(17)	2.413(5)	C(7)	C(8)	1.388(6)
Ti(1)	C(18)	2.381(5)	C(7)	C(12)	1.383(6)
Ti(1)	C(19)	2.336(5)	C(8)	C(9)	1.376(6)
Ti(1)	C(20)	2.388(4)	C(9)	C(10)	1.359(7)
Ti(1)	C(21)	2.394(5)	C(10)	C(11)	1.378(7)
Ti(1)	C(22)	2.402(5)	C(11)	C(12)	1.386(6)
F(1)	C(2)	1.374(5)	C(13)	C(14)	1.406(7)
F(2)	C(3)	1.351(5)	C(13)	C(17)	1.383(6)
F(3)	C(4)	1.338(5)	C(14)	C(15)	1.404(7)
F(4)	C(5)	1.344(5)	C(15)	C(16)	1.385(7)
F(5)	C(6)	1.367(5)	C(16)	C(17)	1.393(7)
F(6)	C(8)	1.362(5)	C(18)	C(19)	1.390(6)
F(7)	C(9)	1.345(5)	C(18)	C(22)	1.386(6)
F(8)	C(10)	1.342(5)	C(19)	C(20)	1.407(6)
F(9)	C(11)	1.338(5)	C(20)	C(21)	1.386(7)
F(10)	C(12)	1.359(5)	C(21)	C(22)	1.397(7)

Table 5-8. Intramolecular Bond Angles[a] for 5

atom	atom	atom	angle	atom	atom	atom	angle
C(1)	Ti(1)	C(7)	102.8(2)	C(14)	Ti(1)	C(22)	129.2(2)
C(1)	Ti(1)	C(13)	111.1(2)	C(15)	Ti(1)	C(16)	33.5(2)
C(1)	Ti(1)	C(14)	131.8(2)	C(15)	Ti(1)	C(17)	55.9(2)
C(1)	Ti(1)	C(15)	105.8(2)	C(15)	Ti(1)	C(18)	170.7(2)
C(1)	Ti(1)	C(16)	76.0(2)	C(15)	Ti(1)	C(19)	136.4(2)
C(1)	Ti(1)	C(17)	79.1(2)	C(15)	Ti(1)	C(20)	115.3(2)
C(1)	Ti(1)	C(18)	79.5(2)	C(15)	Ti(1)	C(21)	120.6(2)
C(1)	Ti(1)	C(19)	97.7(2)	C(15)	Ti(1)	C(22)	148.5(2)
C(1)	Ti(1)	C(20)	131.9(2)	C(16)	Ti(1)	C(17)	33.5(2)
C(1)	Ti(1)	C(21)	132.1(2)	C(16)	Ti(1)	C(18)	146.3(2)
C(1)	Ti(1)	C(22)	98.6(2)	C(16)	Ti(1)	C(19)	128.2(2)
C(7)	Ti(1)	C(13)	129.9(2)	C(16)	Ti(1)	C(20)	130.9(2)
C(7)	Ti(1)	C(14)	95.3(2)	C(16)	Ti(1)	C(21)	151.9(2)
C(7)	Ti(1)	C(15)	79.5(2)	C(16)	Ti(1)	C(22)	172.9(2)
C(7)	Ti(1)	C(16)	100.7(2)	C(17)	Ti(1)	C(18)	119.0(2)
C(7)	Ti(1)	C(17)	133.2(2)	C(17)	Ti(1)	C(19)	94.7(2)
C(7)	Ti(1)	C(18)	107.1(2)	C(17)	Ti(1)	C(20)	103.7(2)
C(7)	Ti(1)	C(19)	130.4(2)	C(17)	Ti(1)	C(21)	136.1(2)
C(7)	Ti(1)	C(20)	108.0(2)	C(17)	Ti(1)	C(22)	150.7(2)
C(7)	Ti(1)	C(21)	76.4(2)	C(18)	Ti(1)	C(19)	34.3(1)
C(7)	Ti(1)	C(22)	75.9(2)	C(18)	Ti(1)	C(20)	56.8(2)
C(13)	Ti(1)	C(14)	34.7(2)	C(18)	Ti(1)	C(21)	56.4(2)
C(13)	Ti(1)	C(15)	56.7(2)	C(18)	Ti(1)	C(22)	33.7(2)
C(13)	Ti(1)	C(16)	56.0(2)	C(19)	Ti(1)	C(20)	34.6(2)
C(13)	Ti(1)	C(17)	33.5(2)	C(19)	Ti(1)	C(21)	56.8(2)
C(13)	Ti(1)	C(18)	114.4(2)	C(19)	Ti(1)	C(22)	56.4(2)
C(13)	Ti(1)	C(19)	80.8(2)	C(20)	Ti(1)	C(21)	33.7(2)
C(13)	Ti(1)	C(20)	75.0(2)	C(20)	Ti(1)	C(22)	56.2(2)
C(13)	Ti(1)	C(21)	104.1(2)	C(21)	Ti(1)	C(22)	33.9(2)
C(13)	Ti(1)	C(22)	130.9(2)	Ti(1)	C(1)	C(2)	128.3(3
C(14)	Ti(1)	C(15)	34.7(2)	Ti(1)	C(1)	C(6)	120.3(3)
C(14)	Ti(1)	C(16)	56.8(2)	C(2)	C(1)	C(6)	111.2(4)
C(14)	Ti(1)	C(17)	56.7(2)	F(1)	C(2)	C(1)	120.2(4)
C(14)	Ti(1)	C(18)	136.5(2)	F(1)	C(2)	C(3)	114.0(4)
C(14)	Ti(1)	C(19)	103.8(2)	C(1)	C(2)	C(3)	125.8(4)
C(14)	Ti(1)	C(20)	81.1(2)	F(2)	C(3)	C(2)	121.3(4)
C(14)	Ti(1)	C(21)	95.3(2)	F(2)	C(3)	C(4)	119.3(4)

Table 5-8. Intramolecular Bond Angles[a] for 8 *(cont'd)*

atom	atom	atom	angle	atom	atom	atom	angle
C(2)	C(3)	C(4)	119.3(4)	Ti(1)	C(13)	C(17)	74.5(3)
F(3)	C(4)	C(3)	120.9(5)	C(14)	C(13)	C(17)	108.0(5)
F(3)	C(4)	C(5)	120.3(4)	Ti(1)	C(14)	C(13)	74.5(3)
C(3)	C(4)	C(5)	118.8(4)	Ti(1)	C(14)	C(15)	74.4(3)
F(4)	C(5)	C(4)	119.2(4)	C(13)	C(14)	C(15)	107.0(5)
F(4)	C(5)	C(6)	122.1(4)	Ti(1)	C(15)	C(14)	70.9(3)
C(4)	C(5)	C(6)	118.6(4)	Ti(1)	C(15)	C(16)	74.9(3)
F(5)	C(6)	C(1)	119.3(4)	C(14)	C(15)	C(16)	108.5(5)
F(5)	C(6)	C(5)	114.4(4)	Ti(1)	C(16)	C(15)	71.6(3)
C(1)	C(6)	C(5)	126.2(4)	Ti(1)	C(16)	C(17)	73.0(3)
Ti(1)	C(7)	C(8)	127.1(4)	C(15)	C(16)	C(17)	107.8(5)
Ti(1)	C(7)	C(12)	120.2(3)	Ti(1)	C(17)	C(13)	72.0(3)
C(8)	C(7)	C(12)	112.4(4)	Ti(1)	C(17)	C(16)	73.5(3)
F(6)	C(8)	C(7)	120.1(5)	C(13)	C(17)	C(16)	108.7(5)
F(6)	C(8)	C(9)	115.0(5)	Ti(1)	C(18)	C(19)	71.1(3)
C(7)	C(8)	C(9)	124.9(5)	Ti(1)	C(18)	C(22)	74.0(3)
F(7)	C(9)	C(8)	120.2(5)	C(19)	C(18)	C(22)	107.7(4)
F(7)	C(9)	C(10)	120.1(5)	Ti(1)	C(19)	C(18)	74.6(3)
C(8)	C(9)	C(10)	119.6(5)	Ti(1)	C(19)	C(20)	74.7(3)
F(8)	C(10)	C(9)	121.6(5)	C(18)	C(19)	C(20)	108.4(5)
F(8)	C(10)	C(11)	119.1(5)	Ti(1)	C(20)	C(19)	70.7(3)
C(9)	C(10)	C(11)	119.3(5)	Ti(1)	C(20)	C(21)	73.4(3)
F(9)	C(11)	C(10)	120.0(5)	C(19)	C(20)	C(21)	107.2(5)
F(9)	C(11)	C(12)	121.4(5)	Ti(1)	C(21)	C(20)	72.9(3)
C(10)	C(11)	C(12)	118.5(5)	Ti(1)	C(21)	C(22)	73.4(3)
F(10)	C(12)	C(7)	120.2(4)	C(20)	C(21)	C(22)	108.3(5)
F(10)	C(12)	C(11)	114.5(5)	Ti(1)	C(22)	C(18)	72.3(3)
C(7)	C(12)	C(11)	125.2(5)	Ti(1)	C(22)	C(21)	72.7(3)
Ti(1)	C(13)	C(14)	70.8(3)	C(18)	C(22)	C(21)	108.4(5)

[a]Angles are in degrees. Estimated standard deviations in the least significant figure are given in parentheses.

two Cp rings are in staggered conformation (Figure 5-11). A characteristic structural feature of this molecule is the existence of a two-fold axis bisecting the CT(1)-Ti-CT(2) and C_{ipso}-Ti-C_{ipso}' angles. Each pentafluorophenyl ring was twisted about 32° from the C_{ipso}-Ti-C_{ipso}' plane although two pentafluorophenyl rings are related via a C_2 axis. This conformation is also the preferred one in solution as the ^{19}F NMR at room temperature shows only five distinct signals (Figure 5-8) at the low temperature limit.

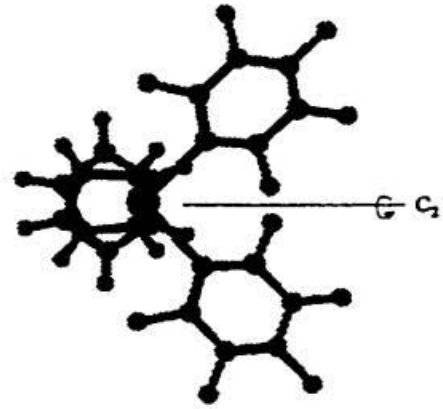

Figure 5-11. Ball-stick drawing (from X-ray crystal data) of two Cp rings projected on C_{ipso}-Ti-C_{ipso}' plane

The average Ti-C_{ipso} bond distance of 2.252Å is slightly shorter than the 2.27Å observed in $Cp_2Ti(C_6H_5)_2$.[368] The CT(1)-Ti-CT(2) angle is 131.1° which is virtually the same (131.0°)[369] observed in the precursor Cp_2TiCl_2 but smaller than 135.1° and 131.8° (two molecules in an asymmetric unit) for $(C_5H_5)(C_5Me_5)TiCl(C_6F_5)$ (1) and 134.5° for $(C_5H_5)(C_5Me_5)TiCl(o\text{-}FC_6H_4)$ (2). The C_{ipso}-Ti-C_{ipso}' angle is 102.8° which is larger than the value 97.3° found for $Cp_2Ti(C_6H_5)_2$[368] indicating F atoms are "bigger,"[370] and larger than 94.5° found in the precursor Cp_2TiCl_2.[369] These

observations suggest that steric factors influence the angle (X-Ti-X) in Cp_2TiX_2.[282]

5.2.8. NMR observations on $(C_5H_5)_2Ti(o\text{-}FC_6H_4)_2$ (6). The synthesis and ^{19}F NMR spectrum of **6** in $CDCl_3$ at 100 MHz have been reported[351] However, no ^1H and ^{13}C NMR data were documented. In order to fully characterize this compound, multinuclear NMR (^1H, ^{13}C and ^{19}F) were recorded at 300 MHz. The ^1H NMR spectrum (in $CDCl_3$) of **6** showed signals at 6.90 (m, 2H), 6.85 (m, 4H), 6.71 (m, 2H), 6.31 ppm(s, 10H). The ^{13}C NMR spectrum of **6** in $CDCl_3$ showed resonances at 164.47 (d, 228.6, C-F), 135.65 (d, 16.5), 126.11 (d, 7.9), 123.16 (s), 115.91(s, Cp) and 114.22 ppm (d, 32.5). The C_{ipso} was not observed. The ^{19}F NMR spectrum (in $CDCl_3$) of **6** showed a singlet at -86.85 ppm at 22.4°C, which is close to the literature value (-86.05 ppm). On lowering the temperature to -90°C, the signal did not split into singlets corresponding to "*out*" and "*in*" rotamers.

5.2.9. Molecular mechanics (MMX) study. The rotational barrier and configurational preference of the fluorine substituted aryl group in the titanocene derivatives (**2** - **6**) were studied by molecular mechanics calculations employing PCMODEL (MMX force field).[334,336] Selected results for complexes **2** - **6** as well as **1** are represented in Table 5-9. The ΔE_{rot} in the table was obtained via the

PCMODEL dihedral driver.

As expected, energy minimization for CpCp*TiCl(*o*-FC_6H_4) (2) starting from the X-ray structure led to a conformer **2a** with *anti* arrangement of Cl and *ortho* F (Figure 5-3 and 5-12). Energy minimization of the *syn* conformer, obtained by rotating the phenyl group about the Ti-C_{ipso} (*o*-FC_6H_4) bond, gave a *syn* conformer **2b** with a higher potential energy. The MMX energy difference between **2a** and **2b** is about 0.8 kcal/mol which is in accord with the *anti* orientation of *ortho* fluorine atoms in the solid state. Other structural parameters from the MMX study such as Cp-Ti-Cp*, Cl-Ti-C_{ipso} angles and torsion angle Cl-Ti-C_{ipso}-C_{ortho} as well as bond distances Ti-Cp, Ti-Cp*, Ti-Cl and TI-C_{ipso} are generally in good agreement with those found by single crystal X-ray analysis. The corresponding angle differences are within 3.5° while the related distances differences are within 0.14 Å (Table 5-9). This close agreement between the molecular mechanics calculated structure and the X-ray structure suggested that the conformation of **2** is dominated by steric effects. This observation parallels literature

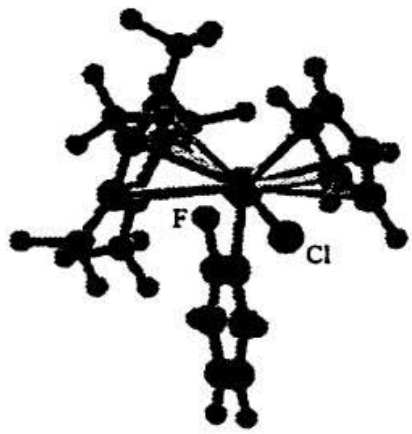

Figure 5-12. Lowest energy conformer found by PCMODEL (MMX force field) for 2a

evidence indicating that F atoms are "bigger" than H atoms and exert a profound steric influence.[370] Similar agreement was found in compound **5**. Comparison of MMX results and X-ray single crystal data for compound $Cp_2Ti(C_6F_5)_2$ (**5**) shows that corresponding structural parameters are also in accord with each other. The difference of important bond and torsion angles as well as bond distances are within 5° and 0.04 Å, respectively.

The calculated rotational barrier for the C_6F_5 rotation around the Ti-C_{ipso} bond in **3** is 15.8 kcal/mol which is in excellent agreement with the value 16.0 kcal/mol found from VT ^{19}F NMR. Again, this agreement implies that the C_6F_5 rotation around the Ti-C_{ipso} bond in **3** is controlled by steric effects. However, the situation is complicated by the ^{19}F NMR results obtained for **5** which indicated that the C_6F_5 rotation around the Ti-C_{ipso} bond in **5** is geared (cf. section 5.2.6). A calculation for geared C_6F_5 rotation around the Ti-C_{ipso} bond was also performed in addition to one for non-geared C_6F_5 rotation (ΔE_{rot} = 31.0 kcal/mol), and gave a rotation barrier of 23.7 kcal/mol. This barrier is much higher than the activation enthalpy $\Delta H^{\ddagger}$ (13.1 kcal/mol) observed for C_6F_5 rotation around the Ti-C_{ipso} bond via DNMR5 analysis of VT ^{19}F NMR data. The discrepancy may be due to dipole or solvent effects, which the MMX force field does not take into account.

Table 5-9. Some Structuraal Parameters from MMX Calculations and X-ray Analysis[a]

Cpd	Cp^1	Cp^2	X	Ar	Cp^1-Ti -Cp^2	X-Ti-C_{ipso}	X-Ti-C_{ipso}-C_{ortho}	Ti-Cp^1	Ti-Cp^2	Ti-X	Ti-C_{ipso}	E_{MMX}	ΔE_{rot}
1	Cp	Cp*	Cl	C_6F_5	137.2 (135.1) (131.8)	99.5 (98.8(7)) (99.7(7))	-6.3 (-14.7) (-13.6)	2.155 (2.080) (2.111)	2.199 (2.120) (2.197)	2.541 (2.32(1)) (2.34(1))	2.249 (2.29(2)) (2.27(2))	-68.5	22.6
2a[b]	Cp	Cp*	Cl	*o*-FC_6H_4	138.0 (134.5)	93.8 (94.61(8))	-6.0 (-5.7(2))	2.134 (2.071)	2.162 (2.089)	2.544 2.4(4)	2.251 (2.209(3))	-79.2	14.2
2b[c]	Cp	Cp*	Cl	*o*-FC_6H_4	137.4	98.6	-4.0	2.134	2.167	2.540	2.251	-78.4	14.3
3	Cp	Cp	Cl	C_6F_5	132.7	100.5	-12.3	2.085	.092	2.540	2.248	-66.8	15.8
4a[b]	Cp	Cp	Cl	*o*-FC_6H_4	134.7	95.8	-8.6	2.076	2.074	2.539	2.247	-72.1	13.5
4b[c]	Cp	Cp	Cl	*o*-FC_6H_4	133.1	98.2	-16.9	2.083	2.083	2.537	2.246	-71.3	14.6
5	Cp	Cp	C_6F_5	C_6F_5	130.6 (131.1)	97.8 (102.8)	-31.7 (-31.2)	2.140 (2.177)	2.134 (2.170)	2.253 (2.290)	2.255 (2.292)	-60.1	31.0 23.7*
6a[d]	Cp	Cp	*o*-FC_6H_4	*o*-FC_6H_4	116.0	96.7	-30.4	2.134	2.045	2.249	2.253	-55.3	33.8
6b[e]	Cp	Cp	*o*-FC_6H_4	*o*-FC_6H_4	130.7	97.7	-31.8	2.138	2.138	2.247	2.245	-55.8	22.2
6c[f]	Cp	Cp	*o*-FC_6H_4	*o*-FC_6H_4	130.8	102.4	-31.5	2.136	2.132	2.249	2.255	-55.4	22.1

[a]Angles in °, distances in Å;C_{ipso} and C_{ortho} are *ipso* and *ortho* carbons of aryl group, respectively; E_{MMX} and ΔE_{rot} are calculated potential energy and barrier for Ti-Ar rotation, respectively, kcal/mol; data in brackets are from X-ray; [b]X and F are *anti*; [c]X and F are *syn*; [d]two F's are both in "*out*" position; [e]two F's are both in "*in*" position; [f]one F is in "*out*" and one F is in "*in*" position. *geared.

5.2.10. Extended Hückel molecular orbital (EHMO) calculations. It is well known[371] that although less precise than *ab initio* studies, molecular orbital calculations at the extended Hückel level have the ability to differentiate more readily between contributions (*e.g.*, specific bonding, orientation of a group) to overall energy changes. Extended Hückel calculations were performed for compounds **2** - **6** using the CACAO package[262] in order to shed some light on possible electronic effects on the aryl rotation barriers and conformational preferences, especially the orientation of the *ortho*-fluorine atom in complex **2**. The starting geometries for **2** and **5** used for EHMO calculations were taken from solid state structures while the geometries for all remaining complexes were those optimized by the MMX force field via PCMODEL 6.0 for Windows.

Complex CpCp*TiCl(*o*-FC_6H_4) (**2**) can, in principle, give rise to two conformational isomers. Both have the F atom in the Cl-Ti-C_{ipso} plane but differ in the relative orientation of the F atom to the ligand Cl. For the "*in*" isomer the F atom lies between the Cl and C_{ipso} in the plane at the open side of the bent metallocene wedge while the "*out*" isomer has the F atom lying away from the Cl atom. The solid state structure of complex **2** shows that the isolated product is the "*out*" isomer (Figure 5-3). The interaction diagram for the "*out*" isomer of **2** and energy profile for the *o*-

FC_6H_4 rotation about the Ti-C_{ipso} bond are given in Figures 5-13 and 5-14, respectively. The "*in*" isomer was obtained from the "*out*" isomer by forcing the *o*-FC_6H_4 rotation about the Ti-C_{ipso} bond until the "*in*" isomer was achieved while keeping the geometry of the CpCp*$TiCl^+$ fragment fixed. EHMO calculations showed that the "*out*" isomer is 0.29 ev (*ca.* 6.7 kcal / mol) more stable than the "*in*" isomer. This energy difference together with a steric contribution of 0.8 kcal / mol from MMX calculation ($\Delta E_{total} = 6.7 + 0.8 = 7.5$ kcal / mol) explains the experimental finding that only the "*out*" isomer was found by X-ray analysis for **2**.

For the purpose of probing the electronic origin of the stability difference between the two conformers of CpCp*TiCl(*o*-FC_6H_4) **2**, the LUMO's of fragment CpCp*$TiCl^+$ (FMO 47 and 48, Figure 5-15) and the HOMO's of fragment *o*-$FC_6H_4^-$ (FMO 108 and 109, Figure 5-16) were also examined. It is interesting to find that both LUMO's of CpCp*$TiCl^+$ have a dominant contribution from titanium (*ca.* 60% for FMO 47 and 78% for FMO 48) but have significant amount of π mixing with Cp and Cp* (*ca.* 28% for FMO 47 and 15% for FMO 48). This observation is similar to those found for Cp_2TiCl^+.[372] The LUMO's with titanium contributions are highlighted in Figure 5-15 by keeping the same geometry and omitting orbital contributions from the Cp and Cp* groups. With respect to the *o*-$FC_6H_4^-$ fragment the first LUMO of

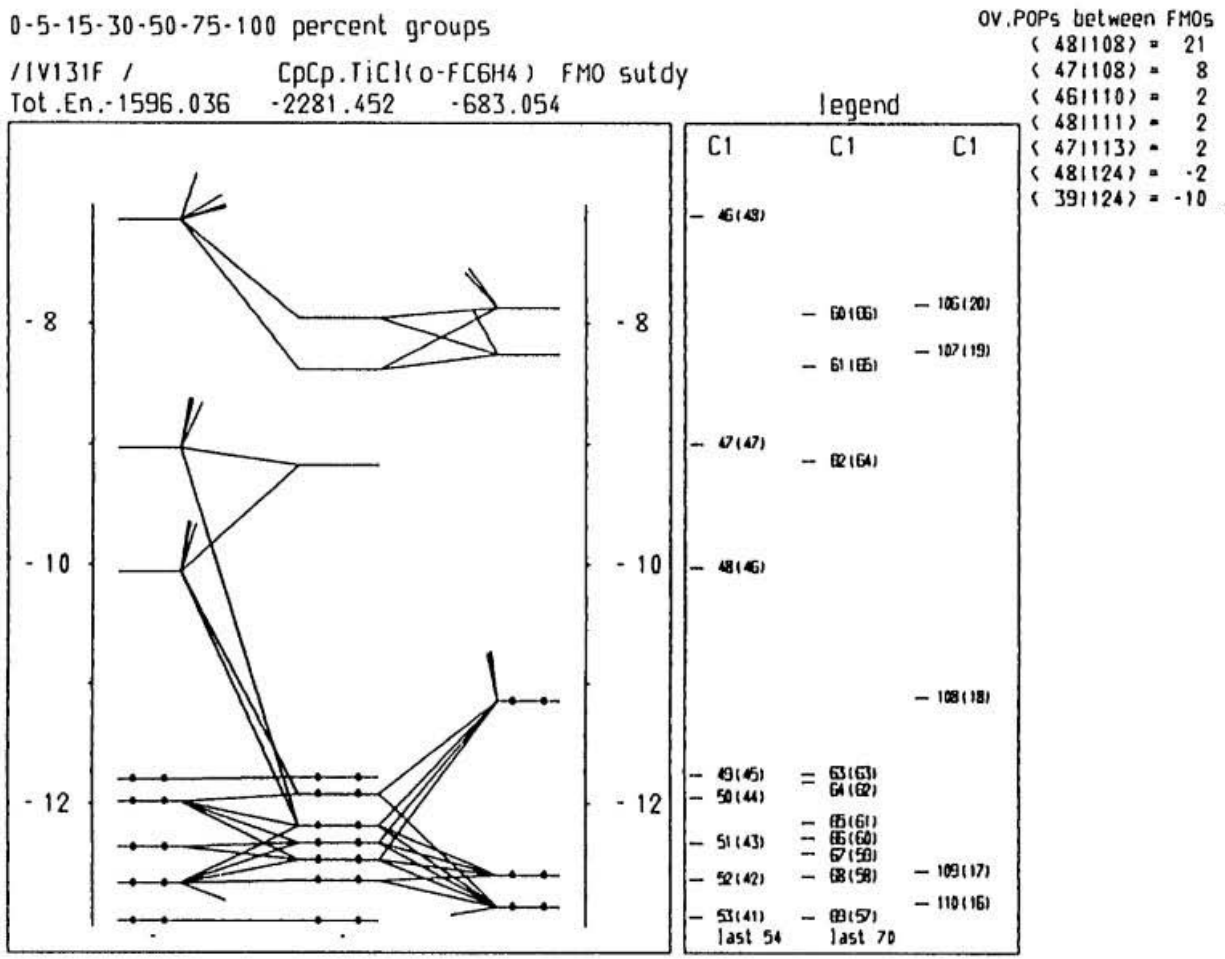

Figure 5-13. Partial interaction diagram for 2 ("out" isomer)

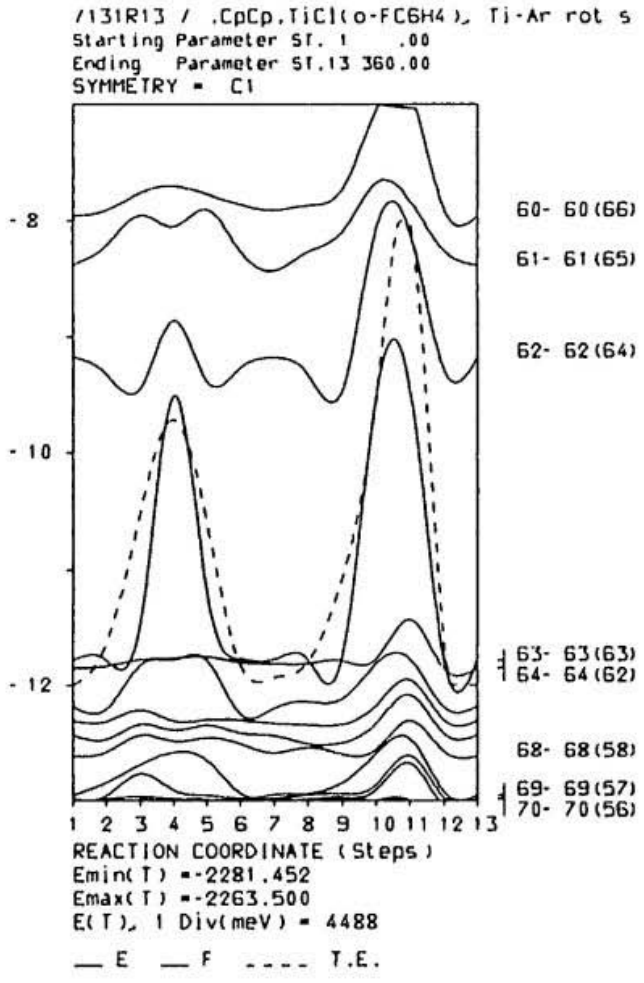

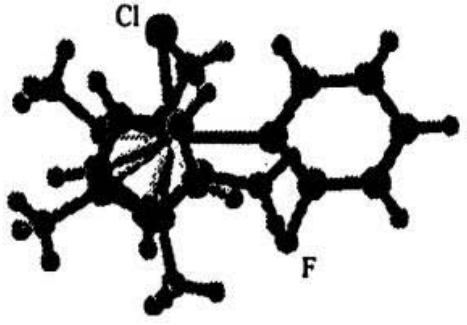

Rotation angles (deg) for step 1-13:
0, 30, 60, 100.9, 120, 150, 180, 210, 240, 259.7, 300, 330, 360

Figure 5-14. Energy profile of rigid rotation of *o*-FC_6H_4 around Ti-C_{ipso} bond for 2

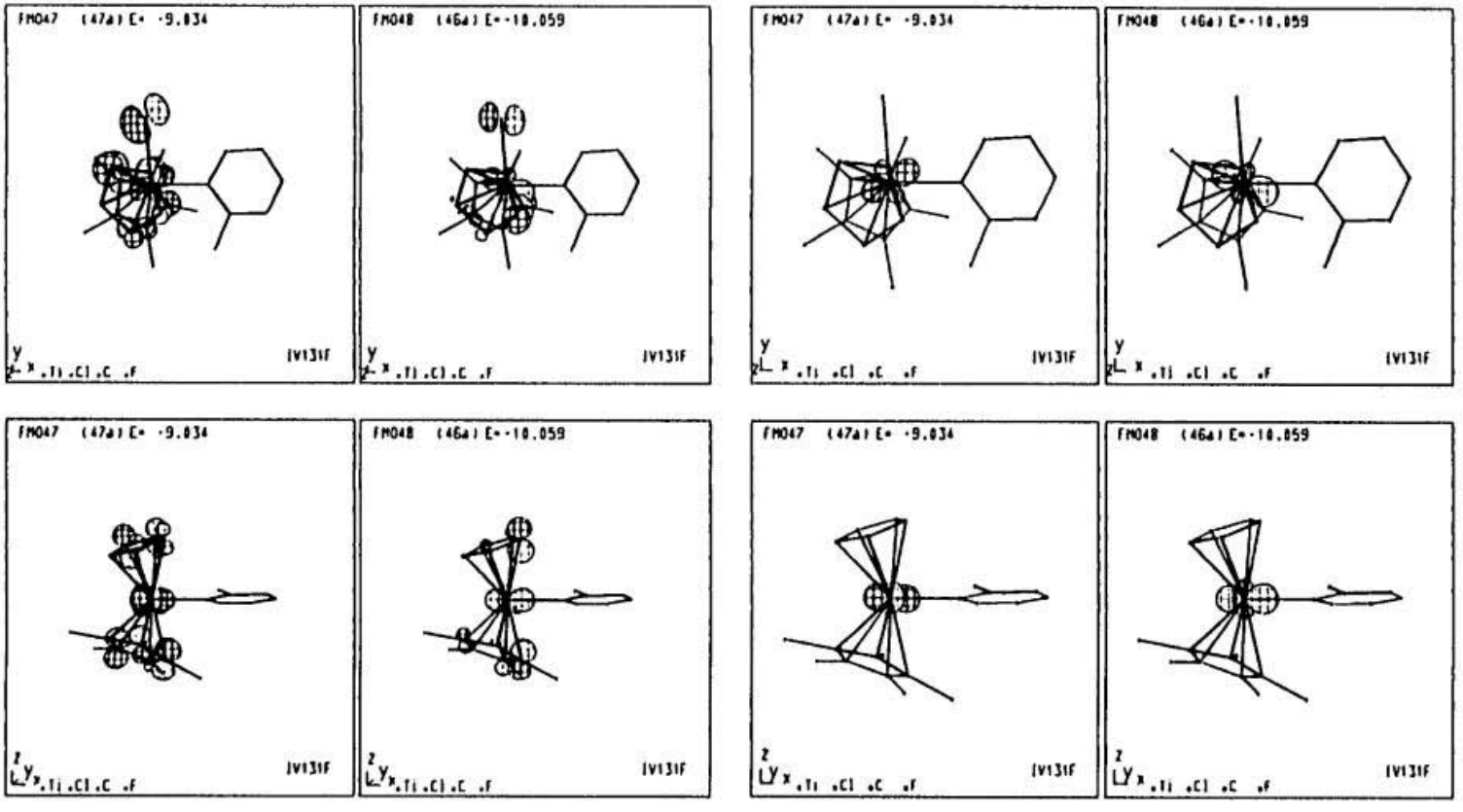

Figure 5-15. LUMOs (FMO 47 and 48) of CpCp*TiCl$^+$, Top view (top), side view (bottom); only contributions from Ti are shown in the top right and bottom right drawings.

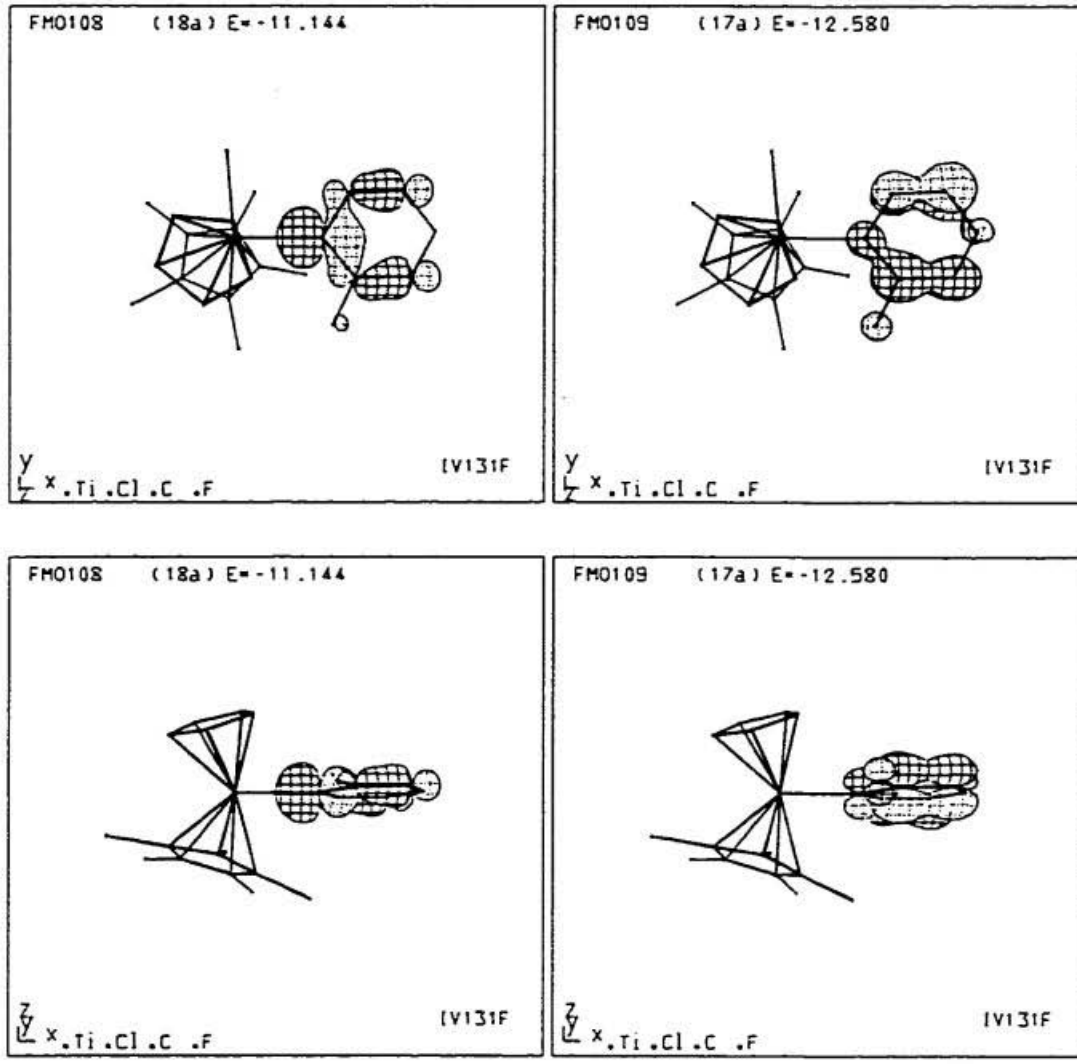

Figure 5-16. HOMOs (FMO 108 and 109) of *o*-$FC_6H_4^-$, Top view (top), side view (bottom)

fragment CpCp*TiCl$^+$ (FMO 47) exhibits roughly σ symmetry while the second LUMO (FMO 48) shows mainly π symmetry (Figure 5-15). Visual examination of Figure 5-16 indicates that the first HOMO of the *o*-$FC_6H_4^-$ unit (FMO 108) is a σ type while the second HOMO (FMO 109) is a π type with π contribution from the *ortho* fluorine atom. Based on symmetry considerations, the first HOMO of the *o*-$FC_6H_4^-$ unit (FMO 108) will only interact with the first LUMO of fragment CpCp*TiCl$^+$ (FMO 47). This σ type interaction will be the same for the *ortho* fluorine atom in the "*in*" and in the "*out*" conformer. However the situation is different for the π interaction. In the "*out*" conformer the *ortho* fluorine atom can interact with one smaller lobe of the metal based orbital pointing toward the fluorine atom in addition to an interaction between the larger lobe located in the +X and +Y quadrant and the π orbital along the C_{ipso}-C_{meta}(*o*-F) bond. On the other hand, there is little or no interaction between the *ortho* fluorine atom and the smaller lobe of the metal based orbital in the "*in*" conformer although the large lobe interaction remains.

Attempts to determine the rotational barrier of the aryl group about the Ti-C_{ipso} bond were made by rotating the aryl group around the Ti-C_{ipso} bond in the range 0 - 360° with a step size of 30° (total 13 steps). When a prohibitive steric interaction between an aryl fluorine atom and a proton in Cp or Cp*, was met, a nearest conformation

(obtained via varying the Ti-Ar rotation angle manually) was used.

The energy profile with the starting geometry and rotation angle corresponding to each step for $(C_5H_5)(C_5Me_5)(Cl)Ti$-(*o*-FC_6H_4) (**2**) (cf. Figure 5-14) shows two barriers which are controlled by the HOMO (MO 63). The maximum at 10.25 eV corresponds to *o*-F passing by the Cp ring while the maximum at 17.95 eV corresponds to *o*-F passing by the bulkier C_5Me_5 ring. The calculated Ti-Ar rotation barrier is 17.95 eV for (**2**). Steric effects (seen by the EHMO method as $4e^-$ repulsions between the two electron pairs of the two contacting atoms) are clearly evident in complex **2** and they are so serious that both 90° and 270° rotations from the optimized starting geometry are prohibited due to unreasonably short contacts between H (Cp*) and *ortho* H (*o*-FC_6H_4) (0.65 Å), and between H (Cp*) and F (*o*-FC_6H_4) (0.364 Å). The overlap population for Ti-C_{ipso} during the 0-360° rotation varies from 0.409 to 0.503 suggesting some π character for the Ti-C_{ipso} bond while the overlap population for the Ti-*o*-F bond changes only from -0.033 to 0.011, which indicates that coordination of *o*-F to Ti is very weak or virtually not existent.

A partial interaction diagram and energy profile for $(C_5H_5)_2Ti(Cl)(C_6F_5)$ (**3**) are given in Figures 5-17 and 5-18. As expected, Figure 5-18 shows an approximately double,

two-fold barrier due to a C_2-axis in the ligand C_6F_5. The barriers at 11.95, 7.02, 12.28 and 8.99 eV are dominated by HOMO (MO 48) (Figure 5-18). The Ti-C_{ipso} overlap population changes from 0.388 to 0.430 suggesting that the Ti-C_{ipso} bond is mostly σ bonding. The two Ti-*o*-F overlap populations are within -0.011 ~ 0.007 and -0.029 ~ 0.011 indicating essentially no interaction between *ortho* fluorine atoms and titanium.

Figures 5-19 and 5-20 show a partial interaction diagram and energy profiles for $(C_5H_5)_2Ti(Cl)(o\text{-}FC_6H_4)$ (4) with the starting geometry (F "*in*") and rotation angle corresponding to each step, respectively. Interestingly, the total energy difference between step 7 (F "*out*") and step 1 (F "*in*"), E_7-E_1, is -0.60 eV (13.8 kcal/mol) which suggested the "*out*" conformer is more stable than the "*in*" conformer. This result is consistent with the result obtained from the molecular mechanics (MMX field) study which showed that the "*out*" conformer is about 0.8 kcal/mol more stable than the "*in*" conformer (Table 5-9). The EHMO and MMX results taken together indicate that the "*out*" conformer still has a *ca.* 14.6 kcal/mol energetic preference over the "*in*" conformer, which conforms well with the solid state structure of the isostructural compound $(C_5H_5)(C_5Me_5)Ti(Cl)(o\text{-}FC_6H_4)$ (2). The overlap populations of the Ti-*o*-F (-0.024 ~ 0.008) and Ti-C_{ipso} (0.399 ~ 0.429) bonds suggest no interaction between

ortho fluorine and titanium and only a small π character for the Ti-C_{ipso} bond. The rotation barriers at step 3, 5, 9 and 11 (Figure 5-20) are 4.36 eV, 5.33, 6.41 and 1.60 eV, respectively.

The energy profile for $(C_5H_5)_2Ti(C_6F_5)_2$ (**5**) with the starting geometry and rotation angle corresponding to each step as well as a partial interaction diagram from FMO analysis are depicted in Figure 5-22 and 5-21, respectively. Both the calculated barrier (34.20 eV) for geared C_6F_5 rotation and the barrier (22.12 eV) for non-geared C_6F_5 rotation are rather high indicating a strong "4 e^- interaction" and imply a profound steric effect during geared and non-geared C_6F_5 rotations. The extremely high barrier obtained suggests either that rigid rotation is not a realistic model or that EHMO method is too simple for this study.

A partial interaction diagram from FMO analysis and energy profile for $(C_5H_5)_2Ti(o\text{-}FC_6H_4)_2$ (**6**) with the starting geometry and rotation angle corresponding to each step are given in Figures 5-23 and 5-24, respectively. The calculated rotation barriers for two fluorine atoms in both "*out*", both "*in*", one "*in*" and one "*out*", geared both "*out*", geared both "*in*", and geared one "*in*" and one "*out*" are 8.47, 24.95, 9.85, 38.61, 37.99 and 15.85 eV, respectively. These data indicate that the geared barrier

is larger. In geared rotation with both F's "*out*", 150° and 330° rotations from the optimized starting geometry of **6** gave *ortho* F - *ortho* F and *ortho* H - *ortho* H contacts of 0.417 Å and 0.662 Å, respectively, and are forbidden since they are much shorter than the sum (0.74 Å for H-H and 1.44 Å for F-F, respectively) of their corresponding covalent radii. In geared rotation with both F's "*in*", 330° rotation was prohibited for the same reason. All these steric effects make the rotational barrier rather high and exaggerated. In the lowest rotation barrier case, *i.e.*, non-geared rotation with both F's "*out*", the overlap population for Ti-*o*-F is still negligible (within -0.023 ~ 0.008) during 0-360° rotation. In other words the coordination of *o*-F to titanium is insignificant.

On balance, it seems to be not reliable to evaluate the aryl rotation barrier in complexes **2** - **6** by the rigid rotation function associated with the CACAO package due to serious steric effects (appears as four electron repulsions in EHMO calculation).[262]

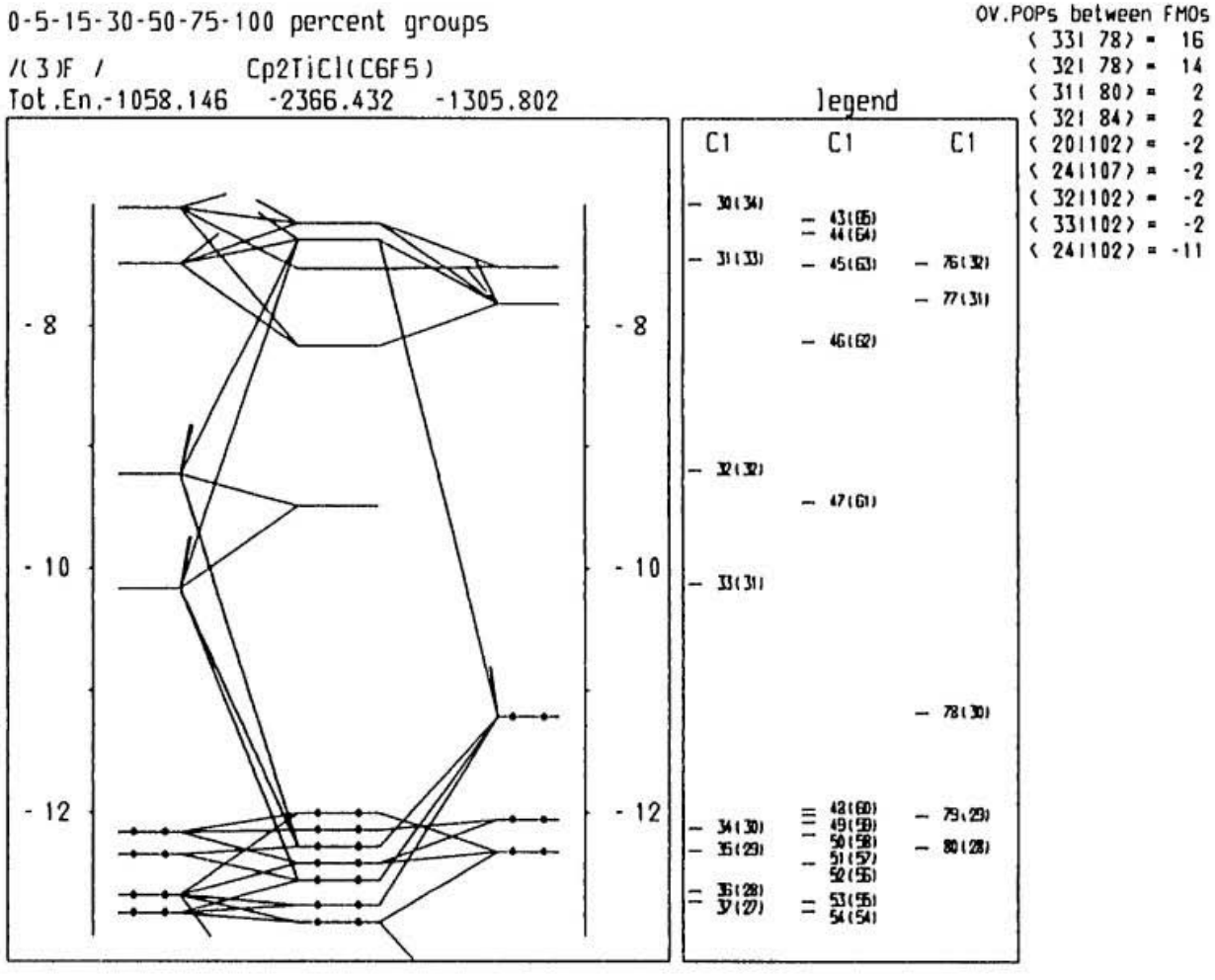

Figure 5-17. Partial interaction diagram for 3

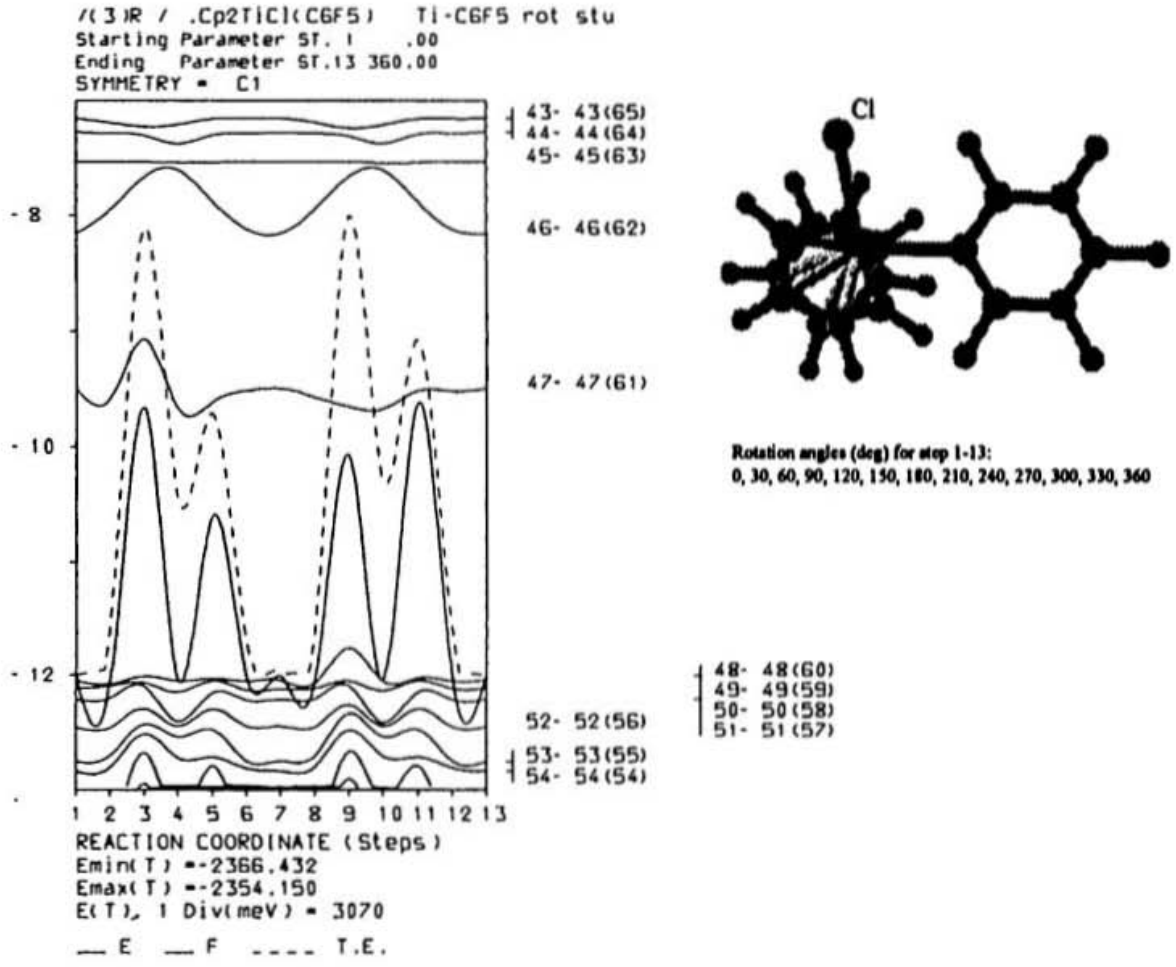

Figure 5-18. Energy profile of rigid rotation of C_6F_5 around Ti-C_{ipso} bond for 3

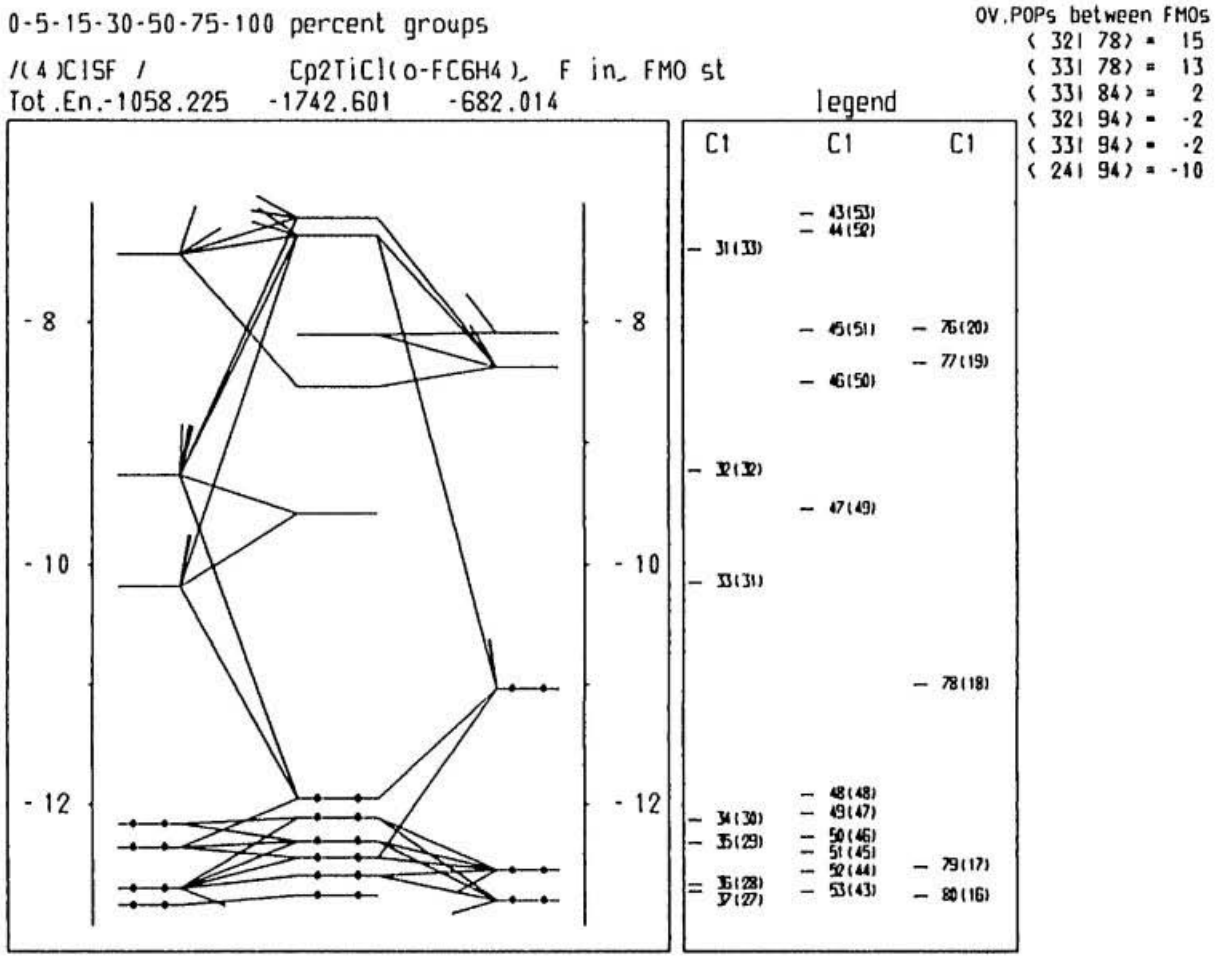

Figure 5-19. Partial interaction diagram for 4, with F "*in*"

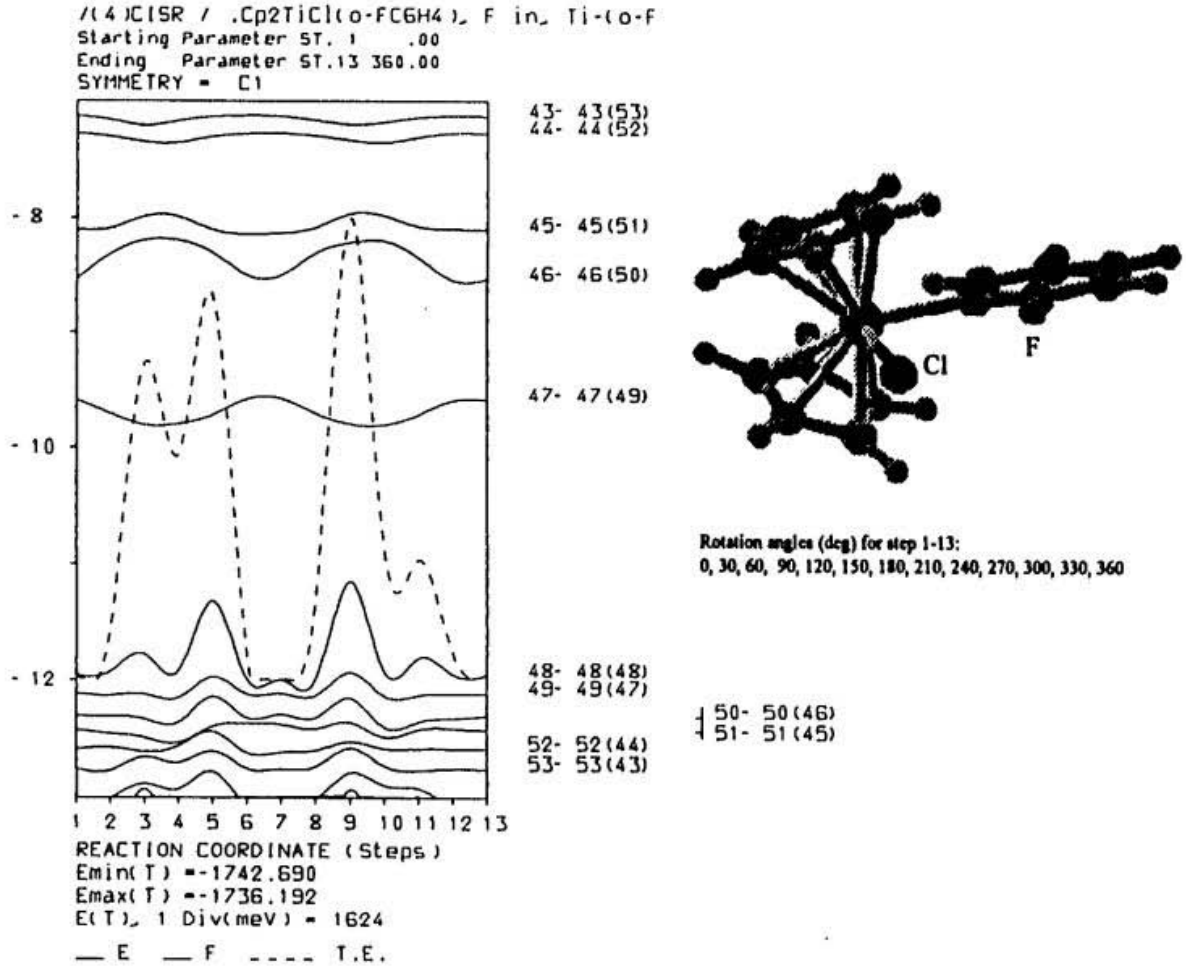

Figure 5-20. Energy profile of rigid rotation of *o*-FC_6H_4 around Ti-C_{ipso} bond for 4, with F "*in*"

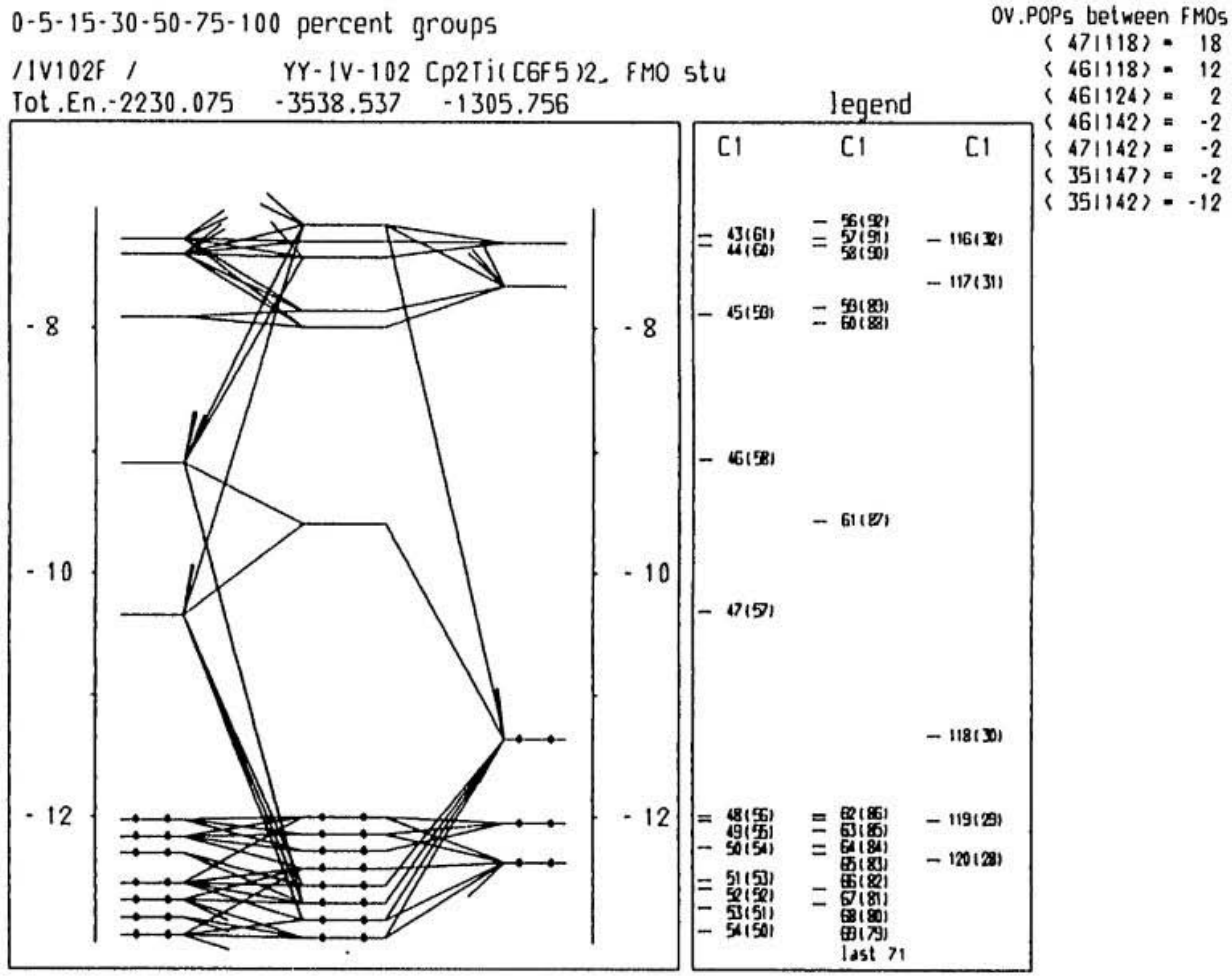

Figure 5-21. Partial interaction diagram for 5

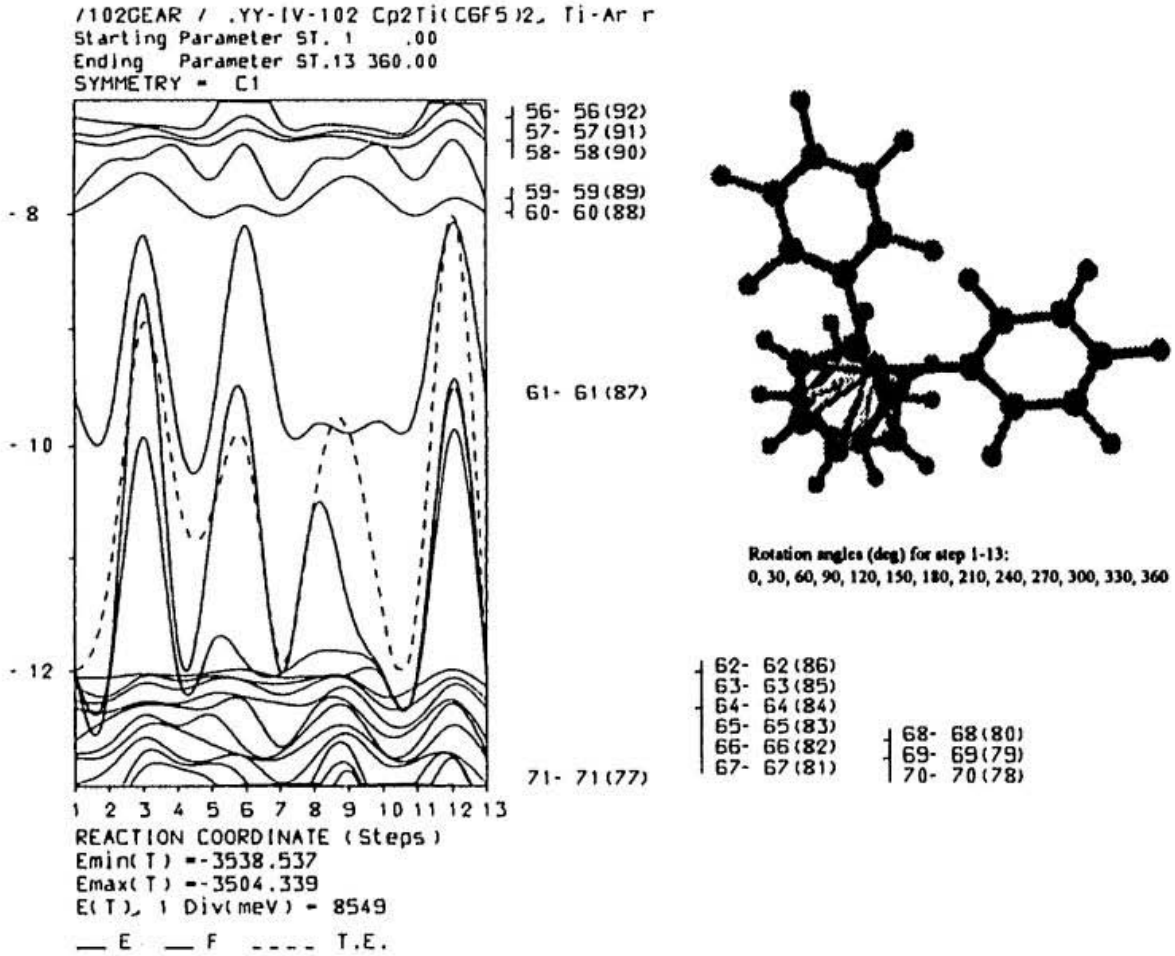

Figure 5-22. Energy profile of rigid rotation of C_6F_5 around Ti-C_{ipso} bond for 5, geared

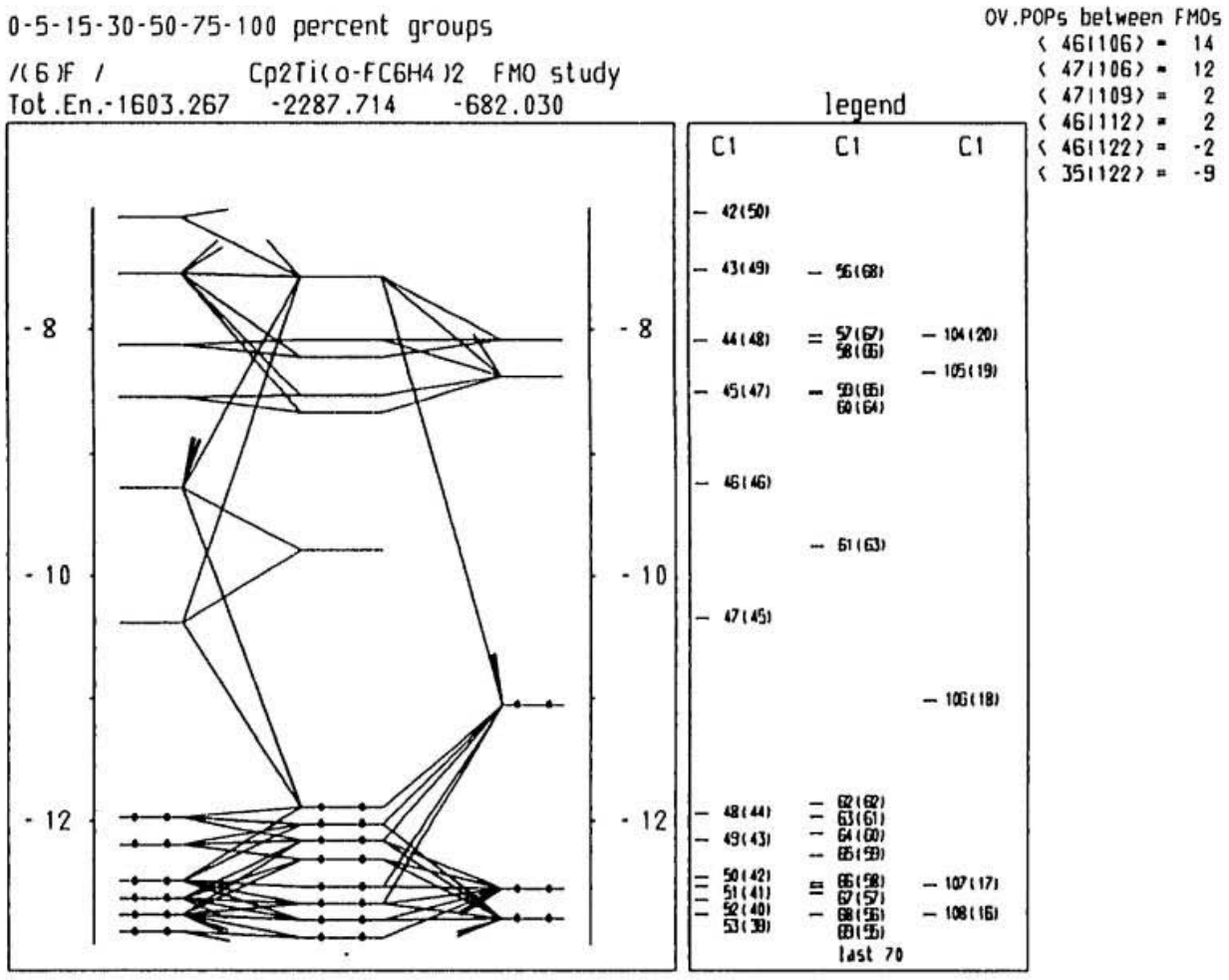

Figure 5-23. Partial interaction diagram for 6, with both F "*out*"

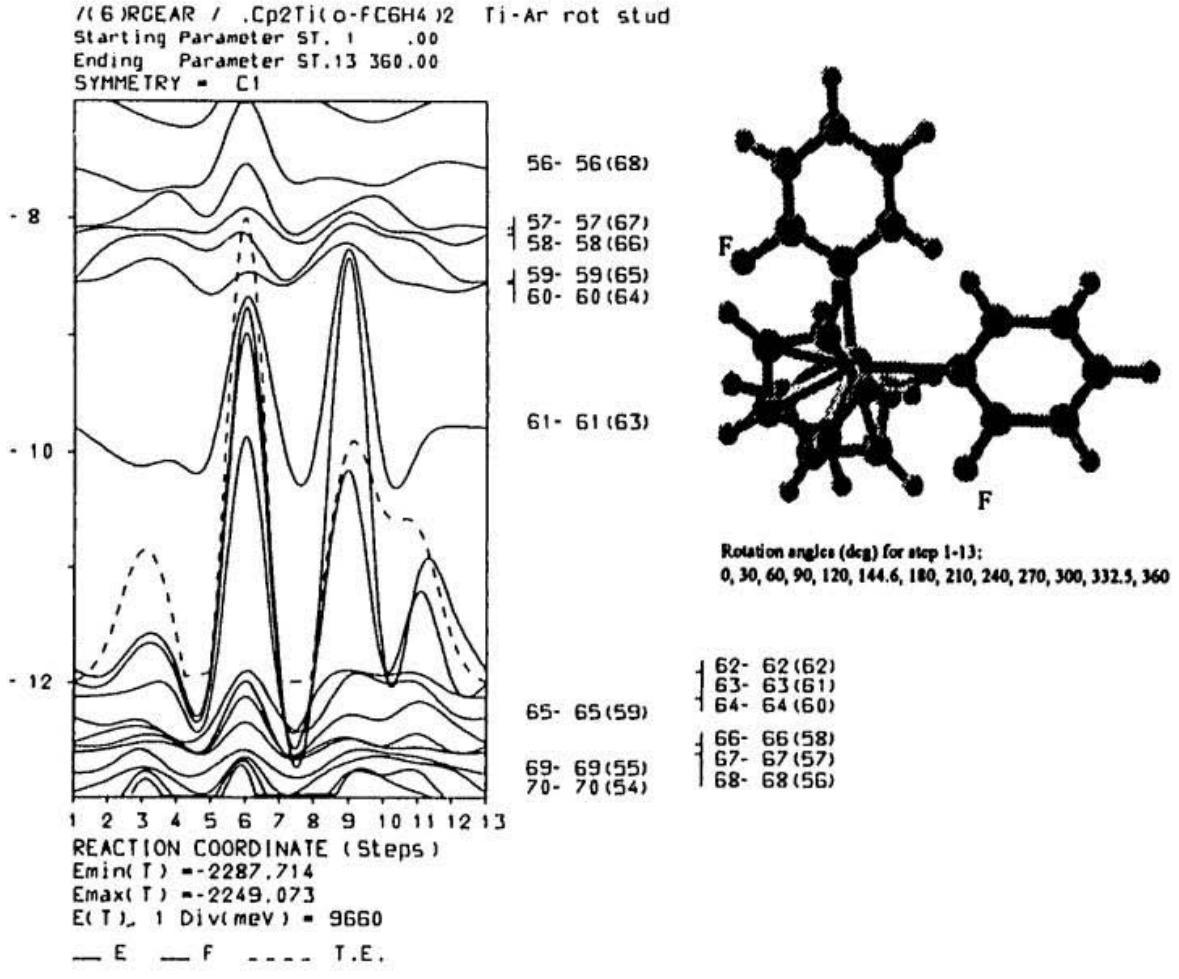

Figure 5-24. Energy profile of rigid rotation of *o*-FC_6H_4 around Ti-C_{ipso} bond for 6, geared with both F "*out*"

5.4. Summary

A series of new and previously known fluorine substituted phenyl titanocene complexes $(C_5H_5)(C_5R_5)TiX(Ar)$ (R = Me, X = Cl, *o*-FC_6H_4 (**2**); R = H, X = Cl, Ar = C_6F_5 (**3**), *o*-FC_6H_4 (**4**), R = H, X = R = C_6F_5 (**5**), *o*-FC_6H_4 (**6**)) were prepared. Aryl rotation around the Ti-C_{ipso} bond and conformational preference were studied by ^{19}F VT NMR, and single crystal X-ray diffraction for compounds **2** and **5**, and by molecular modelling (MMX) and molecular orbital calculations (EHMO). Activation parameters were obtained for the restricted C_6F_5 rotation about the Ti-C_{ipso} bond in **3** and **5** by DNMR5 analysis.

5.5. Experiments

5.5.1. General Procedure. All manipulations were performed under an atmosphere of nitrogen using standard Schlenk techniques. Diethyl ether, THF and toluene were distilled from purple solutions of sodium and benzophenone under nitrogen. Methylene chloride was distilled from CaH_2. Compounds **3**,[339] **4**,[351] **5**[339] and **6**[351] were synthesized by published procedures. *o*-Fluorophenyllithium[373] and pentafluorophenyllithium[343] were prepared from the corresponding bromides and *n*-butyllithium

prior to use. Other experiments were conducted by using the procedure described in Chapter 4.

5.5.2. X-ray Crystallography. Red crystals of **2** suitable for X-ray analysis were obtained by slow evaporation of an ethyl ether / hexane solution of **2**. A red, irregularly shaped crystal having dimensions of 0.300 x 0.250 x 0.400 mm was cut and mounted on a glass fibre. All measurements were made on a Rigaku AFC6S diffractometer using graphite monochromated Mo Kα radiation (λ=0.71069 Å), and a 2 kW sealed tube generator. Cell constants and an orientation matrix for data collection, obtained from a least-squares refinement using the setting angles of 23 carefully centred reflections in the range $36.4 < 2\theta < 40.9°$ are given in Table 5-1. Based on packing considerations, a statistical analysis of intensity distribution and the successful solution and refinement of the structure, the unit cell was identified as monoclinic with space group $P2_1/n$ (#14). The data was collected at a temperature of 26 ± 1 °C using the ω-2θ scan technique to a maximum 2θ value of 50.1°. Omega scans of several intense reflections, made prior to data collection, had an average width at half-height of 0.31° with a take-off angle of 6.0°. Scans $(1.57 + 0.35 \tan \theta)°$ were made at a speed of 4.0°/min (in Omega). Weak reflections ($I < 10.0\sigma(I)$) were rescanned (maximum of 2 rescans) and the counts were accumulated to assure good

counting statistics. Stationary background counts were recorded on each side of the reflection. The ratio of peak counting time to background counting time was 2:1. The diameter of the incident beam collimator was 1.0 mm and the crystal to detector distance was 400.0 mm. The intensity of three representative reflections which were measured after every 150 reflections remained constant throughout data collection indicating crystal and electronic stability (no decay correction was applied). The linear absorption coefficient for Mo Kα is 6.1 cm^{-1}. Azimuthal scans of several reflections indicated no need for an absorption correction. The data were corrected for Lorentz and polarization effects. A correction for secondary extinction was applied (coefficient = 0.56385E-06). The structure was solved by direct methods.[240] The non-hydrogen atoms were refined anisotropically. All calculations were performed using the TEXSAN crystallographic software package of Molecular Structure Corporation. Hydrogens were optimized by positional refinement with isotropic thermal parameters set twenty percent great than those of their bonding partners at the time of inclusion. However they were fixed for the final round of refinement.

The X-ray crystal structure of **5** was similarly determined. Crystallographic data, atomic coordinates, bond distances and intermolecular bond angles for **5** are listed in

Table 5-5, 5-6, 5-7 and 5-8, respectively.

5.5.3. Molecular Mechanics Modelling. The MMX calculation was performed on an IBM compatible PC with a Pentium-133 CPU using PCMODEL for Windows version 6.0.[334, 336] The starting structures for **3**, **4**, and **6** for minimization were obtained by assembling related structural components *via* the associated drawing tool. Starting structures for **2** and **5** were taken from single crystal X-ray analysis. The Cp, Cp*, *o*-FC_6H_4 and C_6F_5 groups were constructed as substructures by the free drawing tool and were separately minimized several times before assembly. The rotational conformational energy profile was calculated utilizing the dihedral driver within PCMODEL.

5.5.4. Molecular orbital calculations. Extended Hückel calculations were conducted with the EH program contained in the CACAO package (version 4.0)[262] on an IBM compatible PC. The default atomic parameters contained in the data file of the CACAO package[262] were used in all calculations. The optimized geometries of complexes **3**, **4**, and **6** were calculated with PCMODEL 6.0 (MMX force field)[334, 336] while the geometries of **2** and **5** were directly taken from X-ray coordinates. The program CHANGE[344] was used to transform either X-ray / fractional coordinates or

Cartesian coordinates to internal coordinates used for the rotation study via the CACAO package. Sample input files for both FMO analysis and the rotation study are given in appendices 2 and 3.

5.5.5. Preparation of CpCp*TiCl(*o*-FC_6H_4) (Cp*=C_5Me_5) (2). A 150-mL, three-neck, round-bottom flask equipped with a magnetic stirring bar, pressure-equalizing addition funnel, nitrogen inlet and outlet was charged with 0.4895 g (1.534 mmol) of CpCp*$TiCl_2$ in 10 mL Et_2O and 20 mL THF and cooled to -78°C. Through the addition funnel, an ether-pentane solution containing 1.534 mmol (*ca.* 45 mL) of *o*-FC_6H_4Li, freshly made from *o*-FC_6H_4Br and n-BuLi in ether using the established literature method,[343] was added dropwise with stirring. After stirring at -78°C for 2 hours, the reaction mixture was allowed to warm to room temperature and stirred for 24 hours. The precipitated LiCl was removed by filtration. Removal of solvent under vacuum afforded a red residue. Chromatographic separation by eluting with 1:4 ether / hexane and work up gave 0.2513 g (66%) of **2** as a dark red crystalline solid. *Anal.* Found (calcd.): C, 66.23 (66.60), H, 6.42 (6.39). ^{1}H NMR ($CDCl_3$, ppm): 7.11(m, 1H), 6.92(m, 1H), 6.76(m, 1H), 6.66(m, 1H), 6.20(s, 5H), 1.88(s, 15H). ^{13}C NMR: 141.03(d, 17.8), 127.68(s), 126.03(d, 8.0), 123.56(s), 119.84(s), 117.21(s, Cp), 113.76(d, 32.8), 13.06 (s, Me). ^{19}F NMR (25, -50, -60 and 140°C): -87.66(s).

References

1. Eliel, E. L.; Wilen, S. H.; Mander, L. N. In *Stereochemistry of Organic Compounds*; John Wiley & Sons, Inc.: New York, 1994.

2. Actually, in achiral environments physical properties of two enantiomers are identical!

3. Thall, E. *J. Chem. Ed.* **1996**, *73*, 481.

4. Coppola, G. M.; Schuster, H. F. In *Asymmetric Synthesis - Construction of Chiral Molecules Using Amino Acids*; John Wiley & Sons: New York, 1987.

5. Collins, A. N.; Sheldrake, G. N.; Crosby, J. In *Chirality in Industry: The Commercial Manufacture and Applications of Optically Active Compounds*; John Wiley & Sons: Chichester, 1992.

6. Mellin, G. W.; Katzenstein, M. *New Engl. J. Med.* **1962**, *267*, 1184.

7. De Camp, W. H. *Chirality* **1989**, *1*, 2.

8. Ager, D. J.; East, M. B. In *Asymmetric Synthetic Methodology*; CRC Press, Inc.: New York, 1996.

9. Aboul-Enein, H. Y.; Basha, L. I. A. In *The impact of Stereochemistry on Drug Development and Use*, 1st; Aboul-Enein, H. Y.; Wainer, I. W., Eds.; Interscience: New York, 1997; p1.

10. Juaristi, E. In *Introduction to Stereochemistry and Conformational Analysis*; John Wiley & Sons, Inc.: New York, 1991.

11. Announcement *Chirality* **1992**, *4*, 338.

12. Sheldon, R. *Chem. Ind.* **1990**, 212.

13. Tombo, G. M. R.; Bellus, D. A. N. I. E. L. *Angew. Chem., Int. Ed. Engl.* **1991**, *30*, 1193.

14. Jacques, J.; Collet, A.; Wilen, S. H. In *Enatiomers, Racemates, and Resolutions*; John Wiley & Sons, Inc.: New York, 1981.

15. Davies, S. G.; Brown, J. M.; Pratt, A. J.; Fleet, G. *Chem. Br.* **1989**, *25*, 259.

16. Armstrong, R. W.; Beau, J.-M.; Cheon, S. H.; Christ, W. J.; Fujioka, H.; Ham, W.-H.; Hawkins, L. D.; Jin, H.; Kan, S. H.; Kishi, Y.; Martinelli, M. J.; McWhorter, W. W.; Mizuno Jr., M.; Nakata, M.; Stutz, A. E.; Talamas, F. X.; Taniguchi, M.; Tino, J. A.; Ueda, K.; Uenishi, J.; White, J. B.; Yonaga, M. *J. Am. Chem. Soc.* **1989**, *111*, 7525.

17. Nogradi, M. In *Selective Synthesis, A Pratical Approach*, 2nd; VCH: Weinheim, 1995.

18. Atkinson, R. S. In *Stereoselective Synthesis*; John Wiley & Sons: Chichester, 1995.

19. Crosby, J. In *Chirality in Industry: the Commercial Manufacture and Applications of Optically Active Compounds*; Collins, A. N.; Sheldrake, G. N.; Crosby, J., Eds.; John Wiley & Sons: Chichester, 1992; p1.

20. Borman, S. *Chem. and Eng. News* **1990**, *July 9*, 9.

21. Kagan, H. B.; Fiaud, J. C. *Top. Stereochem.* **1988**, *18*, 249.

22. Jones, J. B. *Tetrahedron* **1986**, *42*, 3351.

23. Brown, J. M. *Chem. Ind.* **1988**, *Oct. 13*, 612.

24. Noyori, R. In *Asymmetric Catalysis in Organic Synthesis*; Wiley: New York, 1994.

25. Pasteur, L. *Ann. Chim. et Phys.* **1848**, *24*, 442.

26. Cristau, H. J.; Plenat, F. In *The Chemistry of Organophosphorus Compounds*; Hartley, F. R., Ed.; John Wiley & Sons: Chichester, 1994; Vol. 3, p45.

27. Rouhi, M. *Chemical and Engineering News* **1996**, *Aug. 12*, 10.

28. Meyers, A. I. In *Stereoselective Synthesis, A Pratical Approach*, 2nd; Nogradi, M., Ed.; VCH: Weinheim, 1995; .

29. Noyori, R. *Science (Washington, D.C.)* **1990**, *248*, 1194.

30. Sardina, F. J.; Rapoport, H. *Chem. Rev.* **1996**, *96*, 1825.

31. Seebach, D.; Hungerbuhler, E. In *Modern Synthetic Methods 1980*; Scheffold, R.,

Ed.; Salle & Sauerlander: Frankfurt, 1980; .

32. Mehta, G. *Pure Appl. Chem.* **1990**, *62*, 1263.

33. Kunz, H.; Ruck, K. *Angew. Chem., Int. Ed. Engl.* **1993**, *32*, 336.

34. Pietrusiewicz, K. M.; Zablocka, M. *Chem. Rev.* **1994**, *94*, 1375.

35. Ojima, I. In *Catalytic Asymmetric Synthesis*; VCH Publishers: New York, 1993.

36. Morrison, J. D. In *Asymmetric Synthesis - Vol 5. Chiral Catalysis*; Academic Press: Orlando, 1985; Vol. 5,.

37. McQuillin, F. J.; Parker, D. G.; Stephenson, G. R. In *Transition Metal Oranometallics for Organic Synthesis*; Cambridge University Press: Cambridge, 1991.

38. Blystone, S. I. *Chem. Rev.* **1989**, *89*, 1663.

39. Duthaler, R. O.; Hafner, A. *Chem. Rev.* **1992**, *92*, 807.

40. Green, M. L. H.; Davies, S. G. In *The Influence of Organometallic Chemistry on Organic Synthesis: Present and Future*; The Royal Society: London, 1988.

41. Collman, J. P.; Hegedus, L. S.; Norton, J. R.; Finke, R. G. In *Principles and Applications of Organotransition Metal Chemistry*; University Science Books: California, 1987.

42. Hegedus, L. S. In *Transition Metals in the Synthesis of Complex Organic Molecules*; University Science Books: California, 1994.

43. Davies, S. G. In *Organotransition Metal Chemistry: Applications to Organic Synthesis*; Pergamon Press: Oxford, UK, 1982.

44. Brunner, H. *J. Organomet. Chem.* **1995**, *500*, 39.

45. Sawamura, M.; Ito, Y. *Chem. Rev.* **1992**, *92*, 857.

46. Brunner, H. *Top. Stereochem.* **1988**, *18*, 129.

47. Scott, J. W. *Top. Stereochem.* **1989**, *19*, 209.

48. Parshall, G. W.; Ittel, S. D. In *Homogeneous Catalysis - The Application and Chemistry of Catalysis by Soluble Transition Metal Complexes*, 2nd; John Wiley & Sons: New York, 1992.

49. Tonks, L.; Williams, J. M. J. *Contemp. Org. Synth.* **1997**, 353.

50. Regan, A. C. *Contemp. Org. Synth.* **1997**, *4*, 1.

51. Brunner, H. *Synthesis* **1988**, 645.

52. Noyori, R. *Chemtech* **1992**, *22*, 360.

53. Halpern, J. In *Asymmetric Synthesis: Vol. 5, Chiral Catalysis*; Morrison, J. D., Ed.; Academic Press: Orlando, 1985; Vol. 5, p41.

54. Bosnich, B.; Fryzuk, M. D. *Top. Stereochem.* **1981**, *12*, 119.

55. Koenig, K. E. In *Asymmetric Synthesis: Vol. 5, Chiral Catalysis*; Morrison, J. D., Ed.; Academic Press: Orlando, 1985; Vol. 5, p71.

56. Takaya, H.; Ohta, T. *J. Synth. Org. Chem. Jpn.* **1993**, *51*, 1013.

57. Takaya, H.; Ohta, T.; Noyori, R. In *Catalytic Asymmetric Synthesis*; Ojima, I., Ed.; V C H Publishers: New York, 1993; p1.

58. Kagan, H. B.; Sasaki, M. In *The Chemistry of Organophosphorus Compounds*; Hartley, F. R., Ed.; John Wiley & Sons: New York, 1990; Vol. 1, p51.

59. Noyori, R.; Takaya, H. *Acc. Chem. Res.* **1990**, *23*, 345.

60. Ojima, I.; Hirai, K. In *Asymmetric Synthesis: Vol. 5, Chiral Catalysis*; Morrison, J. D., Ed.; Academic Press: Orlando, 1985; Vol. 5, p103.

61. Ojima, I.; Clos, N.; Bastos, C. *Tetrahedron* **1989**, *45*, 6901.

62. Kitamura, M.; Hsiao, Y.; Ohta, M.; Tsukamoto, M.; Ohta, T.; Takaya, H.; Noyori, R. *J. Org. Chem.* **1994**, *59*, 297.

63. Johnson, R. A.; Sharpless, K. B. In *Catalytic Asymmetric Synthesis*; Ojima, I., Ed.; VCH Publishers: New York, 1993; p103.

64. Jacobsen, E. N. In *Catalytic Asymmetric Synthesis*; Ojima, I., Ed.; VCH Publishers: New York, 1993; p159.

65. Finn, M. G.; Sharpless, K. B. In *Asymmetric Synthesis: Vol. 5, Chiral Catalysis*; Morrison, J. D., Ed.; Academic Publication: Orlando, 1985; Vol. 5, p247.

66. Rossiter, B. E. In *Asymmetric Synthesis: Vol. 5, Chiral Catalysis*; Morrison, J. D., Ed.; Academic Press: Orlando, 1985; Vol. 5, p193.

67. Schurig, V.; Betschinger, F. *Chem. Rev.* **1992**, *92*, 873.

68. Hanson, R. M. *Chem. Rev.* **1991**, *91*, 437.

69. Bolm, C. *Angew. Chem., Int. Ed. Engl.* **1991**, *30*, 403.

70. Donohoe, T. J.; Gyo, P. M.; Moore, P. R.; Stevenson, C. A. *Contemp. Org. Synth.* **1997**, *4*, 22.

71. Doyle, M. P.; Protopopova, M. N.; Brandes, B. D.; Davies, H. M. L.; Huby, N. J. S.; Whitesell, J. K. *Synlett* **1993**, 151.

72. Hayashi, T. In *Catalytic Asymmetric Synthesis*; Ojima, I., Ed.; VCH Publishers: New York, 1993; p325.

73. Hayashi, T.; Kumada, M. In *Asymmetric Synthesis: Vol. 5, Chiral Catalysis*; Morrison, J. D., Ed.; Academic Press: Orlando, 1985; Vol. 5, p147.

74. Kinting, A.; Krause, H.; Capka, M. *J. Mol. Catal.* **1985**, *33*, 215.

75. Osborne, J. A.; Jardine, F. H.; Young, J. F.; Wilkinson, G. *J. Chem. Soc., (A)* **1966**, 1711.

76. Horner, L.; Seigel, H.; Buthe, H. *Angew. Chem., Int. Ed. Engl.* **1968**, *7*, 942.

77. Knowles, W. S.; Sabacky, M. J. *J. Chem. Soc., Chem. Commun.* **1968**, 1445.

78. Morrison, J. D.; Burnett, R. E.; Aguiar, A. M.; Morrow, C. J.; Phillips, C. *J. Am. Chem. Soc.* **1971**, *93*, 1301.

79. Kagan, H. B.; Dang, T.-P. *J. Chem. Soc., Chem. Commun.* **1971**, 481.

80. Kagan, H. B.; Dang, T.-P. *J. Am. Chem. Soc.* **1972**, *94*, 6429.

81. Whitesell, J. K. *Chem. Rev.* **1989**, *89*, 1581.

82. Knowles, W. S. *Acc. Chem. Res.* **1983**, *16*, 106.

83. Knowles, W. S. *J. Chem. Ed.* **1986**, *63(3)*, 222.

84. Npyori, R. *Acta Chem. Scand.* **1996**, *50*, 380.

85. Noyoru, R. *Chem. Soc. Rev.* **1989**, *18*, 187.

86. Noyori, R.; Takaya, H. *Chem. Scr.* **1985**, *25*, 83.

87. Ohta, T.; Takaya, H.; Kitamura, M.; Nagai, K.; Noyori, R. *J. Org. Chem.* **1987**, *52*, 3174.

88. Noyori, R.; Ohta, M.; Hsiao, Y.; Kitamura, M.; Ohta, T.; Takaya, H. *J. Am. Chem. Soc.* **1986**, *108*, 7117.

89. Oppolzer, W.; Wills, M.; Starkemann, C.; Bernardinelli, G. *Tetrahedron Lett.* **1990**, *31*, 4117.

90. Brunner, H. *Angew. Chem., Int. Ed. Engl.* **1969**, *8*, 382.

91. Rogers, D. *Acta Crystallogr., Sect. A: Found. Cryst.* **1981**, *37*, 734.

92. Brunner, H. *Adv. Organometal. Chem.* **1980**, *18*, 151.

93. Cahn, R. S.; Ingold, C.; Prelog, V. *Angew. Chem., Int. Ed. Engl.* **1966**, *5*, 385.

94. Lecomte, C.; Dusavsoy, Y.; Protas, J.; Tirouflet, J.; Dormand, A. *J. Organomet. Chem.* **1974**, *73*, 67.

95. Stanley, K.; Baird, M. C. *J. Am. Chem. Soc.* **1975**, *97*, 6598.

96. Attig, T. G.; Wojcicki, A. *J. Am. Chem. Soc.* **1974**, *96*, 262.

97. Brunner, H. *Angew. Chem., Int. Ed. Engl.* **1971**, *10*, 249.

98. Brunner, H.; Jablonski, C. R.; Jones, P. G. *Organometallics* **1988**, *7*, 1283.

99. Brunner, H. In *Chemical Synthesis, Gnosis to Prognosis*; Chatgilialoglu, C.; Snieckus, V., Eds.; NATO ASI Series, Series E: Applied Sciences, Vol.320; Kluwer Academic Publishers: Dordrecht, 1996; p91.

100. Brunner, H. In *The Organic Chemistry of Iron*; Koerner von Gustorf, E. A.; Grevels, F. W.; Fischler, I., Eds.; Academic: New York, 1978; Vol. 1, p299.

101. Brunner, H. *Top. Curr. Chem.* **1975**, *56*, 67.

102. Brunner, H.; Langer, M. *J. Organomet. Chem.* **1973**, *54*, 221.

103. Brunner, H.; Schmidt, E. *J. Organomet. Chem.* **1970**, *21*, P53.

104. Kagan, H. B. In *Comprehensive Organometallic Chemistry*; Pergamon Press: Oxford, 1982; Vol. 8, p463.

105. Brunner, H.; Schmidt, E. *J. Organomet. Chem.* **1973**, *50*, 219.

106. Reisner, M. G.; Bernal, I.; Brunner, H.; Muschiol, M. *Angew. Chem., Int. Ed. Engl.* **1976**, *15*, 776.

107. Reisner, G. M.; Bernal, I.; Brunner, H.; Muschiol, M. *Inorg. Chem.* **1978**, *17*, 783.

108. Bernal, I.; Brunner, H.; Muschiol, M. *Inorg. Chim. Acta* **1988**, *142*, 235.

109. Brunner, H.; Schmidt, E. *J. Organomet. Chem.* **1972**, *36*, C18.

110. Brunner, H.; Langer, M. *J. Organomet. Chem.* **1975**, *87*, 223.

111. Brunner, H.; Aclasis, J.; Langer, M.; Steger, W. *Angew. Chem., Int. Ed. Engl.* **1974**, *13*, 810.

112. Brunner, H.; Steger, W. *J. Organomet. Chem.* **1976**, *120*, 239.

113. Davies, S. G. *Aldrichimica Acta* **1990**, *23*, 31.

114. Davies, S. G. In *Chirality Drug Des. Synth., [Smith Kline French Res. Symp.], 4th*; Brown, C., Ed.; Academic: London, UK., 1990; p181.

115. Davies, S. G.; Bashiardes, G.; Coote, S. J.; Goodfellow, C. L.; McNally, J. P. In *New Aspects Org. Chem. 1, Proc. Int. Kyoto Conf., 4th, Meeting Date 1988*; Yoshida, Z.;

Shiba, T.; Ohshiro, Y., Eds.; Kodansha: Tokyo, Japan., 1989; p81.

116. Brown, J. M.; Davies, S. G. *Nature (London)* **1989**, *342*, 631.

117. Liebeskind, L. S.; Welker, M. E.; Goedkin, V. *J. Am. Chem. Soc.* **1984**, *106*, 441.

118. Liebeskind, L. S.; Welker, M. E. *Tetrahedron Lett.* **1984**, *25*, 4314.

119. Liebeskind, L. S.; Welker, M. E. *Organometallics* **1983**, *2*, 194.

120. Liebeskind, L. S.; Welker, M. E.; Fengl, R. W. *J. Am. Chem. Soc.* **1986**, *108*, 6328.

121. Liebeskind, L. S.; Welker, M. E. *Tetrahedron Lett.* **1985**, *26*, 3079.

122. Davies, S. G.; Seeman, J. I. *Tetrahedron Lett.* **1984**, *25*, 1845.

123. Davies, S. G.; Seeman, J. I.; Williams, I. H. *Tetrahedron Lett.* **1986**, *27*, 619.

124. Blackburn, B. K.; Davies, S. G.; Whittaker, M. In *Stereochemistry of Organometallic and Inorganic Compounds*; Bernal, I., Ed.; Elsevier: Amsterdam, 1989; Vol. 3, p141.

125. Davies, S. G. *Pure Appl. Chem.* **1988**, *60*, 13.

126. Davies, S. G. *Chem. Br.* **1989**, *25*, 268.

127. Kagan, H. B. In *Asymmetric Synthesis, Vol. 5, Chiral Catalysis*; Morrison, J. D., Ed.; Academic Press: Orlando, 1985; Vol. 5, p1.

128. Koenig, K. E.; Sabacky, M. J.; Bachman, G. L.; Christopfel, W. C.; Barnstroff, H. D.; Friedman, R. B.; Knoweles, W. S.; Stults, B. R.; Vineyard, B. D.; Weinkauff, D. J. In *Transition Metal Mediated Organic Synthesis*; Slocum, D. W.; Hughes, O. R., Eds.; Annals of the New York Academy of Science, Vol. 333; The New York Academy of Science: New York, 1980; p16.

129. Fransen, J. R.; Dutton, P. J. *Can. J. Chem.* **1995**, *73*, 2217.

130. Imamoto, T. In *Handbook of Organophosphorus Chemistry*; Engel, R., Ed.; Marcel Dekker, INC: New York, 1992; p1.

131. Harvey, R. G.; de Sombre, E. R. *Top. Phos. Chem.* **1964**, *1*, 57.

132. Lewis, D. E. *J. Chem. Ed.* **1994**, *71*, 93.

133. Bhattacharya, A. K.; Thyagarajan, G. *Chem. Rev.* **1981**, *81*, 415.

134. Engel, R. In *Synthesis of Carbon-Phosphorus Bonds*; CRC Press: Boca Raton, Florida, 1988.

135. Viebrock, H.; Abeln, D.; Weiss, E. *Z. Naturforsch., B: Anorg. Chem., Org. Chem.* **1994**, *49*, 89.

136. Hudson, H. R. *Top. Phos. Chem.* **1983**, *11*, 339.

137. Mikolajczyk, M. *Pure Appl. Chem.* **1980**, *52*, 959.

138. Brill, T. B.; Landon, S. J. *Chem. Rev.* **1984**, *84*, 577.

139. Worms, K. H.; Schmidt-Dunker, M. *Org. Phos. Comp.* **1976**, *7*, 24.

140. Gaydou, E. M.; Bianchini *J. Chem. Soc., Chem. Commun.* **1975**, *14*, 541.

141. Jacobsen, H. I.; Griffin, M. J.; Pries, S.; Jensen, E. V. *J. Am. Chem. Soc.* **1975**, *79*, 1608.

142. Landauer, S. R.; Rydon, H. N. *J. Chem. Soc.* **1953**, 2224.

143. Nakazawa, H.; Ueda, Y.; Nakamura, K.; Miyoshi, K. *Organometallics* **1997**, *16*, 1562.

144. Nakazawa, H.; Fujita, T.; Kubo, K.; Miyoshi, K. *J. Organomet. Chem.* **1994**, *473*, 243.

145. Nakazawa, H.; Kashiwamura, T.; Mizuta, T.; Miyoshi, K. *Organometallics* **1994**, *13*, 941.

146. Nakazawa, H.; Morimasa, K.; Kushi, Y.; Yoneda, H. *Organometallics* **1988**, *7*, 458.

147. Nakazawa, H.; Kadoi, Y.; Mizuta, T.; Miyoshi, K.; Yoneda, H. *J. Organomet. Chem.* **1989**, *366*, 333.

148. Nakazawa, H.; Kadoi, Y.; Miyoshi, K. *Organometallics* **1989**, *8*, 2851.

149. Nakazawa, H.; Yamaguchi, M.; Kubo, K.; Miyoshi, K. *J. Organomet. Chem.* **1992**, *428*, 145.

150. We have named the M-P(O)$(OR)_2$ (metallophosphonates) complexes as organometallic phosphonic acid esters (R'P(O)$(OR)_2$) and the M-P(O)R'(OR) (metallophosphinates) as organometallic phosphinic acid esters (R'_2P(O)(OR)).

151. Haines, R. J.; DuPreez, A. L.; Marais, L. L. *J. Organomet. Chem.* **1971**, *28*, 405.

152. Clemens, J.; Neukomm, H.; Werner, H. *Helv. Chim. Acta* **1974**, *57*, 2000.

153. Harder, V.; Werner, H. *Helv. Chim. Acta* **1973**, *56*, 1620.

154. Harder, V.; Dubler, E.; Werner, H. *J. Organomet. Chem.* **1974**, *71*, 427.

155. King, R. B.; Diefenbach, S. P. *Inorg. Chem.* **1979**, *18*, 63.

156. Newton, M. G.; Pantaleo, N. S.; King, R. B.; Diefenbach, S. P. *J. Chem. Soc., Chem. Commun.* **1979**, 55.

157. Shakir, R.; Atwood, J. L.; Janik, T. S.; Atwood, J. D. *J. Organomet. Chem.* **1980**, *190*, C14.

158. Bruce, M. I.; Shaw, G.; Stone, F. G. A. *J. Chem. Soc., Dalton Trans.* **1973**, 1667.

159. Schubert, U.; Werner, R.; Zinner, L.; Werner, H. *J. Organomet. Chem.* **1983**, *253*, 363.

160. Solar, J. M.; Rogers, R. D.; Mason, W. R. *Inorg. Chem.* **1984**, *23*, 373.

161. King, C.; Roundhill, D. M. *Inorg. Chem.* **1986**, *25*, 2271.

162. Klaui, W.; Buchholz, E. *Inorg. Chem.* **1988**, *27*, 3500.

163. Landon, S. J.; Brill, T. B. *J. Am. Chem. Soc.* **1982**, *104*, 6571.

164. Towle, D. K.; Landon, S. J.; Brill, T. B.; Tulip, T. H. *Organometallics* **1982**, *1*, 295.

165. Landon, S. J.; Brill, T. B. *Inorg. Chem.* **1984**, *23*, 4177.

166. Landon, S. J.; Brill, T. B. *Inorg. Chem.* **1985**, *24*, 2863.

167. Landon, S. J.; Brill, T. B. *Inorg. Chem.* **1984**, *23*, 1266.

168. Sullivan, R. J.; Bao, Q. B.; Landon, S. J.; Rheingold, A. L.; Brill, T. B. *Inorg. Chim. Acta* **1986**, *111*, 19.

169. Bao, Q. B.; Brill, T. B. *Inorg. Chem.* **1987**, *26*, 3447.

170. Jablonski, C. R.; Burrow, T.; Jones, P. G. *J. Organomet. Chem.* **1989**, *370*, 173.

171. Chen, Z.; Jablonski, C.; Bridson, J. *Can. J. Chem.* **1996**, *74*, 2083.

172. Jablonski, C. R.; Ma, H. Z.; Chen, Z.; Hynes, R. C.; Bridson, J. N.; Bubenik, M. P. *Organometallics* **1993**, *12*, 917.

173. Boone, B. J.; Jablonski, C. R.; Jones, P. G.; Newlands, M. J.; Yu, Y. F. *Organometallics* **1993**, *12*, 3042.

174. Zhou, Z.; Jablonski, C.; Bridson, J. *Organometallics* **1993**, *12*, 3677.

175. Zhou, Z.; Jablonski, C.; Bridson, J. *Organometallics* **1994**, *13*, 781.

176. Jablonski, C. R.; Ma, H. Z.; Hynes, R. C. *Organometallics* **1992**, *11*, 2796.

177. Jablonski, C. R.; Zhou, Z. *Can. J. Chem.* **1992**, *70*, 2544.

178. Jablonski, C. R.; Zhou, Z.; Bridson, J. *Inorg. Chim. Acta* **1997**, *254*, 315.

179. Yu, Y.; Jablonski, C.; Bridson, J. *Organometallics* **1997**, *16*, 1270.

180. Schleman, E. V.; Brill, T. B. *J. Organomet. Chem.* **1987**, *323*, 103.

181. Klaui, W. *Angew. Chem., Int. Ed. Engl.* **1990**, *29*, 627.

182. Klaui, W.; Otto, H.; Eberspach, W.; Buchholz, E. *Chem. Ber.* **1982**, *115*, 1922.

183. Klaui, W.; Eberspach, W.; Schwarz, R. *J. Organomet. Chem.* **1983**, *252*, 347.

184. Roman, E.; Tapia, F.; Barrera, M.; Garland, M.-T.; Le Marouille, J.-Y.; Giannotti, C. *J. Organomet. Chem.* **1985**, *297*, C8.

185. Liang, L.; Stevens, E. D.; Nolan, S. P. *Organometallics* **1992**, *11*, 3459.

186. Klaui, W.; Hardt, T.; Schulte, H. J.; Hamers, H. *J. Organomet. Chem.* **1995**, *498*, 63.

187. Klaui, W.; Glaum, M.; Wagner, T.; Bennett, M. A. *J. Organomet. Chem.* **1994**, *472*, 355.

188. Scotti, M.; Valderrama, M.; Campos, P.; Klaui, W. *Inorg. Chim. Acta* **1993**, *207*, 141.

189. Kolle, U.; Ruther, T.; Lenarvor, N.; Englert, U.; Klaui, W. *Angew. Chem., Int. Ed. Engl.* **1994**, *33*, 991.

190. Krampe, O.; Song, C. E.; Klaui, W. *Organometallics* **1993**, *12*, 4949.

191. Scotti, M.; Valderrama, M.; Campos, P.; Klaui, W. *Inorg. Chim. Acta* **1993**, *207*, 141.

192. Klaui, W.; Neukomm, H. *Org. Magn. Reson.* **1977**, *10*, 126.

193. Shinar, H.; Navon, G.; Klaui, W. *J. Am. Chem. Soc.* **1986**, *108*, 5005.

194. Koelle, U.; Ruether, T.; Klaui, W. *J. Organomet. Chem.* **1992**, *426*, 99.

195. Klaui, W.; Neukomm, H.; Werner, H.; Huttner, G. *Chem. Ber.* **1977**, *110*, 2283.

196. Klaui, W. *Helv. Chim. Acta* **1977**, *60*, 1296.

197. Klaui, W. *J. Organomet. Chem.* **1980**, *184*, 49.

198. Holt, E. M.; Klaui, W.; Zuckerman, J. J. *J. Organomet. Chem.* **1987**, *335*, 29.

199. Klaui, W.; Muller, A.; Eberspach, W.; Boese, R.; Goldberg, I. *J. Am. Chem. Soc.* **1987**, *109*, 164.

200. Klaui, W.; Muller, A.; Herbst, R.; Egert, E. *Organometallics* **1987**, *6*, 1824.

201. Klaui, W.; Muller, A.; Scotti, M. *J. Organomet. Chem.* **1983**, *253*, 45.

202. Klaui, W.; Scotti, M.; Valderrama, M.; Rojas, S.; Sheldrick, G. M.; Jones, P. G.; Schroeder, T. *Angew. Chem., Int. Ed. Engl.* **1985**, *24*, 683.

203. Nettle, A.; Valderrama, M.; Contreras, R.; Scotti, M.; Peters, K.; von Schnering, H.

G.; Werner, H. *Polyhedron* **1988**, *7*, 2095.

204. Klaui, W.; Hamers, H. *J. Organomet. Chem.* **1988**, *345*, 287.

205. Klaui, W.; Buchholz, E. *Angew. Chem., Int. Ed. Engl.* **1988**, *27*, 580.

206. Banbery, H. J.; Hussain, W.; Evans, I. G.; Hamor, T. A.; Jones, C. J.; McCleverty, J. A.; Schulte, H.-J.; Engles, B.; Klaui, W. *Polyhedron* **1990**, *9*, 2549.

207. Leung, W.-H.; Chan, E. Y. Y.; Williams, I. D.; Wong, W.-T. *Organometallics* **1997**, *16*, 3234.

208. Kuksis, I.; Baird, M. C. *J. Organomet. Chem.* **1996**, *512*, 253.

209. Goh, L. Y.; D'aniello, M. J.; Slater, S.; Muetterties, E. L.; Tavanaiepour, I.; Chang, M. I.; Fredrich, M. F.; Day, V. W. *Inorg. Chem.* **1979**, *18*, 192.

210. Labinger, J. A. *J. Organomet. Chem.* **1977**, *136*, C31.

211. Fabian, B. D.; Labinger, J. A. *Organometallics* **1983**, *2*, 659.

212. Werner, H.; Feser, R. *Z. Anorg. Allg. Chem.* **1979**, *458*, 301.

213. Nakazawa, H.; Kadoi, Y.; Itoh, T.; Mizuta, T.; Miyoshi, K. *Organometallics* **1991**, *10*, 766.

214. Zhou, Z.; Jablonski, C.; Bridson, J. *J. Organomet. Chem.* **1993**, *461*, 215.

215. Jablonski, C.; Zhou, Z.; Bridson, J. N. *J. Organomet. Chem.* **1992**, *429*, 379.

216. Kepert, D. L. In *The Early Transition Metals*; Academic Press: London, 1972.

217. Shriver, D. F.; Atkins, P. W.; Langford, C. H. In *Inorganic Chemistry*; Oxford University Press: Oxford, 1990.

218. Karl, J.; Erker, G.; Frohlich, R. *J. Am. Chem. Soc.* **1997**, *119*, 11165.

219. Segi, M.; Nakamura, Y.; Nakajama, T.; Suga, S. *Chemistry Letters* **1983**, 913.

220. Braunstein, P.; Cea, S. C.; Bruce, M. I.; Skelton, B. W.; White, A. H. *J. Chem. Soc., Dalton Trans.* **1992**, 2539.

221. Nakazawa, H.; Kubo, K.; Tanisaki, K.; Kawamura, K.; Miyoshi, K. *Inorg. Chim. Acta* **1994**, *222*, 123.

222. Aaron, H. S. In *Topics in Stereochemistry*; Allinger, N. L.; Eliel, E. L., Eds.; Interscience: New York, 1979; Vol. 11, p1.

223. Kovacs, I.; Baird, M. C. *Organometallics* **1995**, *14*, 4084.

224. Day, V. W.; Tavanaiepour, I.; Abdel-Meguid, S. S.; Kirner, J. F.; Goh, L.-Y. *Inorg. Chem.* **1982**, *21*, 657.

225. Antonova, A. B.; Kovalenko, S., V; Korniets, E. D.; Ioganson, A. A.; Struchkov, Y. T.; Akhmedov, A. I.; Yanovskii, A. I. *J. Organomet. Chem.* **1983**, *244*, 35.

226. Walker, N.; Stuart, D. *Acta Crystallogr., Sect. A: Found. Cryst.* **1983**, *A39*, 158.

227. Korp, J. D.; Bernal, I. *J. Organomet. Chem.* **1981**, *220*, 355.

228. Gilheaney, D. G. In *The Chemistry of Organophosphorus Compounds*; Hartley, F. R., Ed.; John Wiley: New York, 1992; Vol. 2, p1.

229. Carlton, L.; Johnston, P.; Coville, N. J. *J. Organomet. Chem.* **1988**, *339*, 339.

230. Gabe, E. J.; LePage, Y.; Charland, J. P.; Lee, F. L.; White, P. S. *J. Appl. Cryst.* **1989**, *22*, 384.

231. Whuler, A.; Brouty, C.; Spinat, P. *Acta Crystallogr., Sect. B: Struct. Sci.* **1980**, *B36*, 1267.

232. Brunner, H.; Riepl, G.; Benn, R.; Rufinska, A. *J. Organomet. Chem.* **1983**, *253*, 93.

233. Bernal, I.; Reisner, G. M.; Brunner, H.; Riepl, G. *Inorg. Chim. Acta* **1985**, *103*, 179.

234. Bernal, I.; Reisner, G. M.; Brunner, H.; Riepl, G. *J. Organomet. Chem.* **1985**, *284*, 115.

235. Brunner, H.; Vogt, H. *J. Organomet. Chem.* **1981**, *210*, 223.

236. Brunner, H.; Rambold, W. *J. Organomet. Chem.* **1974**, *64*, 373.

237. Sloan, T. E. *Top. Stereochem.* **1981**, *12*, 1.

238. Leiva, C.; Mossert, K.; Klahn, A. H.; Sutton, D. *J. Organomet. Chem.* **1994**, *469*, 69.

239. Neuhaus, D.; Williamson, M. P. In *The Nuclear Overhauser Effect in Structural and Conformational Analysis*; VCH Publishers, Inc.: New York, 1989.

240. Gilmore, C. J. *J. Appl. Cryst.* **1984**, *17*, 42.

241. LePage, Y.; Gabe, E. J.; Gainsford, G. J. *J. Appl. Cryst.* **1990**, *23*, 406.

242. Issleib, K.; Seidel, W. *Chem. Ber.* **1959**, *92*, 2681.

243. Arbuzov, B. A.; Yarmukhametova *Dokl. Akad. Nauk SSSR* **1955**, *101*, 675.

244. Rinaldi, P. L. *Pr. Nuc. Mag. Res. Spec.* **1982**, *15*, 291.

245. Brunner, H.; Rambold, W. *Angew. Chem., Int. Ed. Engl.* **1973**, *85*, 1118.

246. Brunner, H.; Doppelberger, J. *Chem. Ber.* **1978**, *111*, 673.

247. Chen, Z. Ph.D. Dissertation, Memorial University, St. John's, 1995.

248. Mata, P.; Lobo, A. M.; Marshall, C.; Johnson, A. P. *Tetrahedron: Asymmetry* **1993**, *4*, 657.

249. Sokolov, V. I. In *Chirality and Optical Activity in Organometallic Compounds*; Gordon and Breach Science Publishers: New York, 1990.

250. Merrifield, J. H.; Fernandez, J. M.; Buhro, W. E.; Gladysz, J. A. *Inorg. Chem.* **1984**, *23*, 4022.

251. Chapman, J. J.; Welker, M. E. *Organometallics* **1997**, *16*, 747.

252. Cavell, R. G. *J. Chem. Soc.* **1964**, 1992.

253. Kruck, T.; Hofler, M.; Jung, H.; Blumer, H. *Angew. Chem., Int. Ed. Engl.* **1969**, *8*, 522.

254. Schadel, E.; Vahrenkamp, H. *Chem. Ber.* **1974**, *107*, 3850.

255. Hofler, M.; Schnitzler, M. *Chem. Ber.* **1972**, *105*, 1133.

288. Schmid, G.; Thealt, U.; Polásek; Mach, K.; Sedmera, P. *J. Organomet. Chem.* **1994**, *482*, 231.

289. Khotsyanova, T. L.; Kuznetsov, S. I. *J. Organomet. Chem.* **1973**, *57*, 155.

290. Mohring, P. C.; Vlachakis, N.; Grimmer, N. E.; Coville, N. J. *J. Organomet. Chem.* **1994**, *483*, 159.

291. Troyanov, S. I.; Rybakov, V. B.; Thewalt, U.; Varga, V.; Mach, K. *J. Organomet. Chem.* **1993**, *447*, 221.

292. Zaegel, F.; Gallucci, J. C.; Meunier, P.; Gautheron, B.; Bzowej, E. I.; Paquette, L. A. *Organometallics* **1995**, *14*, 4576.

293. Howie, R. A.; McQuillan, G. P.; Thompson, D. W.; Lock, G. A. *J. Organomet. Chem.* **1986**, *303*, 213.

294. van Rooyen, P.; Schindehutte, M.; Lota, S. *Organometallics* **1992**, *11*, 1104.

295. Lotz, S.; Vanrooyen, P. H.; Meyer, R. In *Advances in Organometallic Chemistry*; Stone, F. G. A.; West, R., Eds.; Advances in Organometallic Chemistry; Academic Press Inc: 525 B Street Suite 1900 San Diego CA 92101-4495, 1995; Vol. 37, p219.

296. Hoffman, D. M.; Chester, N. D.; Fay, R. C. *Organometallics* **1983**, *2*, 48.

297. Bursten, B. E.; Callstrom, M. R.; Jolly, C. A.; Paquette, L. A.; Sivik, M. R.; Tucker, R. S.; Wartchow, C. A. *Organometallics* **1994**, *13*, 127.

298. Landis, C. R.; Root, D. M.; Cleveland, T. In *Reviews in Computational Chemistry 6*; Lipkowitz, K. B.; Boyd, D. B., Eds.; Reviews in Computational Chemistry; V C H Publishers: 220 E 23RD St Suite 909 New York NY 10010, 1995; Vol. 6, p73.

299. Hutchings, G. J.; Waston, G. W.; Willock, D. J. *Chem. Ind.* **1997**, *15*, 603.

300. Mackie, S. C.; Park, Y. S.; Shurvell, H. F.; Baird, M. C. *Organometallics* **1991**, *10*, 2993.

301. Mackie, S. C.; Baird, M. C. *Organometallics* **1992**, *11*, 3712.

302. Polowin, J.; Mackie, S. C.; Baird, M. C. *Organometallics* **1992**, *11*, 3724.

303. Britten, J.; Mu, Y.; Harrod, J. F.; Polowin, J.; Baird, M. C.; Samuel, E. *Organometallics* **1993**, *12*, 2672.

304. Polowin, J.; Baird, M. C. *J. Organomet. Chem.* **1994**, *478*, 45.

305. Polowin, J.; Poe, R.; Baird, M. C. *Can. J. Chem.* **1995**, *73*, 1078.

306. Yang, K.; Bott, S. G.; Richamond, M. G. *J. Organomet. Chem.* **1994**, *483*, 7.

307. Heyn, R. H.; Stephan, D. W. *Inorg. Chem.* **1995**, *34*, 2804.

308. Nadasdi, T. T.; Huang, Y. J.; Stephan, D. W. *Inorg. Chem.* **1993**, *32*, 347.

309. Kumar, R.; Sierra, M. L.; Oliver, J. P. *Organometallics* **1994**, *13*, 4285.

310. McClain, M. D.; Hay, M. S.; Curtis, M. D.; Kampf, J. W. *Organometallics* **1994**, *13*, 4377.

311. Khan, A. R.; Harvey, P. D.; Socol, S. M. *Inorg. Chim. Acta* **1996**, *251*, 89.

312. Barré, C.; Boudot, P.; Kubicki, M. M.; Moïse, C. *Inorg. Chem.* **1995**, *34*, 284.

313. Sanger, M. J.; Angelici, R. J. *Organometallics* **1994**, *13*, 1821.

314. Yuan, P.; Don, M.-J.; Richmond, M. G.; Schwartz, M. *Inorg. Chem.* **1992**, *31*, 3491.

315. Samuel, E.; Harrod, J. F.; McGlinchey, M. J.; Cabestaing, C. R., Francis. *Inorg. Chem.* **1994**, *33*, 1292.

316. Sapunov, V. N.; Mereiter, K.; Schmid, R.; Kirchner, K. *J. Organomet. Chem.* **1997**, *530*, 105.

317. Malisza, K. L.; Li, L. J.; McGlinchey, M. J. *Can. J. Chem.* **1996**, *74*, 1021.

318. Albright, T. A.; Burdett, J. K.; Whangbo, M. H. In *Orbital Interactions in Chemistry*; John Wiley & Sons: New York, 1985.

319. Albright, T. A.; Hoffmann, R.; Hofmann, P. *Chem. Ber.* **1978**, *111*, 1591.

320. Schilling, G. E. R.; Hoffmann, R.; Faller, J. W. *J. Am. Chem. Soc.* **1979**, *101*, 592.

321. Hoffmann, R.; Hofmann, P. *J. Am. Chem. Soc.* **1976**, *98*, 598.

322. Anh, N. T.; Elian, M.; Hoffmann, R. *J. Am. Chem. Soc.* **1978**, *100*, 110.

323. Albright, T. A.; Hofmann, P.; Hoffmann, R. *J. Am. Chem. Soc.* **1977**, *99*, 7546.

324. Albright, T. A.; Hoffmann, R. *Chem. Ber.* **1978**, *111*, 1578.

325. Curtis, M. D.; Eisenstein, O. *Organometallics* **1984**, *3*, 887.

326. Piers, W. E.; Whittal, R. M.; Ferguson, G.; Gallagher, J. F.; Froese, R. D.; Stronks, H. J.; Krygsman, P. H. *Organometallics* **1992**, *11*, 4015.

327. Downton, P. A.; Sayer, B. G.; McGlinchey, M. J. *Organometallics* **1992**, *11*, 3281.

328. Decken, A.; Britten, J. F.; McGlinchey, M. J. *J. Am. Chem. Soc.* **1993**, *115*, 7275.

329. Bodner, G. S.; Patton, A. T.; Smith, D. E.; Georgiou, S.; Tam, W.; Wong, W.-K.; Strouse, C. E.; Gladysz, J. A. *Organometallics* **1987**, *6*, 1954.

330. Esteruelas, M. A.; Lahuerta, O.; Modrego, J.; Nurnberg, O.; Ore, L. A.; Rodriguez, L.; Sola, E.; Werner, H. *Organometallics* **1993**, *12*, 266.

331. Albright, T. A.; Hofmann, P.; Hoffmann, R.; Lillya, C. P.; Dobosh, P. A. *J. Am. Chem. Soc.* **1983**, *105*, 3396.

332. Ditchfield, R.; Hughes, R. P.; Tucker, D. S.; Bierwagen, E. P.; Robbins, J.; Robinson, D. J.; Zakutansky, J. A. *Organometallics* **1993**, *12*, 2258.

333. Barbaro, P.; Belderrain, T. R.; Bianchini, C.; Scapacci, G.; Masi, D. *Inorg. Chem.* **1996**, *35*, 3362.

334. Gajewski, J. J.; Gilbert, K. E.; McKelvey, J. In *Advances in Molecular Modeling*; Liotta, D., Ed.; JAI Press Inc.: Creenwich, 1990; Vol. 2, p65.

335. Huffman, J. C.; Moloy, K. G.; Marsella, J. A.; Caulton, K. G. *J. Am. Chem. Soc.* **1980**, *102*, 3009.

336. Serena Software, Box 3076, Bloomington, IN 47402-3076.

337. Jones, W. D.; Feher, F. J. *Inorg. Chem.* **1984**, *23*, 2376.

338. Bochmann, M.; Wilson, L. M.; Hursthouse, M. B.; Short, R. L. *Organometallics* **1987**, *6*, 2556.

339. Chaudhari, M. A.; Treichel, P. M.; Stone, F. G. A. *J. Organomet. Chem.* **1964**, *2*, 206.

340. Druce, P. M.; Kingston, B. M.; Lappert, M. F.; Spalding, T. R.; Srivastava, R. C. *J. Chem. Soc., (A)* **1969**, 2106.

341. Huheey, J. E. In *Inorganic Chemistry, Principles of Structure and Reactivity*, 3rd; Harper & Row: New York, 1983.

342. Harger, M. J. P. *Tetrahedron Lett.* **1996**, *37*, 8247.

343. Uson, R.; Launa, A. *Inorg. Synth.* **1982**, *21*, 71.

344. Yu, Y. CHANGE (Version 1.0), A Program for Coordinates Transformation for CACAO, Chemistry Department, Memorial University of Newfoundland, St. John's, Nefoundland, A1B 3X7 Canada.

345. This definition has been relaxed as small distortions in bond angles and bond distances often accompany conformational changes. Moreover, rotations about bonds which have an order greater than one can occur.

346. Albright, T. A. *Acc. Chem. Res.* **1982**, *15*, 149.

347. Leach, A. R. In *Molecular Modelling, Principles and Applications*; Addison Wesley Longman Limited: Singapore, 1996.

348. Luinstra, G. A.; Teuben, J. H. *Organometallics* **1992**, *11*, 1793.

349. Siedle, A. R.; Newmark, R. A.; Lamanna, W. M. *Organometallics* **1993**, *12*, 1491.

350. Gomez, R.; Green, M. L. H.; Haggitt, J. L. *J. Chem. Soc., Dalton Trans.* **1996**, 939.

351. Butler, I. R.; Lindsell, W. E.; Preston, P. N. *J. Chem. Research (M)* **1981**, 2573.

352. Lauher, J.; Hoffmann, R. *J. Am. Chem. Soc.* **1976**, *98*, 1729.

353. Albright, T. A. *Tetrahedron* **1982**, *38*, 1339.

354. Lucas, C. R.; Gabe, E. J.; Lee, F. L. *Can. J. Chem.* **1988**, *66*, 429.

355. Butts, M. D.; Scott, B. L.; Kubas, G., J *J. Am. Chem. Soc.* **1996**, *118*, 11831.

356. Fachinetti, G.; Fochi, G.; Floriani, C. *J. Chem. Soc., Dalton Trans.* **1977**, 1946.

357. Fachinetti, G.; Floriani, C.; Stockli-Evans, H. *J. Chem. Soc., Dalton Trans.* **1977**, 2297.

358. Fagan, P. J.; Manriquez, J. M.; Marks, T. J.; Day, V. W.; Vollmer, S. H.; Day, C. S. *J. Am. Chem. Soc.* **1980**, *102*, 5393.

359. Rausch, M. D. *Pure Appl. Chem.* **1964**, *30*, 523.

360. Casares, J. A.; Espinet, P.; Martinez-Ilarduya, J. M.; Lin, Y.-S. *Organometallics* **1997**, *16*, 770.

361. Stephenson, D. S.; Binsch, G. *J. Magn. Reson.* **1978**, *32*, 142.

362. Stephenson, D. S.; Binsch, G. QCPE Program 365, Department of Chemistry, Indiana University, Bloomington, IN 47405, USA.

363. NUTS - NMR Utility Transform Software for Windows 95/NT, Fremont, CA 94538-6491.

364. YYU - An interface program between NUTS and DNMR5, written originally by Prof. Chet Jablonski and modified by Yongfei Yu, Chemistry Dept., Memorial University, St. John's, Newfoundland, A1B 3X7.

365. Cozzi, F.; Guenzi, A.; Johnson.C.A; Mislow, K.; Hounshell, W. D.; Blount, J. F. *J. Am. Chem. Soc.* **1981**, *103*, 957.

366. Brown, J. M.; Pereztorrente, J. J.; Alcock, N. W. *Organometallics* **1995**, *14*, 1195.

367. Treichel, P. M.; Chaudhari, M. A.; Stone, F. G. A. *J. Organomet. Chem.* **1963**, *1*, 98.

368. Kocman, V.; Rucklidge, J. C.; O'Brien, R. J.; Santo, W. *J. Chem. Soc., Chem. Commun.* **1971**, 1340.

369. Clearfield, A.; Warner, D. K.; Saldarriga-Molina, C. H.; Ropal, R.; Bernal, I. *Can. J. Chem.* **1975**, *53*, 1622.

370. Atherton, M. J.; Fawcett, J.; Hill, A. P.; Holloway, J. H.; Hope, E. G.; Russell, D. R.; Saunders, G. C.; Stead, R. M. J. *J. Chem. Soc., Dalton Trans.* **1997**, 1137.

371. Prosenc, M. H.; Janiak, C.; Brintzinger, H. H. *Organometallics* **1992**, *11*, 4036.

372. Tatsumi, K.; Nakamura, A.; Hofmann, P.; Stauffert, P.; Hoffmann, R. *J. Am. Chem. Soc.* **1985**, *107*, 4440.

373. Gilman, H.; Gorsich, R. D. *J. Am. Chem. Soc.* **1956**, *78*, 2217.

Appendix 1. Source code of *CHANGE* program

```
50   REM PROGRAM "CHANGE VERSION 1.0" © YONGFEI YU, 1994
100 REM THIS IS A COORDINATES TRANSFORMATION SYSTEM.
110 REM IT IS DESIGNED FOR USING CACAO ONLY.
120 REM BEEP
130 GOSUB 8000
140 ON ERROR GOTO 7000
150 REM Max. # OF ATOMS FOR CACAO IS 100
160 DIM AT$(100), X(100, 3), Y(100, 3), V(4, 3), P(2, 3),
RINGX(6), RINGY(6), RINGZ(6)
170 SCREEN 0
180 CLS : COLOR 15, 1
190 ANSWER$ = "": ANSWER = 0
200 FOR I = 1 TO 9: PRINT : NEXT
210 PRINT TAB(27); "1. FROM X-RAY TO CARTESIAN"
220 PRINT TAB(27); "2. FROM CATESAIN TO INTERNAL"
230 PRINT TAB(27); "3. FROM X-RAY TO INTERNAL"
240 PRINT TAB(27); "0. EXIT"
250 FOR I = 1 TO 3: PRINT : NEXT
260 PRINT TAB(27); "YOUR CHOICE:";
270 LOCATE , , 1: ANSWER$ = INKEY$: IF ANSWER$ = "" THEN 270
280 IF ANSWER$ = "1" THEN GOSUB 1000
290 IF ANSWER$ = "2" THEN GOSUB 2000
300 IF ANSWER$ = "3" THEN GOSUB 4000
310 IF ANSWER$ = "0" THEN GOSUB 7600
320 IF ANSWER$ <> "0" THEN 170
330 SCREEN 0: COLOR 7, 0
340 GOSUB 7820
350 SYSTEM


1000 CLS
1010 SCREEN 0
1020 COLOR 15, 2
1030 GOSUB 5000
1040 IF ANS$ = "Y" OR ANS$ = "y" THEN 1050 ELSE 1230
1050 IF A = 1 AND B = 1 AND C = 1 AND ALPH = 90 AND BETA =
90 AND GAMA = 90 THEN 7400
1060 IF A = 1 AND B = 1 AND C = 1 AND ALPH = 90 AND BETA =
90 AND GAMA = 90 THEN 1230
1070 ALPH = ALPH * 22 / (7 * 180): BETA = BETA * 22 / (7 *
180): GAMA = GAMA * 22 / (7 * 180)
1080 U = COS(ALPH) - COS(BETA) * COS(GAMA)
1090 V = SQR(1 - COS(ALPH) ^ 2 - COS(BETA) ^ 2 - COS(GAMA) ^
```

```
2 + 2 * COS(ALPH) * COS(BETA) * COS(GAMA))
1100 OPEN "O", 2, B$
1110 PRINT #2, TITLE$
1120 FOR I = 1 TO N
1130 Y(I, 1) = A * X(I, 1) + B * COS(GAMA) * X(I, 2) + C *
COS(BETA) * X(I, 3)
1140 Y(I, 2) = 0 * X(I, 1) + B * SIN(GAMA) * X(I, 2) + C * U
/ SIN(GAMA) * X(I, 3)
1150 Y(I, 3) = 0 * X(I, 1) + 0 * COS(GAMA) * X(I, 2) + C * V
/ SIN(GAMA) * X(I, 3)
1160 IF LEN(AT$(I)) = 1 THEN AT$(I) = " " + AT$(I)
1170 AT$(I) = AT$(I) + ","
1180 PRINT #2, AT$(I); USING "###.######,"; Y(I, 1); Y(I,
2);
1190 PRINT #2, USING "###.######"; Y(I, 3)
1200 NEXT
1210 CLOSE #2
1220 GOSUB 7200
1230 RETURN


2000 CLS
2010 SCREEN 0
2020 COLOR 15, 3
2030 GOSUB 5000
2040 IF ANS$ = "Y" OR ANS$ = "y" THEN 2050 ELSE 3590
2050 IF ANSWER = 0 THEN 2150
2060 FOR I = 1 TO N
2070 X(I, 1) = X(I, 1) - X(ANSWER, 1)
2080 X(I, 2) = X(I, 2) - X(ANSWER, 2)
2090 X(I, 3) = X(I, 3) - X(ANSWER, 3)
2100 NEXT I
2110 REM acrcos(0)=PI/2=(22/7)/2=11/7
2120 REM arccos(c)=1.5708-2*atn(c/(1+sqr(1-c*c)))
2130 REM arcsin(c)=2*atn(c/(1+sqr(1-c*c)))
2140 REM excerpt from <THE BASIC HANDBOOK> 2rd EDITION, ED.
BY DAVID A. LIEN
2150 DEF FNARCCOS (C) = 11 / 7 - 2 * ATN(C / (1 + SQR(1 - C
* C)))
2160 OPEN "O", 2, B$
2170 PRINT #2, TITLE$
2180 IF ANSWER = 0 THEN ORIGIN$ = "0,0,0,DU"
2190 IF ANSWER = 0 THEN GOTO 2220
2200 IF LEN(AT$(ANSWER)) = 1 THEN AT$(ANSWER) = " " +
AT$(ANSWER)
2210 ORIGIN$ = "0,0,0," + AT$(ANSWER)
```

```
2220 PRINT #2, ORIGIN$
2230 FOR I = 1 TO N
2240 REM PRINT "I,AT$,X(I,0),X(I,?)="; I, AT$(I), X(I, 0),
X(I, 1), X(I, 2), X(I, 3)
2250 IF I = ANSWER THEN 3560
2260 FOR J = 2 TO RX: IF I = RINGX(J) THEN 3560
2270 NEXT J
2280 FOR J = 2 TO RY: IF I = RINGY(J) THEN 3560
2290 NEXT J
2300 FOR J = 2 TO RZ: IF I = RINGZ(J) THEN 3560
2310 NEXT J
2320 H1 = X(I, 0)
2330 IF ANSWER = 0 AND H1 <> -1 THEN 2480
2340 IF ANSWER = 0 THEN 2360
2350 IF H1 <> ANSWER THEN 2480
2360 REM C-D=(0,0,0)-X(I,?)
2370 V(1, 1) = -X(I, 1): V(1, 2) = -X(I, 2): V(1, 3) = -X(I,
3)
2380 REM B-C=(0,0,-1)    (-Z AXIS)
2390 V(2, 1) = 0: V(2, 2) = 0: V(2, 3) = -1
2400 REM IF C-D IS +Z OR -Z AXIS THEN B-C=+Z AXIS
2410 IF V(1, 1) = 0 AND V(1, 2) = 0 THEN V(2, 1) = 0: V(2,
2) = 0: V(2, 3) = 1
2420 REM A-B=(1,0,0)    (X AXIS)
2430 V(3, 1) = 1: V(3, 2) = 0: V(3, 3) = 0
2440 V(4, 1) = V(1, 1) * V(2, 1)
2450 V(4, 2) = V(1, 2) * V(2, 2)
2460 V(4, 3) = V(1, 3) * V(2, 3)
2470 GOTO 2880
2480 H2 = X(H1, 0): IF ANSWER = 0 AND H2 <> -1 THEN 2650
2490 IF ANSWER = 0 THEN 2510
2500 IF X(H1, 0) <> ANSWER THEN 2650
2510 FOR J = 1 TO 3
2520 REM C-D
2530 V(1, J) = X(H1, J) - X(I, J)
2540 NEXT J
2550 REM B-C=(0,0,0)-X(X(I,?))
2560 V(2, 1) = -X(H1, 1): V(2, 2) = -X(H1, 2): V(2, 3) =
-X(H1, 3)
2570 REM B-A=(0,0,-1) (-Z AXIS)
2580 V(3, 1) = 0: V(3, 2) = 0: V(3, 3) = -1
2590 REM IF V(2,?) AND V(3,?) (Z AXIS) ARE COLIENAR THEN
V(3,?)=X AXIS
2600 IF V(2, 1) = 0 AND V(2, 2) = 0 THEN V(3, 1) = 1: V(3,
2) = 0: V(3, 3) = 0
2610 V(4, 1) = V(1, 1) * V(2, 1)
```

```
2620 V(4, 2) = V(1, 2) * V(2, 2)
2630 V(4, 3) = V(1, 3) * V(2, 3)
2640 GOTO 2880
2650 H3 = X(H2, 0): IF ANSWER = 0 AND H3 <> -1 THEN 2780
2660 IF ANSWER = 0 THEN 2680
2670 IF X(H2, 0) <> ANSWER THEN 2780
2680 FOR J = 1 TO 3
2690 REM C-D
2700 V(1, J) = X(H1, J) - X(I, J)
2710 REM B-C
2720 V(2, J) = X(H2, J) - X(H1, J)
2730 REM A-B=(0,0,0)-X(H2,J)
2740 V(3, J) = -X(H2, J)
2750 NEXT J
2760 FOR J = 1 TO 3: V(4, J) = V(1, J) * V(2, J): NEXT J
2770 GOTO 2880
2780 V(1, 1) = X(H1, 1) - X(I, 1)
2790 V(1, 2) = X(H1, 2) - X(I, 2)
2800 V(1, 3) = X(H1, 3) - X(I, 3)
2810 V(2, 1) = X(H2, 1) - X(H1, 1)
2820 V(2, 2) = X(H2, 2) - X(H1, 2)
2830 V(2, 3) = X(H2, 3) - X(H1, 3)
2840 V(3, 1) = X(H3, 1) - X(H2, 1)
2850 V(3, 2) = X(H3, 2) - X(H2, 2)
2860 V(3, 3) = X(H3, 3) - X(H2, 3)
2870 FOR J = 1 TO 3: V(4, J) = V(1, J) * V(2, J): NEXT J
2880 REM PRINT "V1="; V(1, 1); V(1, 2); V(1, 3)
2890 REM PRINT "V2="; V(2, 1); V(2, 2); V(2, 3)
2900 REM PRINT "V3="; V(3, 1); V(3, 2); V(3, 3)
2910 REM PRINT "V4="; V(4, 1); V(4, 2); V(4, 3)
2920 Y(I, 1) = SQR(V(1, 1) ^ 2 + V(1, 2) ^ 2 + V(1, 3) ^ 2)
2930 REM V(1,?) AND V(2,?) ARE COLINEAR? (5210-5300)
2940 K = 0
2950 IF V(1, 1) <> 0 AND V(2, 1) <> 0 THEN K = V(1, 1) /
V(2, 1) ELSE GOTO 2980
2960 IF K > 0 AND V(1, 2) = K * V(2, 2) AND V(1, 3) = K *
V(2, 3) THEN Y(I, 2) = 0: GOTO 3110
2970 IF K < 0 AND V(1, 2) = K * V(2, 2) AND V(1, 3) = K *
V(2, 3) THEN Y(I, 2) = 180: GOTO 3110
2980 IF V(1, 2) <> 0 AND V(2, 2) <> 0 THEN K = V(1, 2) /
V(2, 2) ELSE GOTO 3010
2990 IF K > 0 AND V(1, 1) = K * V(2, 1) AND V(1, 3) = K *
V(2, 3) THEN Y(I, 2) = 0: GOTO 3110
3000 IF K < 0 AND V(1, 1) = K * V(2, 1) AND V(1, 3) = K *
V(2, 3) THEN Y(I, 2) = 180: GOTO 3110
3010 IF V(1, 3) <> 0 AND V(2, 3) <> 0 THEN K = V(1, 3) /
```

```
V(2, 3) ELSE GOTO 3040
3020 IF K > 0 AND V(1, 1) = K * V(2, 1) AND V(1, 2) = K *
V(2, 2) THEN Y(I, 2) = 0: GOTO 3110
3030 IF K < 0 AND V(1, 1) = K * V(2, 1) AND V(1, 2) = K *
V(2, 2) THEN Y(I, 2) = 180: GOTO 3110
3040 C = V(4, 1) + V(4, 2) + V(4, 3)
3050 IF C = 0 THEN Y(I, 2) = 90: GOTO 3110
3060 C = -C / (SQR(V(1, 1) ^ 2 + V(1, 2) ^ 2 + V(1, 3) ^ 2))
3070 C = C / (SQR(V(2, 1) ^ 2 + V(2, 2) ^ 2 + V(2, 3) ^ 2))
3080 REM PRINT "Y(I,2):C, arccos(c)= "; c, FNarccos(c)
3090 Y(I, 2) = 180 / (22 / 7) * FNARCCOS(C)
3100 REM P(1,?),P(2,?) ARE NORMAL TO V1xV2 AND
V2xV3,RESPECTIVELY.
3110 P(1, 1) = V(1, 2) * V(2, 3) - V(1, 3) * V(2, 2)
3120 P(1, 2) = V(1, 3) * V(2, 1) - V(1, 1) * V(2, 3)
3130 P(1, 3) = V(1, 1) * V(2, 2) - V(1, 2) * V(2, 1)
3140 P(2, 1) = V(2, 2) * V(3, 3) - V(2, 3) * V(3, 2)
3150 P(2, 2) = V(2, 3) * V(3, 1) - V(2, 1) * V(3, 3)
3160 P(2, 3) = V(2, 1) * V(3, 2) - V(2, 2) * V(3, 1)
3170 REM PRINT "P1="; P(1, 1), P(1, 2), P(1, 3); " P2=";
P(2, 1), P(2, 2), P(2, 3)
3180 REM P(1,?) AND P(2,?) ARE COLINEAR? (5450-5560)
3190 K = 0
3200 IF P(1, 1) <> 0 AND P(2, 1) <> 0 THEN K = P(1, 1) /
P(2, 1) ELSE GOTO 3230
3210 IF K > 0 AND P(1, 2) = K * P(2, 2) AND P(1, 3) = K *
P(2, 3) THEN Y(I, 3) = 0: GOTO 3420
3220 IF K < 0 AND P(1, 2) = K * P(2, 2) AND P(1, 3) = K *
P(2, 3) THEN Y(I, 3) = 180: GOTO 3420
3230 IF P(1, 2) <> 0 AND P(2, 2) <> 0 THEN K = P(1, 2) /
P(2, 2) ELSE GOTO 3260
3240 IF K > 0 AND P(1, 1) = K * P(2, 1) AND P(1, 3) = K *
P(2, 3) THEN Y(I, 3) = 0: GOTO 3420
3250 IF K < 0 AND P(1, 1) = K * P(2, 1) AND P(1, 3) = K *
P(2, 3) THEN Y(I, 3) = 180: GOTO 3420
3260 IF P(1, 3) <> 0 AND P(2, 3) <> 0 THEN K = P(1, 3) /
P(2, 3) ELSE GOTO 3290
3270 IF K > 0 AND P(1, 1) = K * P(2, 1) AND P(1, 2) = K *
P(2, 2) THEN Y(I, 3) = 0: GOTO 3420
3280 IF K < 0 AND P(1, 1) = K * P(2, 1) AND P(1, 2) = K *
P(2, 2) THEN Y(I, 3) = 180: GOTO 3420
3290 IF P(1, 1) = 0 AND P(1, 2) = 0 AND P(1, 3) = 0 THEN
Y(I, 3) = 0: GOTO 3420
3300 IF P(2, 1) = 0 AND P(2, 2) = 0 AND P(2, 3) = 0 THEN
Y(2, 3) = 0: GOTO 3420
3310 REM S=V(1,?) . P(2,?)
```

```
3320 S = V(1, 1) * P(2, 1) + V(1, 2) * P(2, 2) + V(1, 3) *
P(2, 3)
3330 SIGN = SGN(S)
3340 C = P(1, 1) * P(2, 1) + P(1, 2) * P(2, 2) + P(1, 3) *
P(2, 3)
3350 C = C / (SQR(P(1, 1) ^ 2 + P(1, 2) ^ 2 + P(1, 3) ^ 2) *
(SQR(P(2, 1) ^ 2 + P(2, 2) ^ 2 + P(2, 3) ^ 2)))
3360 REM PRINT "Y(I,3):SIGN,C,ARCCOS(C)= "; SGN(S), c,
FNarccos(c)
3370 IF SIGN >= 0 THEN 3400
3380 Y(I, 3) = 360 - 180 / (22 / 7) * (FNARCCOS(C))
3390 GOTO 3420
3400 Y(I, 3) = 180 / (22 / 7) * FNARCCOS(C)
3410 GOTO 3430
3420 REM PRINT "X(I,0)="; X(I, 0); "I="; I; "AT$="; AT$(I);
" Y1="; Y(I, 1); "Y2="; Y(I, 2); "Y3="; Y(I, 3)
3430 REM TO FIND X(I,0)
3440 GOSUB 14000
3450 REM TO FIND # OF ATOM ORDER
3460 GOSUB 15000
3470 REM  "I,I$="; I, I$
3480 IF I = RINGX(1) OR I = RINGY(1) OR I = RINGZ(1) THEN
3490 ELSE 3510
3490 IF RX = 5 OR RY = 5 OR RZ = 5 THEN AT$(I) = "CP"
3500 IF RX = 6 OR RY = 6 OR RZ = 6 THEN AT$(I) = "BZ"
3510 IF LEN(AT$(I)) = 1 THEN AT$(I) = " " + AT$(I)
3520 Y$ = X$ + I$ + AT$(I)
3530 PRINT #2, Y$;
3540 PRINT #2, USING "###.####,"; Y(I, 1); Y(I, 2);
3550 PRINT #2, USING "###.####"; Y(I, 3)
3560 NEXT I
3570 CLOSE #2
3580 GOSUB 7200
3590 RETURN


4000 CLS
4010 SCREEN 0
4020 COLOR 11, 9
4030 GOSUB 5000
4040 IF ANS$ = "Y" OR ANS$ = "y" THEN 4050 ELSE 4360
4050 IF A = 1 AND B = 1 AND C = 1 AND ALPH = 90 AND BETA =
90 AND GAMA = 90 THEN 4200
4060 ALPH = ALPH * 22 / (7 * 180): BETA = BETA * 22 / (7 *
180): GAMA = GAMA * 22 / (7 * 180)
4070 U = COS(ALPH) - COS(BETA) * COS(GAMA)
```

```
4080 V = SQR(1 - COS(ALPH) ^ 2 - COS(BETA) ^ 2 - COS(GAMA) ^
2 + 2 * COS(ALPH) * COS(BETA) * COS(GAMA))
4090 FOR I = 1 TO N
4100 Y(I, 1) = A * X(I, 1) + B * COS(GAMA) * X(I, 2) + C *
COS(BETA) * X(I, 3)
4110 Y(I, 2) = 0 * X(I, 1) + B * SIN(GAMA) * X(I, 2) + C * U
/ SIN(GAMA) * X(I, 3)
4120 Y(I, 3) = 0 * X(I, 1) + 0 * COS(GAMA) * X(I, 2) + C * V
/ SIN(GAMA) * X(I, 3)
4130 NEXT
4140 FOR I = 1 TO N
4150 X(I, 1) = Y(I, 1)
4160 X(I, 2) = Y(I, 2)
4170 X(I, 3) = Y(I, 3)
4180 REM PRINT "XXX="; X(I, 1), X(I, 2), X(I, 3)
4190 NEXT
4200 IF ANSWER = 0 THEN 4290
4210 XORIGIN = X(ANSWER, 1): YORIGIN = X(ANSWER, 2): ZORIGIN
= X(ANSWER, 3)
4220 FOR I = 1 TO N
4230 REM PRINT "XXXBEFORE="; X(I, 1), X(I, 2), X(I, 3)
4240 X(I, 1) = X(I, 1) - XORIGIN
4250 X(I, 2) = X(I, 2) - YORIGIN
4260 X(I, 3) = X(I, 3) - ZORIGIN
4270 REM PRINT "XXXAFTER="; X(I, 1), X(I, 2), X(I, 3)
4280 NEXT
4290 IF RX = 0 AND RY = 0 AND RZ = 0 AND XYP = 0 AND YZP = 0
AND ZXP = 0 THEN 4300 ELSE 4320
4300 GOSUB 2150
4310 GOTO 4350
4320 GOSUB 8300
4330 REM OPEN "O", 6, "c:\temp4": FOR i = 1 TO n:PRINT #6,
x(i, 0); i; at$(i); x(i, 1); x(i, 2); x(i, 3): NEXT i: CLOSE
#6
4340 GOSUB 2150
4350 GOSUB 7800
4360 RETURN


5000 ANSWER = 0
5010 FOR I = 1 TO 3
5020 CLS : A$ = "": B$ = "": ANS$ = "": FOR J = 1 TO 10:
PRINT : NEXT
5030 IF ANSWER$ = "2" THEN 5060
5040 PRINT TAB(20); "NAME OF X-RAY FILE:"; : INPUT A$
5050 GOTO 5070
```

```
5060 PRINT TAB(20); "NAME OF CARTESIAN FILE:"; : INPUT A$
5070 IF A$ = "QUIT" OR A$ = "quit" THEN 7800
5080 IF A$ = "" THEN 5020
5090 PRINT TAB(20); "CORRECT FILE (Y/N)";
5100 ANS$ = INKEY$: IF ANS$ = "" THEN 5100
5110 IF ANS$ = "Y" OR ANS$ = "y" THEN 5140
5120 NEXT I
5130 IF ANS$ = "Y" OR ANS$ = "y" THEN 5140 ELSE 6000
5140 FOR I = 1 TO 3
5150 CLS : FOR J = 1 TO 10: PRINT : NEXT
5160 PRINT TAB(20); "NAME OF OUPUT FILE:"; : INPUT B$
5170 IF B$ = "QUIT" OR B$ = "quit" THEN 7800
5180 IF B$ = "" THEN 5150
5190 IF B$ <> A$ THEN 5240
5200 PRINT : PRINT TAB(20); "DUPLICATE NAME!"
5210 PRINT TAB(20); "HIT ANY KEY TO CONTINUE...";
5220 ANS$ = INKEY$: IF ANS$ = "" THEN 5220
5230 GOTO 5150
5240 PRINT TAB(20); "NAME OK (Y/N)";
5250 ANS$ = INKEY$: IF ANS$ = "" THEN 5250
5260 IF ANS$ = "Y" OR ANS$ = "y" THEN 5290
5270 NEXT I
5280 IF ANS$ = "Y" OR ANS$ = "y" THEN 5290 ELSE 6000
5290 N = 0: RX = 0: RY = 0: RZ = 0: XYP = 0: YZP = 0: ZXP =
0
5300 FOR I = 1 TO 6: RINGX(I) = 0: RINGY(I) = 0: RINGZ(I) =
0: NEXT I
5310 OPEN "I", 1, A$
5320 LINE INPUT #1, TEMP$
5330 N = N + 1
5340 IF NOT EOF(1) THEN 5320
5350 CLOSE #1
5360 REM N-2=# OF ATOMS
5370 N = N - 2
5380 REM PRINT "N="; N
5390 OPEN "I", 1, A$
5400 LINE INPUT #1, TITLE$
5410 INPUT #1, A, B, C, ALPH, BETA, GAMA
5420 REM "ABCABG="; A, B, C, ALPH, BETA, GAMA
5430 FOR I = 1 TO N: FOR J = 1 TO 3: X(I, J) = 0: Y(I, J) =
0: NEXT J: NEXT I
5440 FOR I = 1 TO N
5450 IF ANSWER$ <> "1" THEN 5490
5460 INPUT #1, AT$(I), X(I, 1), X(I, 2), X(I, 3)
5470 REM PRINT "XXXXANS$"; AT$(I), X(I, 1), X(I, 2), X(I,
3); ANS$
```

```
5480 GOTO 5640
5490 INPUT #1, X(I, 0), AT$(I), X(I, 1), X(I, 2), X(I, 3)
5500 IF X(I, 0) = 0 THEN ANSWER = I
5510 REM PRINT "XXXXANS$"; X(I, 0), AT$(I), X(I, 1), X(I,
2), X(I, 3); ANS$
5520 IF X(I, 1) < 800 THEN 5540
5530 X(I, 1) = X(I, 1) - 900: RX = RX + 1: RINGX(RX) = I:
GOTO 5640
5540 IF X(I, 2) < 800 THEN 5560
5550 X(I, 2) = X(I, 2) - 900: RY = RY + 1: RINGY(RY) = I:
GOTO 5640
5560 IF X(I, 3) < 800 THEN 5580
5570 X(I, 3) = X(I, 3) - 900: RZ = RZ + 1: RINGZ(RZ) = I:
GOTO 5640
5580 IF X(I, 1) < 300 THEN 5600
5590 X(I, 1) = X(I, 1) - 400: YZP = I: GOTO 5640
5600 IF X(I, 2) < 300 THEN 5620
5610 X(I, 2) = X(I, 2) - 400: ZXP = I: GOTO 5640
5620 IF X(I, 3) < 300 THEN 5640
5630 X(I, 3) = X(I, 3) - 400: XYP = I
5640 NEXT
5650 CLOSE #1
5660 RETURN


6000 CLS : FOR I = 1 TO 10: PRINT : NEXT
6010 PRINT TAB(20); "TO SAVE TIME PLEASE REMEMBER YOUR FILE
NAME"
6020 PRINT TAB(20); "BEFORE YOU START THE PROGRAM. THANK
YOU!"
6030 PRINT : PRINT : PRINT TAB(20); "HIT ANY KEY TO RETURN
TO MAIN MENU...";
6040 ANS$ = INKEY$: IF ANS$ = "" THEN 6040
6050 GOSUB 7800
6060 RETURN


7000 CLS : FOR I = 1 TO 9: PRINT : NEXT
7010 PRINT TAB(20); A$
7020 PRINT TAB(20); "IS NOT FOUND OR IN INCORRECT FORMAT."
7030 PRINT : PRINT TAB(20); "OR: THE PATH FOR OUTPUT FILE"
7040 PRINT TAB(20); B$
7050 PRINT TAB(20); "IS WRONG."
7060 PRINT : PRINT : PRINT TAB(20); "HIT ANY KEY TO RETURN
TO MAIN MENU...";
7070 ANS$ = INKEY$: IF ANS$ = "" THEN 7070
```

```
7080 GOSUB 7800
7090 RESUME 170

7200 CLS : FOR I = 1 TO 10: PRINT : NEXT
7210 PRINT TAB(25); A$
7220 PRINT TAB(25); "HAS BEEN SUCCESSFULLY CONVERTED TO"
7230 PRINT TAB(25); B$
7240 PRINT : PRINT : PRINT TAB(25); "HIT ANY KEY TO RETURN
TO MAIN MENU...";
7250 ANS$ = INKEY$: IF ANS$ = "" THEN 7250
7260 GOSUB 7800
7270 RETURN

7400 CLS : FOR I = 1 TO 10: PRINT : NEXT
7410 PRINT TAB(20); A$
7420 PRINT TAB(20); "HAS ALREADY BEEN CATETSIAN FILE!"
7430 PRINT TAB(20); "SEE YOU NEXT TIME!"
7440 PRINT : PRINT : PRINT TAB(20); "HIT ANY KEY TO RETURN
TO MAIN MENU...";
7450 ANS$ = INKEY$: IF ANS$ = "" THEN 7450
7460 GOSUB 7800
7470 RETURN

7600 CLS
7610 SCREEN 0
7620 COLOR 14, 9
7630 CLS : FOR I = 1 TO 10: PRINT : NEXT
7640 PRINT TAB(20); "THANK YOU FOR YOUR USING THIS PROGRAM!"
7650 PRINT TAB(20); "SEE YOU NEXT TIME!"
7660 PRINT : PRINT : PRINT TAB(20); "HIT ANY KEY TO BACK TO
DOS/WINDOWS...";
7670 ANS$ = INKEY$: IF ANS$ = "" THEN 7670
7680 GOSUB 7800
7690 RETURN

7800 SCREEN 0
7810 COLOR 15, 1
7820 CLS
7830 FOR I = 1 TO 24: FOR J = 1 TO 80: PRINT " "; : NEXT:
NEXT
7840 RETURN
```

```
8000 CLS
8010 SCREEN 0
8020 COLOR 14, 9
8030 CLS : PRINT : PRINT
8040 PRINT TAB(10); "╔"; : FOR I = 1 TO 60: PRINT "═"; :
NEXT: PRINT "╗"
8050 PRINT TAB(10); "╟▌ THIS PROGRAM IS DESIGNED TO
TRANSLATE FRACTION COORDINATES╟"
8060 PRINT TAB(10); "╟  TO INTERNAL COORDINATES WHICH ARE
USED BY CACAO ONLY.      ╟"
8070 PRINT TAB(10); "╟▌ IF ANY PROBLEM IS DEVELOPED, PLEASE
LET Mr. Y. YU KNOW.    ╟"
8080 PRINT TAB(10); "╟  THANK YOU FOR YOUR COOPERATION!
                    ╟"
8090 PRINT TAB(10); "╚"; : FOR I = 1 TO 60: PRINT "═"; :
NEXT: PRINT "╝"
8100 PRINT : PRINT : PRINT : PRINT
8110 PRINT TAB(27); "COPYRIGHT (C) 1993, Y. YU"
8120 PRINT TAB(30); "ALL RIGHTS RESERVED"
8130 FOR I = 1 TO 6: PRINT : NEXT
8140 PRINT TAB(27); "HIT ANY KEY TO CONTINUE...";
8150 AN$ = INKEY$: IF AN$ = "" THEN 8150
8160 RETURN


8300 REM TO PUT A CENTROID ON A MAIN AXIS
8310 AVX = 0: AVY = 0: AVZ = 0
8320 IF RX = 0 AND RY = 0 AND RZ = 0 THEN 9370
8330 IF RX > 0 THEN 8360
8340 IF RY > 0 THEN 8420
8350 IF RZ > 0 THEN 8480
8360 RRR = RX: FOR J = 1 TO RRR
8370 AVX = AVX + X(RINGX(J), 1)
8380 AVY = AVY + X(RINGX(J), 2)
8390 AVZ = AVZ + X(RINGX(J), 3)
8400 NEXT J
8410 GOTO 8540
8420 RRR = RY: FOR J = 1 TO RRR
8430 AVX = AVX + X(RINGY(J), 1)
8440 AVY = AVY + X(RINGY(J), 2)
8450 AVZ = AVZ + X(RINGY(J), 3)
8460 NEXT J
8470 GOTO 8540
8480 RRR = RZ: FOR J = 1 TO RRR
8490 AVX = AVX + X(RINGZ(J), 1)
8500 AVY = AVY + X(RINGZ(J), 2)
```

```
8510 AVZ = AVZ + X(RINGZ(J), 3)
8520 NEXT J
8530 REM COORDINATES OF A CENTROID
8540 AVX = AVX / RRR
8550 AVY = AVY / RRR
8560 AVZ = AVZ / RRR
8570 IF RZ = 0 THEN 8760
8580 REM TO PUT THE CENTROID OF THE RING ON A NEW Z-AXIS
8590 REM DIRECTION COSINES OF THE NEW Z-AXIS RELATED TO OLD
COORDINATION SYSTEM
8600 DL3 = AVX / SQR(AVX ^ 2 + AVY ^ 2 + AVZ ^ 2)
8610 DM3 = AVY / SQR(AVX ^ 2 + AVY ^ 2 + AVZ ^ 2)
8620 DN3 = AVZ / SQR(AVX ^ 2 + AVY ^ 2 + AVZ ^ 2)
8630 REM TO FIND A NEW Y-AXIS (1,XYZ,0) ON OLD XY PLANE
8640 REM  (1*DL3+XYZ*DM3+0*DN3)/(|1,XYZ,0|*|DL3,DM3,DN3|)=0
8650 XYZ = -DL3 / DM3
8660 REM DIRECTION COSINES OF THE NEW Y-AXIS
8670 DL2 = 1 / SQR(1 * 1 + XYZ * XYZ + 0 * 0)
8680 DM2 = XYZ / SQR(1 * 1 + XYZ * XYZ + 0 * 0)
8690 DN2 = 0
8700 REM TO FIND A NEW X-AXIS: PRODUCT OF Y x Z
8710 REM DIRECTION COSINES OF THE NEW X-AXIS
8720 DL1 = DM2 * DN3 - DN2 * DM3
8730 DM1 = DN2 * DL3 - DL2 * DN3
8740 DN1 = DL2 * DM3 - DM2 * DL3
8750 GOTO 9140
8760 IF RY = 0 THEN 8950
8770 REM TO PUT CENTROID OF THE RING ON A NEW Y-AXIS
8780 REM DIRECTION COSINES OF A NEW Y-AXIS RELATED TO OLD
COORDINATION SYSTEM
8790 DL2 = AVX / SQR(AVX ^ 2 + AVY ^ 2 + AVZ ^ 2)
8800 DM2 = AVY / SQR(AVX ^ 2 + AVY ^ 2 + AVZ ^ 2)
8810 DN2 = AVZ / SQR(AVX ^ 2 + AVY ^ 2 + AVZ ^ 2)
8820 REM TO FIND A NEW X-AXIS (XYZ,0,1) ON OLD ZX PLANE
8830 REM  (XYZ*DL2+0*DM2+1*DN2)/(|XYZ,0,1|*|DL2,DM2,DN2|)=0
8840 XYZ = -DN2 / DL2
8850 REM DIRECTION COSINE OF THE NEW X-AXIS
8860 DL1 = XYZ / SQR(XYZ * XYZ + 0 * 0 + 1 * 1)
8870 DM1 = 0
8880 DN1 = 1 / SQR(XYZ * XYZ + 0 * 0 + 1 * 1)
8890 REM TO FIND A NEW Z-AXIS: PRODUCT OF X x Y
8900 REM DIRECTION COSINE OF THE NEW Z-AXIS
8910 DL3 = DM1 * DN2 - DN1 * DM2
8920 DM3 = DN1 * DL2 - DL1 * DN2
8930 DN3 = DL1 * DM2 - DM1 * DL2
8940 GOTO 9140
```

```
8950 REM IF RZ=0 AND RY=0 THEN RX>>>0
8960 REM TO PUT THE CENTROID OF THE RING ON A NEW X-AXIS
8970 REM DIRECTION COSINES OF THE NEW X-AXIS RELATED TO OLD
COORDINATION SYSTEM
8980 DL1 = AVX / SQR(AVX ^ 2 + AVY ^ 2 + AVZ ^ 2)
8990 DM1 = AVY / SQR(AVX ^ 2 + AVY ^ 2 + AVZ ^ 2)
9000 DN1 = AVZ / SQR(AVX ^ 2 + AVY ^ 2 + AVZ ^ 2)
9010 REM TO FIND A NEW Z-AXIS (0,1,XYZ) ON OLD YZ PLANE
9020 REM  (0*DL1+1*DM1+XYZ*DN1)/(|0,1,XYZ|*|DL1,DM1,DN1|)=0
9030 XYZ = -DM1 / DN1
9040 REM DIRECTION COSINES OF THE NEW Z-AXIS
9050 DL3 = 0
9060 DM3 = 1 / SQR(0 * 0 + 1 * 1 + XYZ * XYZ)
9070 DN3 = XYZ / SQR(0 * 0 + 1 * 1 + XYZ * XYZ)
9080 REM TO FIND A NEW Y-AXIS: PRODUCT OF Z x X
9090 REM DIRECTION COSINE OF THE NEW Y-AXIS
9100 DL2 = DM3 * DN1 - DN3 * DM1
9110 DM2 = DN3 * DL1 - DL3 * DN1
9120 DN2 = DL3 * DM1 - DM3 * DL1
9130 REM NEW COORDINATES WITH THE CENTROID ON THE MAIN AXIS
X OR Y OR Z
9140 FOR I = 1 TO N
9150 IF I = RINGX(1) THEN 9280
9160 IF I = RINGY(1) THEN 9290
9170 IF I = RINGZ(1) THEN 9300
9180 FOR J = 2 TO RX: IF I = RINGX(J) THEN 9310
9190 NEXT J
9200 FOR J = 2 TO RY: IF I = RINGY(J) THEN 9310
9210 NEXT J
9220 FOR J = 2 TO RZ: IF I = RINGZ(J) THEN 9310
9230 NEXT J
9240 Y(I, 1) = DL1 * X(I, 1) + DM1 * X(I, 2) + DN1 * X(I, 3)
9250 Y(I, 2) = DL2 * X(I, 1) + DM2 * X(I, 2) + DN2 * X(I, 3)
9260 Y(I, 3) = DL3 * X(I, 1) + DM3 * X(I, 2) + DN3 * X(I, 3)
9270 GOTO 9310
9280 Y(I, 1) = SQR(AVX ^ 2 + AVY ^ 2 + AVZ ^ 2): Y(I, 2) =
0: Y(I, 3) = 0: GOTO 9310
9290 Y(I, 1) = 0: Y(I, 2) = SQR(AVX ^ 2 + AVY ^ 2 + AVZ ^
2): Y(I, 3) = 0: GOTO 9310
9300 Y(I, 1) = 0: Y(I, 2) = 0: Y(I, 3) = SQR(AVX ^ 2 + AVY ^
2 + AVZ ^ 2)
9310 NEXT I
9320 FOR I = 1 TO N
9330 X(I, 1) = Y(I, 1): X(I, 2) = Y(I, 2): X(I, 3) = Y(I, 3)
9340 NEXT I
9350 FOR I = 1 TO N: Y(I, 1) = 0: Y(I, 2) = 0: Y(I, 3) = 0:
```

```
NEXT I
9360 REM OPEN "O", 4, "c:\temp2": FOR i = 1 TO n: PRINT #4,
x(i, 0); i; at$(i); x(i, 1); x(i, 2); x(i, 3): NEXT i: CLOSE
#4: STOP
9370 IF YZP > 0 THEN GOSUB 9600
9380 IF ZXP > 0 THEN GOSUB 11000
9390 IF XYP > 0 THEN GOSUB 12000
9400 REM OPEN "O", 5, "c:\temp3": FOR i = 1 TO n: PRINT #5,
x(i, 0); i; at$(i); x(i, 1); x(i, 2); x(i, 3): NEXT i: CLOSE
#5
9410 RETURN


9600 REM TO PUT A SPECEIFIC ATOM ON YZ PLANE
9610 REM TO FIND ANGLE BETWEEN VECTOR O-->S (SPECEFIC ATOM)
AND YZ PLANE
9620 REM IF RX = 0 AND RY = 0 AND RZ = 0 AND YZP>0 THEN
ROTATE AROUND Z AXIS
9630 IF RX = 0 AND RY = 0 AND RZ = 0 THEN 9980
9640 IF RX = 0 THEN 9680
9650 REM IF RX>0 THEN "CANNOT PUT ATOM S ON YZ PLANE EXCEPT
THAT S HAS ALREADY BEEN ON YZ PLANE"
9660 IF RX > 0 AND X(YZP, 1) = 0 THEN 10260
9670 IF RX > 0 AND X(YZP, 1) <> 0 THEN 13000
9680 IF RY = 0 THEN 9970
9690 REM IF RY>0 THEN ROTATE AROUND Y AXIS
9700 REM TO FIND NORMAL TO PLANE O-->S
[X(YZP,1),X(YZP,2),X(YZP,3) AND +Y AXIS
9710 REM NORMAL NORS[X(YZP,3), 0, -X(YZP,1)]
9720 REM ANGLE BETWEEN NORS AND  X-AXIS (NORMAL TO YZ PLANE)
9730 ANG = FNARCCOS((X(YZP, 3) * 1 + 0 * 0 + (-X(YZP, 1)) *
0) / SQR(X(YZP, 3) ^ 2 + 0 * 0 + (-X(YZP, 1)) ^ 2))
9740 REM SS=O-->S . +X AXIS)
9750 SS = X(YZP, 1) * 1 + X(YZP, 2) * 0 + X(YZP, 3) * 0
9760 SIGN = SGN(SS)
9770 IF SIGN < 0 THEN ANG = 2 * 22 / 7 - ANG
9780 FOR I = 1 TO N
9790 IF I = RINGX(1) THEN 9930
9800 IF I = RINGY(1) THEN 9930
9810 IF I = RINGZ(1) THEN 9930
9820 FOR J = 2 TO RX: IF I = RINGX(J) THEN 9950
9830 NEXT J
9840 FOR J = 2 TO RY: IF I = RINGY(J) THEN 9950
9850 NEXT J
9860 FOR J = 2 TO RZ: IF I = RINGZ(J) THEN 9950
9870 NEXT J
```

```
9880 REM TO ROTATE AROUND Y AXIS
9890 Y(I, 1) = COS(ANG) * X(I, 1) + 0 * X(I, 2) +
(-SIN(ANG)) * X(I, 3)
9900 Y(I, 2) = 0 * X(I, 1) + 1 * X(I, 2) + 0 * X(I, 3)
9910 Y(I, 3) = SIN(ANG) * X(I, 1) + 0 * X(I, 2) + COS(ANG) *
X(I, 3)
9920 GOTO 9940
9930 Y(I, 1) = X(I, 1): Y(I, 2) = X(I, 2): Y(I, 3) = X(I, 3)
9940 IF I = YZP THEN Y(I, 1) = 0
9950 NEXT I
9960 GOTO 10250
9970 REM IF RZ = 0 THEN 7340
9980 REM IF RZ>0 THEN ROTATE AROUND Z AXIS
9990 REM TO FIND NORMAL TO PLANE O-->S
[X(YZP,1),X(YZP,2),X(YZP,3) AND +Z AXIS
10000 REM NORMAL NORS[-X(YZP,2), X(YZP,1),0]
10010 REM ANGLE BETWEEN NORS AND  X-AXIS (NORMAL TO YZ
PLANE)
10020 ANG = FNARCCOS((-X(YZP, 2) * 1 + (X(YZP, 1)) * 0 + 0 *
0) / SQR((-X(YZP, 2)) ^ 2 + X(YZP, 1) ^ 2 + 0 * 0))
10030 REM SS=O-->S . +X AXIS
10040 SS = X(YZP, 1) * 1 + X(YZP, 2) * 0 + X(YZP, 3) * 0
10050 SIGN = SGN(SS)
10060 IF SIGN < 0 THEN ANG = 2 * 22 / 7 - ANG
10070 FOR I = 1 TO N
10080 IF I = RINGX(1) THEN 10220
10090 IF I = RINGY(1) THEN 10220
10100 IF I = RINGZ(1) THEN 10220
10110 FOR J = 2 TO RX: IF I = RINGX(J) THEN 10240
10120 NEXT J
10130 FOR J = 2 TO RY: IF I = RINGY(J) THEN 10240
10140 NEXT J
10150 FOR J = 2 TO RZ: IF I = RINGZ(J) THEN 10240
10160 NEXT J
10170 REM TO ROTATE AROUND Z AXIS
10180 Y(I, 1) = COS(ANG) * X(I, 1) + SIN(ANG) * X(I, 2) + 0
* X(I, 3)
10190 Y(I, 2) = -SIN(ANG) * X(I, 1) + COS(ANG) * X(I, 2) + 0
* X(I, 3)
10200 Y(I, 3) = 0 * X(I, 1) + 0 * X(I, 2) + 1 * X(I, 3)
10210 GOTO 10230
10220 Y(I, 1) = X(I, 1): Y(I, 2) = X(I, 2): Y(I, 3) = X(I,
3)
10230 IF I = YZP THEN Y(I, 1) = 0
10240 NEXT I
10250 FOR I = 1 TO N: Y(I, 1) = X(I, 1): Y(I, 2) = X(I, 2):
```

```
Y(I, 3) = X(I, 3): NEXT I
10260 RETURN


11000 REM TO PUT A SPECEIFIC ATOM ON ZX PLANE
11010 REM TO FIND ANGLE BETWEEN VECTOR O-->S (SPECEFIC ATOM)
AND ZX PLANE
11020 REM IF RX = 0 AND RY = 0 AND RZ = 0 AND ZXP>0 THEN
ROTATE AROUND X AXIS
11030 IF RX = 0 AND RY = 0 AND RZ = 0 THEN 11090
11040 IF RY = 0 THEN 11080
11050 REM IF RY>0 THEN "CANNOT PUT ATOM S ON ZX PLANE EXCEPT
THAT S HAS ALREADY BEEN ON ZX PLANE"
11060 IF RY > 0 AND X(ZXP, 2) = 0 THEN 11660
11070 IF RY > 0 AND X(ZXP, 2) <> 0 THEN 13000
11080 IF RX = 0 THEN 11370
11090 REM IF RX>0 THEN ROTATE AROUND X AXIS
11100 REM TO FIND NORMAL TO PLANE O-->S
[X(ZXP,1),X(ZXP,2),X(ZXP,3) AND +X AXIS
11110 REM NORMAL NORS[0, -X(ZXP,3), X(ZXP,2)]
11120 REM ANGLE BETWEEN NORS AND  Y-AXIS (NORMAL TO ZX
PLANE)
11130 ANG = FNARCCOS((0 * 0 + (-X(ZXP, 3)) * 1 + X(ZXP, 2) *
0) / SQR(0 * 0 + (-X(ZXP, 3)) ^ 2 + X(ZXP, 2) ^ 2))
11140 REM SS=O-->S . +Y AXIS)
11150 SS = X(ZXP, 1) * 0 + X(ZXP, 2) * 1 + X(ZXP, 3) * 0
11160 SIGN = SGN(SS)
11170 IF SIGN < 0 THEN ANG = 2 * 22 / 7 - ANG
11180 FOR I = 1 TO N
11190 IF I = RINGX(1) THEN 11330
11200 IF I = RINGY(1) THEN 11330
11210 IF I = RINGZ(1) THEN 11330
11220 FOR J = 2 TO RX: IF I = RINGX(J) THEN 11350
11230 NEXT J
11240 FOR J = 2 TO RY: IF I = RINGY(J) THEN 11350
11250 NEXT J
11260 FOR J = 2 TO RZ: IF I = RINGZ(J) THEN 11350
11270 NEXT J
11280 REM TO ROTATE AROUND X AXIS
11290 Y(I, 1) = 1 * X(I, 1) + 0 * X(I, 2) + 0 * X(I, 3)
11300 Y(I, 2) = 0 * X(I, 1) + COS(ANG) * X(I, 2) + SIN(ANG)
* X(I, 3)
11310 Y(I, 3) = 0 * X(I, 1) + (-SIN(ANG)) * X(I, 2) +
COS(ANG) * X(I, 3)
11320 GOTO 11340
11330 Y(I, 1) = X(I, 1): Y(I, 2) = X(I, 2): Y(I, 3) = X(I,
```

```
3)
11340 IF I = ZXP THEN Y(I, 2) = 0
11350 NEXT I
11360 GOTO 11650
11370 IF RZ = 0 THEN 11660
11380 REM IF RZ>0 THEN ROTATE AROUND Z AXIS
11390 REM TO FIND NORMAL TO PLANE O-->S
[X(ZXP,1),X(ZXP,2),X(ZXP,3) AND +Z AXIS
11400 REM NORMAL NORS[-X(ZXP,2), X(ZXP,1),0]
11410 REM ANGLE BETWEEN NORS AND  Y-AXIS (NORMAL TO ZX
PLANE)
11420 ANG = FNARCCOS((-X(ZXP, 2) * 0 + X(ZXP, 1) * 1 + 0 *
1) / SQR((-X(ZXP, 2)) ^ 2 + X(ZXP, 1) ^ 2 + 0 * 0))
11430 REM SS=O-->S . +Y AXIS
11440 SS = X(ZXP, 1) * 0 + X(ZXP, 2) * 1 + X(ZXP, 3) * 0
11450 SIGN = SGN(SS)
11460 IF SIGN < 0 THEN ANG = 2 * 22 / 7 - ANG
11470 FOR I = 1 TO N
11480 IF I = RINGX(1) THEN 11620
11490 IF I = RINGY(1) THEN 11620
11500 IF I = RINGZ(1) THEN 11620
11510 FOR J = 2 TO RX: IF I = RINGX(J) THEN 11640
11520 NEXT J
11530 FOR J = 2 TO RY: IF I = RINGY(J) THEN 11640
11540 NEXT J
11550 FOR J = 2 TO RZ: IF I = RINGZ(J) THEN 11640
11560 NEXT J
11570 REM TO ROTATE AROUND Z AXIS
11580 Y(I, 1) = COS(ANG) * X(I, 1) + SIN(ANG) * X(I, 2) + 0
* X(I, 3)
11590 Y(I, 2) = -SIN(ANG) * X(I, 1) + COS(ANG) * X(I, 2) + 0
* X(I, 3)
11600 Y(I, 3) = 0 * X(I, 1) + 0 * X(I, 2) + 1 * X(I, 3)
11610 GOTO 11630
11620 Y(I, 1) = X(I, 1): Y(I, 2) = X(I, 2): Y(I, 3) = X(I,
3): GOTO 11640
11630 IF I = ZXP THEN Y(I, 2) = 0
11640 NEXT I
11650 FOR I = 1 TO N: Y(I, 1) = X(I, 1): Y(I, 2) = X(I, 2):
Y(I, 3) = X(I, 3): NEXT I
11660 RETURN


12000 REM TO PUT A SPECEIFIC ATOM ON XY PLANE
12010 REM TO FIND ANGLE BETWEEN VECTOR O-->S (SPECEFIC ATOM)
AND XY PLANE
```

```
12020 REM IF RX = 0 AND RY = 0 AND RZ = 0 AND XYP>0 THEN
ROTATE AROUND Y AXIS
12030 IF RX = 0 AND RY = 0 AND RZ = 0 THEN 12380
12040 IF RZ = 0 THEN 12080
12050 REM IF RZ>0 THEN "CANNOT PUT ATOM S ON XY PLANE EXCEPT
THAT S HAS ALREADY BEEN ON XY PLANE"
12060 IF RZ > 0 AND X(XYP, 3) = 0 THEN 12660
12070 IF RZ > 0 AND X(XYP, 3) <> 0 THEN 13000
12080 IF RX = 0 THEN 12370
12090 REM IF RX>0 THEN ROTATE AROUND X AXIS
12100 REM TO FIND NORMAL TO PLANE O-->S
[X(XYP,1),X(XYP,2),X(XYP,3) AND +X AXIS
12110 REM NORMAL NORS[0, -X(XYP,3), X(XYP,2)]
12120 REM ANGLE BETWEEN NORS AND  Z-AXIS (NORMAL TO XY
PLANE)
12130 ANG = FNARCCOS((0 * 0 + (-X(XYP, 3)) * 0 + X(XYP, 2) *
1) / SQR(0 * 0 + (-X(XYP, 3)) ^ 2 + X(XYP, 2) ^ 2))
12140 REM SS=O-->S . +Z AXIS)
12150 SS = X(XYP, 1) * 0 + X(XYP, 2) * 0 + X(XYP, 3) * 1
12160 SIGN = SGN(SS)
12170 IF SIGN < 0 THEN ANG = 2 * 22 / 7 - ANG
12180 FOR I = 1 TO N
12190 IF I = RINGX(1) THEN 12330
12200 IF I = RINGY(1) THEN 12330
12210 IF I = RINGZ(1) THEN 12330
12220 FOR J = 2 TO RX: IF I = RINGX(J) THEN 12350
12230 NEXT J
12240 FOR J = 2 TO RY: IF I = RINGY(J) THEN 12350
12250 NEXT J
12260 FOR J = 2 TO RZ: IF I = RINGZ(J) THEN 12350
12270 NEXT J
12280 REM TO ROTATE AROUND X AXIS
12290 Y(I, 1) = 1 * X(I, 1) + 0 * X(I, 2) + 0 * X(I, 3)
12300 Y(I, 2) = 0 * X(I, 1) + COS(ANG) * X(I, 2) + SIN(ANG)
* X(I, 3)
12310 Y(I, 3) = 0 * X(I, 1) + (-SIN(ANG)) * X(I, 2) +
COS(ANG) * X(I, 3)
12320 GOTO 12340
12330 Y(I, 1) = X(I, 1): Y(I, 2) = X(I, 2): Y(I, 3) = X(I,
3): GOTO 12350
12340 IF I = XYP THEN Y(I, 3) = 0
12350 NEXT I
12360 GOTO 12650
12370 IF RY = 0 THEN 12660
12380 REM IF RY>0 THEN ROTATE AROUND Y AXIS
12390 REM TO FIND NORMAL TO PLANE O-->S
```

```
[X(XYP,1),X(XYP,2),X(XYP,3) AND +Y AXIS
12400 REM NORMAL NORS[X(XYP,3), 0, -X(XYP,1)]
12410 REM ANGLE BETWEEN NORS AND  Z-AXIS (NORMAL TO XY
PLANE)
12420 ANG = FNARCCOS((X(XYP, 3) * 0 + 0 * 0 + (-X(XYP, 1)) *
1) / SQR(X(XYP, 3) ^ 2 + 0 * 0 + (-X(XYP, 1)) ^ 2))
12430 REM SS=O-->S . +Z AXIS
12440 SS = X(XYP, 1) * 0 + X(XYP, 2) * 0 + X(XYP, 3) * 1
12450 SIGN = SGN(SS)
12460 IF SIGN < 0 THEN ANG = 2 * 22 / 7 - ANG
12470 FOR I = 1 TO N: GOTO 12580
12480 IF I = RINGX(1) THEN 12620
12490 IF I = RINGY(1) THEN 12620
12500 IF I = RINGZ(1) THEN 12620
12510 FOR J = 2 TO RX: IF I = RINGX(J) THEN 12640
12520 NEXT J
12530 FOR J = 2 TO RY: IF I = RINGY(J) THEN 12640
12540 NEXT J
12550 FOR J = 2 TO RZ: IF I = RINGZ(J) THEN 12640
12560 NEXT J
12570 REM TO ROTATE AROUND Y AXIS
12580 Y(I, 1) = COS(ANG) * X(I, 1) + 0 * X(I, 2) +
(-SIN(ANG)) * X(I, 3)
12590 Y(I, 2) = 0 * X(I, 1) + 1 * X(I, 2) + 0 * X(I, 3)
12600 Y(I, 3) = SIN(ANG) * X(I, 1) + 0 * X(I, 2) + COS(ANG)
* X(I, 3)
12610 GOTO 12630
12620 Y(I, 1) = X(I, 1): Y(I, 2) = X(I, 2): Y(I, 3) = X(I,
3)
12630 IF I = XYP THEN Y(I, 3) = 0
12640 NEXT I
12650 FOR I = 1 TO N: X(I, 1) = Y(I, 1): X(I, 2) = Y(I, 2):
X(I, 3) = Y(I, 3): NEXT I
12660 RETURN


13000 CLS : FOR I = 1 TO 10: PRINT : NEXT
13010 IF XYP = 0 THEN 13060
13020 PRINT TAB(20); "ATOM  '"; AT$(XYP); "'  CANNOT BEEN
PUT ON XY PLANE!"
13030 PRINT TAB(20); "BECAUSE YOU WANT PUT A CENTROID OF A
RING"
13040 PRINT TAB(20); "ON THE Z-AXIS AT THE SAME TIME."
13050 GOTO 13140
13060 IF ZXP = 0 THEN 13110
13070 PRINT TAB(20); "ATOM  '"; AT$(ZXP); "'  CANNOT BEEN
```

```
PUT ON ZX PLANE!"
13080 PRINT TAB(20); "BECAUSE YOU WANT PUT A CENTROID OF A
RING"
13090 PRINT TAB(20); "ON THE Y-AXIS AT THE SAME TIME."
13100 GOTO 13140
13110 PRINT TAB(20); "ATOM  '"; AT$(YZP); "'  CANNOT BEEN
PUT ON YZ PLANE!"
13120 PRINT TAB(20); "BECAUSE YOU WANT PUT A CENTROID OF A
RING"
13130 PRINT TAB(20); "ON THE X-AXIS AT THE SAME TIME."
13140 PRINT : PRINT : PRINT TAB(20); "HIT ANY KEY TO RETURN
TO MAIN MENU...";
13150 ANS$ = INKEY$: IF ANS$ = "" THEN 13150
13160 GOSUB 7800
13170 GOTO 170


14000 REM TO DETERMINE X(I,0)
14010 IF ANSWER > 0 THEN 14120
14020 REM X(I,0) WHILE ANSWER=0
14030 X$ = STR$(X(I, 0)) + ","
14040 IF RX > 0 AND RINGX(RX) >= X(I, 0) >= RINGX(1) THEN X$
= STR$(RINGX(1)) + ","
14050 IF RY > 0 AND RINGY(RY) >= X(I, 0) >= RINGY(1) THEN X$
= STR$(RINGY(1)) + ","
14060 IF RZ > 0 AND RINGZ(RZ) >= X(I, 0) >= RINGZ(1) THEN X$
= STR$(RINGZ(1)) + ","
14070 IF RX > 0 AND RINGX(RX) < X(I, 0) THEN X$ = STR$(X(I,
0) + RX) + ","
14080 IF RY > 0 AND RINGY(RY) < X(I, 0) THEN X$ = STR$(X(I,
0) + RY) + ","
14090 IF RZ > 0 AND RINGZ(RZ) < X(I, 0) THEN X$ = STR$(X(I,
0) + RZ) + ","
14100 GOTO 14430
14110 REM X(I,0) WHILE ANSWER>0
14120 X$ = STR$(X(I, 0)) + ","
14130 IF X(I, 0) = ANSWER THEN X$ = " 1,"
14140 REM CASE A: RX=RY=RZ=0
14150 IF RX = 0 AND RY = 0 AND RZ = 0 THEN 14160 ELSE 14180
14160 IF X(I, 0) < ANSWER THEN X$ = STR$(X(I, 0) + 1) + ","
14170 GOTO 14430
14180 REM CASE B: RX>0 OR RY>0 OR RZ>0 AND ANSWER < RINGX(1)
OR RINGY(1) OR RINGZ(1)
14190 IF RX > 0 AND ANSWER > RINGX(1) THEN 14310
14200 IF RY > 0 AND ANSWER > RINGY(1) THEN 14310
14210 IF RZ > 0 AND ANSWER > RINGZ(1) THEN 14310
```

```
14220 IF X(I, 0) < ANSWER THEN X$ = STR$(X(I, 0) + 1) + ","
14230 IF RX > 0 AND RINGX(RX) >= X(I, 0) >= RINGX(1) THEN X$
= STR$(RINGX(1)) + ","
14240 IF RY > 0 AND RINGY(RY) >= X(I, 0) >= RINGY(1) THEN X$
= STR$(RINGY(1)) + ","
14250 IF RZ > 0 AND RINGZ(RZ) >= X(I, 0) >= RINGZ(1) THEN X$
= STR$(RINGZ(1)) + ","
14260 IF RX > 0 AND RINGX(RX) < X(I, 0) THEN X$ = STR$(X(I,
0) + RX) + ","
14270 IF RY > 0 AND RINGY(RY) < X(I, 0) THEN X$ = STR$(X(I,
0) + RY) + ","
14280 IF RZ > 0 AND RINGZ(RZ) < X(I, 0) THEN X$ = STR$(X(I,
0) + RZ) + ","
14290 GOTO 14430
14300 REM CASE C: RX>0 OR RY>0 OR RZ>0 AND ANSWER > RINGX(1)
OR RINGY(1) OR RINGZ(1)
14310 IF RX > 0 AND X(I, 0) < RINGX(1) THEN X$ = STR$(X(I,
0) + 1) + ","
14320 IF RY > 0 AND X(I, 0) < RINGY(1) THEN X$ = STR$(X(I,
0) + 1) + ","
14330 IF RZ > 0 AND X(I, 0) < RINGZ(1) THEN X$ = STR$(X(I,
0) + 1) + ","
14340 IF RX > 0 AND RINGX(RX) >= X(I, 0) >= RINGX(1) THEN X$
= STR$(RINGX(1) + 1) + ","
14350 IF RY > 0 AND RINGY(RY) >= X(I, 0) >= RINGY(1) THEN X$
= STR$(RINGY(1) + 1) + ","
14360 IF RZ > 0 AND RINGZ(RZ) >= X(I, 0) >= RINGZ(1) THEN X$
= STR$(RINGZ(1) + 1) + ","
14370 IF RX > 0 AND RINGX(RX) < X(I, 0) < ANSWER THEN X$ =
STR$(X(I, 0) + 1 + RX) + ","
14380 IF RY > 0 AND RINGY(RY) < X(I, 0) < ANSWER THEN X$ =
STR$(X(I, 0) + 1 + RY) + ","
14390 IF RZ > 0 AND RINGZ(RZ) < X(I, 0) < ANSWER THEN X$ =
STR$(X(I, 0) + 1 + RZ) + ","
14400 IF RX > 0 AND X(I, 0) > ANSWER THEN X$ = STR$(X(I, 0)
+ RX) + ","
14410 IF RY > 0 AND X(I, 0) > ANSWER THEN X$ = STR$(X(I, 0)
+ RY) + ","
14420 IF RZ > 0 AND X(I, 0) > ANSWER THEN X$ = STR$(X(I, 0)
+ RZ) + ","
14430 IF LEN(X$) = 4 THEN X$ = RIGHT$(X$, 3)
14440 RETURN


15000 REM TO DETERMINE NUM (# OF ATOM ORDER)
15010 NUM = 0
```

```
15020 IF ANSWER > 0 THEN 15130
15030 REM X(I,0) WHILE ANSWER=0
15040 NUM = I
15050 IF RX > 0 AND RINGX(RX) >= I >= RINGX(1) THEN NUM =
RINGX(1)
15060 IF RY > 0 AND RINGY(RY) >= I >= RINGY(1) THEN NUM =
RINGY(1)
15070 IF RZ > 0 AND RINGZ(RZ) >= I >= RINGZ(1) THEN NUM =
RINGZ(1)
15080 IF RX > 0 AND RINGX(RX) < I THEN NUM = I + RX
15090 IF RY > 0 AND RINGY(RY) < I THEN NUM = I + RY
15100 IF RZ > 0 AND RINGZ(RZ) < I THEN NUM = I + RZ
15110 GOTO 15440
15120 REM NUM WHILE ANSWER>0
15130 NUM = I
15140 IF I = ANSWER THEN NUM = 1
15150 REM CASE A: RX=RY=RZ=0
15160 IF RX = 0 AND RY = 0 AND RZ = 0 THEN 15170 ELSE 15190
15170 IF I < ANSWER THEN NUM = I + 1
15180 GOTO 15440
15190 REM CASE B: RX>0 OR RY>0 OR RZ>0 AND ANSWER < RINGX(1)
OR RINGY(1) OR RINGZ(1)
15200 IF RX > 0 AND ANSWER > RINGX(1) THEN 15320
15210 IF RY > 0 AND ANSWER > RINGY(1) THEN 15320
15220 IF RZ > 0 AND ANSWER > RINGZ(1) THEN 15320
15230 IF I < ANSWER THEN NUM = I + 1
15240 IF RX > 0 AND RINGX(RX) >= I >= RINGX(1) THEN NUM =
RINGX(1)
15250 IF RY > 0 AND RINGY(RY) >= I >= RINGY(1) THEN NUM =
RINGY(1)
15260 IF RZ > 0 AND RINGZ(RZ) >= I >= RINGZ(1) THEN NUM =
RINGZ(1)
15270 IF RX > 0 AND RINGX(RX) < I THEN NUM = I + RX
15280 IF RY > 0 AND RINGY(RY) < I THEN NUM = I + RY
15290 IF RZ > 0 AND RINGZ(RZ) < I THEN NUM = I + RZ
15300 GOTO 15440
15310 REM CASE C: RX>0 OR RY>0 OR RZ>0 AND ANSWER > RINGX(1)
OR RINGY(1) OR RINGZ(1)
15320 IF RX > 0 AND I < RINGX(1) THEN NUM = I + 1
15330 IF RY > 0 AND I < RINGY(1) THEN NUM = I + 1
15340 IF RZ > 0 AND I < RINGZ(1) THEN NUM = I + 1
15350 IF RX > 0 AND RINGX(RX) >= I >= RINGX(1) THEN NUM =
RINGX(1) + 1
15360 IF RY > 0 AND RINGY(RY) >= I >= RINGY(1) THEN NUM =
RINGY(1) + 1
15370 IF RZ > 0 AND RINGZ(RZ) >= I >= RINGZ(1) THEN NUM =
```

```
RINGZ(1) + 1
15380 IF RX > 0 AND RINGX(RX) < I < ANSWER THEN NUM = I + 1
+ RX
15390 IF RY > 0 AND RINGY(RY) < I < ANSWER THEN NUM = I + 1
+ RY
15400 IF RZ > 0 AND RINGZ(RZ) < I < ANSWER THEN NUM = I + 1
+ RZ
15410 IF RX > 0 AND I > ANSWER THEN NUM = I + RX
15420 IF RY > 0 AND I > ANSWER THEN NUM = I + RY
15430 IF RZ > 0 AND I > ANSWER THEN NUM = I + RZ
15440 I$ = STR$(NUM) + ","
15450 IF LEN(I$) = 4 THEN I$ = RIGHT$(I$, 3)
15460 RETURN
```

Appendix 2. CACAO input file for rotational study of CpCp*TiCl(C_6F_5)

```
CpCp*TiCl(C6F5) 1st molecule in the unit cell, rot study
 48  0DIST  0  1 15
0,14.7,30,60,90,120,150,180,194.7,209.9,240,270,300,330,360
0,0,0,TI
 1, 2,CL  2.3199, 90.0000, 98.8802
 1, 3, C  2.2862, 90.0000,  0.0000,          1
 3, 4, C  1.3937,123.5103,104.7001,          1
 4, 5, C  1.3271,126.3369,177.6341,          1
 5, 6, C  1.4073,118.0895,  3.6762,          1
 6, 7, C  1.3504,117.8464,357.6537,          1
 7, 8, C  1.3378,120.3810,  0.7676,          1
 8, 9, F  1.3636,114.5257,177.9669,          1
 7,10, F  1.3405,118.9599,180.4603,          1
 6,11, F  1.3619,120.5207,179.6772,          1
 5,12, F  1.3002,124.5396,181.7600,          1
 4,13, F  1.3808,120.8772,  3.0201,          1
 1,14, C  2.4146, 11.9204,103.4473
 1,15, C  2.4213, 22.7503,311.9635
 1,16, C  2.3961, 44.9084,262.5067
 1,17, C  2.3679, 50.9753,216.6360
 1,18, C  2.3827, 36.9991,170.3880
14,19, H  0.9530,120.6126,218.2037
15,20, H  0.9414,120.9433,132.6787
16,21, H  0.9548,118.8973,154.5622
17,22, H  0.9535,118.3970,187.3937
18,23, H  0.9371,119.3467,216.5022
 1,24, C  2.4221,145.3441,291.9675
 1,25, C  2.3762,127.6658,248.6664
 1,26, C  2.4019,131.3139,204.1846
 1,27, C  2.4664,153.8942,161.3206
 1,28, C  2.4791,173.0277,  2.2761
24,29, C  1.5427,118.9731, 43.7009
26,30, C  1.5378,118.2374,336.6505
25,31, C  1.5477,117.2563, 12.3159
27,32, C  1.5429,120.5797,307.4177
28,33, C  1.5468,121.1031, 41.1798
29,34, H  0.9129,112.6876,207.7421
29,35, H  0.9276,111.6724,338.7784
29,36, H  1.0352,106.9554, 92.2935
31,37, H  3.7733, 55.4297,255.4795
31,38, H  3.7727, 55.3431,284.4094
31,39, H  2.7055, 71.0873,269.9800
30,40, H  2.8701, 68.9322, 88.2058
30,41, H  3.9041, 53.7018, 73.5181
30,42, H  3.9231, 53.5184,102.0080
32,43, H  0.9861,107.3097,144.3551
32,44, H  0.8877,112.1252,267.3507
32,45, H  0.9747,107.8735, 32.1725
33,46, H  0.9031,112.4956,272.5026
33,47, H  0.9918,108.2513, 34.1096
33,48, H  0.9686,109.3275,147.5504
GR1  1  3 1000., 0.
```

Appendix 3. CACAO input file for FMO study of CpCp*TiCl(C_6F_5)

```
CpCp*TiCl(C6F5) 1st molecule in the unit cell
 48  0DIST
0,0,0,TI
 1, 2,CL  2.3199, 90.0000, 98.8802
 1, 3, C  2.2862, 90.0000,  0.0000
 3, 4, C  1.3937,123.5103,104.7001
 4, 5, C  1.3271,126.3369,177.6341
 5, 6, C  1.4073,118.0895,  3.6762
 6, 7, C  1.3504,117.8464,357.6537
 7, 8, C  1.3378,120.3810,  0.7676
 8, 9, F  1.3636,114.5257,177.9669
 7,10, F  1.3405,118.9599,180.4603
 6,11, F  1.3619,120.5207,179.6772
 5,12, F  1.3002,124.5396,181.7600
 4,13, F  1.3808,120.8772,  3.0201
 1,14, C  2.4146, 11.9204,103.4473
 1,15, C  2.4213, 22.7503,311.9635
 1,16, C  2.3961, 44.9084,262.5067
 1,17, C  2.3679, 50.9753,216.6360
 1,18, C  2.3827, 36.9991,170.3880
14,19, H  0.9530,120.6126,218.2037
15,20, H  0.9414,120.9433,132.6787
16,21, H  0.9548,118.8973,154.5622
17,22, H  0.9535,118.3970,187.3937
18,23, H  0.9371,119.3467,216.5022
 1,24, C  2.4221,145.3441,291.9675
 1,25, C  2.3762,127.6658,248.6664
 1,26, C  2.4019,131.3139,204.1846
 1,27, C  2.4664,153.8942,161.3206
 1,28, C  2.4791,173.0277,  2.2761
24,29, C  1.5427,118.9731, 43.7009
26,30, C  1.5378,118.2374,336.6505
25,31, C  1.5477,117.2563, 12.3159
27,32, C  1.5429,120.5797,307.4177
28,33, C  1.5468,121.1031, 41.1798
29,34, H  0.9129,112.6876,207.7421
29,35, H  0.9276,111.6724,338.7784
29,36, H  1.0352,106.9554, 92.2935
31,37, H  3.7733, 55.4297,255.4795
31,38, H  3.7727, 55.3431,284.4094
31,39, H  2.7055, 71.0873,269.9800
30,40, H  2.8701, 68.9322, 88.2058
30,41, H  3.9041, 53.7018, 73.5181
30,42, H  3.9231, 53.5184,102.0080
32,43, H  0.9861,107.3097,144.3551
32,44, H  0.8877,112.1252,267.3507
32,45, H  0.9747,107.8735, 32.1725
33,46, H  0.9031,112.4956,272.5026
33,47, H  0.9918,108.2513, 34.1096
33,48, H  0.9686,109.3275,147.5504
FMO
 -2 11 37 -1  1
  3  4  5  6  7  8  9 10 11 12 13
```

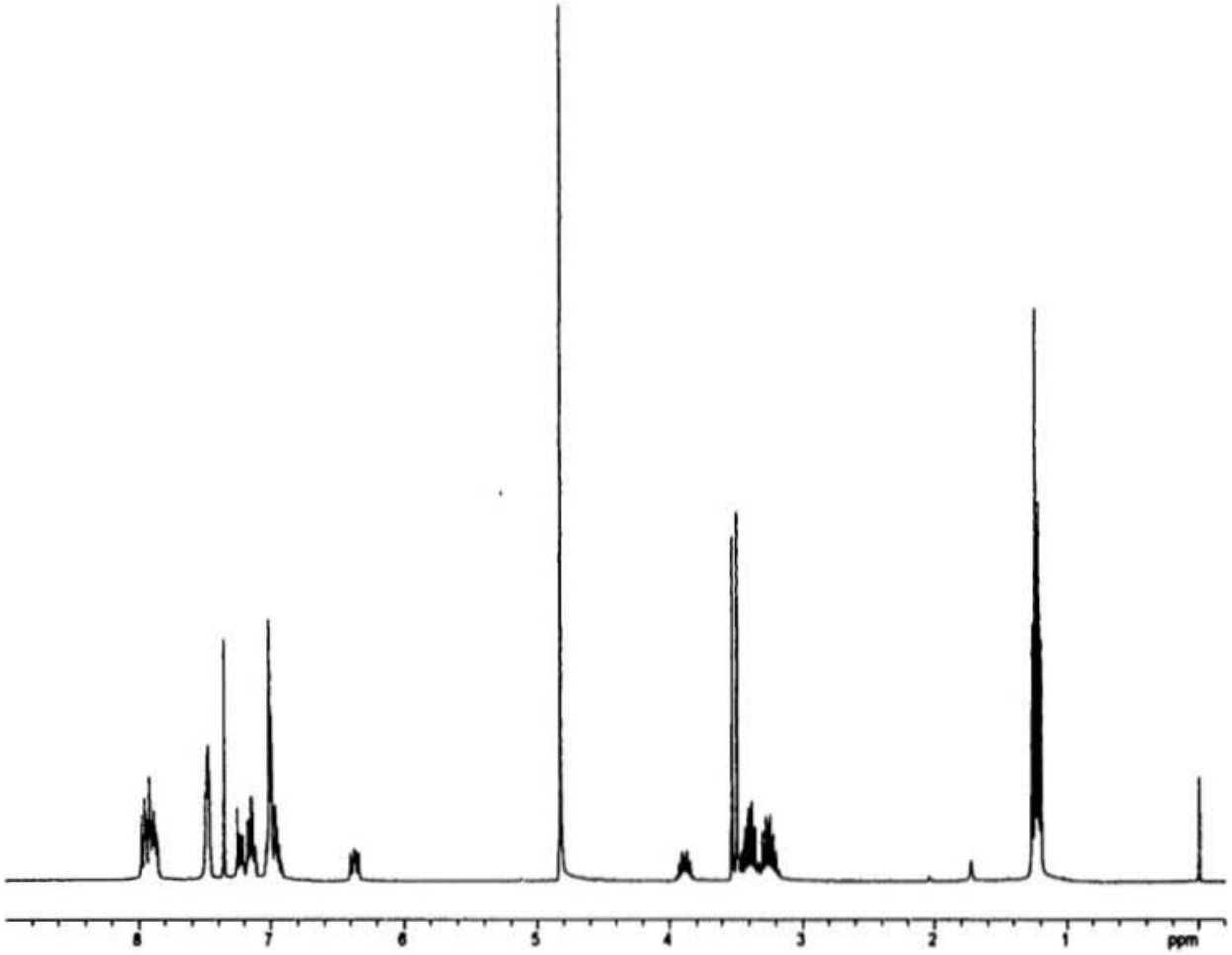

Appendix 4. 300.1 MHz ^{1}H NMR of $R_{Co}S_PS_C$-CpCo(I)($Et_2NP(O)(OMe)$)($PPh_2NHCH(Me)Ph$) (3a-2 in Chapter 2) in $CDCl_3$ at room temperature

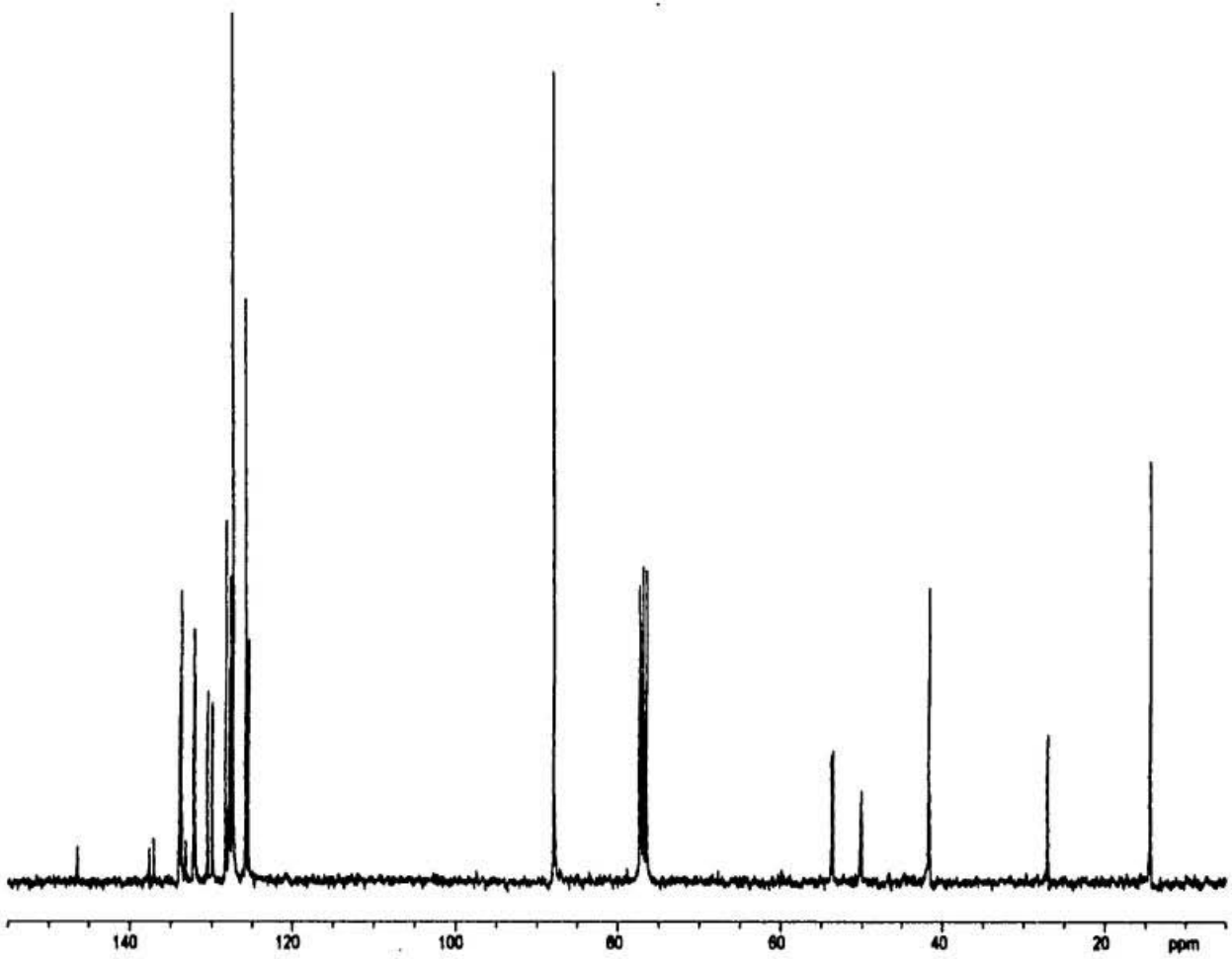

Appendix 5. 75.5 MHz ^{13}C NMR of $R_{Co}S_PS_C$-CpCo(I)($Et_2NP(O)(OMe)$)($PPh_2NHCH(Me)Ph$) (3a-2 in Chpater 2) in $CDCl_3$ at room temperature

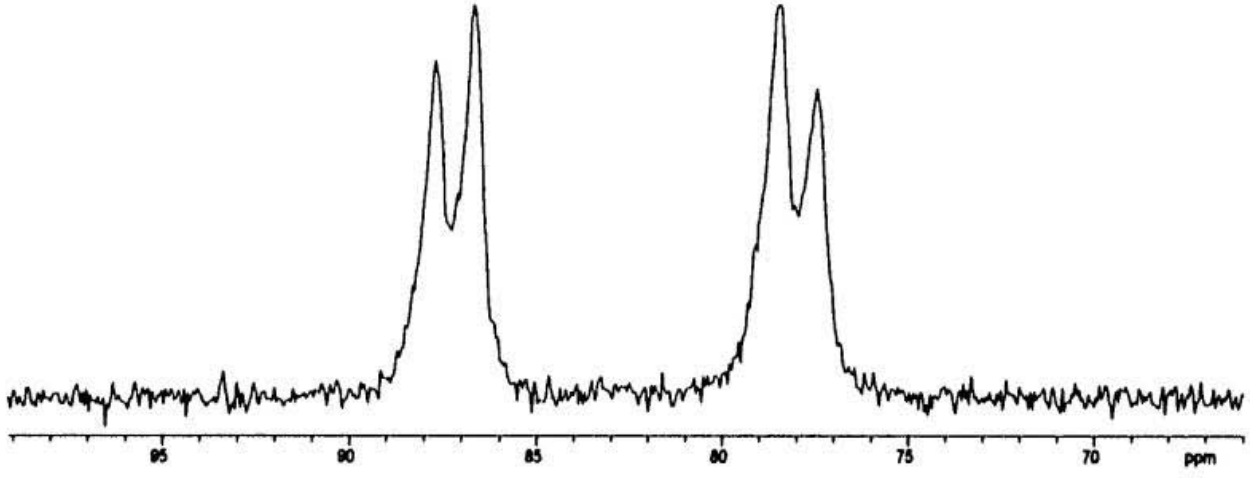

Appendix 6. 121.5 MHz ^{31}P NMR of $R_{Co}S_PS_C$-CpCo(I)(Et$_2$NP(O)(OMe))(PPh$_2$NHCH(Me)Ph) (3a-2 in Chapter 2) in CDCl$_3$ at room temperature

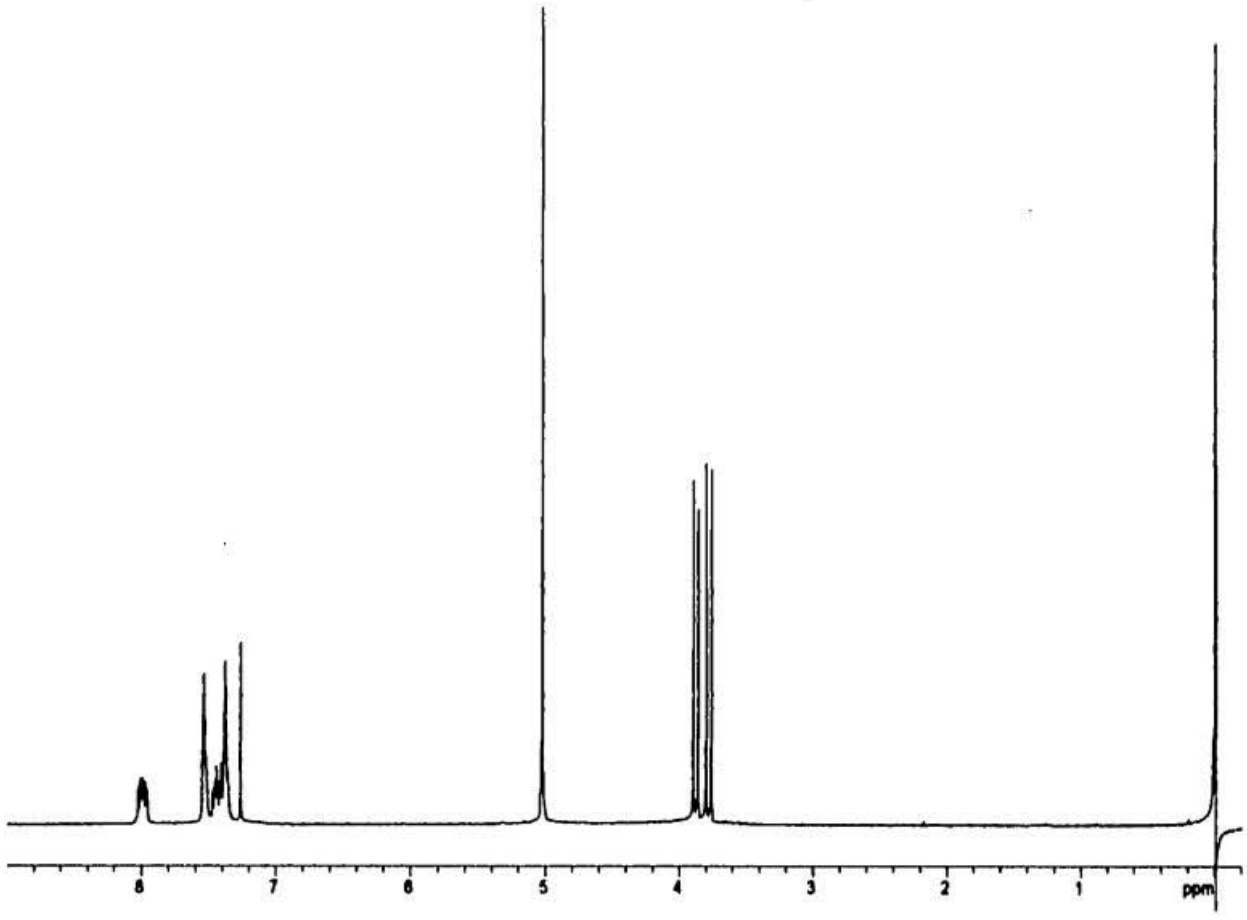

Appendix 7. 300.1 MHz ^{1}H NMR of R_{Co}-CpCo(I)(P(O)(OMe)$_2$)(PPh$_2$OH) (3a-2 in Chapter 3) in CDCl$_3$ at room temperature

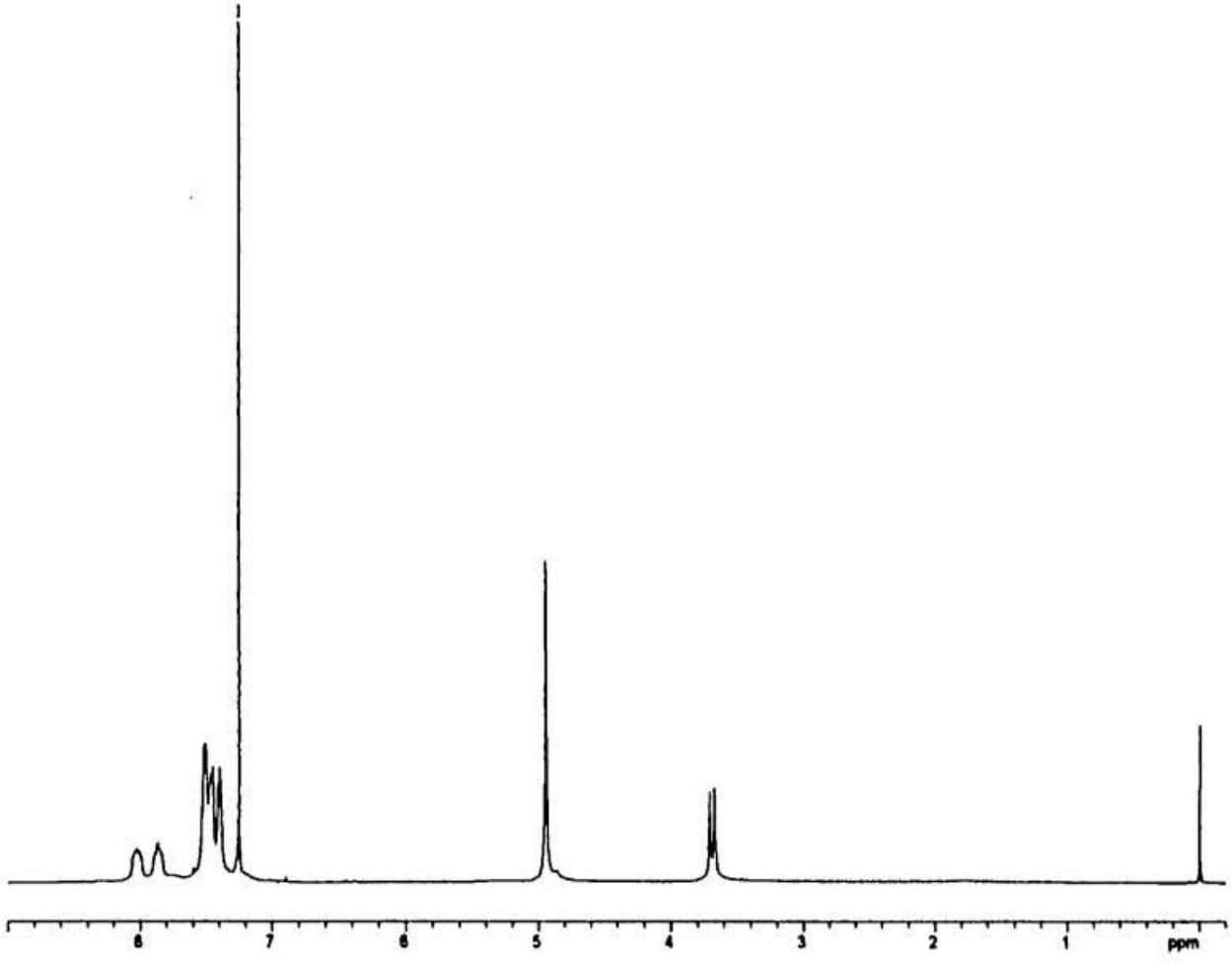

Appendix 8. 300.1 MHz ^{1}H NMR of (R_{Co},S_p)-CpCo(I)(PhP(O)(OMe))(PPh$_2$OH) (3b-2 in Chapter 3) in CDCl$_3$ at room temperature

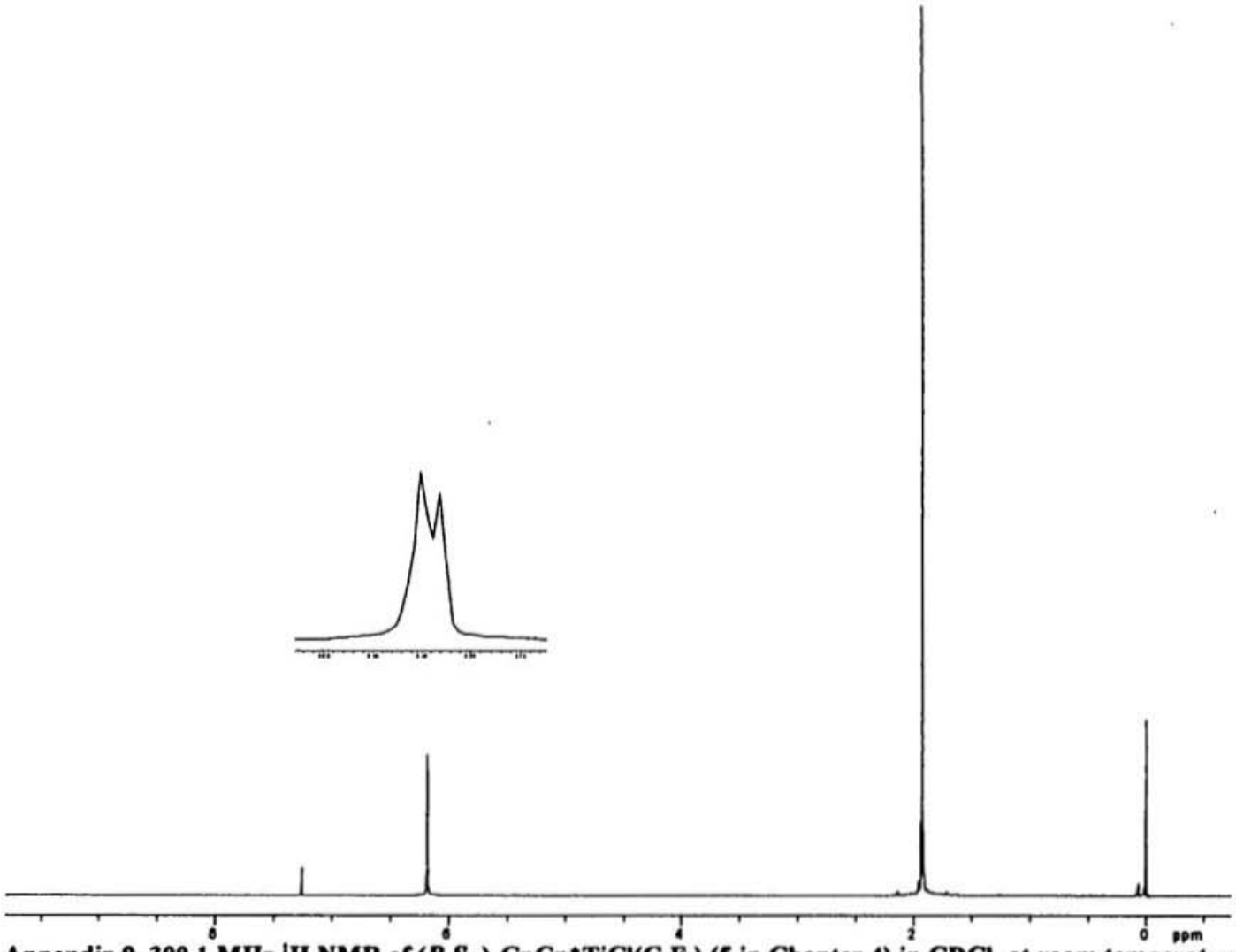

Appendix 9. 300.1 MHz ^{1}H NMR of ($R_r S_{Ti}$)-CpCp*TiCl(C_6F_5) (5 in Chapter 4) in $CDCl_3$ at room temperature

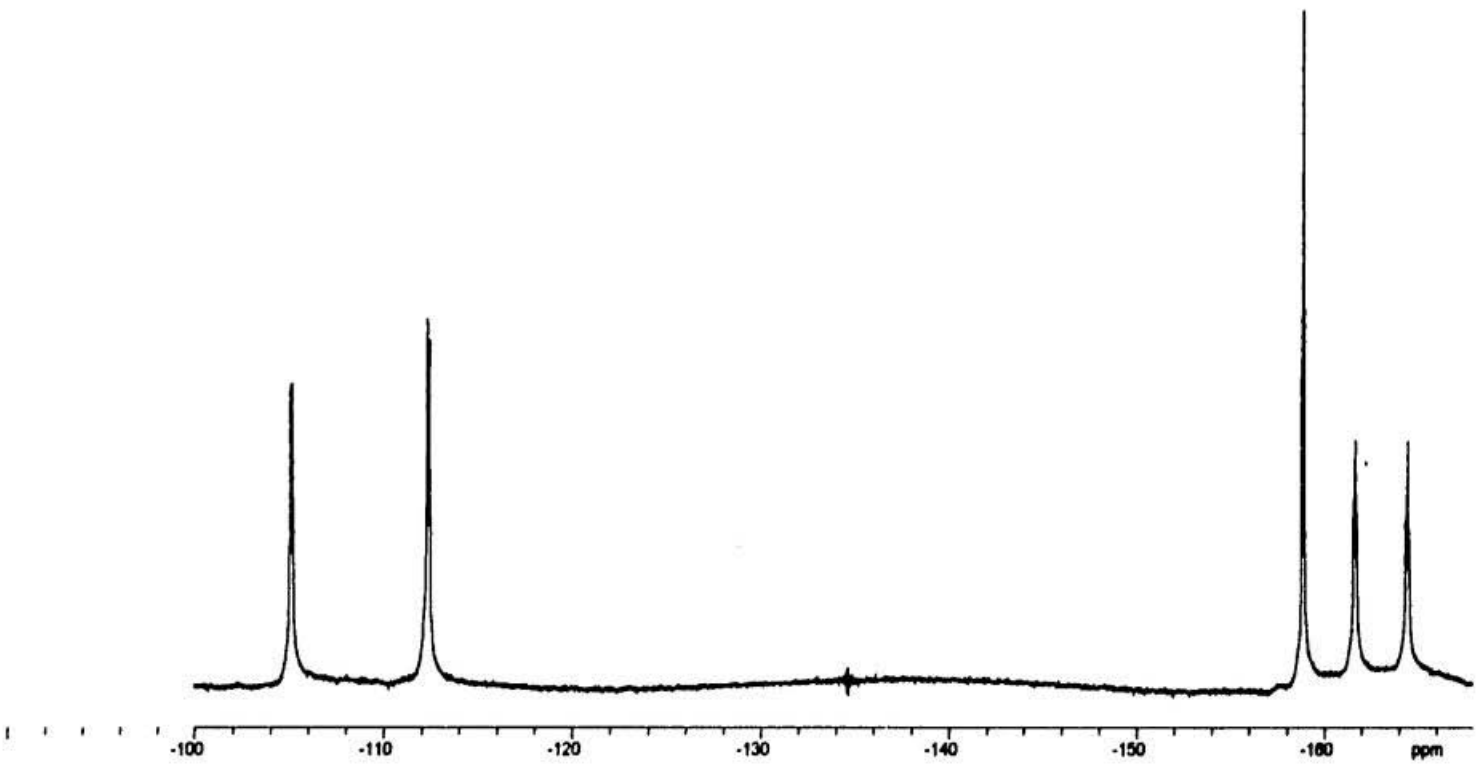

Appendix 10. 282.4 MHz ^{19}F NMR of (R,S_{Ti})-CpCp*TiCl(C_6F_5) (5 in Chapter 4) in $CDCl_3$ at room temperature

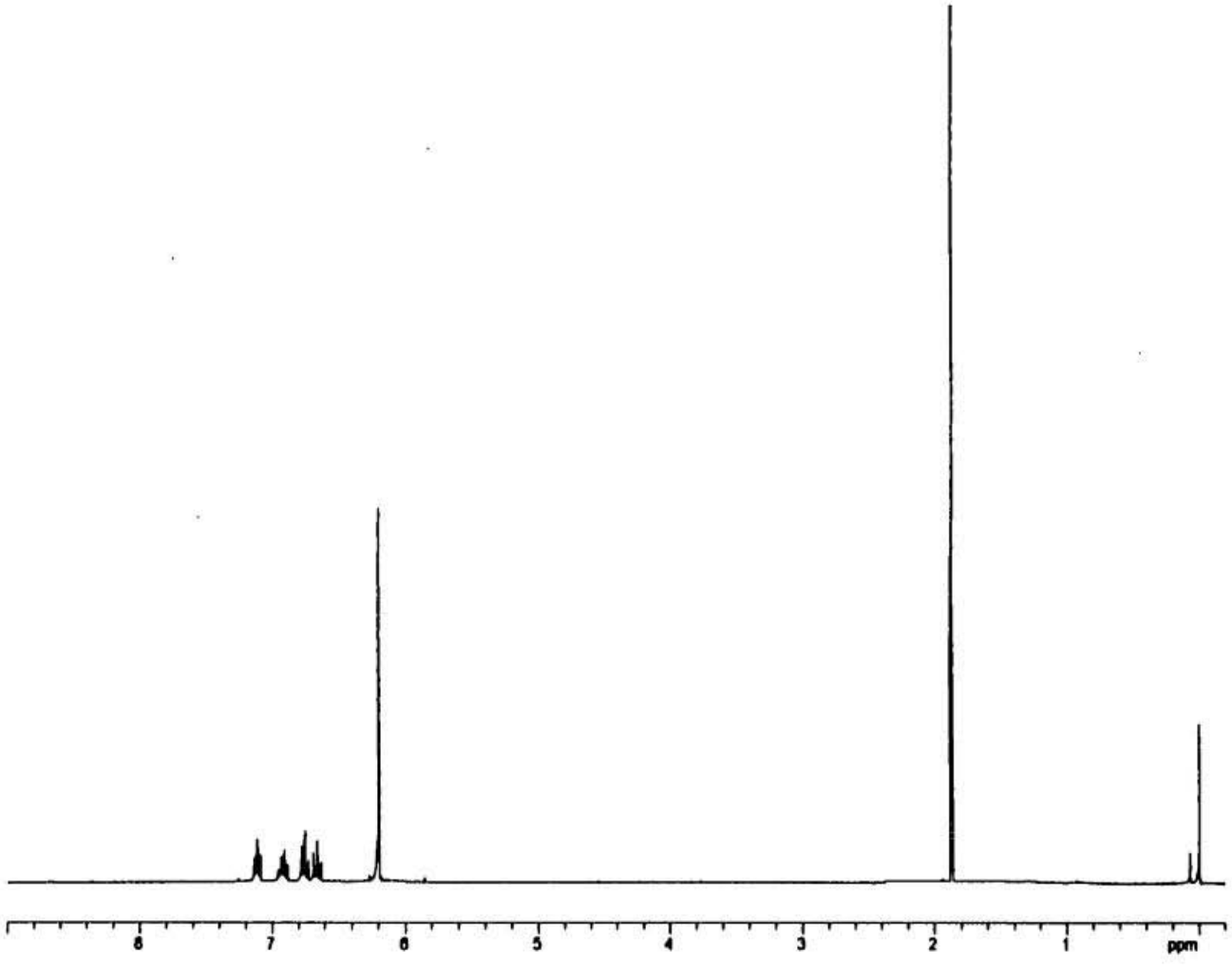

Appendix 11. 300.1 MHz ^{1}H NMR of CpCp*TiCl(*o*-FC_6H_4) (2 in Chapter 5) in $CDCl_3$ at room temperature